ISBN 978-82-326-1610-7 (printed version)
ISBN 978-82-326-1611-4 (electronic version)
ISSN 1503-8181

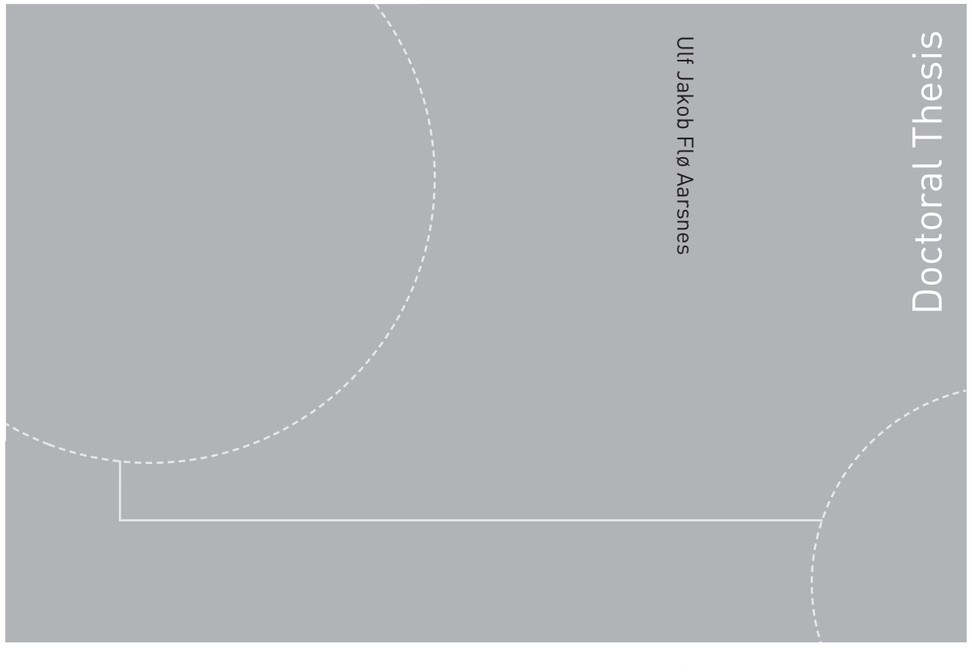

Doctoral theses at NTNU, 2016:136

Ulf Jakob Flø Aarsnes

Modeling of Two-Phase Flow for Estimation and Control of Drilling Operations

NTNU
Norwegian University of
Science and Technology

NTNU
Norwegian University of
Science and Technology

Doctoral theses at NTNU, 2016:136

NTNU

NTNU
Norwegian University of
Science and Technology
Faculty of Information Technology,
Mathematics and Electrical Engineering
Department of Engineering Cybernetics

NTNU
Norwegian University of
Science and Technology

Ulf Jakob Flø Aarsnes

Modeling of Two-Phase Flow for Estimation and Control of Drilling Operations

Thesis for the degree of Philosophiae Doctor

Trondheim, May 2016

Norwegian University of Science and Technology
Faculty of Information Technology,
Mathematics and Electrical Engineering
Department of Engineering Cybernetics

NTNU
Norwegian University of
Science and Technology

NTNU
Norwegian University of Science and Technology

Thesis for the degree of Philosophiae Doctor

Faculty of Information Technology,
Mathematics and Electrical Engineering
Department of Engineering Cybernetics

ISBN 978-82-326-1610-7 (printed version)
ISBN 978-82-326-1611-4 (electronic version)
ISSN 1503-8181

Doctoral theses at NTNU, 2016:136
ITK-report: 2016-10-W

Printed by Skipnes Kommunikasjon as

Summary

Modern approaches to process monitoring, optimization and control promise enhanced robustness and performance through the merger of process knowledge encoded in mathematical models with real-time measurements from the process. Such design techniques, often referred to as model-based estimation and control, require a mathematical model with the right balance between complexity and fidelity: i.e. the complexity must be limited to facilitate the use of established mathematical analysis and design techniques, while the qualitative response of the process is retained.

Finding such models amenable for estimation and control of two-phase flow in drilling is particularly challenging due to the relative complexity of both the mathematical models and the dynamics to be represented. In particular the timescale separation between dominating dynamic effects, distributed nature of important transport phenomena and the nonlinear coupling between them entails very rich dynamics with modes over a broad frequency range and bifurcations between potential operating points.

This thesis uses the classical transient drift flux model as a starting point for heuristically distinguishing between three qualitatively different dynamic effects, each of which dominates the transient response in a given frequency range: ~ 10 seconds, the distributed pressure dynamics, $\sim 1-10$ minutes, a slow compressional pressure mode, and finally ~ 10 minutes to hours, the advection of a two-phase void wave.

Since the distributed pressure waves operate in a high-frequency range, it is of little impact for operations concerned with slower phenomena. This insight is employed to develop simplified model descriptions of the slow pressure mode, and void wave advection, which are amenable for certain model-based control and estimation applications. In particular the description is used to develop an RLS estimator of reservoir pressure during a gas influx.

The heuristic for characterizing the dominating effect after frequency range (or timescale) is also used to develop a robust pressure controller using an automatically controlled back-pressure choke. The approach retains the dominating dynamic effect in the frequency range of interest (the slow pressure mode) while ensuring robustness to the discarded high-frequency pressure waves.

The thesis gives examples from the industry to problems and processes which can be dealt with through use of model-based estimation and control techniques and provides a framework for designing such algorithms.

Preface

This thesis is submitted in partial fullfilment of the requirements for the degree of Philosphiae Doctor (PhD) at the Norwegian University of Science and Technology (NTNU). The research has been conducted at the Department of Engineering Cybernetics (ITK) from August 2012 to December 2015.

This time period included a two month internship at the Statoil Research centre, Porsgrunn, Norway, February to April 2015, a two month visit to MINES ParisTech, Paris, France, May to June 2013, a six month visit to the University of Texas at Austin, Austin, Texas, May to November 2014, and a one month secondment to Blade Energy Partners, Frisco, Texas, October 2016. Funding for the project was provided by Statoil ASA and the Research Council of Norway (NFR project 210432/E30 Intelligent Drilling).

I would like to thank my supervisor, Professor Ole Morten Aamo, and my co-supervisor, Adjunct Professor Glenn-Ole Kaasa, for their help and encouragement throughout the PhD.

Thanks to Professor Florent Di Meglio of Mines ParisTech for welcoming me to Paris and for our continued collaboration. Thanks to Adrian Ambrus at the University of Texas at Austin who contributed significantly to this thesis. Also thanks to Professor Eric van Oort, Professor Behçet Açıkmeşe and Dr. Ali Karimi Vajargah at the University of Texas at Austin, for hosting me and starting a successful collaboration. Thanks to Martin Culen and Oscar Gabaldon of Blade Energy Partners for inviting me to visit, work with and learn from the engineers at Blade. Thanks to Robert Graham of Well Advanced Solutions, Dr. Tore Flåtten at the Oil and Gas Process Technology, Sintef, for their collaboration and input. Thanks to Dr. Qin Li, Dr. Henrik Manum and Dr. Alexey Pavlov at the Statoil Research center in Porsgrunn.

Thanks to my colleagues in the Intelligent Drilling research group Dr. Anders Willersrud, Torbjørn Pedersen, Amirhossein Nikoofard and Dr. Agus Hasan, the supervisors and collaborators Professor Lars Imsland, Professor Tor Arne Johansen, Adjunct Professor John-Morten Godhavn, Dr. Jan Einar Gravdal and Adjunct professor Gerhard Nygaard, and the staff and my colleagues at the Department.

Finally, thank you to my family.

Ulf Jakob F. Aarsnes
Trondheim, December 2015

Contents

1. Introduction 1
   1.1. Pressure Control 2
   1.2. Two-phase flow in MPD: well control 6
   1.3. Underbalanced drilling 7
   1.4. Use of Fit-for-purpose models 12
   1.5. Two-phase modeling and timescales 13
   1.6. Outline and contribution 17

2. Models of gas-liquid two-phase flow in drilling for control and estimation applications 23
   2.1. Introduction 23
   2.2. High fidelity models 28
   2.3. Drift-Flux Models (DFM) 33
   2.4. Simplified ODE models 38
   2.5. Numerical Schemes 41
   2.6. Simulation Study 42
   2.7. Conclusion 48

3. A methodology for classifying operating regimes in underbalanced drilling operations 51
   3.1. Introduction 51
   3.2. Stable and unstable equilibria of dynamical systems 53
   3.3. The Drift Flux Model at steady-state 56
   3.4. UBD operating envelope 58
   3.5. Classification of operating regimes 64
   3.6. Choke opening sensitivity analysis 68
   3.7. Dynamic instability: severe slugging in UBO 68
   3.8. Summary and conclusions 71
   3.A. Loop Transfer Function derivation 74
   3.B. The Nyquist Stability Criterion 76

4. A Simplified Two-Phase Flow Model Using a Quasi-Equilibrium Momentum Balance 79
   4.1. Introduction 79
   4.2. The Drift Flux Model 81
   4.3. Derivation of the new formulation 86

4.4. Some Numerical Examples 90
4.5. Summary and conclusions 94

5. Model-Based Estimation of Reservoir Inflow and Pore Pressure 95
5.1. Introduction 95
5.2. The Reduced Drift Flux Model 98
5.3. Model Validation 100
5.4. Experimental data 103
5.5. Proposed Methodology for Pore Pressure and Reservoir Inflow Estimation 106
5.6. Validation of Estimation Methodology 110
5.7. Conclusions 116
5.A. Recursive Least Squares Algorithm 116

6. Robust Controller Design for Automated Kick Handling in Managed Pressure Drilling 119
6.1. Introduction 119
6.2. Model Description 122
6.3. Proposed Controller Structure 128
6.4. Controller Design and Results 131
6.5. Simulations 136
6.6. Conclusion and Future Work 138
6.A. Hydraulic Transmission line modelling 141
6.B. Linearized Two-Phase Choke Equation 142

7. Concluding remarks 145

Appendices 147

A. The Drift-Flux Model 147
A.1. Governing Equations 147
A.2. Numerical Implementations 149

Abbreviations

BHP/BHCP	Bottom-Hole (Circulating) Pressure: $p_{bh} = P(0)$.
DFM	Drift Flux Model.
IPR	Inflow Performance Relationship.
LOL-model	Low Order Lumped-model.
LMI	Linear Matrix Inequality
MPD	Managed Pressure Drilling.
NPW	No pressure wave: NPW DFM = Reduced DFM.
ODE	Ordinary Differential Equation.
PI	Production Index.
PDE	Partial Differential Equation.
RIPI	Rate-integral production index.
UBD	Under-Balanced Drilling.
UBO	Underbalanced Operations.
WHP	Well-Head Pressure: $p_a, p_c = P(L)$.

Chapter 1

Introduction

The process of oil well drilling, schematically depicted on Figure 1.1, consists in boring a hole several kilometers deep into the ground, until a reservoir is reached. The hole is created by rotating a bit to which a downward force is applied (Bourgoyne et al., 1986). The force, and in most cases the rotation, is applied by a rotary drilling rig to sections of heavy thick-walled pipe, called the *drill-string*, which transfers it to the bit. The drilling rig can be located on onshore or on an offshore platform, then either as a rig anchored on the sea bed or as floating a drilling ship or semi-submersible.

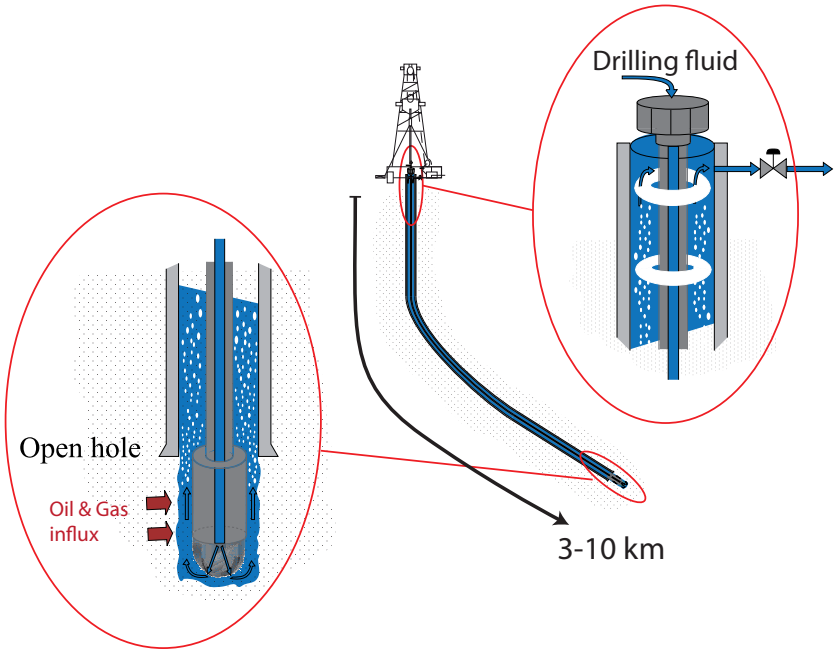

Figure 1.1.: Schematic of a well being drilled.

During the drilling operation, drilling fluid, also known as *mud* is pumped through the drill-string, exits through the drill bit nozzles, cools and lubricates

the bit and the drill-string, and carries drilled cuttings to the surface. An essential function of the drilling mud is to provide the hydrostatic pressure, added to the frictional pressure drop in the annular space between the drill-string and wellbore/casing, required to balance the reservoir formation pressure. Consequently, the point where wellbore pressure equals the reservoir pore pressure is referred to as the *balance point*, and when the pressure in the wellbore exceeds and is less than the reservoir pressure, the well is said to be *overbalanced* and *underbalanced*, respectively.

The drill-string typically consists of 9 meter long pipe sections which are added as drilling progresses. This procedure, referred to as a *connection*, involves halting the drilling process, including the injection of mud, so as to enable connecting a new pipe section.

As drilling progresses, casing is set at preplanned intervals to isolate the wellbore from the surrounding formation. The casing is a steel cylinder which is hammered into the open hole and cemented in place. The section of the well that has been drilled since the last casing was set, is susceptible to pressure changes in the wellbore and is called the *exposed zone*. Controlling pressure in the exposed zone is a major challenge in drilling.

1.1. Pressure Control

1.1.1. Conventional drilling

In conventional drilling, it is desired to keep the well overbalanced so as to prevent any influx of formation fluids (oil, gas or water) to the wellbore. However, if wellbore pressure is too high, it can exceed the fracture initiation pressure, resulting in rock breakdown and loss of drilling fluid to the formation. This can be costly due to potential damage to the reservoir, high price of the lost fluid, and may in some cases prevent drilling from proceeding altogether. Therefore, in overbalanced drilling, wellbore pressure should be managed to stay above the formation pore and collapse pressures and below the fracture pressure in the exposed zone, see Fig. 1.2.

That is, we can write the pressure $P(x)$, at position x in the well, as

$$P(x) = P_{atm} + \text{Fric}(x,t) + \text{Grav}(x), \tag{1.1}$$

where the wellhead pressure is atmospheric WHP $= P_{atm}$. Hence, changing the pressure in the well must be achieved by circulating a new mud with different density, so as to affect the $\text{Grav}(x)$ term. This distributed pressure is then to be kept within lower and upper pressure margins, which in this case are the pore pressure and fracture pressure, respectively:

$$P_{pore}(x) < P(x,t) < P_{frac}(x), \qquad \text{for } x \text{ in the exposed zone.} \tag{1.2}$$

For convenience, the distributed pressure in the exposed zone is often lumped to a single point and referred to as the bottom-hole (circulating) pressure (BHP/BHCP).

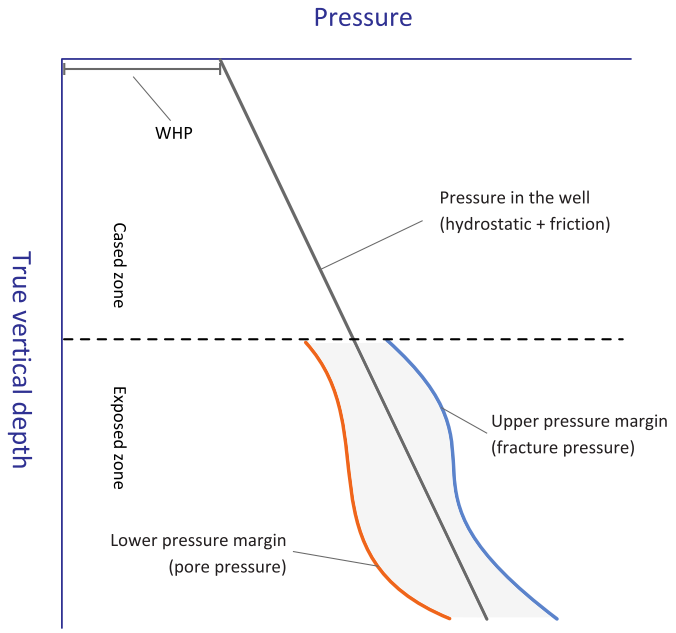

Figure 1.2.: Distributed pressure margins for overbalanced drilling including MPD.

1.1.2. Managed pressure drilling

In narrow margin wells such as deep-water offshore wells, formation and fracture pressures are very close. Managing the annular pressure is challenging and plays a vital role in successful drilling of these wells. Managed Pressure Drilling (MPD) techniques have been introduced in recent years to more precisely control the annular pressure profile throughout the wellbore of narrow margin wells in particular (Malloy et al., 2009). MPD differs from conventional drilling in that a rotating control device (RCD), see Fig. 1.3, is used to create a seal around the drill-string at the wellhead, which, together with a *back-pressure choke*, enables manipulating the WHP. This is sometimes also coupled with a dedicated back-pressure pump to enable control even when the main pump is shut off.

A key advantage of MPD is that it enables the drilling of wells where pressure margins are too narrow for conventional drilling. However, it is also often used to handle uncertainty of the reservoir and well plan in that it enables the driller to better and more quickly adapt to the scenario that is actually encountered (Saponja et al., 2006). This is primarily due to the improved well control capabilities offered by MPD (Smith and Patel, 2013; Gabaldon et al., 2014; Kinik et al., 2015)

For MPD we have

$$P(x) = \mathrm{WHP}(t) + \mathrm{Fric}(x,t) + \mathrm{Grav}(x), \tag{1.3}$$

where WHP can be effectively controlled by manipulating the opening of the back-

pressure choke.

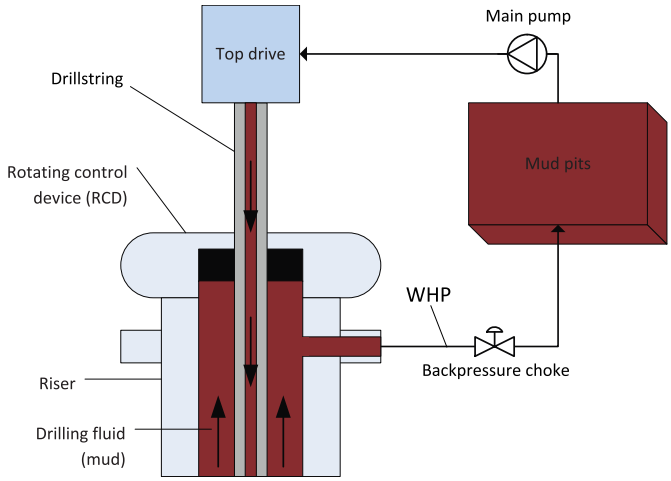

Figure 1.3.: Topside part of a the closed circulation MPD system which enables the application of back-pressure, (Hauge, 2013).

1.1.3. Underbalanced drilling

Drilling with a BHCP intentionally lowered to below the reservoir pressure, such that the well is producing fluid from the reservoir while drilling, see Fig. 1.4, is called *underbalanced drilling* (UBD) (Saponja, 1998). The pressure differential between the reservoir and open-hole wellbore is called *drawdown* and is defined as positive when underbalanced. Key drivers for employing UBD include

- **Reduced formation damage:** Overbalanced drilling operations cause invasion of filtrate into near-wellbore regions resulting in reduced producion index (PI). (Suryanarayana et al., 2007b; Al-Saadi et al., 2006).
- **Increased rate of penetration:** Lower pressure in the wellbore invaribly increases penetration rates, resulting in improved bit life and reduced drilling time (Bourgoyne, Jr., 1997; Bennion et al., 1996).
- **Reservoir characterization:** Estimating reservoir pressure and productivity while drilling offers unique insights as the reservoir can be characterized in zones as it is drilled. (Culen and Killip, 2005; Suryanarayana et al., 2007a; Wu and Suryanarayana, 2011)
- **Enabling technology:** in dealing with reservoirs with small or vanishing pressure margins (Pickles et al., 2004).

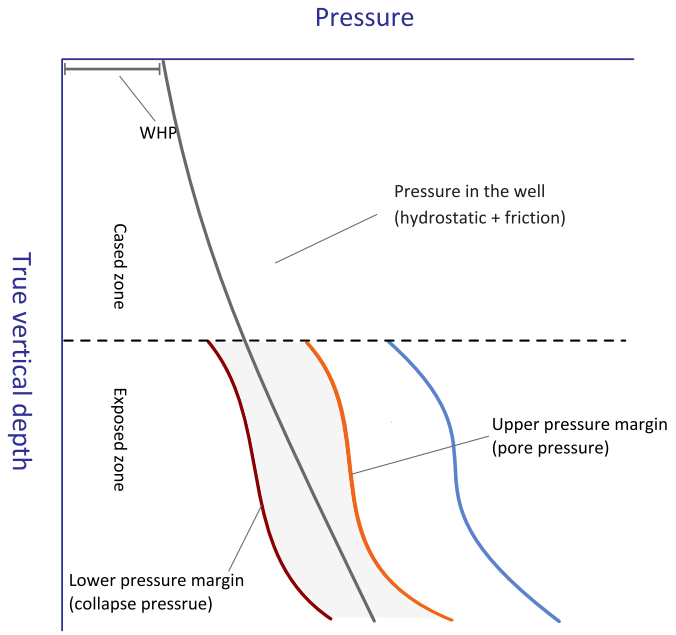

Figure 1.4.: Distributed pressure margins for underbalanced drilling.

UBD requires additional equipment and procedures to handle the produced fluids while the well is being drilled. The produced fluids may include gas which makes the wellbore flow two-phase and affect the hydrostatic pressure when entering the vertical section of the annulus. Since the influx from the reservoir depends on the pressure in the exposed zone, the well-reservoir interaction effectively creates a feedback system which can give rise to complex, non-linear, dynamics such as multiple equilibria, non-minimum phase response and bifurcations.

UBD also requires the use of a RCD and a back-pressure choke, hence

$$P(x) = \mathrm{WHP}(t) + \mathrm{Fric}(x,t) + \mathrm{Grav}(x,t), \tag{1.4}$$

where the significant difference is that the $\mathrm{Grav}(x,t)$ term now varies in time with the amount of gas in the well. When applying UBD the pressure control goal will depend on the well in question as well as the reasons for choosing UBD. Key factors deciding the optimal drawdown during UBD is that (Guo and Ghalambor, 2006): the BHCP should be high enough to avoid risk of collapse (Bennion et al., 1996) and limit the influx to a level that can be handled by separators and storage facilities. The BHCP should be low enough to avoid mud damaging the reservoir (i.e. lower than pore pressure) and cause sufficient influx to obtain stable operating conditions (Saponja, 1998) and hole cleaning (Doan et al., 2003). In addition, constant pressure during drilling is desirable to enhance reservoir characterization.

As a minimum, the following limitations on pressure are enforced during UBD:

$$P_{collapse}(x) < P(x,t) < P_{pore}(x), \qquad \text{for } x \text{ in the exposed zone.} \tag{1.5}$$

1.2. Two-phase flow in MPD: well control

As mentioned before, when wellbore pressure opposite a permeable zone is below the formation pore pressure, formation fluids and/or gas may flow into the wellbore. This phenomenon is commonly referred to as a gas or liquid "kick". Gas kicks tend to be more severe and hazardous than liquid kicks due to gas expansion in the annulus and higher magnitudes and variations in annular pressure (Karimi Vajargah, 2013). If the kick migrates to the surface in an uncontrolled manner, a *blow-out* scenario can occur. Blow-outs pose severe threats to rig crew safety, the surrounding environment, company and industry reputation, project economics, etc. Detection and handling of gas kicks in a timely manner is referred to as *well control* and is a major concern in any drilling operation.

The traditional procedure for the handling of a confirmed kick is to perform *shut-in* operations and apply a well control method to remove it. Shutting in entails halting the drilling operation, stopping the rig pumps and closing the blow-out preventers (BOPs), a set of valves capable of sealing the annulus at the wellhead (see Fig. 1.1), thus letting the pressure in the well increase until the bottom-hole pressure (i.e. the combination of the muds hydrostatic head and the shut-in pressure at surface) reaches the reservoir pressure so that the influx stops. This increase in pressure is referred to as *killing* the well. Kick detection and shut-in operations are cumbersome and stressful for the crew, cause significant downtime and entail significant pressure transients that may damage the well and/or the reservoir (Gravdal et al., 2013).

However, the added actuation introduced by MPD equipment enables circulating influxes of small and medium size out of the well without needing to perform a shut-in operation (Bacon et al., 2015). Increasing the surface backpressure to attenuate the kick can be used as a viable alternative to shutting in the well (Karimi Vajargah et al., 2014). Back-pressure is applied by means of the dedicated MPD choke, the operation of which can be automated. The gas influx is circulated out through the MPD choke manifold, similarly to the first circulation phase of the Drillers Method (Smith and Patel, 2013). Once gas exits the choke, it is vented through the mud gas separator. This *dynamic well control* can only be used for influxes up to a certain volumetric size, the limit being as low as 10 barrels in some deepwater operations (Karimi Vajargah et al., 2014). An influx larger than this size may cause the annular pressure to exceed the integrity limits of weak formations exposed in the open-hole section (i.e. the part of the well that is not protected by casing and cement) or those of the MPD surface equipment. In that case, conventional shut-in and well control methods need to be used. Nevertheless, in situations where dynamic kick handling is feasible, it is essential to keep bottom-hole pressure

constant at a value sufficient to prevent further influx from the formation on the one hand and prevent fracture initiation on the other. To maintain the correct constant bottom-hole pressure during influx removal, proper and robust estimation of formation pressure and influx rate and volume is vital. Handling the changing well dynamics when taking and circulating out gas, while staying within pressure constraints, is also considered a challenge (Reitsma and Couturier, 2012).

1.3. Underbalanced drilling

This section contains suggestions for how applied control theory can make an impact in UBD.

1.3.1. Reservoir Characterization

Reservoir characterization is often a major driver for performing a drilling operation underbalanced. State of the art reservoir characterization while drilling uses a combination of dedicated flow and pressure buildup tests and analysis of changes in production rates while drilling (Shayegi et al., 2012).

Flow tests

Flow and pressure buildup test have to be performed for sufficient time to elicit the transient response of the reservoir that is used to characterize it (Hasan and Kabir, 1983; Wu and Suryanarayana, 2011). As such, performing these tests during a UBD operation causes significant flat time, see Fig 1.5, and consequently these tests are typically mainly performed for wells which are drilled UBD for the sake of reservoir characterization. These tests mimic the ones performed in reservoir engineering, although at shorter time-scales.

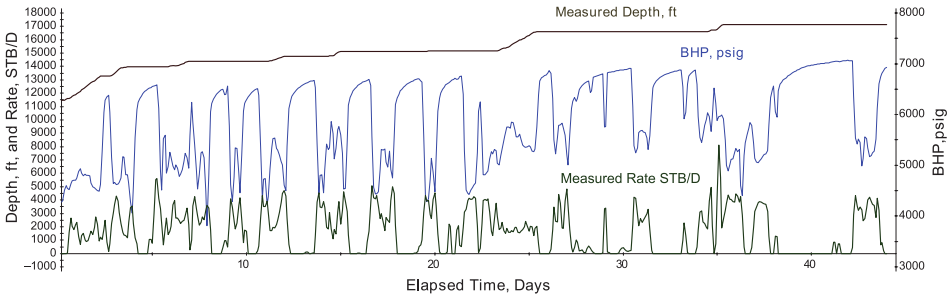

Figure 1.5.: Flow tests take up significant time of UBD operations done for the purpose of reservoir characterization, resulting in so-called *flat time*. Figure by Shayegi et al. (2012).

Rate transient analysis

Production rates while drilling are typically analyzed using a rate-integral production index (RIPI) in a process referred to as rate transient reservoir characterization (RTRC). RIPI is an averaged quantity used to interpret flow data (Gauthier et al., 2007). Specifically, it is desirable to estimate the Production Index of water, gas and oil, and how it changes while the well is drilled (Culen and Killip, 2005). Due to transient events and measurement noise, discerning the production index, k, in the relation

$$q(t) = k(t)\Delta P(t) \tag{1.6}$$

where ΔP is the drawdown and q is the produced quantity, can be challenging. The RIPI was defined by Suryanarayana et al. (2007a) as

$$\mathrm{RIPI}(t) = \frac{1}{t\Delta P(t)} \int_0^t q(\tau)\mathrm{d}\tau, \tag{1.7}$$

which is intended to smoothen out the effect of noise, defined as wellbore transients.

Potential for improvements

Estimating production rates is often complicated by wellbore transients. Specifically, it is desired to correlate estimates of the production rates as the flow enters the wellbore from the reservoir (at the sandface) to the current BHCP. The actual production measurements are, however, at the wellhead.

This problem can be mitigated by reducing transient effects, i.e. by using automatic control. Steady operating conditions significantly improve the quality of the analysis. Using model based estimation schemes which take the transient effects into account can further improve the results.

Finally, combining a transient wellbore model with a near-reservoir model, so that both reservoir and wellbore transients are represented (Nævdal et al., 2002), could improve reservoir characterization capabilities and reduce the need for dedicated tests.

1.3.2. Connection transients

One of the major inhibitors of steady drilling conditions in UBD is the drill-string connection procedure. As the connection requires the halting of liquid injection, the result is a large temporary change in the downhole void fraction, which then propagates through the wellbore causing variations in pressure and production rates if not controlled properly (Perez-Tellez, 2003).

During this transient process, the operator will dynamically control the backpressure choke opening, attempting to keep the BHP constant, see Fig. 1.6. Given the appropriate model, an automatic controller can be designed which would improve

this procedure, i.e. which keeps BHP within some predefined constraint for the duration of the connection (Nygaard et al., 2004).

A particularly challenging case is shown in Fig. 1.7. For wells close to conditions with severe slugging, either due to casing heading or to gas production (as in this case), the connection induced transients are particularly problematic. As is illustrated in the figure, the well is in an almost perpetual transient condition due to the connections.

1.3.3. Severe slugging in UBD

Severe slugging in production has been extensively studied in the literature but very little research exists on this topic related to underbalanced drilling. The two phenomena are, however, closely related. The possible causes for severe slugging in drilling include

- **Casing heading:** Well known from production, see e.g. Torre et al. (1987); Eikrem et al. (2008), is also known to occur in drilling (Mykytiw et al., 2003) when gas is injected from a separate conduit, see Fig. 1.8. Casing heading is caused by an interaction between the dynamic pressure and outflow of the casing and two-phase flow in the wellbore (Sinegre et al., 2006).

- **Density wave:** This instability occurs for a simple vertical conduit with a constant gas rate and a pressure dependent liquid rate, see Sinegre et al. (2005); Di Meglio (2011), and is thus known from oil production with gas lifts, where the liquid production rate is dependent on drawdown.

- The final type of instability is for conduits with a constant liquid rate and pressure dependent gas rate (Aarsnes et al., 2016c). This configuration is encountered in UBD in gas dominated wells, see Fig. 1.8 by (Graham and Culen, 2004), but has not previously been described in the literature due to not being encountered in production. As such the mechanism is not well understood, but seems to rely on a large increase in WHP caused by produced gas exiting through the back-pressure choke.

1.3.4. Extending the Operating Envelope to the Unstable Regime

When drilling underbalanced in gas dominated wells, the well behavior changes depending on operating conditions. This is due to the interaction between the wellbore BHP and the reservoir influx. Heuristically, at low drawdowns and gas rates, transients are long and the well difficult to control (Perez-Tellez, 2003; Saponja, 1998). In fact, as will be shown in this thesis (Aarsnes et al., 2016c), at low draw-downs there can be regions which are inoperable due to instabilities caused by severe slugging or a so-called *static* instablity (Hu, 2004).

These points are illustrated by Fig. 1.9, where a steady-state 2-phase model of flow in a wellbore has been used to plot BHCP against WHP in a gas dominated

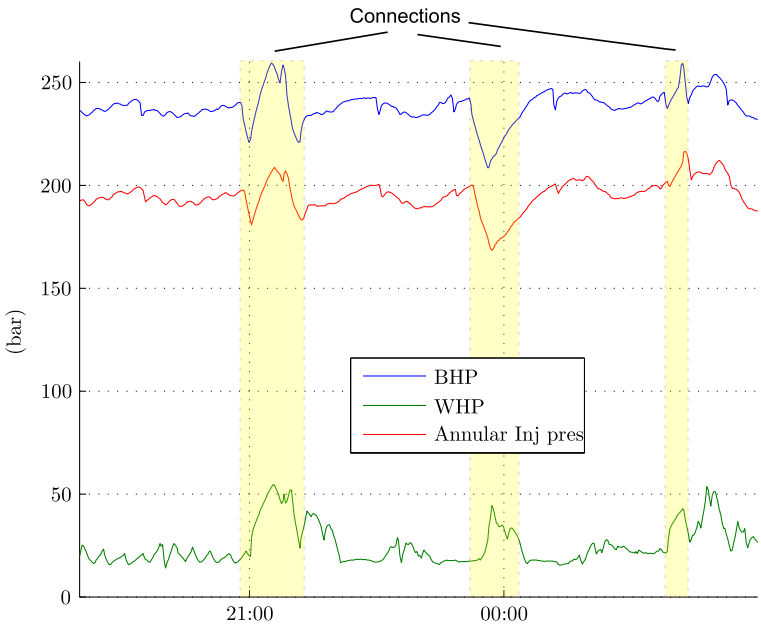

Figure 1.6.: Wellbore transients induced by connections.

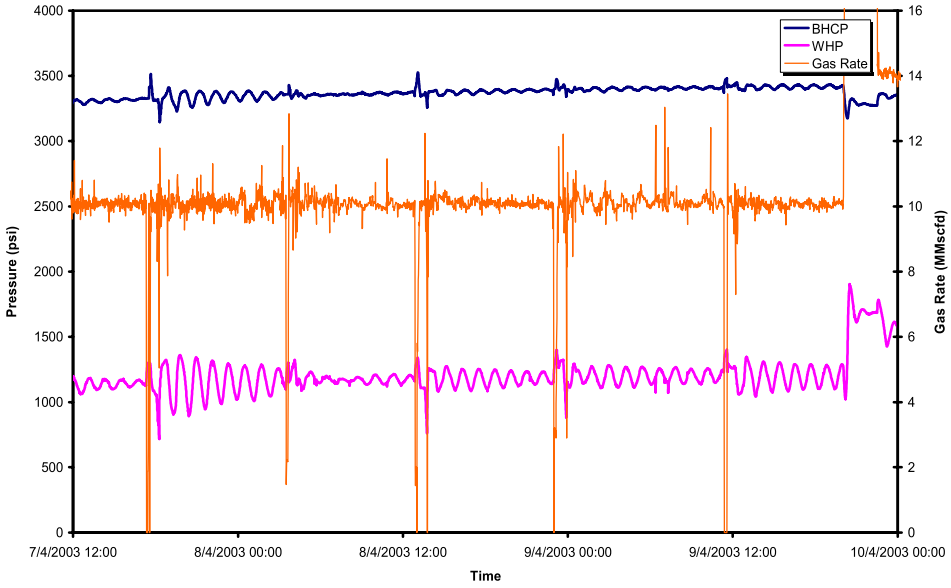

Figure 1.7.: Connection induced transients are especially problematic when the well is close to conditions with severe slugging. Connections are indicated by downward spikes in the gas rate. Figure by Graham and Culen (2004).

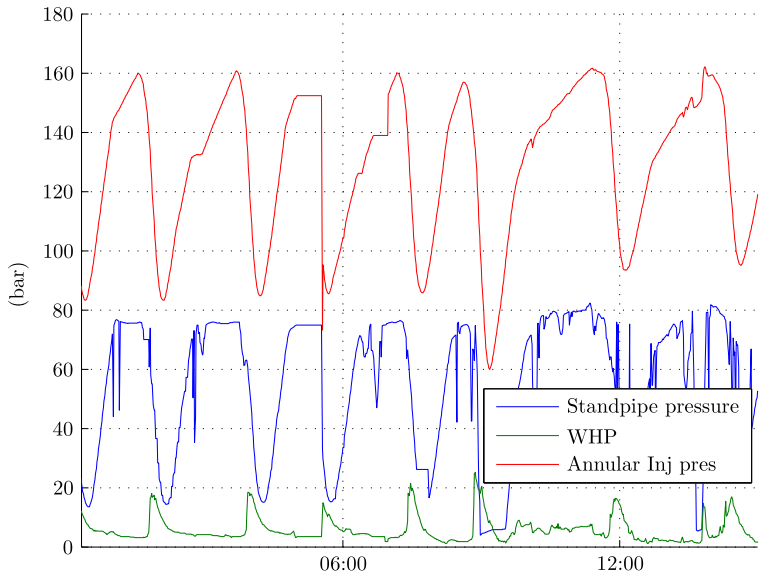

Figure 1.8.: Severe slugging caused by casing heading when attempting to get a well underbalanced.

well. The unstable and non-intuitive labels denote regions at low drawdown which are currently not considered for operations due to the difficult conditions. Using automatic control, these regions can be stabilized, thereby extending the operating envelope, potentially enabling more cost effective and environmentally friendly operations due to reduced flaring of unused produced gas, and enabling UBD in wells with narrow pressure margins.

1.3.5. Problem formulations

As a rule, steady operation of the drilling system translates into a better performance and improved safety. However, as has been discussed, the process is subject to various perturbations, uncertainties and instabilities. Automated estimation and control algorithms have the potential to improve operations with regards to many of these challenges, as is suggested in Table 1.1.

Table 1.1.: Examples of industrial challenges that can be reformulated as estimation and control problems.

Industrial challenge	**Control problem reformulation**
Characterize operating conditions	Linear stability analysis
Respect pressure constraints	Stabilization & trajectory planning
Estimate gas quantity and pressure	Distributed state estimation
Identify reservoir characteristics	Parameter identification

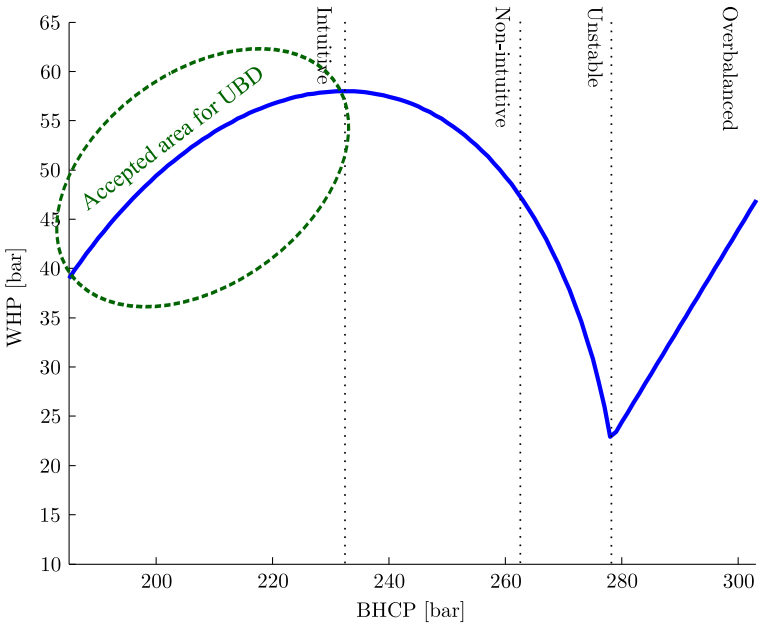

Figure 1.9.: UBD operating envelope showing regions that are challenging due to transient well dynamics. The significant drawdown required for *intuitive* operating conditions can be a challenge in reservoirs with small pressure margins.

1.4. Use of Fit-for-purpose models

Using a mathematical model as the basis for design of a control or estimation algorithm, so-called model-based design is a staple of modern approaches within the field, (Åström and Murray, 2010; Anderson and Moore, 1990) and classical references also typically use first principle models as basis for analysis and design (Maxwell, 1867). Many applications are enabled by the use of models (see e.g. Willersrud (2015) for recent relevant examples), and others can be significantly improved (Eykhoff, 1994).

Modeling for estimation and control poses distinct requirements on model development: model complexity must be limited to facilitate the use of established mathematical analysis and design techniques, while the qualitative response, that is to be controlled or estimated, is retained: effectively echoing the popular adage that *everything sould be made as simple as possible, but not simpler*. Different applications, then, will necessarily pose different requirements on the model, and as such one can often find, in the literature, multiple mathematical models of a single phenomena, each amenable for a different application. These models are variably be referred to as *control oriented*, *simplified* or *fit-for-purpose models*, where the last term is primarily adopted in the present work.

This thesis will propose a novel version of the no-pressure-wave drift flux model,

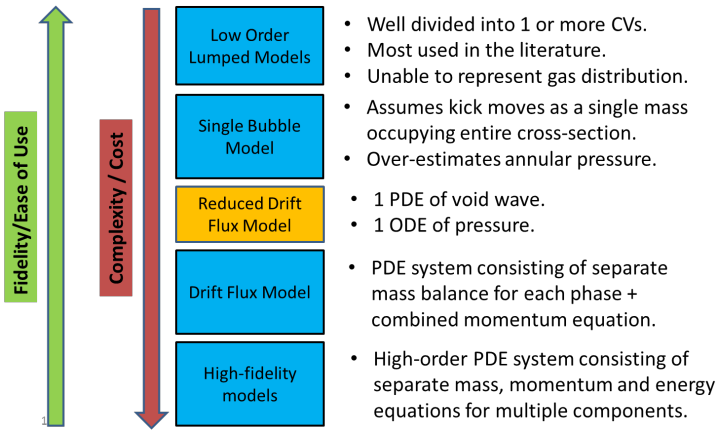

Figure 1.10.: Proposed model compared to existing models.

sometimes referred to as the reduced drift flux model, which aims to be amenable as a fit-for-purpose model of two-phase flow in drilling. The complexity of this model is schematically illustrated in Fig. 1.10. We will later argue that the models above the proposed model lack the capability to sufficiently represent the two-phase dynamics of certain scenarios, while the models below are too complicated, or computationally expensive, for many applications. Identifying which model is amenable for which scenario is an important part of successful algorithm development.

1.5. Two-phase modeling and timescales

Having introduced these industry problems, related to two-phase flow in drilling, it is pertinent to note that most of them will not be dealt with directly in this thesis. What will be attempted in this thesis is to propose a framework for developing model-driven control and estimation solutions to problems related to two-phase flow. The key to this approach is to understand what specific property is required by the model for a given application, and which models offer these properties. Answering these queries will necessarily rely on heuristics, however, heuristics are a staple of petroleum engineering and can be effective in developing engineering solutions.

The central heuristic developed and employed by this work is the following: ignoring the energy dynamics, the flow-pressure behavior of two-phase flow in a long (0.5–10 km), slim, conduit can be divided into three time-scales as summarized in Table 1.2.

Table 1.2.: Time-scale heuristic.

Time-scale	**Dominating dynamics**
~ 10 seconds	Distributed pressure dynamics
$\sim 1{-}10$ minutes	Slow compression pressure mode
~ 10 minutes to hours	Void wave advection

The classical drift flux model equations

We can argue for this heuristic by some basic considerations on the DFM, using the classical formulation of Gavrilyuk and Fabre (1996) (with incompressible liquid):

$$\frac{\partial \alpha_\ell \rho_\ell}{\partial t} + \frac{\partial \alpha_\ell \rho_\ell v_\ell}{\partial x} = 0 \tag{1.8}$$

$$\frac{\partial \alpha_\mathrm{g} \rho_\mathrm{g}}{\partial t} + \frac{\partial \alpha_\mathrm{g} \rho_\mathrm{g} v_\mathrm{g}}{\partial x} = 0 \tag{1.9}$$

$$\frac{\partial \alpha_\ell \rho_\ell v_\ell + \alpha_\mathrm{g} \rho_\mathrm{g} v_\mathrm{g}}{\partial t} + \frac{\partial P + \alpha_\ell \rho_\ell v_\ell^2 + \alpha_\mathrm{g} \rho_\mathrm{g} v_\mathrm{g}^2}{\partial x} = S, \tag{1.10}$$

where α_i, v_i, ρ_i denote the volume fraction, velocity and density, respectively, of phase $i = \mathrm{g}, \ell$ (gas or liquid), P is pressure and S is a momentum source term. We also have the closure relations:

$$\alpha_\mathrm{g} + \alpha_\ell = 1, \qquad P = \rho_\mathrm{g} c_\mathrm{g}^2, \tag{1.11}$$

and the slip law

$$v_\mathrm{g} = \frac{\alpha_\mathrm{g} v_\mathrm{g} + \alpha_\ell v_\ell}{1 - \alpha_\ell^*} + v_\infty \tag{1.12}$$

where $\alpha_\ell^* \in [0, 1)$ and $v_\infty \geq 0$ are constant parameters.

Without going into too much detail, we can employ the transformation due to Gavrilyuk and Fabre (1996)

$$\mathbf{u} = (\chi_\ell, \rho, v_\mathrm{g}) = \left(\frac{(\alpha_\ell - \alpha_\ell^*)\rho_\ell}{\rho_M - \alpha_\ell^* \rho_\ell}, \rho_M - \alpha_\ell^* \rho_\ell, v_\mathrm{g} \right), \tag{1.13}$$

and discard the second-order terms in (1.10) (as was justified by Masella et al. (1998)) to approximate (1.8)–(1.12) as:

$$\frac{\partial}{\partial t} \begin{bmatrix} \chi_\ell \\ \rho \\ v_\mathrm{g} \end{bmatrix} + \begin{bmatrix} v_\mathrm{g} & 0 & 0 \\ 0 & v_\mathrm{g} & \rho \\ \frac{\bar{\alpha}_0(\mathbf{u}) c_M^2(\mathbf{u})}{\rho} & \frac{c_M^2(\mathbf{u})}{\rho} & v_\mathrm{g} \end{bmatrix} \frac{\partial}{\partial x} \begin{bmatrix} \chi_\ell \\ \rho \\ v_\mathrm{g} \end{bmatrix} = \begin{bmatrix} 0 \\ 0 \\ \tilde{S} \end{bmatrix}, \tag{1.14}$$

where $\bar{\alpha}_0(\mathbf{u}), c_M(\mathbf{u}), \tilde{S}$ are rather complicated and implicitly given by (1.13). We see from (1.14) that the pseudo mass concentration χ_ℓ is a Riemann invariant

convecting to the right with velocity v_{g}. This is a representation of the slow void wave dynamics which dominate a low frequencies.

For high frequencies the mass rate influx can be assumed constant and the remaining pressure dynamics can be approximated with the one-dimensional wave equation with a mixture sound velocity, as is shown in the following. Assuming that the liquid and gas mass-rates on the left boundary are constant we have

$$\left[\alpha_\ell \rho_\ell v_\ell\right]_{x=0} = \left[\chi_\ell \rho v_{\mathrm{g}} - \rho_\ell (1-\alpha_\ell^*) v_\infty\right]_{x=0} = \text{const.} \tag{1.15}$$

$$\left[\alpha_{\mathrm{g}} \rho_{\mathrm{g}} v_{\mathrm{g}}\right]_{x=0} = \left[(1-\chi_\ell)\rho v_{\mathrm{g}}\right]_{x=0} = \text{const.} \tag{1.16}$$

Note that this implies that the quantity $\left[\chi_\ell \rho v_{\mathrm{g}}\right]_{x=0}$ is also constant. Thus, from (1.15)-(1.16): $\left[\rho v_{\mathrm{g}}\right]_{x=0} = \text{const.}$ meaning that $\chi_\ell(x,t) = \text{const.}$ for all x, t.

The remaining dynamics, after having enforced constant mass-rates, can now be expressed as a second-order PDE retaining only the lower right 2×2 part of the transport matrix in (1.14), i.e.:

$$\frac{\partial u_s}{\partial t} + A_s(u_s)\frac{\partial u_s}{\partial x} = S_s(u_s), \tag{1.17}$$

$$A_s = \begin{bmatrix} v_{\mathrm{g}} & \rho \\ \frac{c_M^2(\mathbf{u})}{\rho} & v_{\mathrm{g}} \end{bmatrix}, \quad u_s = \begin{bmatrix} \rho \\ v_{\mathrm{g}} \end{bmatrix}. \tag{1.18}$$

We recognize (1.17)–(1.18) as the system matrix from the 1-D shallow water equations, also known as the Saint Venant equation (Andréa-Novel et al., 2009). This 2×2 system has the eigenvectors and eigenvalues

$$\begin{bmatrix} l_{s1} \\ l_{s2} \end{bmatrix} = \begin{bmatrix} \frac{c_M(\mathbf{u})}{\rho} & 1 \\ -\frac{c_M(\mathbf{u})}{\rho} & 1 \end{bmatrix}, \quad \begin{bmatrix} \lambda_{s1} \\ \lambda_{s2} \end{bmatrix} = \begin{bmatrix} v_{\mathrm{g}} + c_M(\mathbf{u}) \\ v_{\mathrm{g}} - c_M(\mathbf{u}) \end{bmatrix}, \tag{1.19}$$

where $c_M(\mathbf{u})$ is an approximate mixture sound velocity. We typically have: $c_M(\mathbf{u}) \gg v_{\mathrm{g}}$, and using this approximation the subsystem (1.17)–(1.18) results in the classical one-dimensional wave equations used to describe the distributed pressure dynamics in one-phase wells and transmission lines (Stecki and Davis, 1986; Aarsnes et al., 2012; Landet et al., 2013).

Finally we note how using a flow rate as a boundary condition at $x = L$ introduces an additional slow compressional pressure mode. E.g. specifying flow out using a choke equation results in dynamics as shown in Fig. 1.11. If one intends to discard the fast pressure dynamics, this pressure mode can be kept by lumping the distributed pressure.

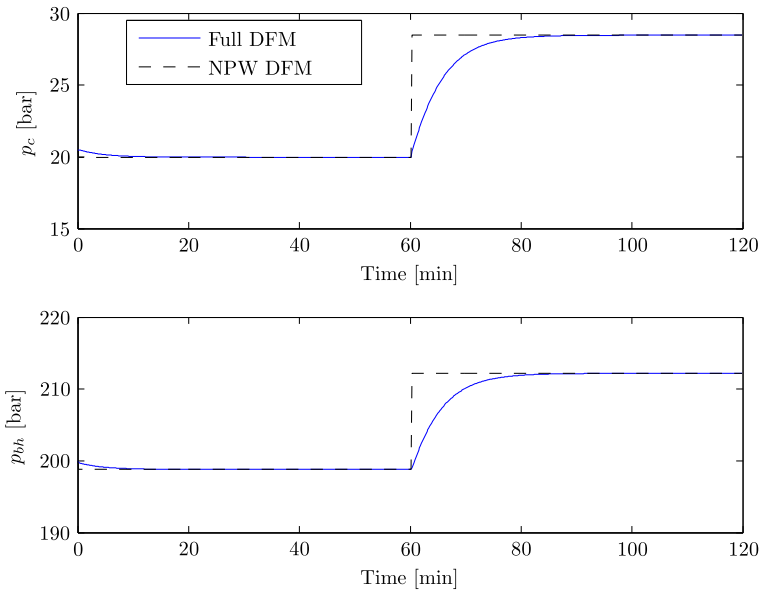

Figure 1.11.: Comparison between the DFM and the NPW DFM (referring to the DFM with discarded pressure dynamics) showing the slow pressure mode introduced by the choke equation, here in the response of choke and bottom-hole pressure (p_c, p_{bh}) with a step change in choke opening.

1.5.1. Time-scale heuristic summary

$\sim$ **10 seconds:** Distributed pressure dynamics. Behaves approximately as the wave equation used for one-phase flow, i.e.:

$$\frac{\partial P}{\partial t} + \beta \frac{\partial v}{\partial x} = 0 \tag{1.20}$$

$$\rho \frac{\partial v}{\partial t} + \frac{\partial P}{\partial x} = F(v) + G \tag{1.21}$$

with pressure, P, and velocity, v. The density ρ and bulk modulus β, and source terms F, G can change significantly at two-phase flow, however.

1−10 minutes: Slow compression pressure mode introduced by using flow as boundary conditions on both sides of (1.20)–(1.21). This mode can be modeled by lumping the distributed pressure into a single control volume with volume V:

$$\frac{\partial P(x{=}L)}{\partial t} = \frac{\beta}{V}\big(q(x{=}0) - q(x{=}L) + T_{E_G}\big), \tag{1.22}$$

where T_{E_G} accounts for in-domain gas expansion in the case of two-phase flow. The total bulk modulus β will change with the void fraction profile.

10 minutes to hours: Void wave advection

$$\frac{\partial \chi_\ell}{\partial t} + v_\mathrm{g} \frac{\partial \chi_\ell}{\partial x} = 0, \tag{1.23}$$

where the pseudo mass concentration χ_ℓ propagates with the gas velocity, thus determining hydrostatic pressure.

Understanding and recognizing this distinction enables us to retain and deal with only the dynamics in the frequency range of interest. Consider the following illustrative examples:

- When controlling downhole pressure in the heave problem, see Aarsnes et al. (2014c), the fast distributed pressure dynamics, (1.20)–(1.21), must be retained and used in controller design (Aamo, 2013; Landet et al., 2013).
- When controlling gas kicks, see Aarsnes et al. (2016a), we retain only the slow pressure mode (1.22) as it is the dominating dynamic around the desired cross-over frequency. Due to the difficulty in modeling the fast pressure waves in a (continuously changing) two-phase mixture (Flåtten and Lund, 2011) pushing the closed-loop control to a higher frequency range is not to be recommended. The controller still has to be made robust to these uncertain high-frequency dynamics.
- In production monitoring and optimization, time-scales are large and model based procedures are typically based on steady-state models. However, in some cases it is desirable to perform optimization on the time-scale of hours (Willersrud et al., 2015b) where dynamics have to be represented, in which case it should be sufficient to employ a dynamics model of only the void wave advection (1.23). This equation could then be coupled to the existing steady-state models to obtain pressure gradients.

1.6. Outline and contribution

The following five chapters of the thesis describe the development and application of fit-for-purpose models of gas-liquid dynamics in a well. The chapters are reprints of published and submitted papers with minor changes to improve the readability of the thesis.

- **Chapter 2** reviews the existing literature on one-dimensional two-phase models, and motivates the development of an appropriate fit-for-purpose model. It is showed how relaxation techniques are used to derive simplified models by imposing instantaneous steady-state between phases, or by lumping distributed dynamics. Depending on the phenomenon to be represented, these

relaxation techniques can be employed to obtain a simplified model by discarding dynamics not needed. The reduced DFM is found to qualitatively recreate the dynamics for many important scenarios.

The chapter is based on Aarsnes et al. (2016d).

- **Chapter 3** concerns describing the dynamics encountered in a gas-dominant UBD well. Four distinct operating regimes are identified and located in terms of drawdown, and the behavior in each of them is described. Understanding the qualitative changes in dynamics between these regimes can improve operations and well design. A major contribution of this chapter is that a particular kind of severe slugging is investigated that have previously not received significant interest in the literature. Furthermore, a potential novel application of automated choke control by feedback is pointed out which can enable drilling at low drawdown by stabilizing the nominally unstable regime.

  The chapter is based on Aarsnes et al. (2016c)

- **Chapter 4** concerns the development of a simplified two-phase flow model by building on previous results on simplifying the drift flux model by using a quasi-steady momentum balance (i.e. a reduced DFM). This simplification results in a hyperbolic-parabolic PDE system with a single finite eigenvalue. In somewhat simplified terms, one can say that the single hyperbolic PDE represents the void wave advection, with the two parabolic relations giving the pressure and velocity profiles. Finding appropriate approximations for the pressure and velocity, explicit in the state (void fraction) and exogenous variables, a novel formulation for a fast and robust fit-for-purpose model is obtained.

  The chapter is based on Aarsnes et al. (2016b).

- **Chapter 5** includes testing of this model against full scale experimental data. To illustrate the use of the model, a RLS estimator that can be used to estimate reservoir pressure and track the gas propagation is developed and tested against OLGA and field data from a dynamically controlled kick incident.

  The chapter is based on Ambrus et al. (2015); Aarsnes et al. (2015); Ambrus et al. (2016).

- **Chapter 6** describes the development of a robust pressure controller using an automatic back-pressure choke. The approach uses the previously developed understanding of the time-scale heuristic to show that the dynamics in the frequency range of interest is dominated by a single slow pressure mode. This pressure mode represents the lumped compression of the fluid mixture, and as such is dependent on the void fraction distribution. By measuring or estimating the characteristic time associated with this mode and encoding the

information into an automatic controller, performance can be significantly improved. Robustness towards the discarded high-frequency pressure dynamics is ensured using an LMI formulation. The presented approach, of explicitly capturing the effect of the gas influx and incorporate this in a model-based controller design, is a first for this problem.

The chapter is based on Aarsnes et al. (2016a).

1.6.1. Publications

First-Author papers

The contributions of the candidate have been published in the following journal papers and conference papers with peer review:

Journal papers

- U. J. F. Aarsnes, M. S. Gleditsch, O. M. Aamo, and A. Pavlov, "Modeling and Avoidance of Heave-Induced Resonances in Offshore Drilling," *SPE Drill. Complet.*, vol. 29, no. 04, pp. 454-464, Dec. 2014.
- U. J. F. Aarsnes, F. Di Meglio, R. Graham, and O. M. Aamo, "A methodology for classifying operating regimes in underbalanced drilling operations," *SPE J.*, SPE Journal, 21(02), pp. 243433, Apr. 2016.
- U. J. F. Aarsnes and O. M. Aamo, "Linear stability analysis of self-excited vibrations in drilling using an infinite dimensional model," *J. Sound Vib.*, vol. 360, pp. 239259, Jan. 2016.
- U. J. F. Aarsnes, T. Flåtten, and O. M. Aamo, "Models of gas-liquid two-phase flow in drilling for control and estimation applications," In review.
- U. J. F. Aarsnes, A. Ambrus, F. Di Meglio, A. K. Vajargah, O. M. Aamo, and E. Van Oort, "A Simplified Two-Phase Flow Model Using a Quasi-Equilibrium Momentum Balance," *Int. J. Multiph. flow*, 83(July), pp. 77-85, Jul. 2016.
- U. J. F. Aarsnes, B. Açıkmeşe, A. Ambrus and O. M. Aamo, "Robust Controller Design for Automated Kick Handling in Managed Pressure Drilling," In review.

Conference papers

- U. J. F. Aarsnes, O. M. Aamo, and A. Pavlov, "Quantifying Error Introduced by Finite Order Discretization of a Hydraulic Well Model," in *Australian Control Conference*, 2012, pp. 54–59.

- U. J. F. Aarsnes, O. M. Aamo, E. Hauge, and A. Pavlov, "Limits of Controller Performance in the Heave Disturbance Attenuation Problem," in *European Control Conference (ECC)*, 2013, pp. 1070–1076.
- U. J. F. Aarsnes, F. Di Meglio, S. Evje, and O. M. Aamo, "Control-Oriented Drift-Flux Modeling of Single and Two-Phase Flow for Drilling," in *ASME Dynamic Systems and Control Conference*, 2014.

Co-Author papers

In addition, the candidate has contributed as co-author to the following journal papers and conference papers with peer review.

Journal papers

- A. Nikoofard, U. J. F. Aarsnes, T. A. Johansen, and G.O. Kaasa, "State and Parameter Estimation of a Drift-Flux Model for Under Balanced Drilling Operations". In review.
- A. Ambrus, U. J. F. Aarsnes, A. Karimi, B. Akbari, E. van Oort and O. M. Aamo, "Real-Time Estimation of Reservoir Influx Rate and Pore Pressure Using a Simplified Transient Two-Phase Flow Model," *J. Nat. Gas Sci. Eng.*, to appear.

Conference papers

- F. Di Meglio and U. J. F. Aarsnes, "A distributed parameter systems view of control problems in drilling," in *2nd IFAC Workshop on Automatic Control in Offshore Oil and Gas Production*, 2015.
- F. Di Meglio, D. Bresch-Pietri, and U. J. F. Aarsnes, "An Adaptive Observer for Hyperbolic Systems with Application to UnderBalanced Drilling," in *IFAC World Congress 2014*, South Africa, 2014, pp. 11391–11397.
- A. Nikoofard, U. J. F. Aarsnes, T. A. Johansen, and G.-O. Kaasa, "Estimation of States and Parameters of a Drift-Flux Model with Unscented Kalman Filter," in *2nd IFAC Workshop on Automatic Control in Offshore Oil and Gas Production*, 2015.

Publications without peer review

The following papers have been published without peer review:

- U. J. F. Aarsnes, F. Di Meglio, O. M. Aamo, and G.-O. Kaasa, "Fit-for-Purpose Modeling for Automation of Underbalanced Drilling Operations," in *SPE/IADC Managed Pressure Drilling & Underbalanced Operations Conference & Exhibition*, 2014.

- U. J. F. Aarsnes, H. Mahdianfar, O. M. Aamo and A. Pavlov. " Rejection of Heave-Induced Pressure Oscillations in Managed Pressure Drilling," presented at the *Colloquium on Nonlinear Dynamics and Control of Deep Drilling Systems*, Minneapolis, Minnesota, May 2014. (Invited Paper).

- U. J. F. Aarsnes, A. Ambrus, A. Karimi Vajargah, O. M. Aamo, and E. van Oort, "A simplified gas-liquid flow model for kick mitigation and control during drilling operations," in *Proceedings of the ASME 2015 Dynamic Systems and Control Conference*, 2015.

- A. Ambrus, U. J. F. Aarsnes, A. Karimi Vajargah, B. Akbari and E. van Oort, "A Simplified Transient Multi-Phase Model for Automated Well Control Applications," in *9th International Petroleum Conf. (IPTC)*, 2015.

Chapter 2

Models of gas-liquid two-phase flow in drilling for control and estimation applications

This chapter is based on the work presented in Aarsnes et al. (2016d).

Summary

Most model-based control and estimation techniques put limitations on the structure and complexity of the models to which they are applied. This has motivated the development of simplified models of gas-liquid two-phase flow in drilling for control and estimation applications. This paper reviews the literature for such models. The models are categorized in terms of complexity and the physical interpretation of the simplifications employed. A simulation study is used to evaluate their ability to qualitatively represent dynamics of 3 different gas-liquid scenarios encountered in drilling, based on which conclusions are drawn.

2.1. Introduction

Drilling for hydrocarbons is the process of creating a wellbore, sometimes extending several thousand meters into the ground, until it reaches an oil or gas reservoir (Fig. 2.1). There is a multitude of risks and challenges associated with this process, particularly in regards to controlling the distributed pressure in the well within the constraints imposed by the operation.

Dealing with these challenges has entailed an increasing drive for automation in many aspects of drilling (Thorogood et al., 2010; Godhavn, 2011). Simultaneously, a goal of improved drilling efficiency is pursued through reducing Non-Productive Time, optimizing operations, and detecting and avoiding incidents before adverse consequences occur (Cayeux et al., 2013). The trend for drilling deeper and more complex wells (Lukawski et al., 2014) is also a driver for automation as an enabling technology, allowing for continued exploration of difficult and mature reservoirs.

Following the demand of the drilling industry, high fidelity simulators of the drilling process have been developed. Applications of these include training of drilling personnel and real time decision support (Petersen et al., 2008; Rommetveit

Notation

c	Sound speed
$m = \alpha_\ell \rho_\ell$	Liquid mass
$n = \alpha_\mathrm{g} \rho_\mathrm{g}$	Gas mass
q	Volumetric flow-rate
t	Time, independent variable
v	Velocity
v_∞	Slip relation drift velocity
w	Mass flow-rate
x	Position, independent variable
C_0	Slip relation profile parameter
F	Frictional pressure loss
G	Gravitational pressure loss
P	Pressure
T	Temperature
V	Volume
α	Volume fraction
β	Bulk modulus
γ	Adiabatic index
ρ	Density
μ	Chemical potential
$\mathcal{J}, \mathcal{K}, \mathcal{M}, \mathcal{H}$	Relaxation coefficients

Subscripts

a	Lumped annulus parameter
c	At or exiting through the choke
d	Lumped drill string parameter
i	Interface
M	Mixture
ℓ	Liquid phase
g	Gas phase
bit	Entering the annulus from the drill string
inj	Injected into the drill string
res	Entering the annulus from the reservoir

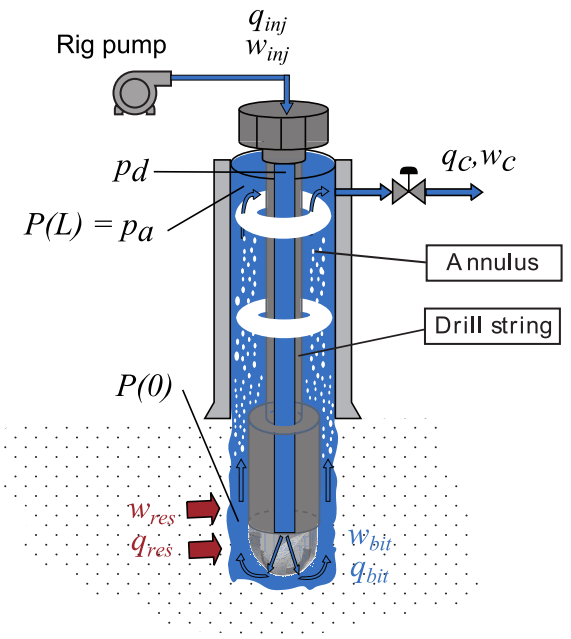

Figure 2.1.: Schematic of the system under consideration.

et al., 2004). At the same time, automated control systems for controlling various aspects of the drilling process have been developed and are gradually being accepted by the industry (Santos et al., 2007).

Modern approaches to process monitoring, optimization and control promise to enhance robustness and performance of such automation through the merger of process knowledge encoded in mathematical models with real-time measurements from the process. By intelligently combining predictions from the mathematical model with information from multiple sensors one can estimate unmeasured quantities, optimize automatic control procedures, predict future behavior, and plan countermeasures for unwanted incidents. Such design techniques, often referred to as model based estimation and control (Åström and Murray, 2010; Anderson and Moore, 1990), require a mathematical model with the right balance between complexity and fidelity: i.e. the complexity must be limited to facilitate the use of established mathematical analysis and design techniques, while the qualitative response of the process is retained.

Models that strike the right balance between complexity and fidelity are sometimes referred to as fit-for-purpose models, and have been employed in control (Stamnes et al., 2011a) and monitoring (Willersrud, 2015) of drilling processes in one-phase flow regimes. Obtaining such simplified models becomes significantly more difficult for gas-liquid two-phase dynamics due to the significant complexity and distributed nature of multiphase pipe flow (Aarsnes et al., 2014b, 2016c).

Table 2.1.: The three components of a complete simulation model

Mathematical Structure	**Closure Relations**	**Numerical Scheme**
PDE or ODE	Slip law	Numerical accuracy
Hyperbolic or Parabolic	Equation of State	Numerical robustness
Number of equations	Frictional pressure loss	Complexity
Stiffness	Other source terms	Solution speed

This makes the reduction to fit-for-purpose models for scenarios such as gas kick incidents, and underbalanced operations, challenging.

Consequently, several different approaches have been suggested in the literature, ranging from using complicated high-order numerical schemes with advanced multiphase-flow models to simplified low-order or black-box step response representations. The present paper presents a review of these models used for designing control and estimation/monitoring algorithms of gas-liquid two-phase dynamics encountered in drilling. The survey will focus on the models used and not the methods in themselves.

2.1.1. Components of a simulation model

To structure the following discussion, it is useful to identify the distinct components which make up a complete simulation model. The three components are *Mathematical structure*, *Closure Relations* and the *Numerical Scheme* and they are summarized in Table 2.1.

The complexity of a model is mainly determined by its mathematical structure. This is the type and number of dynamical equations needed to describe the model. Determining the mathematical structure of the model also determines, cially in our case, the mathematical tools and the model based estimation and control algorithms which can be employed with it.

The *closure relations* that are used will necessarily depend on the mathematical structure of the model. When a model is simplified, the closure relations will often also have to be modified to accommodate for the simplification, typically in such a way as to retain the steady state profile. Closure relations can also be chosen and *tuned* based on experiments or measurements, and consequently, given a mathematical structure, the accuracy of the model will mostly be determined by the value and form of the closure relations chosen.

The final component to a simulation model is the *numerical scheme*. This is the way the mathematical equations are approximated in order for them to be solved numerically. The solution procedures that can be utilized have varying degrees of accuracy and solution speeds. Crucially for our purposes are the numerical stability, robustness and implementation complexity of the numerical scheme chosen.

2.1.2. A coarse classification and outline

To structure the paper we split the models found in the literature into the three broad categories according to their overarching mathematical structure.

High fidelity models:

This category encompasses models which are designed to be highly accurate and have a high degree of predictive power over a wide range of application scenarios. They are often used for training, analysis and planning of operations and are not created for the application to a specific scenario or use with mathematical algorithms. They are thus not fit-for-purpose models.

Drift Flux Models (DFM):

We use this category to denote a set of distributed (i.e. PDE) models which are very popular in the literature due to their reasonable accuracy and relative simplicity compared to the high fidelity models. They are essentially simplifications of these models in that they require significantly fewer equations and they can be rigorously derived from the high fidelity models through the process of relaxation of dynamics explained in Section 2.2.1. The DFMs have reduced predictive power compared to high fidelity models, but high accuracy can be retained through selection of closure relations adapted to the considered scenario. Estimation and control results do exist for these models, although their distributed nature often makes these results non-standard and limited to specialists.

Simplified ODE models:

This category refers to models which can be represented with low-order ODEs. This means that the models are unable to represent the full richness of dynamics inherent in distributed models, and consequently they are highly specialized with a limited range of operation. Their simplicity, however, makes them very well suited for the design of algorithms, often allowing for the use of highly effective and well established design procedures.

Outline

This paper will consider each of these categories, review their basic mathematical structure and their uses in control and estimation applications. Then, in section 2.5 a brief review of numerical schemes is presented. Finally, in Section 2.6, a simulation study is performed to evaluate the ability of the models to qualitatively capture the dynamics of drilling scenarios involving gas-liquid flow.

2.1.3. Note on the equations

The equations given in this paper to represent the models are not exhaustive, but are meant to give a general idea of the model properties and structure. The reader is referred to the specific original literature for the full, rigorous, model representations.

2.2. High fidelity models

In one space dimension, the PDE formulation of dynamic distributed models may be written in a highly general form

$$\frac{\partial \mathbf{U}}{\partial t} + \mathbf{A}(\mathbf{U}, x, t)\frac{\partial \mathbf{U}}{\partial x} = \mathbf{D}(\mathbf{U}, x, t)\frac{\partial^2 \mathbf{U}}{\partial x^2} + \mathbf{Q}(\mathbf{U}, x, t). \tag{2.1}$$

Herein, each term affects the *mathematical structure* of the model in its own unique way. In particular:

- $\boldsymbol{U}(x, t)$ represents the vector of unknowns, i.e. the independent variables needed to represent the physical state at each point in space and time. The dimension of the vector $\boldsymbol{U}$ depends on the level of detail and complexity we want represented in the model. As the dynamical equations represent transport of conserved quantities in physical space, the components of $\boldsymbol{U}$ would typically represent density, momentum and energy. Through variable transformations, the equations could also be expressed in terms of more directly observable physical quantities such as temperature or pressure (Fjelde and Karlsen, 2002).

- $\boldsymbol{A}$ encodes information that propagates with a finite speed across the computational domain, and represents transport effects such as convection or momentum transfer through pressure. The fundamental underlying physical structure of the model is encoded here. Furthermore, this term has a dominating effect on the the velocity of the high-frequency waves in the system (Solem et al., 2015).

- $\boldsymbol{D}$ represents irreversible diffusive effects in the flow direction, such as viscosity, or heat or mass diffusion. Loss of information due to upscaling may be one mechanism behind terms in this form. If the symmetric part of $\boldsymbol{D}$ is positive definite, then $\boldsymbol{D}$ will have a stabilizing effect on the system, acting more strongly on higher frequencies.

  For the discretized equations used in practical simulations, this term is often small compared to the artificial numerical diffusion (Bruce Stewart and Wendroff, 1984).

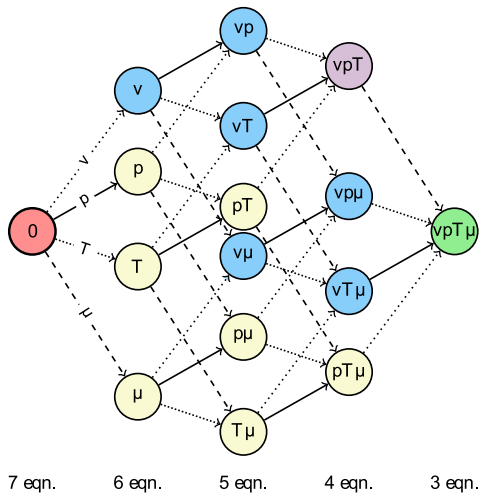

Figure 2.2.: The 4-dimensional hypercube representing the model hierarchy of two-fluid relaxation models. Each vertex represents a unique model in the hierarchy where the leftmost one is the seminal formulation of Baer and Nunziato (1986). The edges correspond to relaxation processes in the variables p (pressure), T (temperature), μ (chemical potential) and v (velocity). Models with a v relaxation are typically referred to as *Drift Flux Models*. Adapted from (Linga, 2015).

- $\boldsymbol{Q}$ represents source terms, i.e. exchanges between the state and the environment, or exchanges between separate state variables at each point. Interactions with the environment may include friction terms, gravity terms and heat transfer. Exchanges between state variables may include heat, volume, mass and momentum transfer.

  In the limit that $\boldsymbol{Q}$ acts infinitely fast, we obtain a *reduced model* where the information represented by $\boldsymbol{Q}$ is incorporated into the matrix $\boldsymbol{A}$ (Flåtten and Lund, 2011; Lund, 2012). This model reduction, termed *relaxation*, is illustrated in Figure 2.2 where the Baer-Nunziato model (Baer and Nunziato, 1986) is the starting point.

  This term has a dominating effect on the velocity of the longest wavelengths in the system (Solem et al., 2015).

2.2.1. The Baer-Nunziato model

The physical structure of a flow model is mainly determined from the description of how the physical variables are transported, and the process to approach full thermodynamic equilibrium.

Following the classical approach of Baer and Nunziato (1986), we may then write the foundation for one-dimensional two-phase flow modeling as a set of hyperbolic

partial differential equations in the following form (Linga, 2015):

- Volume advection:

$$\frac{\partial \alpha_{\mathrm{g}}}{\partial t} + v_p \frac{\partial \alpha_{\mathrm{g}}}{\partial x} = \mathcal{J}(P_{\mathrm{g}} - P_\ell), \tag{2.2}$$

- Mass conservation:

$$\frac{\partial}{\partial t}\left(\rho_{\mathrm{g}}\alpha_{\mathrm{g}}\right) + \frac{\partial}{\partial x}\left(\rho_{\mathrm{g}}\alpha_{\mathrm{g}}v_{\mathrm{g}}\right) = \mathcal{K}(\mu_\ell - \mu_{\mathrm{g}}), \tag{2.3}$$

$$\frac{\partial}{\partial t}\left(\rho_\ell\alpha_\ell\right) + \frac{\partial}{\partial x}\left(\rho_\ell\alpha_\ell v_\ell\right) = \mathcal{K}(\mu_{\mathrm{g}} - \mu_\ell), \tag{2.4}$$

- Momentum balance:

$$\frac{\partial}{\partial t}\left(\rho_{\mathrm{g}}\alpha_{\mathrm{g}}v_{\mathrm{g}}\right) + \frac{\partial}{\partial x}\left(\rho_{\mathrm{g}}\alpha_{\mathrm{g}}v_{\mathrm{g}}^2 + \alpha_{\mathrm{g}}P_{\mathrm{g}}\right) - p_{\mathrm{i}}\frac{\partial \alpha_{\mathrm{g}}}{\partial x} = v_{\mathrm{i}}\mathcal{K}(\mu_\ell - \mu_{\mathrm{g}}) + \mathcal{M}(v_\ell - v_{\mathrm{g}}), \tag{2.5}$$

$$\frac{\partial}{\partial t}\left(\rho_\ell\alpha_\ell v_\ell\right) + \frac{\partial}{\partial x}\left(\rho_\ell\alpha_\ell v_\ell^2 + \alpha_\ell P_\ell\right) + p_{\mathrm{i}}\frac{\partial \alpha_{\mathrm{g}}}{\partial x} = v_{\mathrm{i}}\mathcal{K}(\mu_{\mathrm{g}} - \mu_\ell) + \mathcal{M}(v_{\mathrm{g}} - v_\ell), \tag{2.6}$$

- Energy balance:

$$\frac{\partial E_{\mathrm{g}}}{\partial t} + \frac{\partial}{\partial x}\left(E_{\mathrm{g}}v_{\mathrm{g}} + \alpha_{\mathrm{g}}P_{\mathrm{g}}v_{\mathrm{g}}\right) - p_{\mathrm{i}}v_p\frac{\partial \alpha_{\mathrm{g}}}{\partial x} = -p_{\mathrm{i}}\mathcal{J}(P_\ell - P_{\mathrm{g}}) + \left(\mu_{\mathrm{i}} + \frac{1}{2}v_{\mathrm{i}}^2\right)\mathcal{K}(\mu_\ell - \mu_{\mathrm{g}}) + v_p\mathcal{M}(v_\ell - v_{\mathrm{g}}) + \mathcal{H}(T_\ell - T_{\mathrm{g}}), \tag{2.7}$$

$$\frac{\partial E_\ell}{\partial t} + \frac{\partial}{\partial x}\left(E_\ell v_\ell + \alpha_\ell P_\ell v_\ell\right) + p_{\mathrm{i}}v_p\frac{\partial \alpha_{\mathrm{g}}}{\partial x} = -p_{\mathrm{i}}\mathcal{J}(P_{\mathrm{g}} - P_\ell) + \left(\mu_{\mathrm{i}} + \frac{1}{2}v_{\mathrm{i}}^2\right)\mathcal{K}(\mu_{\mathrm{g}} - \mu_\ell) + v_p\mathcal{M}(v_{\mathrm{g}} - v_\ell) + \mathcal{H}(T_{\mathrm{g}} - T_\ell). \tag{2.8}$$

Herein, the terms representing interactions with the environment and diffusive terms are not included. In the context of (2.1), the left-hand sides of (2.2)–(2.8) contribute to the $\partial_t \boldsymbol{U} + \boldsymbol{A}\partial_x \boldsymbol{U}$ terms and the right-hand sides contribute to the $\boldsymbol{Q}$ term.

Furthermore, α_k, ρ_k, v_k, P_k, μ_k and T_k represent, respectively, the volume fraction, density, velocity, pressure, chemical potential and temperature of each phase and the interface $k \in \{\mathrm{g}, \ell, \mathrm{i}\}$, and v_p the volume advection velocity. However, the model is equally valid regardless of whether g and ℓ represent gases, liquids or solids.

The relaxation coefficients $\mathcal{J}, \mathcal{K}, \mathcal{M}$ and $\mathcal{H}$ are all non-negative so as to induce

1. volume transfer towards the phase with the highest pressure,
2. mass transfer towards the phase with the lowest chemical potential,
3. momentum transfer towards the phase with the lowest velocity and
4. heat transfer towards the phase with the lowest temperature.

The model has been extended to three phases, herein care must be taken to ensure compliance with the second law of thermodynamics (Hérard, 2007).

This highly general model is unnecessarily complex for the drilling applications considered in this paper. Significant model reduction is desirable, and one main path of achieving this model reduction is the process of *relaxation*, where the dynamical equations representing non-equilibrium processes are replaced by static equilibrium assumptions. For the Baer-Nunziato model, such model reductions have been studied extensively in for instance (Flåtten and Lund, 2011; Linga, 2015; Lund, 2012).

In this respect, a important and relevant concept is the *subcharacteristic condition* (Chen et al., 1994; Solem et al., 2015). Simply put, it states that every reduction of the model through relaxation will reduce the velocity of information propagation in the system, sometimes to a very large degree (Flåtten and Lund, 2011; Lund, 2012). This effect must be considered when evaluating the validity of simplified models for control applications. Another main theme is the discarding of the energy equations, motivated by the assumption that temperature transients have no significant effect on the macroscopic flow dynamics on the time scale of interest. This fundamental simplification will be described in more detail below.

2.2.2. Discarding the energy equation

Fundamental thermodynamics dictates that density is a state function $\rho(P, T)$. In the context of the Baer-Nunziato model, the pressure dynamics is normally dominated by the mass equations and the temperature dynamics by the energy equations. In the limit $\mathcal{H} \to \infty$ of the Baer-Nunziato model, the energy equations may be replaced by one single energy equation describing the evolution of the common temperature $T = T_{\mathrm{g}} = T_{\ell}$.

Further, there are many situation of interest where a temperature distribution $T(x, t) = T(x)$ is known (to sufficient approximation) a priori. This can occur for instance when

1. The flow may be assumed to be always in thermal equilibrium with the environment.
2. The temperature boundary conditions do not change significantly over time, and the heat exchange with the environment is not sensitive to the flow transients.

3. The temperature is measured and can be treated as an exogenous variable.

If phase transitions are important for our application, the dynamics may easily be very sensitive to $T(x,t)$, Otherwise, in situations where any of 1.–3. are valid we may replace the energy PDE with the given approximate temperature distribution $T(x)$, and the density may now be obtained as

$$\rho(P,T) = \rho(P,T(x)) = \rho(P,x). \tag{2.9}$$

Herein, we remark that this simplification can at best be fully valid only for slow dynamics. The sound speed (giving the propagation velocity of pressure waves) is generally given as

$$c^2 = \left(\frac{\partial P}{\partial \rho}\right)_x. \tag{2.10}$$

However, from (2.9) we see that the corresponding value $\bar{c}$ in models with no energy equations will be more akin to

$$\bar{c}^2 = \left(\frac{\partial P}{\partial \rho}\right)_T, \tag{2.11}$$

and hence from fundamental thermodynamic stability

$$\bar{c} \leq c. \tag{2.12}$$

Hence, we may expect that reducing the model through discarding the energy equation will tend to *under-predict* the velocity of pressure propagation.

2.2.3. Examples from literature

High fidelity models used for flow assurance and production design include the OLGA (Bendiksen et al., 1991) and LedaFlow (Danielson et al., 2011) commercial simulators. These are both 3-phase flow 1D models, imposing instantaneous pressure equilibrium in all phases. LedaFlow has the option of solving separate energy equations for each phase, and for both simulators the energy equations can be discarded as described in the previous section.

LedaFlow also incorporates additional mass equations to allow for the possibility of the phases being dispersed in each other.

Although not focusing on drilling applications, the commercial real-time multiphase flow simulator FlowManager$^{\text{TM}}$ Dynamic (Holmås and Løvli, 2011) is worthy of mention. This is a tool used for on-line surveillance and optimization of subsea oil and gas production. The underlying model consists of three mass conservation equations (oil, gas and water), one total momentum conservation equation and one total energy equation.

Other high-fidelity multiphase flow simulators for drilling include WeMod, developed by the International Research Institute of Stavanger (IRIS) based on a R&D

program started in the early 2000's in collaboration with Petrobras (Rommetveit and Lage, 2001), and a simulator due to Sintef Petroleum Research (Bjorkevoll et al., 2010; Petersen et al., 2008).

Due to their complexity, the application of high-fidelity models to model based control and estimator design is limited to the use with general, high order, numerical schemes. A promising application is the flow metering and estimation of states and parameters in production based on indirect measurements. This application is sometimes referred to as *soft sensing*, see e.g. (Gryzlov, 2011; de Kruif et al., 2008; Lorentzen et al., 2010). Herein, a popular approach is using so-called particle filters, where an ensemble of simulations are performed in parallel with the uncertain states and parameters perturbed. This ensemble is used to develop statistics of the uncertainties which can then be combined with measurements to produce estimates. This approach is still being refined with more sophisticated particle filters being applied to more complicated multiphase models (Luo et al., 2014; Lorentzen et al., 2014, 2015).

2.3. Drift-Flux Models (DFM)

Probably the most widely used model in the literature on two-phase flow in drilling is the 3-PDE drift-flux model

$$\frac{\partial}{\partial t}\left(\alpha_{\mathrm{g}}\rho_{\mathrm{g}}\right)+\frac{\partial}{\partial x}\left(\alpha_{\mathrm{g}}\rho_{\mathrm{g}}v_{\mathrm{g}}\right)=\Gamma \tag{2.13}$$

$$\frac{\partial}{\partial t}\left(\alpha_{\ell}\rho_{\ell}\right)+\frac{\partial}{\partial x}\left(\alpha_{\ell}\rho_{\ell}v_{\ell}\right)=-\Gamma \tag{2.14}$$

$$\frac{\partial}{\partial t}\left(\alpha_{\ell}\rho_{\ell}v_{\ell}+\alpha_{\mathrm{g}}\rho_{\mathrm{g}}v_{\mathrm{g}}\right)+\frac{\partial}{\partial x}\left(\alpha_{\ell}\rho_{\ell}v_{\ell}^{2}+\alpha_{\mathrm{g}}\rho_{\mathrm{g}}v_{\mathrm{g}}^{2}+P\right)=-F-G, \tag{2.15}$$

where the source terms are: the mass transfer term $\Gamma=\mathcal{K}\left(\mu_{\ell}-\mu_{\mathrm{g}}\right)$ often assumed zero, viscous pressure loss F and gravitational pressure loss $G=\rho_{M}g\sin\theta$.

This model is equivalent to the four eqn. *vpT* node in Fig. 2.2 with, additionally, the energy equation discarded. The two different fields for mass transport (2.13) and (2.14) are required since typically the two phases are represented by two or more different components[1]. This model may be obtained from the Baer-Nunziato system by discarding the energy equations and imposing velocity and pressure equilibrium. Herein, velocity equilibrium does not necessarily imply $v_{\mathrm{g}}=v_{\ell}$: Due to averaging and external interactions, it is stated in a more general form known as the *slip relation*:

$$v_{\mathrm{g}}-v_{\ell}=\Phi(\boldsymbol{U}), \tag{2.16}$$

i.e. the relative velocity between the phases is determined by the local full flow configuration.

The slip relation is one of three *closure relations* needed to complete the model.

[1]e.g. nitrogen and water are different components (Crowe et al., 2011).

2.3.1. Closure relations

When choosing closure relations for the DFM, two different approaches are taken in the literature. The more complicated approach, sometimes referred to as mechanistic models, predicts local flow regimes and then uses different correlations depending on the regime predicted, see e.g. Fjelde et al. (2003); Perez-Tellez et al. (2003). This typically entails solving implicit relations using an iterative numerical procedure.

The alternative approach is to use flow-pattern independent closure relations which allow for simpler solution procedure.

Slip relation

For the case of two-phase flow in inclined pipes, several flow pattern independent correlations have been suggested. Recent comparisons of such correlations can be found in (Bhagwat and Ghajar, 2014; Choi et al., 2012).

A simple correlation is the *Zuber-Findlay slip law* (Zuber and Findlay, 1965), which determines the relative velocity between the phases. Writing the mixture velocity as $v_M = \alpha_{\mathrm{g}} v_{\mathrm{g}} + \alpha_\ell v_\ell$ the classical formulation is:

$$v_{\mathrm{g}} = C_0 v_M + v_\infty, \tag{2.17}$$

where C_0 is called the profile parameter and v_∞ the drift velocity (Zuber and Findlay, 1965; Bhagwat and Ghajar, 2014). This is most naturally interpreted in the context of bubbly flows.

A mechanistic approach for finding correlations, which considers the annular geometry and upward flow encountered in drilling, was developed by Lage and Time (2000); Lage et al. (2000); Lage and Time (2002), which uses five different flow patterns: *bubble, slug, churn, annular* and *dispersed bubble*. This approach was further studied by Perez-Tellez (2003); Perez-Tellez et al. (2003) and employed on Iranian field data by Ashena and Moghadasi (2010).

Closure relations for counter-current flow were considered by Taitel and Barnea (1983); Hasan et al. (1994).

Viscous pressure loss

A frequently used structure for the relation of viscous pressure loss is

$$F = f \rho_M v_M |v_M|, \tag{2.18}$$

with f sometimes set as a constant friction coefficient dependent on viscosity and flow geometry, and other times given by the multiphase Reynolds number.

In mechanistic models (2.18) is used for bubble flow while other, modified, relations are used for other flow regimes (Lage and Time, 2002).

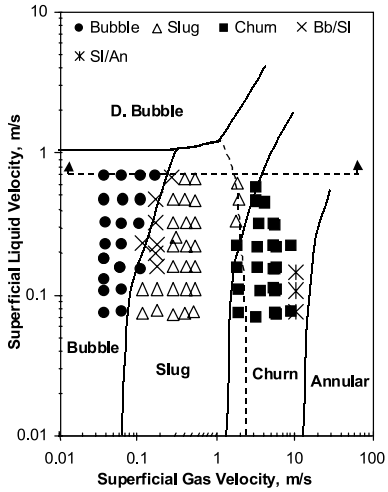

Figure 2.3.: Flow pattern map of upward air/water flow in an annulus, by Lage and Time (2002).

Equation of state

When the energy equation has been discarded, the *equation of state* is reduced to a relation between the principal variables and the pressure. Assuming the conserved quantities $n = \rho_{\mathrm{g}}\alpha_{\mathrm{g}}$ and $m = \alpha_\ell\rho_\ell$ to be our principal variables, the simplest relation available is obtained by using the ideal gas law and assuming incompressible liquid

$$P = \frac{nc_{\mathrm{g}}^2}{1 - \frac{m}{\rho_\ell}}, \tag{2.19}$$

where c_{g}, c_ℓ are the sound speed of the gas and liquid phase respectively. With a compressible liquid, but still using the ideal gas law, the relation becomes more involved. From (Evje and Fjelde, 2002; Aarsnes et al., 2014b):

$$\alpha_{\mathrm{g}} = \frac{1}{2} - \frac{\frac{c_{\mathrm{g}}^2}{c_\ell^2}n + m + \sqrt{\Delta}}{2\rho_{\ell,0}}, \tag{2.20a}$$

$$\Delta = \left(\rho_{\ell,0} - \frac{c_{\mathrm{g}}^2}{c_\ell^2}n + m\right)^2 + 4\frac{c_{\mathrm{g}}^2}{c_\ell^2}\rho_{\ell,0}, \tag{2.20b}$$

$$P = \begin{cases} \left(\frac{m}{1-\alpha_{\mathrm{g}}} - \rho_{\ell,0}\right)c_\ell^2, & \text{if } 1-\alpha_{\mathrm{g}} > \epsilon \\ \frac{n}{\alpha_{\mathrm{g}}}c_{\mathrm{g}}^2, & \text{otherwise.} \end{cases} \tag{2.20c}$$

2.3.2. Model range of operation

Some models have limited ranges of operation due to unboundedness introduced by simplifying assumptions: A model assuming incompressible liquid becomes invalid when gas disappears as the distributed pressure becomes undefined, see (2.19).

The slip relation can also limit the applicability of the model. By inspecting (2.17) we see that

$$C_0 < \frac{1}{\alpha_{\mathrm{g}}} \tag{2.21}$$

must be enforced. Representing the slip in annular flow regimes has proven to be challenging (Lage and Time, 2002), and it is often recommended to use a two-fluid model (i.e. a model without a relaxed momentum transfer) in such a case (Masella et al., 1998).

2.3.3. Application to estimation and control

Despite its relative complexity, the DFM has seen some use in state and parameter estimation.

The mechanistic model of Lage et al. (2000); Lorentzen et al. (2001) was used with an ensemble Kalman filter to tune coefficients in the slip law and frictional pressure loss by Lorentzen et al. (2003, 2001), and for estimating reservoir parameters by Vefring et al. (2003). Vefring et al. (2002) used a similar approach, but with a least squares fitting procedure in place of the ensemble Kalman filter.

A similar approach to reservoir characterization was implemented by Nygaard et al. (2007a), using an Unscented Kalman Filter (UKF). This was combined with a Nonlinear Model Predictive Control (NMPC) scheme to automatically control BHP during UBD connections.

Results on the simpler Drift Flux Model, without flow regime predictions, include using an Unscented Kalman Filter by (Nikoofard et al., 2015), and an extended Kalman filter by Bloemen et al. (2006) and Aarsnes et al. (2014a).

Finally, emerging results from the field of control and estimation of hyperbolic systems are starting to reach a degree of sophistication that enables working with (linearized versions of) the DFM directly (Di Meglio and Aarsnes, 2015). Di Meglio et al. (2014) designed an adaptive observer that could estimate the states and a boundary reflection coefficient of a so-called $n + 1$ hyperbolic system (n characteristics moving right and 1 moving left), of which the DFM, (2.13)–(2.15), is an instance (Di Meglio, 2011). The result was consequently applied to estimating the reservoir pressure in UBD. Di Meglio et al. (2013) derived a controller for the $n+1$ system, which was generalized to disturbance attenuation by Hasan (2014) and to $n+m$ systems by Hu et al. (2015). Ongoing work will introduce further extensions such as estimating multiple boundary parameters simultaneously and only using topside measurements (Anfinsen et al., 2016a,b).

2.3.4. Reduced Drift Flux model

In attempting to reduce the complexity of the two-phase flow models, a particular approach has been proposed where the distributed pressure dynamics are relaxed, thus neglecting the fast pressure waves (Di Meglio, 2011), while keeping the dynamics of the slow gas propagation.

This approach was used by Taitel et al. (1989) where the resulting model was described by a single transient PDE of the liquid continuity, obtained by assuming incompressible liquid, and a set of steady state relations. The closure relations are flow regime dependent, making the model mechanistic. The approach was expanded upon by Taitel and Barnea (1997), where the assumption of incompressible liquid was dropped, yielding two transient equations. A similar model was investigated by Masella et al. (1998), here called the No Pressure-Wave (NPW) model. In this particular incarnation, the resulting equations are (2.13)–(2.14) but in place of (2.15) the static relation

$$\frac{\partial P}{\partial x} = -F - G, \tag{2.22}$$

is used to relate the steady-state pressure drop to frictional and gravitational source terms.

Further, the DynaFloDrill (Rommetveit et al., 2005) simulator is based on this approach, solving for seven mass equations (for oil, water, gas, mud and cuttings plus dispersion fields) coupled to a static momentum balance.

A similar model is used by Choi et al. (2013), except that here the steady-state pressure drop is found from a fitted correlation given as

$$\frac{2}{\rho_\ell(\alpha_\ell v_\ell)^2}\frac{\partial P}{\partial x} = -\frac{2G}{\rho_\ell(\alpha_\ell v_\ell)^2} + A\left(\frac{\alpha_\ell \rho_\ell v_\ell}{\alpha_{\mathrm{g}}\rho_{\mathrm{g}} v_{\mathrm{g}}}\sqrt{\frac{\rho_{\mathrm{g}}}{\rho_\ell}}\right)^B, \tag{2.23}$$

where A and B are tuning coefficients.

A 1-equation PDE, coupled with an ODE, based on the Lagrangian formulation of (Gavrilyuk and Fabre, 1996) is used in (Aarsnes et al., 2015) to estimate reservoir parameters during a kick incident. An alternate version of this model is derived in (Ambrus et al., 2015), where the idea of (Taitel et al., 1989) is expanded upon to derive a PDE-ODE model on the form

$$\dot{p}_a = \frac{\beta_a}{V_a}\big(q_{inj} - q_c + q_{res} + A\int_0^L E_{\mathrm{g}}\mathrm{d}x\big), \tag{2.24}$$

$$E_{\mathrm{g}} = \frac{\alpha_{\mathrm{g}}(1 - C_0\alpha_{\mathrm{g}})\alpha_\ell}{\gamma}\frac{1}{P}\left(\frac{\partial P}{\partial t} + v_{\mathrm{g}}\frac{\partial P}{\partial x}\right). \tag{2.25}$$

$$\frac{\partial \alpha_{\mathrm{g}}}{\partial t} + v_{\mathrm{g}}\frac{\partial \alpha_{\mathrm{g}}}{\partial x} = E_{\mathrm{g}}, \tag{2.26}$$

The ODE, (2.24), represents the slow pressure mode of the annulus with the last term of (2.24), given by (2.25), accounting for the total gas expansion in the well.

In (2.25) γ is the adiabatic index. The gas propagation dynamics is given by (2.26). The pressure profile must then be given by a closure relation, and approaches such as (2.22) or (2.23) can be used.

2.4. Simplified ODE models

In this section we consider ODE-models which do not attempt to capture the distributed nature of the system through high order spatial discretizations, but lump the dynamics into one, or a few, control volumes.

2.4.1. One-phase model

A popular, simple, liquid only model of the drilling hydraulics from the literature is due to (Kaasa et al., 2012), and is given by

$$\dot{p}_a = \frac{\beta_a}{V_a}\big(q_{bit} + q_{res} - q_c\big), \tag{2.27}$$

$$\dot{p}_d = \frac{\beta_d}{V_d}\big(q_{inj} - q_{bit}\big), \tag{2.28}$$

$$\dot{q}_{bit} = \frac{1}{M}\big(p_{bd} - p_{ad}\big), \tag{2.29}$$

$$p_{bd} \equiv p_d + G_d - F_d(q_{bit}), \tag{2.30}$$

$$p_{ad} \equiv p_a + G_a + F_a(q_{bit}). \tag{2.31}$$

Here M represents the fluid inertance and gives the relaxation time of the pressure between the control volumes representing the annulus a and drill string d. For many applications, however, the volume of the drill-string can be assumed small which allows for the further approximation

$$\dot{p}_a = \frac{\beta_a}{V_a}\big(q_p + q_{res} - q_c\big). \tag{2.32}$$

This is equivalent to the pressure dynamics in the reduced DFM (2.24), i.e. when the gas dynamics have been discarded.

This formulation and variations thereof have, due to their simplicity, seen a wide range of applications as a dynamic model for both estimation (Stamnes et al., 2011a,b; Kaasa et al., 2011), fault detection (Willersrud et al., 2013, 2015b, 2014) and control (Godhavn, 2011; Asgharzadeh Shishavan et al., 2015). As mentioned, the model does not capture two-phase flow, but has still been applied to kick detection applications (Willersrud et al., 2015a; Zhou et al., 2011).

The effect of ignoring the spatially distributed dynamics for this model was studied in (Aarsnes et al., 2012), where it is noted that models of the same type (i.e. lumped models) with a higher order spatial discretizations can be obtained, as suggested in (Landet et al., 2012, 2013). The deciding factor for whether the distributed pressure dynamics are required is the frequency range for which the model

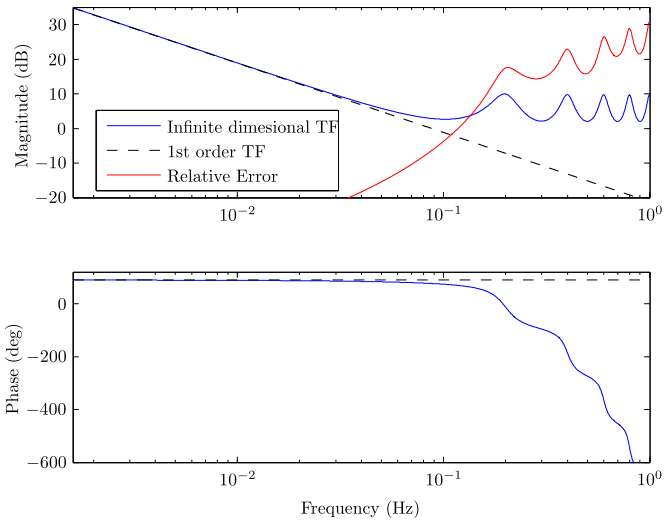

Figure 2.4.: Comparison of the transfer function of a distributed PDE model (i.e. the DFM (2.13)–(2.15) with liquid only) vs the first order approximation (2.32), with input q_c and p_{bh} (normalized amplitude). The effect would be similar when discarding the distributed pressure dynamics in the 2-phase case, i.e. comparing the DFM (2.13)–(2.15) with the reduced DFM (2.24)–(2.26).

is required to be valid. This can be observed in Fig. 2.4, which compares the transfer functions of a PDE representation of the pressure dynamics vs the 1st order ODE of (2.32). This comparison is also broadly valid for 2-phase flow, i.e. in the comparison between the full and the reduced DFM.

2.4.2. Lagrangian two-phase model

An interesting approach to representing the effect of gas-liquid flow of a single bubble in the annulus, while still retaining the simplicity of an ODE model, is the Lagrangian formulation proposed by Hauge et al. (2013b); Hauge (2013) (cf. Gavrilyuk and Fabre (1996); Aarsnes et al. (2015)). Here the dynamics are given through the states L_1, V_G representing the bubble position and size:

$$\dot{L}_1 = -\frac{2(q_c - q_{bit})}{A_p \alpha_{dist}} + v_{\mathrm{g}} \tag{2.33}$$

$$\dot{V}_G = q_c - q_{bit}. \tag{2.34}$$

where the first term in (2.33) accounts for the gas expansion with α_{dist} being a distribution parameter set to 0.21, and v_G found from a slip law. Equation (2.34) is obtained by assuming the liquid incompressible.

This model was shown to be adept at tracking a bubble's position and expansion in a kick scenario, and was used to estimate these values in the paper. However,

due to the Lagrangian formulation tracking a single bubble, it is unable to handle the continuous influx encountered in underbalanced operations.

2.4.3. Low order lumped two-phase models

A range of low order lumped models have seen success in modeling for control of severe slugging in two-phase production risers, such as Di Meglio et al. (2009); Eikrem et al. (2008); Esmaeil and Skogestad (2011); Storkaas et al. (2003).

Such models have been applied to UBD in the literature, in particular the model suggested by Nygaard and Nævdal (2005), which shares several features with the "slugging models". Using as states n, m representing total gas and liquid mass in the drill-string and annulus denoted by the subscripts a, d respectively, the model is given as:

$$\dot{n}_d = w_{\mathrm{g},inj} - w_{\mathrm{g},bit} \tag{2.35}$$
$$\dot{m}_d = w_{\ell,inj} - w_{\ell,bit} \tag{2.36}$$
$$\dot{n}_a = w_{\mathrm{g},bit} + w_{\mathrm{g},res} - w_{\mathrm{g},c} \tag{2.37}$$
$$\dot{m}_a = w_{\ell,bit} + w_{\ell,res} - w_{\ell,c} \tag{2.38}$$

where the mass rates $w_{\mathrm{g},bit}, w_{\ell,bit}$ are found through considering a pressure balance over the bit. The model lumps the spatial dynamics into a drill string (2.35)–(2.36) and an annular (2.37)–(2.38) control volume, but is unable to represent the gas distribution profile within the control volumes.

In (Nygaard and Nævdal, 2005) this model was used to tune a PI controller for use in a connection scenario during UBD, and a similar model with the drill string dynamics discarded (thus retaining only (2.37)–(2.38)) was applied to estimation in (Nikoofard et al., 2014a,b) and control in (Nikoofard et al., 2013).

ODE-models from identification techniques

Due to the high level of complexity encountered when deriving two-phase models from first principles, using black box or step response models are an attractive approach. The downside is that it might be difficult to identify and handle situations when the two-phase system exhibits changes in qualitative response, see Aarsnes et al. (2016c).

Model identification techniques were used to obtain 1st-order delay models for control of UBO using Model Predictive Control (MPC) by Pedersen and Godhavn (2013), with extensions in Pedersen et al. (2015). This is similar to the technique used in (Nygaard et al., 2007b) where a NMPC controller was designed based on identified time constants. Here it was concluded that this approach was significantly simpler to implement and analyze than the Nonlinear MPC controller of (Nygaard et al., 2007a), designed using the full DFM, and, furthermore, outperformed this controller in the scenario considered.

The approach of identifying time constants of the response was also taken by Carlsen et al. (2013) where the identification was used to design automatic controllers evaluated in a dynamic kick handling scenario.

2.5. Numerical Schemes

For control and estimation purposes, an essential feature of the simulation is the numerical procedure to solve the underlying equations. The choice of numerical scheme may influence the accuracy, stability and computational speed of the ultimate predictions.

Numerical methods in use typically build on established methods for classical computational fluid dynamics, and may be divided into two main lines:

- *Pressure-based methods.* These are typically variations of the SIMPLE[2] method (Patankar and Spalding, 1972), where the pressure is solved for as a primary variable. Herein, a staggered grid is typically used, where the pressure is resolved at the cell centers and velocities are resolved at the cell interfaces.

- *Density-based methods* (Roe, 1981). These methods typically guarantee mass conservation directly, and are commonly formulated on the simpler collocated grids. However, they are prone to introducing pressure oscillations for low Mach number flows (Guillard and Viozat, 1999).

Methods may be further classified into *explicit* (e.g. forward Euler time discretization) and *implicit* (e.g. backward Euler time discretization) schemes.

Explicit schemes are simpler to implement than implicit schemes, and their fast computation time per iteration facilitates using smaller time steps making them well suited for representing fast dynamics such as pressure waves. Explicit schemes, however, are typically bound[3] by the Courant-Friedrichs-Lewy (CFL) condition limiting time-steps according to:

$$|\lambda|\frac{\Delta t}{\Delta x} \leq 1, \tag{2.39}$$

where Δt is the time step, Δx is the grid cell size and λ is the velocity of the characteristic being resolved. This restriction is very limiting in the case of multiphase flow since Δt must be designed to allow for the worst-case value of λ which in most cases is the sound velocity of liquid $\sim$ 1000 m/s, much greater than the other transport phenomena of interest (Lorentzen and Fjelde, 2005).

Consequently, when computational efficiency is essential, implicit schemes are normally superior due to their potential for large time steps. An alternative is

[2]Semi-Implicit Method for Pressure Linked Equations

[3]There are exceptions known as explicit large time step schemes.

the semi-implicit schemes which resolve the slow characteristics, related to mass propagation, explicitly while the fast pressure characteristics are resolved implicitly.

Both the OLGA (Bendiksen et al., 1991) and LedaFlow (Danielson et al., 2011) numerical schemes are pressure-based and implicit. The FlowManager^{TM} scheme due to Evje and Flåtten (2006); Holmås and Løvli (2011) is essentially a density-based implicit method, incorporating some ideas from the classical pressure-based schemes. WeMod, developed by IRIS, uses a semi-implicit scheme with a slopelimiter technique which can be categorized as a finite element pressure-based method (Lorentzen and Fjelde, 2005).

Among the explicit schemes, the density-based AUMSV scheme (Evje and Fjelde, 2002) has proved useful for the drift-flux model (Udegbunam et al., 2014), as it provides an efficient combination of simplicity, accuracy and robustness. Consequently it is used in the Straume^{TM} Hydraulic Simulator developed by Kelda Drilling Controls (2015b).

2.6. Simulation Study

In this section we evaluate and compare the ability of the models covered in the preceding survey to qualitatively recreate the dynamics of three different gas-liquid flow scenarios encountered in drilling. The parameters are identical over the three scenarios except for the parameter changes indicated in Table 2.3.

2.6.1. Models used

In the simulations study, a total of 6 models are used for the kick scenario and 5 for the two UBD scenarios. These are summarized in Table 2.2. Here we use OLGA as reference to illustrate the dynamics that we would like to recreate with the simpler models.

At this point we again refer to Table 2.1 and note that we are only investigating the ability of the different mathematical structures represented to capture the qualitative transient behavior of the scenario. That is, we do not evaluate quantitative performance of the models, as this is mainly determined by which closure relations are used and these are beyond the scope of this paper.

2.6.2. **Scenario 1**: Dynamically handled gas kick

In this scenario, see Fig. 2.5 (a), a well is drilled using MPD at BHP = 260 bar when a high pressure zone of 270 bar is encountered. This causes a gas influx for the next 10 minutes, at which point the choke opening is decremented, increasing back-pressure and attenuating the kick. The gas is then circulated out.

Table 2.2.: Ability of models used in the simulation study to qualitatively represent dynamics in given scenario.

Model	Equations	Reference	Scenario Suitability		
			Scenario 1	Scenario 2	Scenario 3
High fidelity models:					
OLGA	-	(Bendiksen et al., 1991)	Reference model		
Drift flux models:					
Full DFM	(2.13)–(2.15)	(Lage et al., 2000)	Good	Good	Good*
Red DFM	(2.24)–(2.26)	(Ambrus et al., 2015)	Good†	Good	Good*
ODE models:					
LOL mod	(2.35)–(2.36)	(Nygaard and Nævdal, 2005)	Poor	Fair*	Fair*
1-ph mod	(2.32)	(Kaasa et al., 2012)	Poor	Poor	Poor
Lagrangian	(2.33)–(2.34)	(Hauge et al., 2013b)	Good	N/A	N/A

*Requires extra modifications to closure relations to fit specific scenario.
†Difficulty with shut-in and liquid back-flow.

Model performance

The drift flux models, Fig. 2.5 (a), are able to give a good qualitative representation of the kick incident. It is unclear, however, how to enable the reduced DFM to capture a shut-in incident with liquid back-flow. This can limit the applicability of this model in some instances.

The LOL model fails due to its inability to account for the gas position as it percolates through the well, see Fig. 2.5 (b). The Lagrangian model is able to amend this by using a state to track the position of the gas bubble. This model works well for single bubble dynamics, i.e. when the duration of the influx is limited, however, it stops working when the gas reaches the choke.

Finally, the 1-phase model does not include 2-phase dynamics and so only captures the changes in flow rate and choke opening. We note that this might still be enough for certain control applications, although one has to handle the large changes in the effective bulk modulus that occurs when gas enters the well.

2.6.3. **Scenario 2**: UBD connection

This scenario recreates the dominating dynamics of a connection in an underbalanced well by ramping down the liquid injection rate, keeping it at zero flow for 20 minutes, and then ramping it back up again, see Fig. 2.6 (a). This causes the gas in the well to start replacing the liquid causing lower bottom-hole pressure and

increased gas influx consequently resulting in an increase in the WHP.

Model performance

Again we conclude that the DFM show satisfactory performance, see Fig. 2.6 (a). The majority of the discrepancies that can be observed between the high-fidelity models and the DFMs are due to the large effect of differences in choke models resulting in varying WHPs.

Due to the inability of the lumped model to capture the gas distribution accurately, the hydrostatic pressure difference over the well had to be significantly modified, see Fig. 2.6 (b). A reasonable closure relation to deal with this issue can likely be developed with some effort. Given that this is fixed, however, the LOL model gives a reasonable representation of the response of the bottom-hole pressure, and consequently the increased gas influx and its corresponding increase in WHP.

2.6.4. **Scenario 3**: UBD operating envelope

This scenario is inspired by the fact that an underbalanced, gas producing, well exhibits very different dynamics when operating at different draw-downs, see (Aarsnes et al., 2016c). At two hour intervals the choke opening is decremented and the well allowed to reach steady-state. As the well nears the balance point, the WHP exhibits a characteristic inverse response, and then goes overbalanced toward the very end of the simulation, see Fig. 2.7 (a).

Model performance

In this scenario the DFMs give a largely correct representation of the behavior, and they are able to capture the qualitative effects of the different operating regimes (Aarsnes et al., 2016c), see Fig. 2.7 (a):

1. Intuitive regime
2. Non-intuitive regime
3. Unstable/slugging regimes close to the balance point.
4. Overbalanced regime.

There is a discrepancy, however, in regard to at which points the qualitative response of the models change. This is determined in large part by the closure relations, hence these should be tuned/adapted to the observed response or selected with care.

The lumped model is also able to represent the difference between the intuitive and non-intuitive response, but again the pressure drop over the well requires tuning to obtain this, see Fig. 2.7 (b).

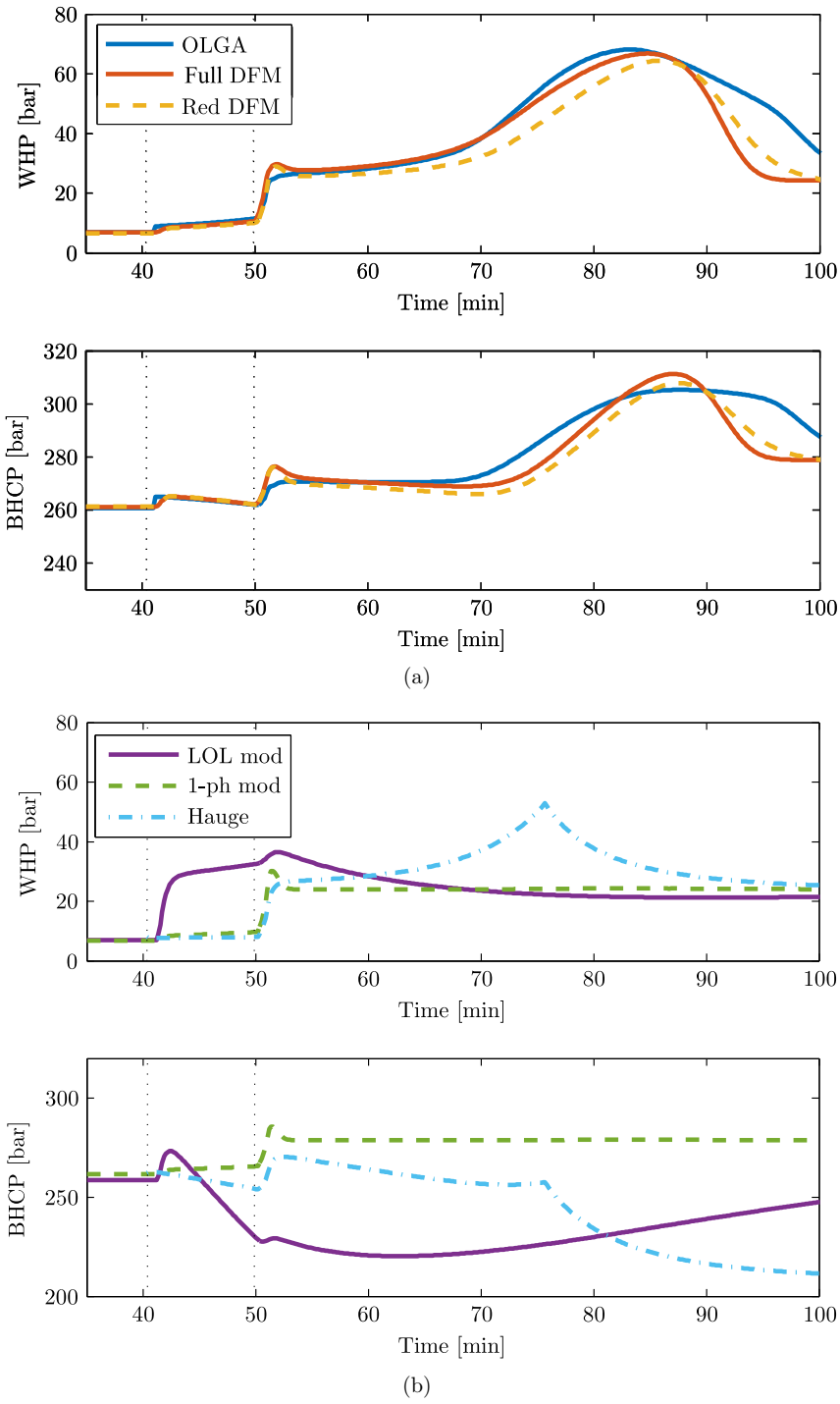

Figure 2.5.: Pressure trends for **Scenario 1**.

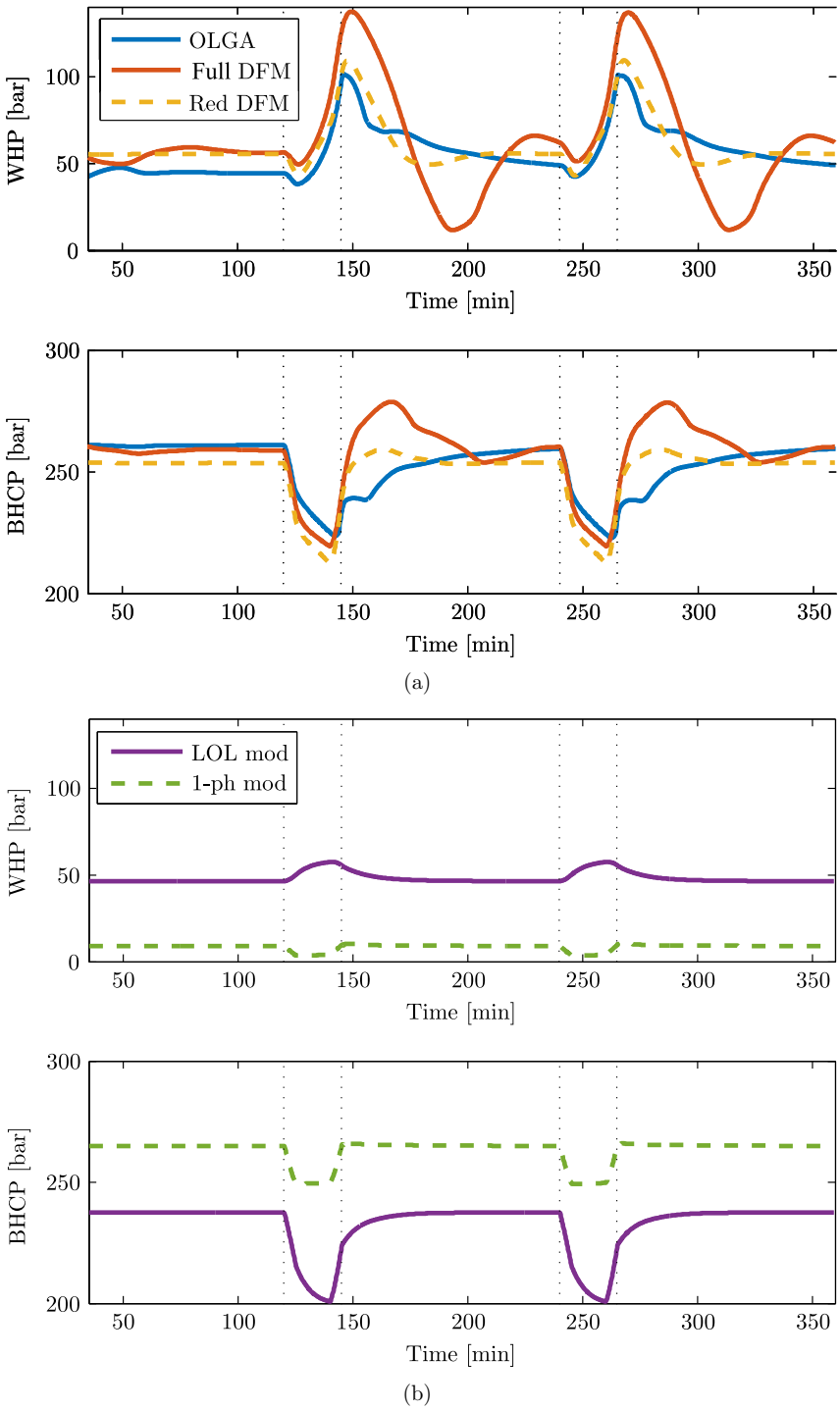

Figure 2.6.: Pressure trends for **Scenario 2**.

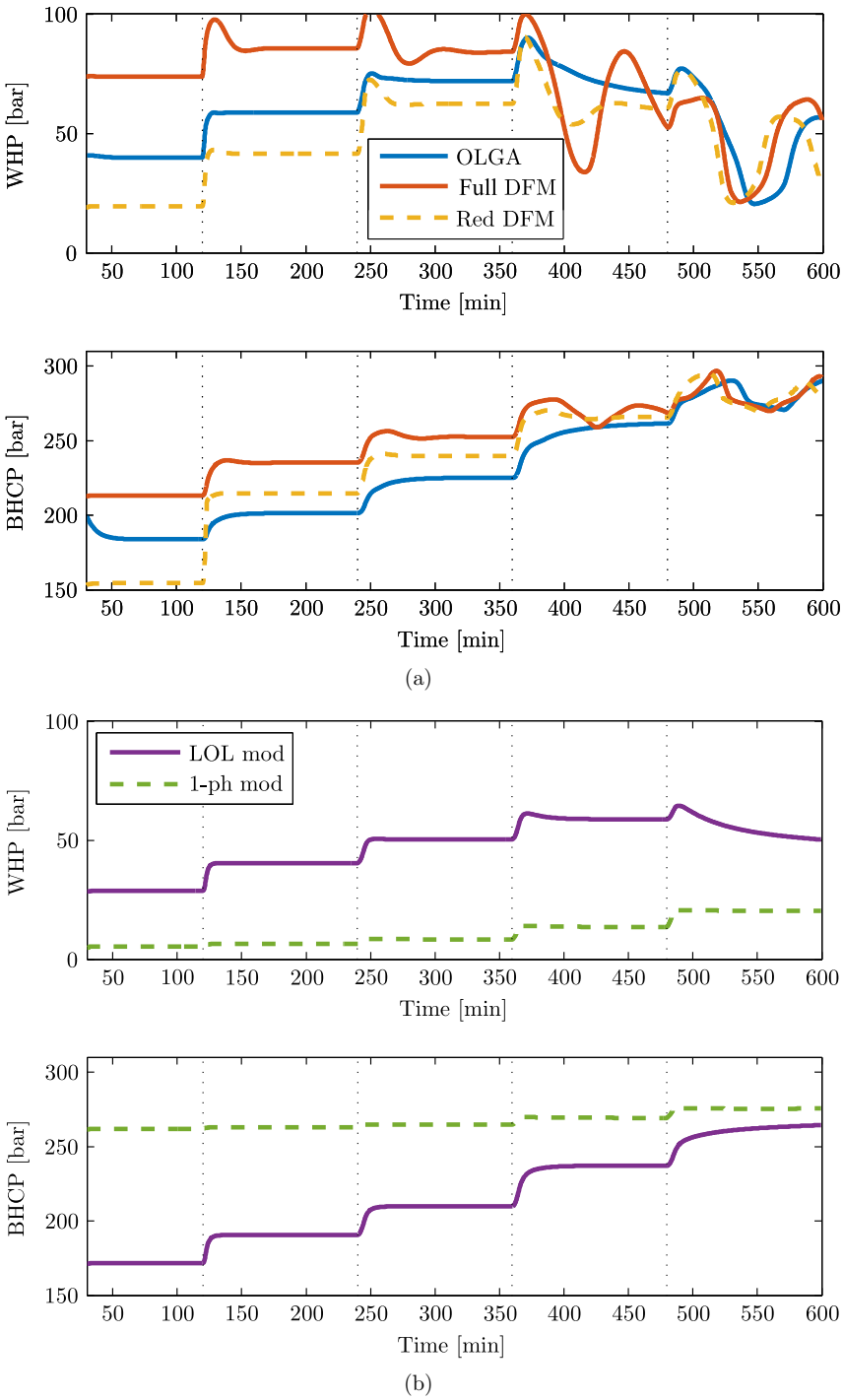

Figure 2.7.: Pressure trends for **Scenario 3**.

Table 2.3.: Simulation scenarios

Scenario 1: MPD gas kick

Time:	Reservoir pressure:	Choke-opening:
0 minutes	200 bar	$Z = 6\%$
40 minutes	270 bar	$Z = 6\%$
50 minutes	270 bar	$Z = 3\%$

Scenario 2: UBD connection

Time:	Rig pump:
0 minutes	$q_L = 0.133$ m^3/s
120 minutes	$q_L = 0$ m^3/s
140 minutes	$q_L = 0.133$ m^3/s
240 minutes	$q_L = 0$ m^3/s
260 minutes	$q_L = 0.133$ m^3/s

Scenario 3: UBD operating envelope

Time:	Choke opening:
0 minutes	$Z = 20\%$
120 minutes	$Z = 12\%$
240 minutes	$Z = 8\%$
360 minutes	$Z = 5\%$
480 minutes	$Z = 3.5\%$

2.7. Conclusion

This paper has considered the topic of obtaining models representing gas-liquid flow dynamics encountered in drilling for the purpose of model based estimation and control design. We have used the framework that a complete simulation model is made up of a *mathematical structure*, *closure relations* and a *numerical scheme*, and argued that while the qualitative behavior of the model to a large degree is determined by the mathematical structure, the quantitative accuracy is primarily given by the closure relations.

For model based controller and estimator design it is desirable to have simpler models than what is obtained from general first principle considerations. Significant simplifications necessarily entail removing equations, thus altering the mathematical structure. This can be interpreted physically as imposing instantaneous equilibrium of certain dynamics, which yields static relations in place of the dynamic equations removed.

Simplifications reviewed in this paper employed imposing equilibriums:

- Between two phases: interphasic relaxation.
- Between two or more spatial locations: lump dynamics.
- Overall: discard dynamics.

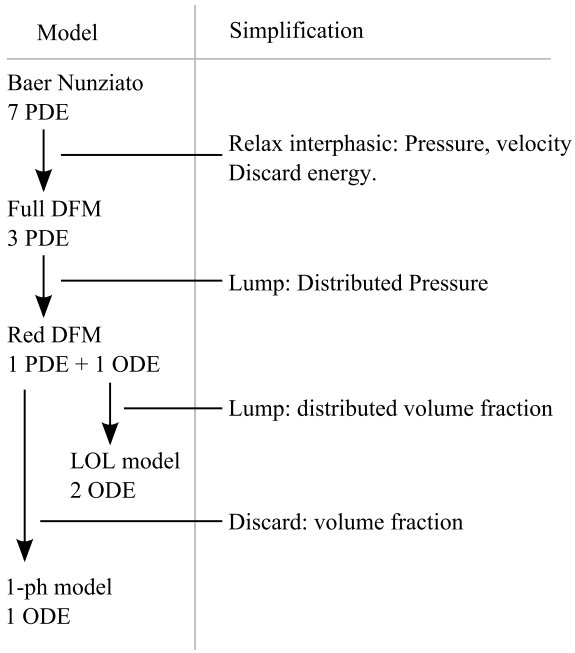

Figure 2.8.: Relation between the models considered in this paper.

Using these processes one can extend the hierarchy of relaxation models derived from the Baer-Nunziato model, shown in Fig. 2.2. Specifically, the models considered in this paper follow the simplification processes as shown in Fig. 2.8.

The literature survey combined with a simulation study that was performed indicates that quite significant simplifications can be undertaken without removing essential qualitative behavior required to represent two-phase drilling dynamics. The optimal blend between accuracy and simplicity for several applications seems to be somewhere in between the classical 3 PDE drift flux model, and the lumped ODE models. The reduced drift flux model that has seen renewed interest in recent years is consequently very promising.

The main challenges to be dealt with in future work are to adapt closure relations to simplified models and investigate how these can be effectively combined with estimation techniques. Dealing directly with PDEs for controller and estimator design in a robust manner also remains a challenge due to the complexity of most such proposed solutions.

Chapter 3

A methodology for classifying operating regimes in underbalanced drilling operations

This chapter is based on the work presented in Aarsnes et al. (2016c).

Summary

This paper proposes an extension to an existing operating envelope technique used for underbalanced drilling to enhance control of bottomhole pressure and inflow parameters. Using an implementation of the drift flux model with boundary conditions typically encountered in Underbalanced Operations (UBO), a steady-state analysis of the system is performed. Through this analysis, four distinct operating regimes are identified and the behavior in each of them is investigated through steady-state calculations and transient simulations. In particular, the analysis reveals that a section of the operating envelope previously believed to be unstable/transient is in fact stable/steady when a fixed choke opening is used as independent variable in place of a fixed well-head pressure. This results in the steady-state operating envelope being extended and gives an increased understanding of the well behavior encountered in UBO towards enabling the introduction of automated control. Finally we investigate the mechanism behind severe slugging in UBO and argue that the cause is different from that of the slugging encountered in production and multiphase transport.

3.1. Introduction

Recent years have seen an increasing degree of automation in Managed Pressure Drilling (MPD) (Thorogood et al., 2010). The pay-off has been increased safety as well as enabling the drilling of previously undrillable wells, due to tighter control of downhole pressure (Godhavn, 2010, 2011). It is natural to believe that we will see a similar development towards increased automation, in Underbalanced Operations (UBO).

Unfortunately, in the context of automated pressure and flow control, the dynamics of the two-phase flow encountered in UBO is significantly more complicated than

the single-phase flow of conventional drilling: In single-phase flow any operating point is inherently stable, transients are short and predictable and, barring certain well control incidents, operating conditions are reasonably homogeneous. By contrast, in two-phase UBO, the distributed gas–liquid flow and the reservoir–well interaction result in classical non-linear behavior (see Khalil (2002) for description of non-linear behavior of dynamics systems.) such as multiple steady-states, limit cycles and bifurcations as described by Aarsnes et al. (2014a,b); Mykytiw et al. (2003, 2004). Hence, to enable safe and robust algorithms for automated control to be developed for UBO, increased understanding of these phenomena, their potential occurrence in UBO and the behavior of the coupled well-reservoir dynamics are required.

3.1.1. Contribution

The main contribution of this paper is the classification of operating points in UBO. The associated analysis done to attain this classification also yields understanding of the behavior of the system.

More precisely, a comprehensive steady-state analysis of a Drift Flux model coupled with a reservoir is performed. The dynamics of this model replicates those which are encountered in underbalanced operations in gas dominant reservoirs. Investigating the steady states of a model also reveals a lot of the transient behavior.

To this end we present an extension to the operating envelope analysis technique presented by Graham and Culen (2004) and used by Mykytiw et al. (2004), which have properties that are particularly beneficial from a pressure control point of view compared to the conventional UBO operating envelope analysis technique, used in e.g. Saponja (1998); Guo and Ghalambor (2002).

This new technique, combined with analysis tools from dynamic systems theory, is used to investigate when the flow in the well is stable/steady and when it might become unstable. In particular it is shown that whether a well is hydrostatic or friction dominated (in the sense used by Saponja (1998)) is not the determining factor for flow stability in UBO. Instead a new classification of the UBO envelope is proposed where the part with stable flow can be identified as either an **intuitive regime** with short and well-behaved transient dynamics, or a **non-intuitive regime** with an inverted response in the Wellhead Pressure (WHP). In addition an **unstable regime** with no stable steady-states, an operating region with potential slugging, and finally conventional overbalanced drilling round out the classification to 5 distinct regimes.

3.1.2. Outline

In the next section some concepts from dynamic systems theory are introduced which will be helpful in the later discussion on the dynamics. Next, the Drift Flux Model at steady-state is described with the full model given in Appendix A. Using a short transient simulation case an alternative operating envelope analysis

technique is hypothesized and then proposed. This is then used to identify and classify 5 distinct operating regimes in UBO, when including severe slugging as a distinct regime (as the potential occurrence of severe slugging is not captured directly by this technique it is given its own treatment.) This is the main result of the paper. We end the paper with a conclusion section and some thoughts on the potential of automatic control in light of the preceding analysis.

3.2. Stable and unstable equilibria of dynamical systems

This section introduces some well-known concepts and results from the field of dynamic systems theory that will be useful in the following discussion. For a more comprehensive treatment the interested reader is referred to Khalil (2002).

Consider the autonomous system

$$\dot{x} = f(x), \tag{3.1}$$

where x is a vector of system states and $\dot{x}$ denotes the time derivative of these states such that the dynamics of the system are described by the function $f(x)$. A state $\bar{x}$ is an equilibrium of (3.1) if it satisfies $f(\bar{x}) = 0$. The following definition will be of importance.

Definition 3.1. *The equilibrium point $\bar{x}$ of* (3.1) *is*

- *stable if, for each $\epsilon > 0$, there is $\delta = \delta(\epsilon) > 0$ such that*

$$\|x(0) - \bar{x}\| < \delta \implies \|x(t) - \bar{x}\| < \epsilon, \quad \forall t \geq 0 \tag{3.2}$$

- *unstable if it is not stable*
- *asymptotically stable if it is stable and δ can be chosen such that*

$$\|x(0) - \bar{x}\| < \delta \implies \lim_{t \to \infty} x(t) = \bar{x} \tag{3.3}$$

The implication of this definition is that a system will diverge away from an *unstable* equilibrium, remain close to a *stable* equilibrium and converge to an *asymptotically stable* equilibrium. The following example is illustrative.

Example

Consider the pendulum system shown in Fig. 3.1. The pendulum equation can be derived using Newton's second law of motion and written as

$$\dot{\theta}_1 = \omega \tag{3.4}$$

$$\dot{\omega}_2 = -\frac{g}{l}\sin(\theta) - \frac{k}{m}\omega \tag{3.5}$$

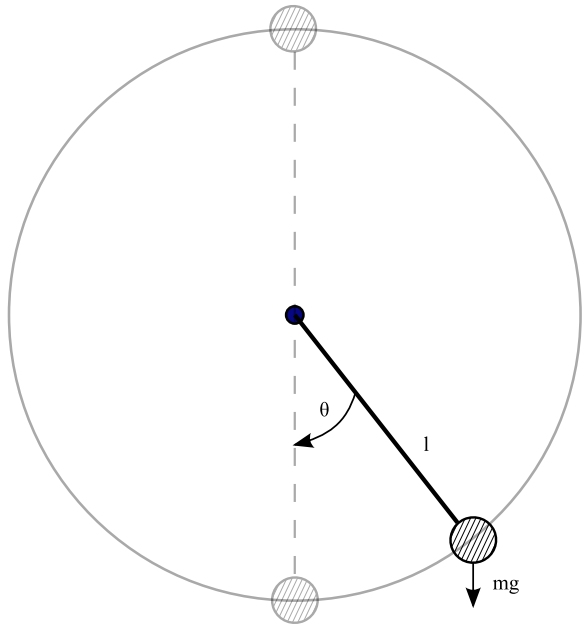

Figure 3.1.: Pendulum.

where θ, ω denote the angular position and velocity and k is the frictional coefficient. This system has two equilibrium points $\theta = 0,\ \omega = 0$ and $\theta = \pi,\ \omega = 0$. Starting in an equilibrium point, the system will remain stationary, i.e. at steady-state. However, for the second equilibrium point at $\theta = \pi$, all trajectories starting arbitrarily close will eventually diverge and leave the ball $\|x - \bar{x}\| \leq \epsilon$. This point clearly does not satisfy the $\epsilon - \delta$ requirement for stability and is hence an unstable equilibrium point. Unstable points are not uninteresting, however, since they can be rendered stable by feedback control and yield insight into the behavior of the system. The equilibrium at $\theta = 0$ is asymptotically *stable as nearby trajectories will not only remain close, thus satisfying the $\epsilon - \delta$ requirement, but converge to the equilibrium point as time tends to infinity due to frictional damping.*

3.2.1. Analysis through linearization

A well known technique in analyzing non-linear systems is to exploit the fact that, close to an equilibrium, a system's behavior matches closely that of its linear approximation. In fact, the stability of an equilibrium point can in most instances be determined by checking the stability of the linearized system, as per Lyapunov's indirect method (Khalil, 2002). This is usually done by utilizing a classic result which states that a linear system is unstable if one or more of its poles (i.e. zeros of the systems characteristic equation) are in the right half plane (i.e. have a positive

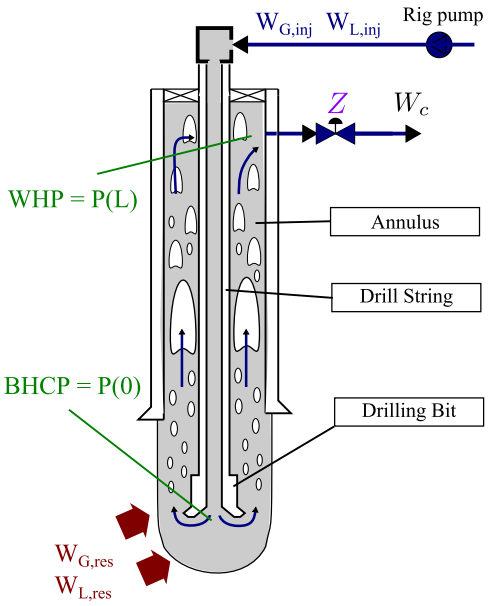

Figure 3.2.: UBD schematic.

real part) (Åström and Murray, 2010). Furthermore, two different types of unstable poles can be identified according to their location in the right half plane.

1. Pole on the real axis in the right half plane.

2. Complex conjugate pair of poles in the right half plane,

We will in the following refer to 1. as a static instability and 2. as a dynamic instability. Since a system can have several modes, an equilibrium can have both static and dynamic instabilities.

Close to the equilibrium, qualitative different behavior can be discerned between the two cases (Xu and Golan, 1989): static instabilities exhibit a simple exponential divergence from the equilibrium, while the dynamic instability causes the system to oscillate around the equilibrium point with an exponentially increasing magnitude. In the case of both dynamic and static instabilities, one of them will typically dominate the behavior.

By identifying all equilibriums of a system and determining their properties through linear analysis, one can make predictions about the full non-linear dynamics as well. However, if the system's trajectory becomes removed from the analyzed equilibria, the predictions from the linear approximations might become invalid. Thus predictions on behavior should be substantiated through further analysis and transient simulations to obtain a comprehensive understanding of the system.

$n = \alpha_{\mathrm{g}}\rho_{\mathrm{g}}$	Gas mass variable	$m = \alpha_\ell\rho_\ell$	Liquid mass variable
$W_{\mathrm{g}} = Anv_{\mathrm{g}}$	Gas mass rate	$W_\ell = Amv_\ell$	Liquid mass rate
α_{g}	Void fraction	α_ℓ	Liquid holdup
ρ_{g}	Gas density	ρ_ℓ	Liquid density
v_{g}	Gas velocity	v_ℓ	Liquid velocity
v_M	Mixture velocity	P	Distributed pressure

Table 3.1.: List of dependent variables

3.3. The Drift Flux Model at steady-state

To model the pressure and flow dynamics in the well, we will use the Drift Flux Model (DFM), which is a frequently used model of multi-phase flow in drilling. The DFM requires one distributed state for each phase to model the mass balance while the momentum of the mixture is lumped into one equation. Seminal references on two phase flow and the DFM are Wallis (1969); Ishii (1977).

In the context of drilling, seminal work was done by Lage et al. (2000) which concluded that the DFM formulation was "broadly validated through full-scale experimental data". This work was extended by Fjelde et al. (2003) who again confirmed that a "good agreement can be observed with the experimental data", but also concluded that accuracy improved when using flow pattern identification and separate closure relations for each flow pattern. This again is consistent with the results found by Lage and Time (2002) who proposed such closure relations to be used for drilling with a steady state DFM, and then did extensive comparisons with experimental data.

In the present work a DFM is used with simple friction and slip correlations independent of flow patterns. This simplifies the analysis of the model, and although the accuracy is reduced, the qualitative behavior is retained.

A description of the full Drift Flux Model is given in Appendix A. What follows is the boundary conditions and steady-state version of the DFM equations, which are used to calculate the operating envelope. Description of dependent variables is given in Table 3.1 and parameters in Table 3.2.

Boundary Conditions

Let $x \in [0, L]$ denote the space variable. For clarity purposes we will denote the pressure at the boundaries as $P(x = 0) = \mathrm{BHCP}$ and $P(x = L) = \mathrm{WHP}$. Boundary conditions on the downhole boundary are given by the mass rates of gas and liquid injected from the drilling rig and flowing in from the reservoir. Denoting the cross-sectional flow area by A, the boundary fluxes are given as:

$$Amv_\ell|_{x=0} = k_\ell \max(P_{res} - \mathrm{BHCP}, 0) + W_{\ell,inj}(t), \tag{3.6}$$

$$Anv_{\mathrm{g}}|_{x=0} = k_{\mathrm{g}} \max(P_{res} - \mathrm{BHCP}, 0) + W_{\mathrm{g},inj}(t). \tag{3.7}$$

Description	Symbol	Value	Unit
Area of flow	A	6.8×10^{-3}	m^2
Gas Production Index	k_g	5×10^{-7}	kg/s/Pa
Liquid Production Index	k_ℓ	0	kg/s/Pa
Slip Parameter	K	1.5	-
Slip Parameter	S	1.0	m/s
Inclination	$\phi(x)$	$\pi/2$	-
Measured Depth	L	2530	m
Reservoir pressure	P_{res}	279	bar
Reference liquid density	$\rho_{0,\ell}$	1000	kg/m^3

Table 3.2.: List of parameters

Here P_{res} denotes the reservoir pore pressure and k_g, k_ℓ are the production index (PI) of the gas and liquid respectively. The injection mass rates of gas and liquid, $W_{G,inj}, W_{L,inj}$, are specified by the driller and can, within some constraints, be considered as manipulated variables. The inflow from the reservoir is dependent on the pressure on the left boundary, usually given by a Vogel-Type Inflow performance relationship (IPR) (Wiggins et al., 1996), but within the operational range of a typical UBD operation, a linear approximation should suffice.

We will consider two different topside boundary conditions, corresponding to two potential operating scenarios.

1. the WHP is set to be constant:

$$\text{WHP} = \text{const.} \tag{3.8}$$

2. WHP is dependent on the topside liquid and gas mass rates through a valve equation:

$$\frac{mv_\ell}{\sqrt{\rho_\ell}} + \frac{nv_g}{Y\sqrt{\rho_g}}\Big|_{x=L} = \frac{C_v\big(Z(t)\big)}{A}\sqrt{\text{WHP} - P_s}, \tag{3.9}$$

where C_v is the choke opening given by the manipulated variable Z, $Y \in [0, 1]$ is a gas expansion factor for the gas flow and P_s is the separator pressure, i.e. the pressure downstream the choke.

3.3.1. Steady-state Equations

The model is said to be at an equilibrium, or at steady-state, when both the boundary conditions (3.6)–(3.7) and (3.9) or (3.8), and the distributed equations (A.2)–(A.4) with the $\frac{\partial \cdot}{\partial t}$ terms set as zero, are satisfied. That is, at steady-state we

have:

$$\frac{\partial m v_\ell}{\partial x} = 0, \tag{3.10}$$

$$\frac{\partial n v_\mathrm{g}}{\partial x} = 0, \tag{3.11}$$

$$\frac{\partial P + m v_\ell^2 + n v_\mathrm{g}^2}{\partial x} = -(m+n) g \sin\phi(x) - \frac{2 f (m+n) v_M |v_M|}{D}. \tag{3.12}$$

From (3.10)–(3.11) we have that the mass flux is constant w.r.t. the variable s. Combining this with the boundary conditions and integrating (3.12) we find that the system at steady-state must satisfy

$$\mathrm{WHP} = \mathrm{BHCP} + \int_0^L - \underbrace{\frac{\partial m v_\ell^2 + n v_\mathrm{g}^2}{\partial s}}_{\text{Acceleration}} - \underbrace{(m+n) g \sin\phi(x)}_{\text{Gravity}} - \underbrace{\frac{2 f (m+n) v_M |v_M|}{D}}_{\text{Friction}} \mathrm{d}x, \tag{3.13}$$

$$A m v_\ell = k_\ell \max(P_{res} - \mathrm{BHCP}, 0) + W_{\ell,inj}(t), \tag{3.14}$$

$$A n v_\mathrm{g} = k_\mathrm{g} \max(P_{res} - \mathrm{BHCP}, 0) + W_{\mathrm{g},inj}(t), \tag{3.15}$$

and the topside boundary condition (3.8) or (3.9).

3.4. UBD operating envelope

In UBD well engineering, using a steady-state multiphase flow simulator is a popular approach to develop an *operating envelope*, or *operating window*. This allows the engineer to gauge the WHP and injection rates required to achieve the desired BHCP as well as satisfying hole cleaning requirements. Publications referring the use of such a technique are also numerous, see e.g. Saponja (1998); Guo and Ghalambor (2002); Udegbunam et al. (2013); Nguyen et al. (2009); Suryanarayana et al. (2006); Guo (2002); Pickles et al. (2004).

In the following, we consider an example case to illustrate the failure of the conventional operating envelope to predict stability of certain equilibria due to the assumption of constant WHP. An alternative approach that amends this problem is then proposed. For the case considered, no gas injected and no liquid produced (i.e. a constant liquid rate and pressure dependent gas rate), is assumed. See Table 3.2 for full list of parameter values used.

3.4.1. Conventional operating envelope analysis

The conventional way of developing the operating envelope is to assume a fixed WHP, thus satisfying (3.8), and then specify a gas mass-rate nv_G and solve (3.13)–(3.14) to find the corresponding BHCP. This is then repeated over a range of gas mass rates thus creating the Tubing performance curve (see. Fig. 3.3). This curve gives

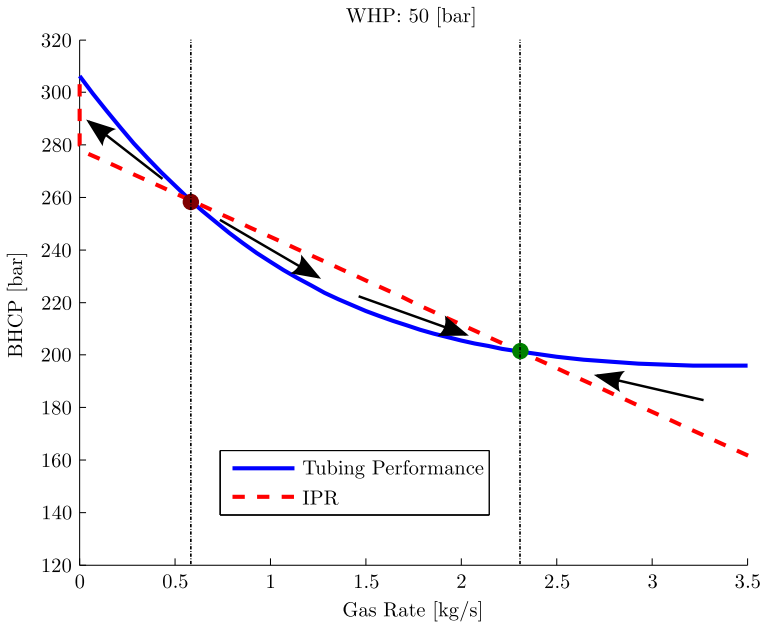

Figure 3.3.: Stable and unstable equilibrium in an UB operation.

the *potential* steady-state operating points of the well. To find the actual equilibria of the system we need to overlay the solution of equation (3.15), which is the inflow performance relationship (IPR) curve. The intersection points of these two curves corresponds to an equilibrium, as it indicates that the full set of equations (3.8),(3.13)–(3.15) are satisfied. These equilibria can be either stable or unstable, see Definition 3.1.

In Fig. 3.3, there are two intersection points, but only one of these is stable and a suitable operating point. By inspecting the curves we see that for gas rates where the IPR curve is above the 'Tubing Performance' curve, the well is not in a steady-state but tends to a higher gas rate and vice versa, see Fig. 3.4. The intersection point denoted by the red dot, then, is unstable: a slight perturbation from this point to an increased BHCP would cause a reduced gas inflow further increasing the BHCP. Vice versa, for a slight decrease in BHCP, the increased gas-influx will displace the liquid in the well further decreasing BHCP and causing yet more gas influx. Hence this is an unstable equilibrium caused by a statically unstable pole, from which nearby trajectories will diverge.

For the steady-state denoted by the green dot, the intersection between the two curves is in the opposite direction making this an attractive (i.e. stable) equilibrium.

In the field, changing BHCP is typically achieved by controlling the WHP. The effect of changing the WHP for the current scenario can be seen in Fig. 3.5, where the well will tend to the intersection denoted by the green dot for the 'Tubing

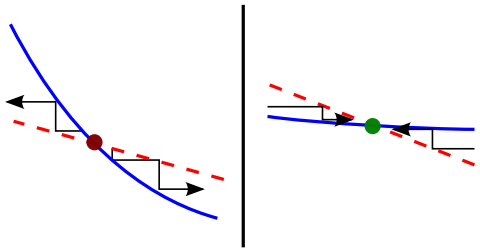

Figure 3.4.: Dynamics of an unstable and a stable equilibrium.

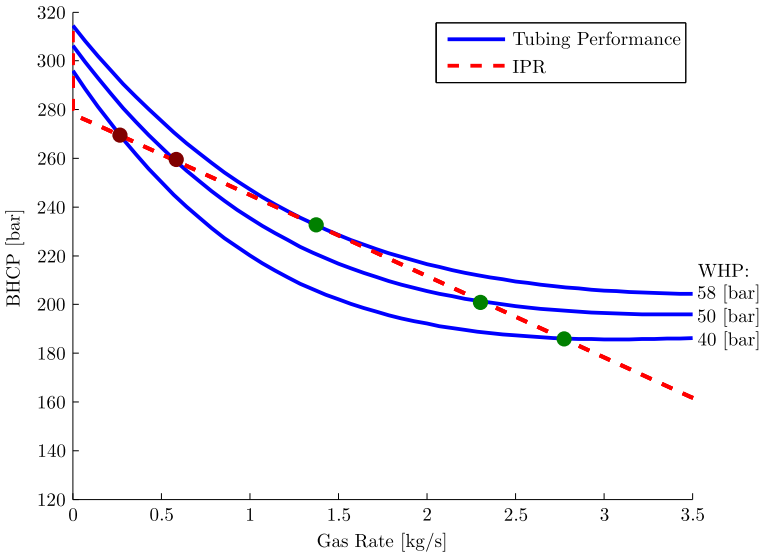

Figure 3.5.: Highest achievable BHCP with a constant WHP.

Performance curve' corresponding to the current WHP. Hence, according to this analysis, the highest underbalanced BHCP at a stable steady-state that can be achieved for this well by changing the WHP is 235 bar achieved with a WHP of 58 bar. Enforcing a WHP higher than this will lead to the well becoming overbalanced.

3.4.2. Alternative technique

In this section we present an alternative approach to finding equilibria in underbalanced operations. The basis is similar to the techniques used by Mykytiw et al. (2004); Graham and Culen (2004), but where these papers concluded that (what we call) the non-intuitive regime is unstable, we show that this only is true when using a constant WHP, i.e. (3.8), as a boundary condition. When we control by setting a fixed choke opening instead, i.e. using (3.9), the stable regime is expanded

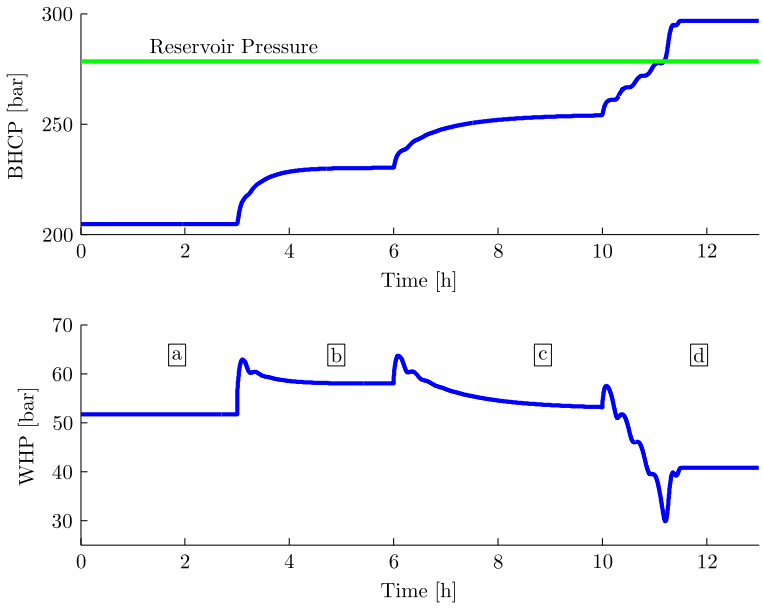

Figure 3.6.: Transient simulation with decreasing choke opening.

as will be shown in the following.

Transient Simulation

To give an impression of the thinking behind this approach, consider a transient simulation of the same well studied in the previous section but with the topside boundary condition (3.9), see Fig. 3.6. Again, the injected liquid rate is kept constant, the gas rate is dependent on the BHCP according to (3.15) and the only manipulated variable is the choke opening. Note that the effect of changing the choke opening is to change the WHP required to have a given mass-rate flowing out of the well as given by (3.9).

Initially, the choke opening is set to **a** (see Table 3.3) and is changed (slightly closed) to **b**,**c** and **d** after 3,6 and 10 hours. When the choke opening is changed, there is a transient period before the pressure settles to the new steady-state. We note the qualitatively different responses for each of the changes in choke opening. For the change from **a** to **b**, both the WHP and BHCP increase as the choke opening is decreasing, as expected. For the decrease in choke opening from **b** to **c**, however, after an initial increase in WHP, a counter-intuitive response follows, where the WHP decreases and settles at a lower value than the previous equilibrium. Finally, when the choke opening is set to **d** after 10 hours the system drifts to overbalance.

Time:	1–3[h]	3–6[h]	6–10[h]	10–12[h]
Choke opening:	a=12%	b=10%	c=8.5%	d=7%

Table 3.3.: Choke stepping program.

Steady-State Analysis

It is clear that this transient behavior cannot be fully understood by the conventional operating envelope analysis, and the reason for this is the failure of that method to take the effect of the back-pressure choke, (3.9), into account. Specifically, the conventional operating envelope analysis considers the WHP as the independent (i.e. exogenous) variable when in practice, the choke opening is the independent variable, which allows for including (3.9).

Instead, to understand this behavior, we return to the steady-state equations of the DFM, but, following the suggestion of Graham and Culen (2004), we combine the Tubing performance curve and the IPR to plot the curve shown in Fig. 3.7. The blue WHP curve in this figure is calculated by fixing the BHCP, figuring out the inflow rates using (3.14)–(3.15), and then finding the corresponding WHP by integrating (3.13). Equilibria can then be found by overlaying either (3.8) (which corresponds to Fig. 3.7) or (3.9) (corresponding to Fig. 3.8) according to which the boundary condition is enforced.

By comparing Fig. 3.7 to Fig. 3.5, it is seen that the same equilibria points are identified by both approaches. However, to understand the behavior from the transient simulation, the boundary condition with the back-pressure choke, i.e. (3.9), must be enforced. Overlaying (3.9) with the values in Table 3.3 yields Fig. 3.8. Again, for certain choke openings such as **c**, there are multiple points of intersection between the curves and correspondingly multiple equilibria. These can be checked for static instabilties in a similar fashion as for the conventional technique: When the red line is below the blue line, there is more mass flowing out of the well than into the well and BHCP will decrease and vice versa. Hence, we can identify the qualitative behavior of the system and heuristically determine the stability or instability of the equilibria (Note that this heuristic is only able to detect static instabilities.), see Fig. 3.9. In this figure the behavior of the well is also indicated by the arrows: if the well is initiated with a BHCP lower than that which corresponds to the unstable equlibrium, we see that the red curve is below the blue and the system moves to a lower BHCP corresponding at the stable equlibrium indicated by the green dot. Thus the behavior of the transient simulation shown in Fig. 3.6 can be understood from Fig. 3.8.

Considering the transient simulation (Fig. 3.6) in the context of Fig. 3.8, we see that moving from choke opening **a** to **b**, we have an intuitive response as the system moves to the apex of the steady-state WHP curve. Moving to choke opening **c**, however, results in a decreased steady-state WHP as indicated by Fig. 3.8, and finally at **d** there are no intersections between the two curves at underbalanced BHCPs and the well moves to the only equilibrium which is in overbalanced

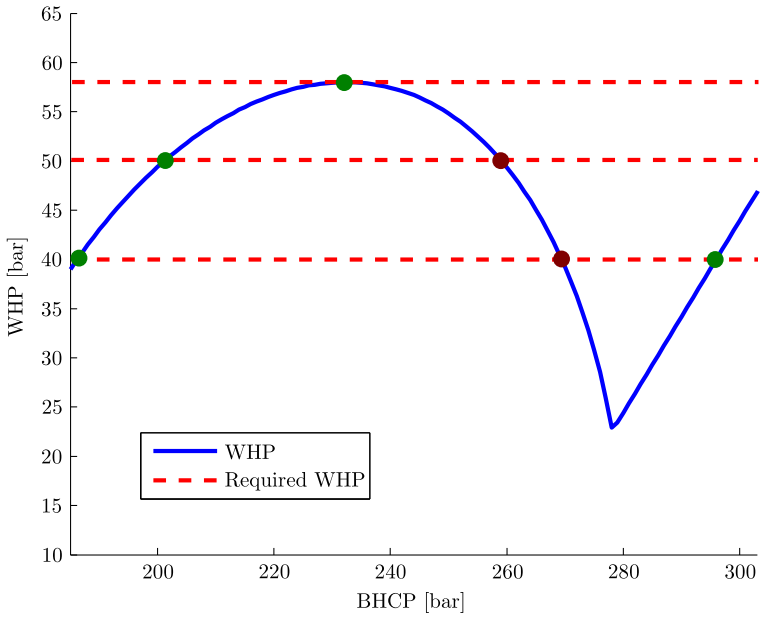

Figure 3.7.: Operating envelope technique as suggested by Graham and Culen (2004).

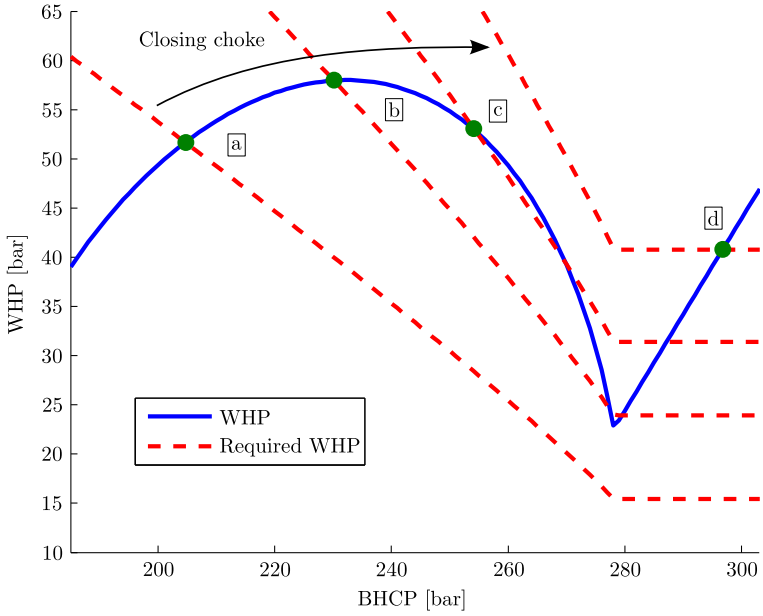

Figure 3.8.: Effect of using a valve equation at the boundary.

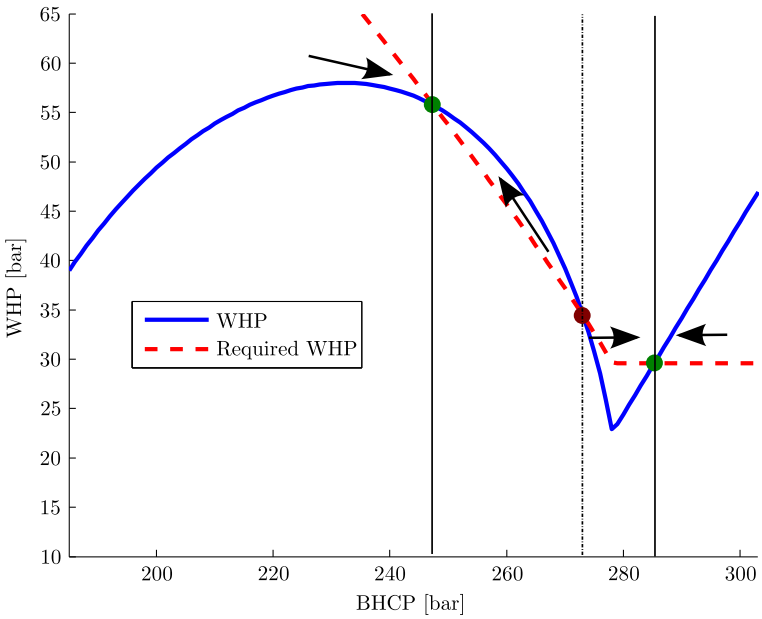

Figure 3.9.: Characterising equilibria and transient response.

conditions.

3.5. Classification of operating regimes

Using the techniques presented in the previous section, 4 distinct regimes for the UBD well in question can be identified, see Fig. 3.10. In addition, there is a fifth regime caused by a dynamic instability which is characterized by a severe slugging limit cycle. This is investigated in a later section.

Intuitive regime

This regime corresponds to BHCPs below (i.e. left in Fig. 3.10) the apex of the WHP curve. The well in this regime is stable and well behaved without exhibiting inverse responses.

Non-intuitive regime

In this regime the well exhibits inverse response in the WHP compared to BHCP. To explain this phenomenon, consider the following approximation of (3.13), obtained by neglecting the acceleration term:

$$\text{BHCP} = F + G + \text{WHP}, \tag{3.16}$$

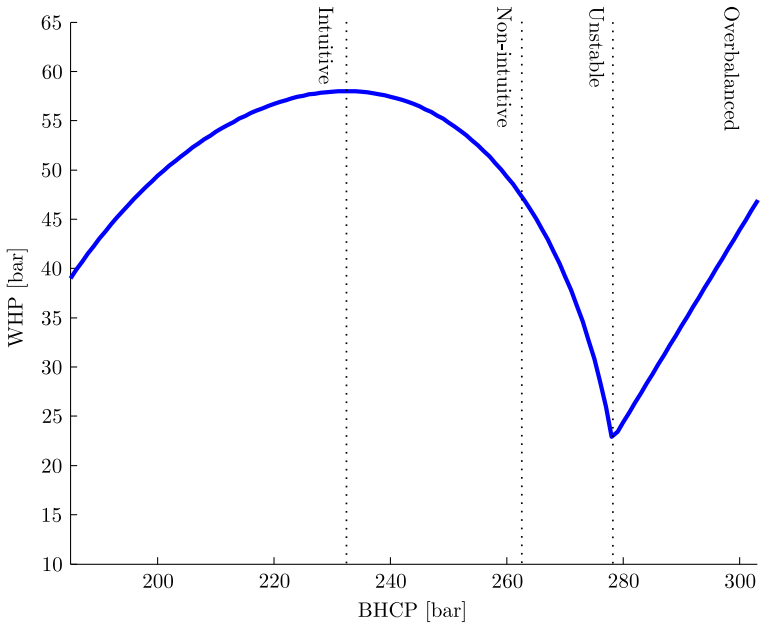

Figure 3.10.: The four distinct operating regimes.

where F denotes the integrated frictional pressure drop and G the hydrostatic pressure. Let Δ denote a steady-state change in value. We have

$$\Delta\text{WHP} = \Delta\text{BHCP} - \Delta F - \Delta G, \tag{3.17}$$

$$\implies \frac{\Delta\text{WHP}}{\Delta\text{BHCP}} = 1 - \frac{\Delta F}{\Delta\text{BHCP}} - \frac{\Delta G}{\Delta\text{BHCP}}. \tag{3.18}$$

Inserting (3.15):

$$\frac{\Delta\text{WHP}}{\Delta W_\text{g}} = -\frac{1}{k_\text{g}} - \frac{\Delta F}{\Delta W_\text{g}} - \frac{\Delta G}{\Delta W_\text{g}}. \tag{3.19}$$

Hence we get the non-intuitive response when[1]

$$\frac{1}{k_\text{g}} + \frac{\Delta F}{\Delta W_\text{g}} + \frac{\Delta G}{\Delta W_\text{g}} < 0, \tag{3.20}$$

and the apex of the curve in Fig. 3.10 corresponds to the point when the left side of (3.20) equals 0. Note that this condition is different from the one typically used

[1]Unfortunately this criterion requires a steady-state model of the well to find $\frac{\Delta F}{\Delta W_\text{g}}$; $\frac{\Delta G}{\Delta W_\text{g}}$, and cannot be computed explicitly from well parameters alone.

to identify a hydrostatically dominated well, which is:

$$\frac{\Delta(\text{BHCP} - \text{WHP})}{\Delta W_{\text{g}}} < 0 \tag{3.21}$$

$$\implies \frac{\Delta F}{\Delta W_{\text{g}}} + \frac{\Delta G}{\Delta W_{\text{g}}} < 0. \tag{3.22}$$

We emphasize that the determining factor for the behavior of the well is condition (3.20) and *not* (3.22).

In this non-intuitive regime the pressure settles at a lower value, but since the system's initial response is an increase (see. Fig. 3.6) we get an inverse response in the WHP. This phenomenon is referred to as the system being non-minimum phase in systems theory. *Because of this non-minimum phase response, the BHCP should not be controlled on WHP in this regime.* This is why steady-states in this regime appear unstable when the conventional technique shown in Fig. 3.5 is used. In this regime, BHCP should be controlled on choke opening.

Unstable regime

For larger values of BHCP, there are no stable equilibria. Closing the choke further, e.g. from **c** to **d**, will cause the well to enter a limit cycle of severe slugging or drift towards the steady-state in overbalanced conditions.

We note, however, that there are nominally unstable equilibria in this regime which can be made stable through automatic feedback control of the choke using BHCP measurements, i.e. by creating the appropriate dynamic mapping $Z(t) = C(\text{BHCP})$. Thus, the UBD operating envelope can be extended, which would enable performing UBO on wells with tight margins between fracture and collapse pressure or with stringent limits on the amount of gas that can be flared.

Overbalanced regime

In this regime, for the given well, the system contains only liquid, which makes the difference BHCP − WHP constant. Hence all steady-states are stable with short predictable transients.

3.5.1. Identifying operating regime

As was shown, the operating envelope can be extended by using the choke opening as the independent variable in place of WHP. While keeping the well under control in this manner, the well's operating regime can be identified by reducing the choke opening and observing the corresponding change in WHP (see Fig. 3.6). In the intuitive region far from the apex of the WHP curve (see fig. 3.10), the well quickly goes to steady-state after the change, without any overshoot and with an increase in steady-state WHP. Closer to the apex of the WHP curve (and thus closer to the limit to the non-intuitive region), the well will need more time to reach steady-state and

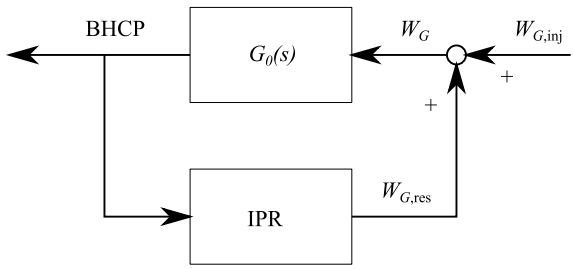

Figure 3.11.: Block diagram of the feedback loop which potentially causes instability.

the WHP response will have an overshoot. In the non-intuitive regime, the WHP will have an inverse response, and the well will need increasingly more time to reach steady-state as the limit to the unstable regime or severe slugging is approached.

3.5.2. Validity of stability heuristic

In the previous sections, the stability of an equilibrium was determined by a heuristic using the direction the steady-state curves of the operating envelope cross each other, which is thus only able to detect static instabilities. A more rigorous way of determining stability is to use the well-known Nyquist stability criterion, see e.g. Åström and Murray (2010).

To use this criterion, we need to linearize the system and derive the Loop Transfer function of a known stable loop. Assuming a well with constant choke opening and constant gas and liquid mass rates entering at the bottom to be stable, we can analyze the system by breaking the loop between the reservoir and the well, see Fig. 3.11. In this block diagram, $G_0(s)$ denotes the linearized system dynamics between a gas mass rate entering at the bottom of the system and the BHCP. By closing the loop with the IPR, we obtain the full system with the boundary conditions discussed previously. Hence, we can evaluate the stability of the system by employing the Nyquist criterion on the Loop Transfer function of $G_0(s)$ multiplied with the linearized IPR, here denoted by k_{g}.

The loop transfer function is derived in Appendix 3.A, while the Nyquist criterion is restated in Appendix 3.B. Using this theorem we can investigate the validity of the heuristic. Consider again the equilibria shown in Fig. 3.9. The Nyquist contours corresponding to the two underbalanced equilibria are shown in Fig. 3.12. The equilibrium denoted as unstable has several encirclements of the -1 point (i.e. the complex number $-1 + 0j$), meaning it is in fact unstable, thus confirming the heuristic in this case.

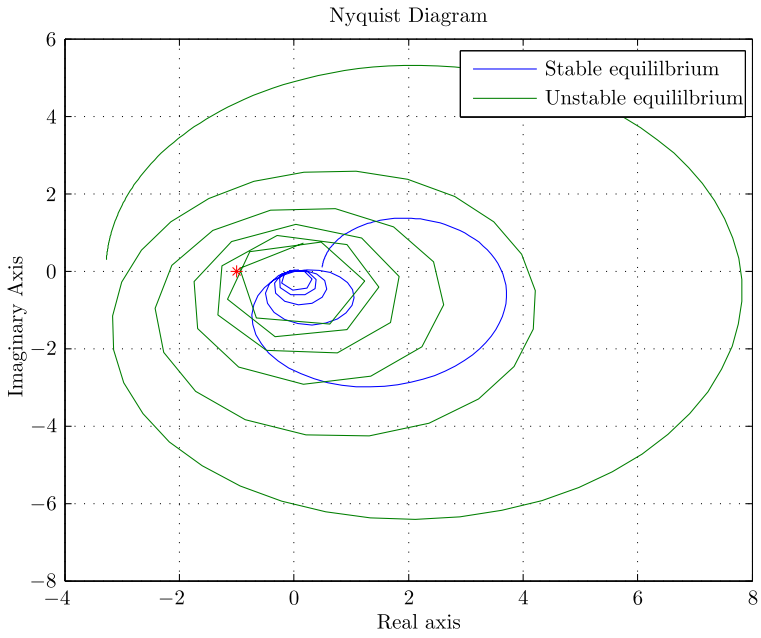

Figure 3.12.: Comparison of the Nyquist contours.

3.6. Choke opening sensitivity analysis

When controlling the BHCP by manipulating the opening of the back-pressure valve, either through an automatic algorithm or with a "bloke on the choke", it is desirable to understand how the well reacts to this actuation. This is shown in Fig. 3.13. The steady-state values of BHCP and WHP (i.e. the green and red dots in Fig. 3.9) are plotted over a range of choke openings given on the x-axis.

Consider a well initially in the overbalanced regime. Closing the choke will cause the system to move along the red line until a choke opening of 8%. This corresponds to a choke opening where the red dotted line in Fig. 3.8 is below the WHP minimum occurring at the transition to underbalanced conditions. The system will then move to the stable steady-states given by the blue curve in Fig. 3.13. Reducing the choke opening when the system is in this state will make it move along the blue curve. The end of the blue curve, moving towards left, is the limit of the stable regime. Closing the choke past this point will either cause the system to go to the overbalanced regime or enter a severe slugging limit cycle.

3.7. Dynamic instability: severe slugging in UBO

As have been discussed above, an equilibrium must be checked for dynamic instabilities to guarantee a stable operating point. For the considered UBO scenario, where

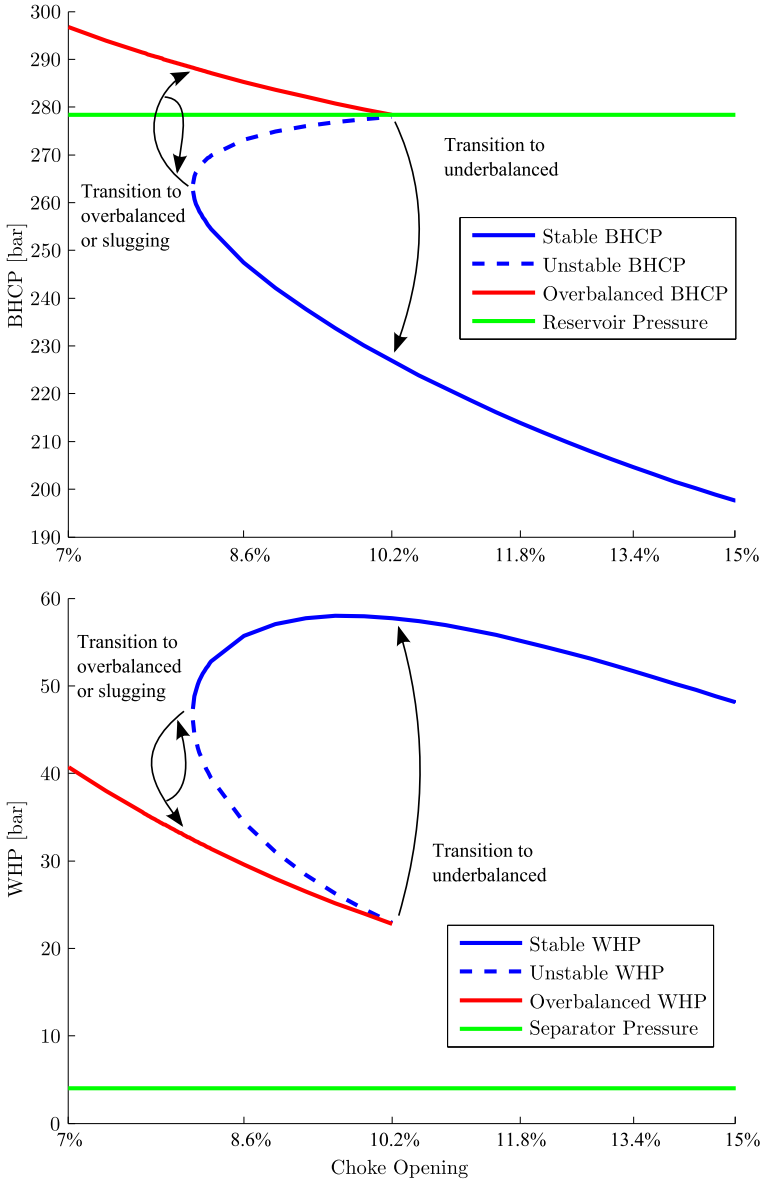

Figure 3.13.: Control envelope showing steady-state points plotted against choke opening. The system shows a hysteresis-like behaviour in that it will converge to different steady-states depending on whether the system is over- or under-balanced.

the liquid rate is constant and the gas rate is dependent on drawdown, there have been reports from the field by Graham and Culen (2004); Mykytiw et al. (2004), of instabilities associated with low gas rates leading to a limit cycle of severe slugging. (Note that by severe slugging we mean a violent, low frequency cycling between long liquid slugs and a high gas flow rate, and *not* a slug flow pattern.) In recreating this behavior in simulations it was found that the severe slugging could occur even when there was no static instability. This leads us to conclude that the instability associated with this severe slugging is caused by a dynamic instability.

In the literature, we find that there can be different mechanisms for severe slugging, e.g.: **terrain slugging** (Jansen et al., 1996; Taitel, 1986), **casing heading** (Eikrem et al., 2006, 2008) and **density-wave** (Sinegre, 2006; Hu, 2004). However, none of these mechanisms matches exactly with the boundary conditions of constant liquid rate and drawdown-dependent gas rate, which are explored in this paper.

Thus it seems that this particular mechanism for severe slugging in UBD has not been extensively studied in the literature and hence is not yet clearly understood. It is, however, known to be associated with low gas rates, meaning it tends to occur close to the balance point. Furthermore, it seems to be caused by increases in WHP due to gas flowing out through the choke. Thus keeping WHP constant would remove the slugging but would initiate a static instability instead if the well is in the non-intuitive regime.

To recreate slugging with the DFM, the back-pressure choke equation (3.9) with a very small Y is required. The effect of this is that variations in gas flow through the choke cause large changes in WHP. The operating envelope of a well that exhibits slugging is shown in Fig. 3.14, here $Y = 0.025$ was used. Fig. 3.14 also shows the Required WHP curves of two slightly different choke openings: one which corresponds to a stable equilibrium and one that has a dynamic instability. With such a low Y constant, the unstable regime discussed in the previous section, caused by the static instability, is avoided due to the steepness of the Required WHP curves. Instead the occurrence of severe slugging becomes possible. To evaluate the stability of these equilibria, we again find the loop transfer function using the method described in Appendix 3.A and the Nyquist theorem from Appendix 3.B.

The loop transfer functions and the Nyquist contours of the linearized systems obtained around the two equilibria are shown in Fig. 3.15. The loop transfer function shows the frequency domain response of the system to an impulse of increased gas influx. In the Nyquist plot we see that the slugging instability in this case is caused by two unstable modes in the 2×10^{-3}–1×10^{-2} (rad/s) frequency range. This is consistent with the transient simulation shown in Fig. 3.16 where the slugging has approximately a 20 minute period, which corresponds to 5×10^{-3} (rad/s).

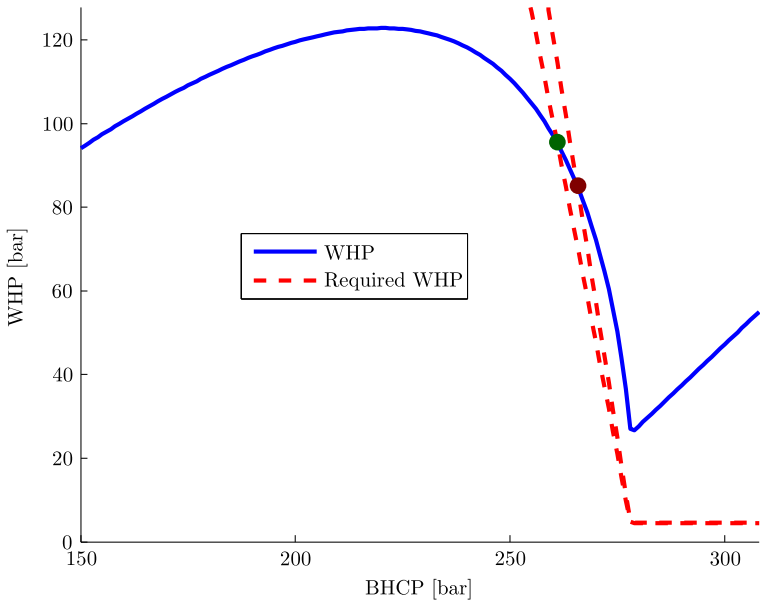

Figure 3.14.: Operating envelope showing the equilibria at the transition to severe slugging.

3.8. Summary and conclusions

In this paper, an operating envelope technique for analyzing dynamics encountered in UBO is presented. Using this technique we are able to identify 5 distinct operating regimes:

- *Intuitive regime* with short and intuitive transient dynamics, associated with high gas rates.
- *Non-intuitive regime* with an inverted Wellhead Pressure (WHP) response, associated with low to mid-range gas rates.
- *Unstable regime, static instability*, with no stable steady-states due to a static instability, associated with low gas rates.
- *Unstable regime, severe slugging*, with no stable steady-states due to the well tending to a severe slugging limit cycle, caused by dynamic instability, associated with low gas rates.
- *Overbalanced regime*, with no reservoir influx and stable steady-states.

The accompanying analysis reveals that an important factor deciding the behavior of an underbalanced gas well is not whether the well is frictionally or hydrostatically dominated, but instead the limit between the intuitive and non-intuitive

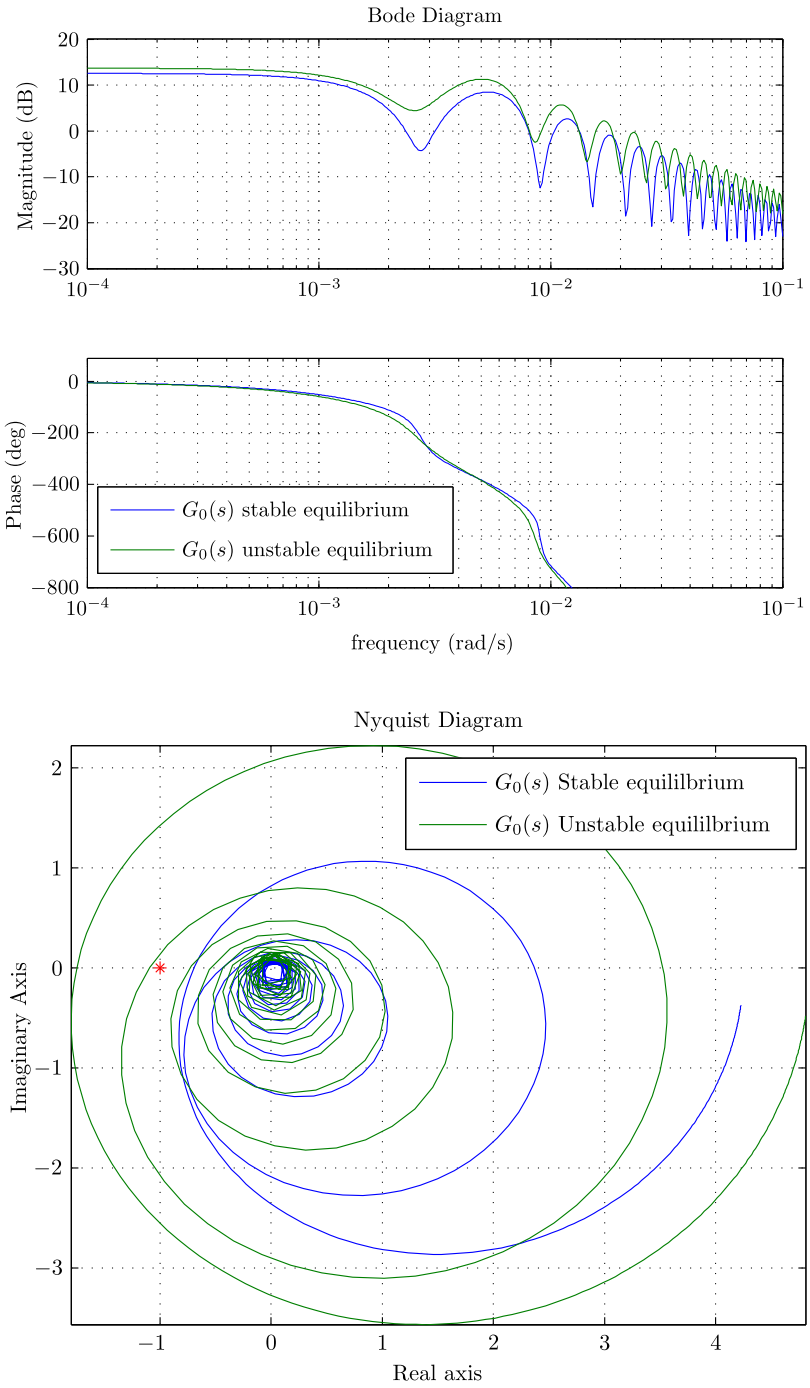

Figure 3.15.: Loop transfer functions (**top**) and Nyquist plot (**bottom**) of well entering a severe slugging limit cycle by decreasing the choke opening.

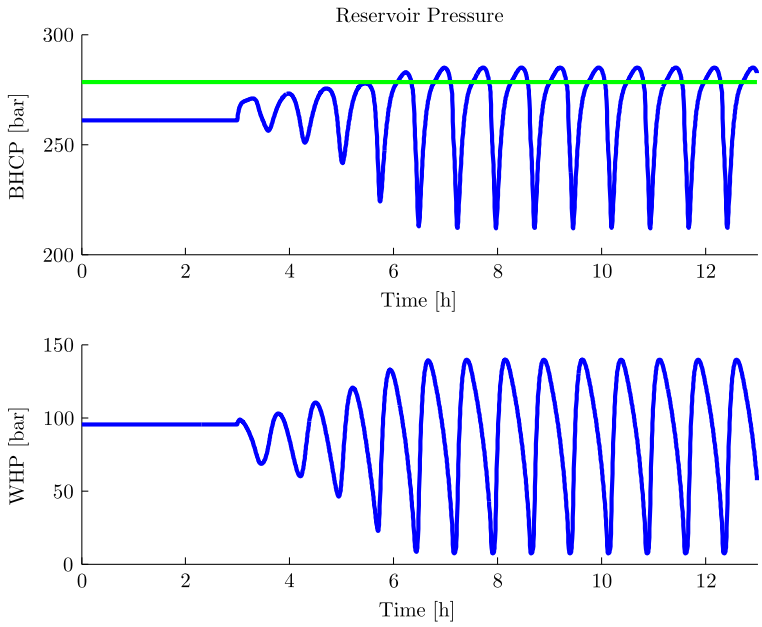

Figure 3.16.: Transient simulation of the well entering a slugging limit cycle when changing choke opening at 3 hours.

regimes, given by the point when

$$\frac{1}{k_{\mathrm{g}}} + \frac{\Delta F}{\Delta W_{\mathrm{g}}} + \frac{\Delta G}{\Delta W_{\mathrm{g}}} = 0. \tag{3.23}$$

Another important determining factor for the behavior are the limits to the two unstable regimes. It can be shown that both a steep and flat slope of the 'Required WHP' curve of the back-pressure choke can cause instabilities:

- A static instability in the case of a flat curve, see Fig. 3.9 and 3.12.
- A dynamic instability causing severe slugging in the case of a steep curve, see Fig. 3.14 and 3.15.

The location of the limits to these two regimes will typically be uncertain, but it was shown that they are both associated with low gas rates, and some insight can be gained by deriving the loop transfer function and employing the Nyquist stability criterion, as described in Appendices 3.A and 3.B.

3.8.1. Potential for automatic control

The analysis and classification provided in this paper could serve as a decision support tool to identify operating conditions and anticipate the behavior of the

system. This should allow operators to avoid counter-productive operation of the choke, as is reported in Graham and Culen (2004).

An even more promising line of future research, however, is the potential for automatic control. There are many examples from other industries where feedback control has been utilized to turn a nominally unstable equilibrium into a stable one (see e.g. Krstic et al. (1995)), hence making it a possible operating point.

By stabilizing the unstable regions with feedback control, UBO could be performed arbitrarily close to the balance point, thus avoiding excessive flaring of produced gas and enabling underbalanced drilling of wells with low collapse margins. Conceptually, stabilizing an underbalanced well can be understood as analogous to controlling a pendulum at the upper equilibrium: straightforward to do with an actuator controlled with feedback from position measurements, but possibly challenging and tiring if done manually. This topic will be investigated in future publications.

Appendix

3.A. Loop Transfer Function derivation

The goal of this section is to develop the system's transfer functions of various input/output configurations of interest. To do this, following the lines of Aarsnes et al. (2014c); Aarsnes and Aamo (2016), we linearise the system around a steady-state profile and take the Laplace transform of the system with regards to time. We then obtain a third order linear, but space variant, ODE in space. This ODE must be solved for its boundary conditions. There are two boundary conditions on the left (downhole) boundary and one on the right (topside). Hence we must obtain the transition matrix to transport the basis of the solution from the right side to the left (or vice versa) to obtain the specific solution.

3.A.1. Linearization

The system (A.2)-(A.4) with boundary conditions (3.6)-(3.9) can be written on the quasilinear form

$$\frac{\partial q(x,t)}{\partial t} + A\big(q(x,t)\big)\frac{\partial q(x,t)}{\partial x} = S(q(x,t)), \tag{3.24}$$

with boundary conditions

$$h_1\big(q(0,t),U(t)\big) = h_2\big(q(0,t),U(t)\big) = h_3\big(q(L,t),V(t)\big) = 0, \tag{3.25}$$

where $q = \begin{bmatrix} m & n & I \end{bmatrix}$ is the state vector and the actuation acts through the exogenous variables $U(t) = \begin{bmatrix} W_{\ell,\text{inj}} & W_{\text{g,inj}} \end{bmatrix}^T$ and $V(t) = Z$.

Let $\tilde{q}(x,t) = q(x,t) - \bar{q}(x)$ denote the distance from some equilibrium profile $\bar{q}$. Close to this equilibrium profile the dynamics of the system can be approximated by the linear system (Di Meglio, 2011)

$$\frac{\partial \tilde{q}(x,t)}{\partial t} + A\big(\bar{q}(x)\big)\frac{\partial \tilde{q}(x,t)}{\partial x} = \left[-\frac{\partial A}{\partial q}\cdot \bar{q}'(x) + \frac{\partial S}{\partial q}\right]_{q=\bar{q}} \tilde{q}(x,t), \tag{3.26}$$

where we have used the fact that the equilibrium satisfies

$$A(\bar{q})\bar{q}'(x) = S(\bar{q}). \tag{3.27}$$

Also, note the notation:

$$\frac{\partial A}{\partial q}\cdot \bar{q}'(x)\Big|_{q=\bar{q}} = \left[\frac{\partial A}{\partial m}\bar{m}'(x) + \frac{\partial A}{\partial n}\bar{n}'(x) + \frac{\partial A}{\partial I}\bar{I}'(x)\right]_{q=\bar{q}}. \tag{3.28}$$

Taking the Laplace transform of (3.26) in time, denoting the Laplace variable by s we get the following ODE in space

$$\frac{\partial \tilde{q}(x,s)}{\partial x} = \bar{A}(x,s)\tilde{q}(x,s), \tag{3.29}$$

$$\bar{A}(x,s) \equiv A^{-1}(\bar{q})\left[-\frac{\partial A}{\partial q}\cdot \bar{q}'(x) + \frac{\partial S}{\partial q} - sI^{3\times 3}\right]_{q=\bar{q}}. \tag{3.30}$$

3.A.2. Numerical solution

Since (3.29) is a linear ODE we can superimpose solutions to construct the transition matrix. This is done by solving the system (3.29) from x_0 to x_1 three times with the initial conditions:

$$\tilde{q}^1(x_0,s) = \begin{bmatrix}1\\0\\0\end{bmatrix}, \quad \tilde{q}^2(x_0,s) = \begin{bmatrix}0\\1\\0\end{bmatrix}, \quad \tilde{q}^3(x_0,s) = \begin{bmatrix}0\\0\\1\end{bmatrix}. \tag{3.31}$$

The solutions, denoted as $\tilde{q}^1(x_1,s), \tilde{q}^2(x_1,s), \tilde{q}^3(x_1,s)$, make up the transition matrix:

$$\Phi(x_1,x_0) = \begin{bmatrix}\tilde{q}^1(x_1) & \tilde{q}^2(x_1) & \tilde{q}^3(x_1)\end{bmatrix}, \tag{3.32}$$

which has the property

$$\tilde{q}(x_1,s) = \Phi(x_1,x_0)\tilde{q}(x_0,s). \tag{3.33}$$

3.A.3. Boundary Condition

Consider the following linearisation of the boundary conditions

$$\frac{\partial h_1}{\partial q}\tilde{q}(0,s) = -\frac{\partial h_1}{\partial U}\tilde{U}(s), \tag{3.34}$$

$$\frac{\partial h_2}{\partial q}\tilde{q}(0,s) = -\frac{\partial h_2}{\partial U}\tilde{U}(s), \tag{3.35}$$

$$\frac{\partial h_3}{\partial q}\tilde{q}(1,s) = -\frac{\partial h_3}{\partial V}\tilde{V}(s), \tag{3.36}$$

where the partial derivatives are evaluated at $q = \bar{q}, U = \bar{U}, V = \bar{V}$. Using the derived transition matrix we can write these in matrix form

$$\tilde{q}(0,s) = \begin{bmatrix} \frac{\partial h_1}{\partial q} \\ \frac{\partial h_2}{\partial q} \\ \frac{\partial h_3}{\partial q}\Phi(1,0) \end{bmatrix}^{-1} \begin{bmatrix} -\frac{\partial h_1}{\partial U}\tilde{U}(s) \\ -\frac{\partial h_2}{\partial U}\tilde{U}(s) \\ -\frac{\partial h_3}{\partial V}\tilde{V}(s) \end{bmatrix}_{\substack{U=\bar{U} \\ V=\bar{V} \\ q=\bar{q}}}. \tag{3.37}$$

The states at other positions can be obtained using (3.33).

3.A.4. Transfer function

Finally, we can obtain the desired transfer functions. Considering the output $g(q)$ with perturbations denoted $\tilde{g}\big(q(0,s)\big) = g\big(q(0,s)\big) - g\big(\bar{q}(0)\big)$, the transfer function from e.g. the choke input $Z(s) = V(s)$ is given as

$$\frac{\tilde{g}}{\tilde{Z}}(s) = \frac{\partial g}{\partial q}\begin{bmatrix} \frac{\partial h_1}{\partial q} \\ \frac{\partial h_2}{\partial q} \\ \frac{\partial h_3}{\partial q}\Phi(1,0) \end{bmatrix}^{-1} \begin{bmatrix} 0 \\ 0 \\ -\frac{\partial h_3}{\partial V} \end{bmatrix}_{\substack{U=\bar{U} \\ V=\bar{V} \\ q=\bar{q}}}. \tag{3.38}$$

3.B. The Nyquist Stability Criterion

Assuming that for constant influx rates of gas and liquid the DFM is stable, the cause for the potential instability must be the interaction between the dynamics in the well and the Inflow Performance Relationship (IPR), see Fig 3.11.

Stability of an equilibrium point can be determined by checking the stability of the linearized system, as per Lyapunov's indirect method (Khalil, 2002). Hence we can determine the stability of equilibria encountered in UBD by employing the Nyquist criterion on the loop transfer function developed in Appendix 3.A. A restatement of the Nyquist criterion is as follows (Åström and Murray, 2010):

Theorem 3.1. *Let $G_0(s)k_g$ be the loop transfer function for a negative feedback system (as shown in Fig. 3.11) and assume that $G_0(s)k_g$ has no poles in the closed right half-plane (Re $s \geq 0$) except for single poles on the imaginary axis. Then*

the closed loop system is stable if and only if the closed contour given by $\Omega = \{G_0(j\omega)k_{\mathrm{g}} : -\infty < \omega < \infty\} \subset \mathbb{C}$ *has no net encirclements of the critical point* $s = -1$.

Chapter 4

A Simplified Two-Phase Flow Model Using a Quasi-Equilibrium Momentum Balance

This chapter is based on the work presented in Aarsnes et al. (2016b).

Summary

We propose a novel simple model of two-phase gas-liquid flow by imposing a quasi-equilibrium on the mixture momentum balance of the classical transient drift-flux model. This reduces the model to a single hyperbolic PDE, describing the void wave, coupled with two static relations giving the void wave velocity from the now static momentum balance. Exploiting this, the new model uses a single distributed state, the void fraction, and with a suggested approximation of the two remaining static relations, all closure relations are given explicitly in, or as quadrature of functions of, the void fraction and exogenous variables. This makes model implementation, simulation and analysis very fast, simple and robust. Consequently, the proposed model is well-suited for model-based control and estimation applications concerning two-phase gas-liquid flow.

4.1. Introduction

Multi-phase flow simulation models have evolved significantly over the last couple of decades. With the increase in computational power and sophistication of numerical schemes, simulating two-phase pipe flow no longer suffers the same limitations on computational size, and state of the art high-fidelity models such as OLGA (Bendiksen et al., 1991) and LedaFlow (Danielson et al., 2011) typically run many times faster than real-time on a standard desktop computer.

Before this development, however, significant efforts were devoted to obtaining simplifications of multi-phase flow models which could ease implementation and increase their simulation speed. The Drift Flux Model (DFM) (Ishii, 1977) was first proposed by Zuber and Findlay (1965) as a correlation for predicting steady-state void-fraction profiles and later used in transient representations of two-phase flow (Pauchon and Dhulesia, 1994). In this form it is a simplification of the transient two-fluid model obtained by relaxing (i.e. imposing immediate steady-state

on (Flåtten and Lund, 2011)) the dynamic momentum equation of each phase, replacing them with a mixture momentum equation and a static relation typically called a *slip law*.

Further simplification can be achieve by using a similar approach to other parts of the dynamics deemed insignificant for the application at hand. Specifically, by imposing steady state on the momentum balance, the pressure wave dynamics are neglected, yielding so-called "No Pressure Wave" (NPW) models or "Reduced DFMs". This simplification is motivated by applications for which slow gas propagation dynamics are more critical than fast pressure wave propagation. Furthermore, it has been shown that the validity of the Drift-Flux models representation of the fast pressure dynamics is imprecise in many scenarios due to the relaxation involved in the full formulation of Baer and Nunziato (1986) which lowers the sonic velocity (Flåtten and Lund, 2011; Linga, 2015). Thus, if the "medium" complexity DFM representation of the pressure waves is imprecise, the argument can be made that they could be discarded.

This approach was used by Taitel et al. (1989) where the resulting model was described by a single transient PDE of the liquid continuity, obtained by assuming incompressible liquid, and a set of steady-state relations. The resulting model was further investigated by Minami and Shoham (1994) where it was found to be amenable for certain scenarios. The approach was expanded upon by Taitel and Barnea (1997), where the assumption of incompressible liquid was dropped, yielding two transient equations. A similar model was investigated by Masella et al. (1998), here called the "No Pressure Wave" (NPW) model. More recent additions to the literature on models using quasi-equilibrium momentum balance include Choi et al. (2013); Aarsnes et al. (2015); Ambrus et al. (2015).

Interestingly, many of these recent studies have not been motivated by the desire to reduce computational complexity. Rather, the advent of computerized automation and optimization in the oil and gas industry has created new applications for various forms of simplified models, causing renewed interest in these models.

4.1.1. Application

Modern approaches to process monitoring, optimization and control promise to enhance the robustness and performance of automation through the merger of process knowledge encoded in mathematical models with real-time measurements (Aarsnes et al., 2016d). By intelligently combining predictions from the mathematical model with information from multiple sensors one can estimate unmeasured quantities, optimize automatic control procedures, predict future behavior, and plan countermeasures for unwanted incidents. Such design techniques, often referred to as model-based estimation and control (Åström and Murray, 2010; Anderson and Moore, 1990), require a mathematical model with the proper balance between complexity and fidelity, i.e. the complexity must be limited to facilitate the use of established mathematical analysis and design techniques, while the qualitative response of the process is retained.

Models that achieve such balance between complexity and fidelity are sometimes referred to as fit-for-purpose models. Obtaining such models often proves difficult for gas-liquid two-phase dynamics due to the significant complexity and distributed nature of multi-phase pipe flow (Aarsnes et al., 2014b, 2016c).

If the appropriate model can be developed, however, it could see a wide range of uses in model-based control and estimation applications where two-phase pipe flow is encountered, such as underbalanced drilling of oil and gas wells (Pedersen et al., 2015), well control (both in conventional and Managed Pressure Drilling) (Carlsen et al., 2008), riser gas handling (Hauge et al., 2015), hydrocarbon production monitoring (Bloemen et al., 2006; Teixeira et al., 2014) and mitigating severe slugging during hydrocarbon production (Eikrem et al., 2008; Esmaeil and Skogestad, 2011; Di Meglio et al., 2010).

4.2. The Drift Flux Model

In applications where the flow regime is most often bubble or slug flow, such as in drilling, the preferred model for representing one-dimensional two-phase flow dynamics at an acceptable fidelity is the classical three-state transient Drift Flux Model (DFM), see e.g. Lage and Time (2000); Fjelde et al. (2003); Aarsnes et al. (2014b).

For certain boundary conditions, the existence of solutions has been proven (Evje and Wen, 2013, 2015), and it is well known that the DFM is, in most practical situations, hyperbolic, with three (two fast and one slow) characteristic velocities (Di Meglio, 2011). The two fast characteristics represent the fast pressure dynamics in the pipe, while the slow characteristic velocity is associated with the transport of matter, also sometimes referred to as the void wave (Lorentzen and Fjelde, 2005; Masella et al., 1998).

In this section we restate the classical equations of the transient drift-flux model and then cast the system in canonical form using the eigenvectors of the transport matrix, which poses the model as a single Riemann invariant governing the propagation of the void wave, coupled to the pressure dynamics, given by two PDEs, through the gas velocity. We then show how the approximation employed by e.g. Masella et al. (1998); Choi et al. (2013), using a static relation in place of a dynamic momentum balance, is related to relaxing both of the two PDEs describing the pressure dynamics. Consequently this leads to a mixed hyperbolic/parabolic system with one hyperbolic PDE with one finite eigenvalue.

4.2.1. The Drift Flux Model equations

We start the development of the proposed two-phase model from the classical Drift Flux Model (DFM) formulation, described by the following equations (Gavrilyuk

and Fabre, 1996; Evje and Wen, 2015):

$$\frac{\partial(\alpha_\ell \rho_\ell)}{\partial t} + \frac{\partial(\alpha_\ell \rho_\ell v_\ell)}{\partial x} = \Gamma_\ell, \tag{4.1}$$

$$\frac{\partial(\alpha_\mathrm{g} \rho_\mathrm{g})}{\partial t} + \frac{\partial(\alpha_\mathrm{g} \rho_\mathrm{g} v_\mathrm{g})}{\partial x} = \Gamma_\mathrm{g}, \tag{4.2}$$

$$\frac{\partial(\alpha_\ell \rho_\ell v_\ell + \alpha_\mathrm{g} \rho_\mathrm{g} v_\mathrm{g})}{\partial t} + \frac{\partial(P + \alpha_\mathrm{g} \rho_\mathrm{g} v_\mathrm{g}^2 + \alpha_\ell \rho_\ell v_\ell^2)}{\partial x} = S, \tag{4.3}$$

where the independent variables t, x represent time and position along the pipe, respectively, and the momentum source term, S is typically given as

$$S = -\rho_M g \sin\theta(x) - \frac{2 f \rho_M v_M |v_M|}{D} \tag{4.4}$$

with the mixture relations

$$\rho_M = \alpha_\mathrm{g} \rho_\mathrm{g} + \alpha_\ell \rho_\ell, \qquad v_M = \alpha_\mathrm{g} v_\mathrm{g} + \alpha_\ell v_\ell, \tag{4.5}$$

and where $\alpha_i, v_i, \rho_i, \Gamma_i$ denote the volume fraction, velocity, density and mass source-term, respectively, of phase $i = \mathrm{g}, \ell$ (gas or liquid). Finally, f is the friction coefficient, D the hydraulic diameter, g is the acceleration of gravity and θ is the pipe inclination angle (relative to the horizontal). For the remainder of this section we will assume $\Gamma_\ell = \Gamma_\mathrm{g} = 0$.

Eqs. (4.1)-(4.2) represent the mass balance for the liquid and gas phases, while (4.3) is the conservation of momentum for the gas-liquid mixture.

The following closure relations are needed to complete the system:

$$\alpha_\ell + \alpha_\mathrm{g} = 1, \qquad P = c_\mathrm{g}^2 \rho_\mathrm{g}, \tag{4.6}$$

where P is the pressure, and c_g is the velocity of sound in the gas, while the liquid is assumed incompressible. Finally the slip law

$$v_\mathrm{g} = \frac{v_M}{1 - \alpha_\ell^*} + v_\infty = C_0 v_M + v_\infty \tag{4.7}$$

where the profile parameter $\alpha_\ell^* \in [0, 1)$, usually given as the distribution parameter $C_0 = 1/(1-\alpha_\ell^*)$, and drift parameter $v_\infty \geq 0$ determine the relative velocity between the phases. These parameters typically depend on factors such as superficial velocities and inclination (Shi et al., 2005). Multiple correlations for obtaining α_ℓ^*, v_∞ exist in the literature, see e.g. Zuber and Findlay (1965); Bhagwat and Ghajar (2014); Choi et al. (2012).

4.2.2. Variable Change

To better highlight interesting features of the model, we rewrite (4.1)–(4.3) using a transformation in accordance with Gavrilyuk and Fabre (1996) to obtain a new set of variables

$$(\chi_\ell, \rho, v_\mathrm{g}) = \left(\frac{(\alpha_\ell - \alpha_\ell^*)\rho_\ell}{\rho_M - \alpha_\ell^* \rho_\ell}, \rho_M - \alpha_\ell^* \rho_\ell, v_\mathrm{g} \right). \tag{4.8}$$

The resulting equations allow the quasilinear formulation

$$\frac{\partial \mathbf{u}}{\partial t} + A(\mathbf{u})\frac{\partial \mathbf{u}}{\partial x} = \mathbf{Q}(\mathbf{u}), \qquad \mathbf{u} = \begin{bmatrix} \chi_\ell \\ \rho \\ v_\mathrm{g} \end{bmatrix}, \tag{4.9}$$

with $A(\mathbf{u})$ given as

$$A(\mathbf{u}) = \begin{bmatrix} v_\mathrm{g} & 0 & 0 \\ 0 & v_\mathrm{g} & \rho \\ A_{31}(\mathbf{u}) & A_{32}(\mathbf{u}) & A_{33}(\mathbf{u}) \end{bmatrix}, \tag{4.10}$$

$$A_{31}(\mathbf{u}) \equiv c_\mathrm{g}^2 \frac{\rho_\mathrm{g}(\mathbf{u}) - \rho_\ell}{\alpha_\mathrm{g}(\mathbf{u})\rho_\ell} - \big(v_\mathrm{g} - v_\ell(\mathbf{u})\big)^2, \tag{4.11}$$

$$A_{32}(\mathbf{u}) \equiv c_\mathrm{g}^2 \frac{(1-\alpha_\ell^*)\rho_\mathrm{g}(\mathbf{u})}{\alpha_\mathrm{g}(\mathbf{u})\rho^2} - \big(v_\mathrm{g} - v_\ell(\mathbf{u})\big)^2 \frac{\chi_\ell}{\rho}, \tag{4.12}$$

$$A_{33}(\mathbf{u}) \equiv v_\mathrm{g} - 2\chi_\ell(v_\mathrm{g} - v_\ell(\mathbf{u})), \tag{4.13}$$

and

$$\mathbf{Q}(\mathbf{u}) = \begin{bmatrix} 0 \\ 0 \\ Q(\mathbf{u}) \end{bmatrix}, \tag{4.14}$$

$$Q(\mathbf{u}) = -\left(1 + \frac{\alpha_\ell^* \rho_\ell}{\rho}\right)\Bigg(g\sin\theta + \frac{2f\big((1-\alpha_\ell^*)v_\mathrm{g} - v_\infty\big)|(1-\alpha_\ell^*)v_\mathrm{g} - v_\infty|}{D}\Bigg), \tag{4.15}$$

where all dependent variables are in boldface.

For the case of a vanishing liquid mass source term $\Gamma_\ell = 0$, the first state χ_ℓ is a *Riemann invariant*: it satisfies a pure transport equation at the velocity v_g. The eigenvalues of the transport matrix, $A(\mathbf{u})$, are (Di Meglio, 2011):

$$\begin{bmatrix} \lambda_1 \\ \lambda_2 \\ \lambda_3 \end{bmatrix} = \begin{bmatrix} v_\mathrm{g} \\ v_\mathrm{g} + \chi_\ell\big(v_\ell(\mathbf{u}) - v_\mathrm{g}\big) + c_M(\mathbf{u}) \\ v_\mathrm{g} + \chi_\ell\big(v_\ell(\mathbf{u}) - v_\mathrm{g}\big) - c_M(\mathbf{u}) \end{bmatrix}, \tag{4.16}$$

with the mixture sound velocity

$$c_M(\mathbf{u}) = \sqrt{\chi_\ell(\chi_\ell - 1)\big(v_\mathrm{g} - v_\ell(\mathbf{u})\big)^2 + \frac{(1-\alpha_\ell^*)c_\mathrm{g}^2\rho_\mathrm{g}(\mathbf{u})}{\alpha_\mathrm{g}(\mathbf{u})\rho}}, \tag{4.17}$$

and the left eigenvectors

$$\begin{bmatrix} l_1 \\ l_2 \\ l_3 \end{bmatrix} = \begin{bmatrix} 1 & 0 & 0 \\ \frac{A_{31}(\mathbf{u})}{A_{32}(\mathbf{u})} & 1 & \frac{\rho}{\chi_\ell(v_\mathrm{g} - v_\ell(\mathbf{u})) + c_M(\mathbf{u})} \\ \frac{A_{31}(\mathbf{u})}{A_{32}(\mathbf{u})} & 1 & \frac{\rho}{\chi_\ell(v_\mathrm{g} - v_\ell(\mathbf{u})) - c_M(\mathbf{u})} \end{bmatrix}. \tag{4.18}$$

We note from this derivation that v_{g} shows up as an eigenvalue in the transport matrix and that the void wave dynamics are relatively simple due to our state transformation. The relations for the fast pressure dynamics are much more complicated and challenging to work with. In particular, finding a diagonalizing transformation of the system is not feasible, if at all possible.

4.2.3. Relaxation of the distributed pressure dynamics

Multiplying (4.9) with the left eigenvectors yields:

$$l_1(\mathbf{u})\Big[\frac{\partial \mathbf{u}}{\partial t} + \lambda_1(\mathbf{u})\frac{\partial \mathbf{u}}{\partial x} - \mathbf{Q}(\mathbf{u})\Big] = 0 \tag{4.19}$$

$$l_2(\mathbf{u})\Big[\frac{\partial \mathbf{u}}{\partial t} + \lambda_2(\mathbf{u})\frac{\partial \mathbf{u}}{\partial x} - \mathbf{Q}(\mathbf{u})\Big] = 0 \tag{4.20}$$

$$l_3(\mathbf{u})\Big[\frac{\partial \mathbf{u}}{\partial t} + \lambda_3(\mathbf{u})\frac{\partial \mathbf{u}}{\partial x} - \mathbf{Q}(\mathbf{u})\Big] = 0. \tag{4.21}$$

Following Di Meglio (2011), we proceed to a model reduction analogous to singular perturbation techniques. Indeed, eigenvalues λ_2 and λ_3 correspond to sound wave propagation (see, e.g. Masella et al. (1998); Lorentzen and Fjelde (2005)) and are at least one order of magnitude greater than λ_1, which corresponds to the transport of the pseudo-holdup χ_ℓ. This suggests that the fast transport dynamics corresponding to (4.20) and (4.21) can be relaxed when concerned with the slower time scale of the void wave Eq. (4.19). Imposing instantaneous steady state for (4.20) and (4.21) yields:

$$l_1(\mathbf{u})\Big[\frac{\partial \mathbf{u}}{\partial t} + \lambda_1(\mathbf{u})\frac{\partial \mathbf{u}}{\partial x} - \mathbf{Q}(\mathbf{u})\Big] = 0 \tag{4.22}$$

$$l_2(\mathbf{u})\Big[\lambda_2(\mathbf{u})\frac{\partial \mathbf{u}}{\partial x} - \mathbf{Q}(\mathbf{u})\Big] = 0 \tag{4.23}$$

$$l_3(\mathbf{u})\Big[\lambda_3(\mathbf{u})\frac{\partial \mathbf{u}}{\partial x} - \mathbf{Q}(\mathbf{u})\Big] = 0, \tag{4.24}$$

where by inserting for the eigenvectors and eigenvalues we can write the resulting system as

$$\frac{\partial \chi_\ell}{\partial t} + v_{\mathrm{g}}\frac{\partial \chi_\ell}{\partial x} = 0 \tag{4.25}$$

$$\frac{\partial \rho}{\partial x} = -\frac{A_{31}(\mathbf{u})}{A_{32}(\mathbf{u})}\frac{\partial \chi_\ell}{\partial x} + \frac{\rho Q(\mathbf{u})}{A_{32}(\mathbf{u})\rho - A_{33}(\mathbf{u})v_{\mathrm{g}}}. \tag{4.26}$$

$$\frac{\partial v_{\mathrm{g}}}{\partial x} = \frac{v_{\mathrm{g}}Q(\mathbf{u})}{A_{33}(\mathbf{u})v_{\mathrm{g}} - A_{32}(\mathbf{u})\rho} \tag{4.27}$$

The consequence of this is that χ_ℓ is still a Riemann invariant propagating with velocity v_{g} given implicitly by the relations (4.26)–(4.27).

Relation to the No-Pressure-Wave Model

In Masella et al. (1998) and Choi et al. (2013) a reduced DFM referred to as the *No Pressure Wave* (NPW) model is obtained by removing the time derivative term in (4.3) and computing the pressure from the resulting static relation. Consider again the original set of equations (4.1)–(4.2) but in place of the mixture momentum equation (4.3) use the static force balance

$$\frac{\partial P}{\partial x} = S. \tag{4.28}$$

In Masella et al. (1998) it is noted that the resulting model has a single finite eigenvalue, and that the remaining two states corresponds to eigenvalues that are infinite, which is similar to the system of (4.25)–(4.27). This means that using (4.28) in place of (4.3) effectively relaxes both the two characteristics associated with the fast pressure waves. Hence, using a simpler approximation in place of the expressions for ρ, v_{g} it is possible to obtain a simple first-order PDE of the two-phase flow dynamics. In the following we exploit these facts to develop such a simple representation of the void wave propagation that remains when the pressure dynamics have been relaxed.

New Approach

An approach to exploit the structure revealed by (4.25)–(4.27) was suggested in Aarsnes et al. (2015) where a simplified model representation of these relaxed dynamics was developed. The problem with this approach is that pressure is given implicitly in the states (due to the source term) such that the resulting simulation requires the solution of an ODE for every time step. This problem is avoided in the present paper by using α_{g} as the distributed state in place of χ_ℓ, which allows for finding an *approximate* relation for the pressure gradient which yields pressure explicit in the states and exogenous variables.

More specifically the pseudo-holdup,

$$\chi_\ell = \frac{(\alpha_\ell - \alpha_\ell^*)\rho_\ell}{\rho_M - \alpha_\ell^*\rho_\ell}, \tag{4.29}$$

changes according to:

$$\mathrm{d}\chi_\ell = \frac{\rho_{\mathrm{g}}(\alpha_\ell^* - 1)\mathrm{d}\alpha_{\mathrm{g}} + \alpha_{\mathrm{g}}(\alpha_{\mathrm{g}} + \alpha_\ell^* - 1)\mathrm{d}\rho_{\mathrm{g}}}{\left(\alpha_{\mathrm{g}}\rho_{\mathrm{g}} - \rho_\ell(\alpha_{\mathrm{g}} + \alpha_\ell^* - 1)\right)^2}. \tag{4.30}$$

Plugging (4.30) into (4.25) we get the equation:

$$\frac{\partial \alpha_{\mathrm{g}}}{\partial t} + v_{\mathrm{g}}\frac{\partial \alpha_{\mathrm{g}}}{\partial x} = -\frac{\alpha_{\mathrm{g}}(\alpha_{\mathrm{g}} + \alpha_\ell^* - 1)}{\rho_{\mathrm{g}}(\alpha_\ell^* - 1)}\left(\frac{\partial \rho_{\mathrm{g}}}{\partial t} + v_{\mathrm{g}}\frac{\partial \rho_{\mathrm{g}}}{\partial x}\right) \tag{4.31}$$

where ρ_{g} is given by the pressure. This motivates the approach taken in the following section.

4.3. Derivation of the new formulation

The full three-state drift-flux model is too complicated for most model-based estimation and control approaches (Aarsnes et al., 2016d), hence simplification is desirable. Based on the analysis of the previous section it should be possible to reduce the full DFM down to a first order PDE when discarding the pressure wave dynamics.

For this derivation we will again start with the classical Drift Flux formulation (4.1)–(4.7). First note the relation from the slip law (4.7):

$$\alpha_\ell v_\ell = (\alpha_\ell - \alpha_\ell^*)v_\mathrm{g} - (1-\alpha_\ell^*)v_\infty. \tag{4.32}$$

From (4.1) we have (Gavrilyuk and Fabre, 1996):

$$\frac{\partial \alpha_\ell}{\partial t} + \frac{\partial (\alpha_\ell - \alpha_\ell^*)v_\mathrm{g}}{\partial x} = \frac{\Gamma_\ell}{\rho_\ell} \tag{4.33}$$

$$\implies \frac{\partial \alpha_\mathrm{g}}{\partial t} + v_\mathrm{g}\frac{\partial \alpha_\mathrm{g}}{\partial x} = (\alpha_\ell - \alpha_\ell^*)\frac{\partial v_\mathrm{g}}{\partial x} - \frac{\Gamma_\ell}{\rho_\ell} \tag{4.34}$$

where the first term on the RHS of (4.34) is due to gas expansion which necessarily translates to acceleration of the gas.

From (4.2) we have

$$\begin{aligned}\frac{\partial v_\mathrm{g}}{\partial x} =& \frac{\Gamma_\mathrm{g}}{\alpha_\mathrm{g}\rho_\mathrm{g}} - \frac{1}{\alpha_\mathrm{g}\rho_\mathrm{g}}\left(\frac{\partial \alpha_\mathrm{g}\rho_\mathrm{g}}{\partial t} + v_\mathrm{g}\frac{\partial \alpha_\mathrm{g}\rho_\mathrm{g}}{\partial x}\right) &(4.35)\\ =& \frac{\Gamma_\mathrm{g}}{\alpha_\mathrm{g}\rho_\mathrm{g}} - \frac{1}{\rho_\mathrm{g}}\left(\frac{\partial \rho_\mathrm{g}}{\partial t} + v_\mathrm{g}\frac{\partial \rho_\mathrm{g}}{\partial x}\right) \\ & - \frac{1}{\alpha_\mathrm{g}}\left(\frac{\partial \alpha_\mathrm{g}}{\partial t} + v_\mathrm{g}\frac{\partial \alpha_\mathrm{g}}{\partial x}\right). &(4.36)\end{aligned}$$

Inserting (4.36) into (4.34)

$$\begin{aligned}&\frac{\partial \alpha_\mathrm{g}}{\partial t}\left(1 + \frac{\alpha_\ell - \alpha_\ell^*}{\alpha_\mathrm{g}}\right) + v_\mathrm{g}\frac{\partial \alpha_\mathrm{g}}{\partial x}\left(1 + \frac{\alpha_\ell - \alpha_\ell^*}{\alpha_\mathrm{g}}\right) \\ &= (\alpha_\ell - \alpha_\ell^*)\frac{\Gamma_\mathrm{g}}{\alpha_\mathrm{g}\rho_\mathrm{g}} - \frac{(\alpha_\ell - \alpha_\ell^*)}{\rho_\mathrm{g}}\left(\frac{\partial \rho_\mathrm{g}}{\partial t} + v_\mathrm{g}\frac{\partial \rho_\mathrm{g}}{\partial x}\right).\end{aligned} \tag{4.37}$$

Thus, defining the convenience variable E_g:

$$E_\mathrm{g} \equiv -\frac{\alpha_\mathrm{g}(\alpha_\ell - \alpha_\ell^*)}{(1-\alpha_\ell^*)\rho_\mathrm{g}}\left(\frac{\partial \rho_\mathrm{g}}{\partial t} + v_\mathrm{g}\frac{\partial \rho_\mathrm{g}}{\partial x}\right), \tag{4.38}$$

we have from (4.37)

$$\frac{\partial \alpha_\mathrm{g}}{\partial t} + v_\mathrm{g}\frac{\partial \alpha_\mathrm{g}}{\partial x} = E_\mathrm{g} + \frac{1}{1-\alpha_\ell^*}\left((\alpha_\ell - \alpha_\ell^*)\frac{\Gamma_\mathrm{g}}{\rho_\mathrm{g}} - \alpha_\mathrm{g}\frac{\Gamma_\ell}{\rho_\ell}\right). \tag{4.39}$$

Then, defining the source terms $\Gamma_{\mathrm{g}}^*, \Gamma_\ell^*$:

$$\Gamma_{\mathrm{g}}^* \equiv \frac{\alpha_\ell - \alpha_\ell^*}{(1-\alpha_\ell^*)\rho_{\mathrm{g}}}\Gamma_{\mathrm{g}}, \quad \Gamma_\ell^* \equiv \frac{\alpha_{\mathrm{g}}}{(1-\alpha_\ell^*)\rho_\ell}\Gamma_\ell, \tag{4.40}$$

we have

$$\frac{\partial \alpha_{\mathrm{g}}}{\partial t} + v_{\mathrm{g}}\frac{\partial \alpha_{\mathrm{g}}}{\partial x} = E_{\mathrm{g}} + \Gamma_{\mathrm{g}}^* - \Gamma_\ell^*. \tag{4.41}$$

4.3.1. Pressure profile

The distributed, quasi-steady pressure is obtained from (4.28) and the pressure boundary condition $P(x{=}L) = P_L$:

$$P(x) = P_L + \int_L^x S(\xi)\mathrm{d}\xi. \tag{4.42}$$

This expression is implicit in that it is dependent on v_M which is in turn dependent on $E_{\mathrm{g}}(P)$, and $\rho_{\mathrm{g}}(P)$. To avoid this complication a simplification should be used, e.g. by assuming v_M uniform in space when calculating the pressure profile. Essentially, what is modeled is

$$P(x) = P_L + F(x) + G(x), \tag{4.43}$$

where $F(x), G(x)$ is the frictional pressure drop and hydrostatic pressure. Let q_ℓ, q_{g} denote the exogenous variables liquid, respectively gas, volumetric flow rates entering at the bottom of the well. Then one possible approximation of (4.4) is

$$S(x) \approx -\bar{\rho}_M(x)\left(g\sin\theta(x) + \frac{2f(q_{\mathrm{g}}+q_\ell)|q_{\mathrm{g}}+q_\ell|}{A^2 D}\right), \tag{4.44}$$

$$\bar{\rho}_M = (\rho_\ell \alpha_\ell(x) + \bar{\rho}_{\mathrm{g}}\alpha_{\mathrm{g}}(x)), \tag{4.45}$$

i.e. a mean approximate gas density is used, which is an amenable approximation for $\alpha_{\mathrm{g}}\rho_{\mathrm{g}} \ll \alpha_\ell\rho_\ell$. This makes the source term S explicit in the state α_{g} and the exogenous variables.

4.3.2. Boundary condition and velocity profile

Defining $v_{\mathrm{g}0} \equiv v_{\mathrm{g}}(x{=}0, t)$, we have from (4.7):

$$v_{\mathrm{g}0} = \frac{C_0}{A}(q_{\mathrm{g}} + q_\ell) + v_\infty. \tag{4.46}$$

The downhole boundary condition of (4.41) is given as

$$\alpha_{\mathrm{g}}(x{=}0, t) = \frac{q_{\mathrm{g}}}{A v_{\mathrm{g}0}}, \tag{4.47}$$

The velocity gradient is obtained by combining (4.36) and (4.41):

$$\frac{\partial v_{\mathrm{g}}}{\partial x} = \frac{E_{\mathrm{g}} + \Gamma_{\mathrm{g}}^* - \Gamma_\ell^* + \Gamma_\ell/\rho_\ell}{\alpha_\ell - \alpha_\ell^*}, \tag{4.48}$$

$$= \frac{E_{\mathrm{g}} + \Gamma_{\mathrm{g}}^*}{\alpha_\ell - \alpha_\ell^*} + \frac{1}{1-\alpha_\ell^*}\frac{\Gamma_\ell}{\rho_\ell}. \tag{4.49}$$

Now note the relation for the gas density in (4.6). In the following we will make this relation slightly more general by instead using

$$\frac{\rho_{\mathrm{g}}^\gamma}{P} = C, \tag{4.50}$$

where C is a constant and γ is the adiabatic gas constant equal to one for constant temperature. In differential form, we can write (4.50) as

$$\gamma \rho_{\mathrm{g}}^{\gamma-1} \mathrm{d}\rho_{\mathrm{g}} = C \mathrm{d}P, \tag{4.51}$$

and substituting the value of C from (4.50), we further have:

$$\frac{\mathrm{d}\rho_{\mathrm{g}}}{\rho_{\mathrm{g}}} = \frac{\mathrm{d}P}{\gamma P}. \tag{4.52}$$

Note that the term γP is equivalent to the isentropic bulk modulus of an ideal gas. Eq. (4.52) allows us to recast (4.38) in terms of the pressure profile, $P(x)$:

$$E_{\mathrm{g}} = -\frac{\alpha_{\mathrm{g}}(1 - C_0\alpha_{\mathrm{g}})}{\gamma P}\left(\frac{\partial P}{\partial t} + v_{\mathrm{g}}\frac{\partial P}{\partial x}\right), \tag{4.53}$$

For deriving the velocity, we neglect the $\frac{\partial \rho_{\mathrm{g}}}{\partial t}$ term from (4.38). Furthermore, in implementation, the singularity at $\alpha_\ell = \alpha_\ell^*$ should be avoided, hence we rewrite (4.49) as:

$$\frac{\partial v_{\mathrm{g}}}{\partial x} = C_0\left(-\frac{\alpha_{\mathrm{g}} v_{\mathrm{g}}}{P\gamma} S + \frac{c_{\mathrm{g}}^2}{P\gamma}\Gamma_{\mathrm{g}} + \frac{1}{\rho_\ell}\Gamma_\ell\right), \tag{4.54}$$

and consequently, by defining the integral

$$I_v(x) = \int_0^x \frac{C_0\alpha_{\mathrm{g}}(\xi)}{P(\xi)\gamma} S(\xi)\mathrm{d}\xi, \tag{4.55}$$

the distributed velocity is obtained as

$$v_{\mathrm{g}}(x) = e^{-I_v(x)}\Bigg(v_{\mathrm{g}0} + C_0\int_0^x \left(\frac{c_{\mathrm{g}}^2(\zeta)}{P(\zeta)\gamma}\Gamma_{\mathrm{g}}(\zeta) + \frac{1}{\rho_\ell}\Gamma_\ell(\zeta)\right)e^{I_{v_{\mathrm{g}}}(\zeta)}\mathrm{d}\zeta\Bigg). \tag{4.56}$$

4.3.3. Lumped pressure dynamics

For the case when the pressure at the topside boundary is exogenous, the equations in the previous sections give a complete description of the simplified two-phase flow model. In many cases, however, the topside boundary pressure is indirectly determined by additional dynamics, e.g. when controlling pressure with a choke valve in Managed Pressure Drilling (Godhavn, 2011; Kaasa et al., 2012).

To model this scenario we use a lumped expression for the pressure dynamics:

$$\frac{\partial P_L}{\partial t} = \frac{\beta_\ell}{V}\left(q_\ell + q_{\mathrm{g}} + T_{E_{\mathrm{g}}} - q_c\right), \tag{4.57}$$

with q_c the volumetric flow rate through the choke, and $T_{E_{\mathrm{g}}}$ the effect of in-domain gas expansion on the lumped pressure dynamics. The term $T_{E_{\mathrm{g}}}$ can be found by integrating the gradient of the gas velocity along the well. Including the $\frac{\partial \rho_{\mathrm{g}}}{\partial t}$ term in (4.38), $T_{E_{\mathrm{g}}}$ can be written as:

$$T_{E_{\mathrm{g}}} = A\int_0^L \frac{E_{\mathrm{g}} + \Gamma_{\mathrm{g}}^*}{\alpha_\ell - \alpha_\ell^*} + \frac{1}{1-\alpha_\ell^*}\frac{\Gamma_\ell}{\rho_\ell}\mathrm{d}x. \tag{4.58}$$

We will now show that the total gas expansion, $T_{E_{\mathrm{g}}}$, can be split into a term affecting the effective bulk modulus of the gas-liquid mixture, $\bar{\beta}$, and a remaining term, T_{XE}, accounting for source terms and the gas expansion when propagating through the negative pressure gradient.

Express the gas expansion dynamics in the principal variables:

$$E_{\mathrm{g}} = -\frac{\alpha_{\mathrm{g}}(\alpha_\ell - \alpha_\ell^*)}{(1-\alpha_\ell^*)\gamma P}\left(\frac{\partial P}{\partial t} + v_{\mathrm{g}}\frac{\partial P}{\partial x}\right), \tag{4.59}$$

$$\frac{\partial P(x,t)}{\partial x} = S(x), \tag{4.60}$$

$$\frac{\partial P(x,t)}{\partial t} \approx \frac{\partial P_L}{\partial t} = \frac{\beta_\ell}{V}\left(q_\ell + q_{\mathrm{g}} + T_{E_{\mathrm{g}}} - q_c\right), \tag{4.61}$$

and consequently the T_{EG} term can be split into a term which includes $\frac{\partial P_L}{\partial t}$ and a remainder

$$T_{E_{\mathrm{g}}} = T_{XE} - A\int_0^L \frac{C_0\alpha_{\mathrm{g}}}{\gamma P}\mathrm{d}x\frac{\partial P_L}{\partial t}, \tag{4.62}$$

$$T_{XE} = A\big(v_{\mathrm{g}}(L) - v_{\mathrm{g}0}\big), \tag{4.63}$$

where we have used the fact that the remainder equals the integrated velocity gradient with the $\frac{\partial \rho_{\mathrm{g}}}{\partial t}$ term excluded.

Inserting the total gas expansion (4.62) into the pressure dynamics (4.57):

$$\frac{\partial P_L}{\partial t} = \frac{\beta_\ell}{V}\left(q_\ell + q_{\mathrm{g}} - q_c - T_{XE} - A\int_0^L \frac{C_0\alpha_{\mathrm{g}}}{\gamma P}\mathrm{d}x\frac{\partial P_L}{\partial t}\right), \tag{4.64}$$

we get

$$\frac{\partial P_L}{\partial t}\left(1+\frac{\beta_\ell}{L}\int_0^L \frac{C_0\alpha_{\rm g}}{\gamma P}\mathrm{d}x\right)=\frac{\beta_\ell}{V}\big(q_\ell+q_{\rm g}-q_c+T_{XE}\big), \tag{4.65}$$

hence

$$\frac{\partial P_L}{\partial t}=\frac{\bar{\beta}}{V}\big(q_\ell+q_{\rm g}-q_c+T_{XE}\big), \tag{4.66}$$

$$\bar{\beta}\equiv\frac{\beta_\ell}{1+\frac{\beta_\ell}{L}\int_0^L\frac{C_0\alpha_{\rm g}}{\gamma P}\mathrm{d}x}, \tag{4.67}$$

where we have defined the effective bulk modulus $\bar{\beta}$.

The complete model is restated in Table 4.1 for convenience.

4.4. Some Numerical Examples

In this section two numerical examples are considered. The first one highlights the effect of removing the pressure dynamics, while the second numerical example illustrates the feasibility of employing the model in a typical scenario from underbalanced drilling.

For both scenarios we consider a 1000-meter long domain with $c_{\rm g}=300\,m/s$, $\rho_\ell=1000\;kg/m^3$, $v_\infty=\alpha_\ell^*=0$. The full Drift-Flux model equations (4.1)–(4.3) are implemented with the AUSM scheme of Evje and Fjelde (2002) while the PDE of the simplified model is implemented with a first order upwind scheme and the integrals evaluated with trapezoidal quadrature. In both cases a grid size of Δx=1 m are used.

4.4.1. Shock Tube

We initially investigate the model in a so-called shock-tube scenario, see Evje and Fjelde (2002). The source terms are set to zero, corresponding to a frictionless horizontal tube, and the simulation is initialized with the domain split in half with $\alpha_{\rm g}=0.2$ and $\alpha_{\rm g}=0.8$ for the right and left domain respectively, and with a right boundary condition of $P(x{=}L)=1$ bar.

The simulation results are shown in Fig. 4.1, where the void wave can be seen propagating towards the right while the faster pressure waves in the full DFM travel back and forth in the domain, being reflected at the boundaries. These pressure oscillations cause perturbations in the void fraction around the *nominal* trajectory followed by the simplified model.

Table 4.1.: The complete Simplified Two-Phase Model

Pressure dynamics:

$$\frac{\partial}{\partial t}P_L(t) = \frac{\bar{\beta}(t)}{V}\big(q_\ell(t) + q_{\mathrm{g}}(t) - q_c(t) + T_{XE}(t)\big), \tag{4.68}$$

$$T_{XE}(t) = A\big(v_{\mathrm{g}}(L,t) - v_{\mathrm{g0}}(t)\big), \tag{4.69}$$

$$\bar{\beta}(t) \equiv \frac{\beta_\ell}{1 + \frac{\beta_\ell}{L}\int_0^L \frac{C_0\alpha_{\mathrm{g}}(x,t)}{\gamma P(x,t)}\mathrm{d}x}, \tag{4.70}$$

Distributed dynamics:

$$\frac{\partial}{\partial t}\alpha_{\mathrm{g}}(x,t) + v_{\mathrm{g}}(x,t)\frac{\partial}{\partial x}\alpha_{\mathrm{g}}(x,t) = E_{\mathrm{g}}(x,t) + \Gamma^*_{\mathrm{g}}(x,t) - \Gamma^*_\ell(x,t), \tag{4.71}$$

$$\alpha_{\mathrm{g}}(x{=}0,t) = \frac{q_{\mathrm{g}}(t)}{C_0(q_{\mathrm{g}}(t) + q_\ell(t)) + Av_\infty}. \tag{4.72}$$

$$\Gamma^*_{\mathrm{g}}(x,t) \equiv \frac{1 - C_0\alpha_{\mathrm{g}}(x,t)}{\rho_{\mathrm{g}}(x,t)}\Gamma_{\mathrm{g}}(x,t), \tag{4.73}$$

$$\Gamma^*_\ell(x,t) \equiv \frac{C_0\alpha_{\mathrm{g}}(x,t)}{\rho_\ell}\Gamma_\ell(x,t), \tag{4.74}$$

Closure relations:

$$\bar{S}(x,t) = -\bar{\rho}_M(x,t)\left(g\sin\theta(x) + \frac{2f(q_{\mathrm{g}}(t) + q_\ell(t)|q_{\mathrm{g}}(t) + q_\ell(t)|}{A^2D}\right), \tag{4.75}$$

$$\bar{\rho}_M(x,t) = \rho_\ell\alpha_\ell(x,t) + \bar{\rho}_{\mathrm{g}}\alpha_{\mathrm{g}}(x,t), \tag{4.76}$$

$$P(x,t) = P_L(t) - \int_L^x \bar{S}(\xi,t)\mathrm{d}\xi, \tag{4.77}$$

$$v_{\mathrm{g}}(x,t) = e^{-I_v(x,t)}\left(v_{\mathrm{g0}}(t) + C_0\int_0^x\left(\frac{c_{\mathrm{g}}^2}{P(\zeta,t)\gamma}\Gamma_{\mathrm{g}}(\zeta,t) + \frac{1}{\rho_\ell}\Gamma_\ell(\zeta,t)\right)e^{I_{v_{\mathrm{g}}}(\zeta,t)}\mathrm{d}\zeta\right), \tag{4.78}$$

$$I_v(x,t) = \int_0^x \frac{C_0\alpha_{\mathrm{g}}(\xi,t)}{P(\xi,t)\gamma}S(\xi,t)\mathrm{d}\xi, \tag{4.79}$$

$$v_{\mathrm{g0}}(t) \equiv \frac{C_0}{A}\big(q_{\mathrm{g}}(t) + q_\ell(t) + v_\infty\big). \tag{4.80}$$

$$E_{\mathrm{g}}(x,t) \equiv -\frac{\alpha_{\mathrm{g}}(x,t)(1 - C_0\alpha_{\mathrm{g}}(x,t))}{\gamma P(x,t)}\left(\frac{\partial}{\partial t}P_L(t) + v_{\mathrm{g}}(x,t)\bar{S}(x,t)\right), \tag{4.81}$$

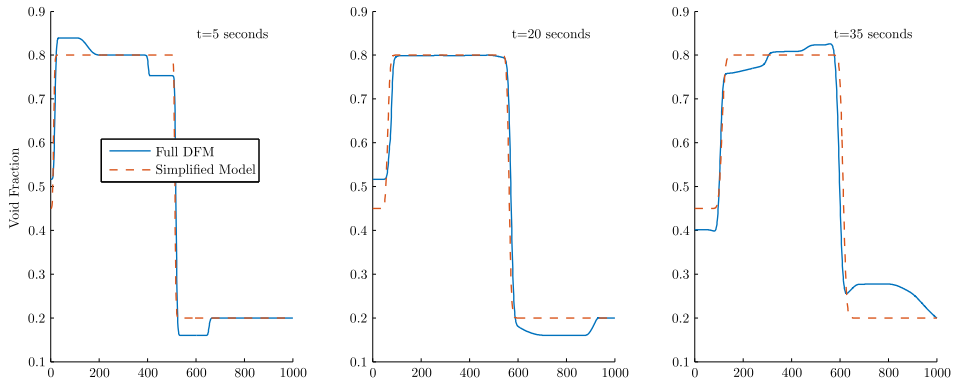

Figure 4.1.: Shock tube test with all source terms set to zero. The pressure dynamics, discarded in the relaxed model, causes the full model to oscillate around the trajectory of the relaxed model. With no source terms to drive the pressure dynamics to the equilibrium, these oscillations would in theory continue indefinitely, although here the effect of numerical diffusion can be seen.

4.4.2. Underbalanced Drilling Connection

Next we consider a scenario relevant for the potential application of the model to underbalanced drilling. When performing a pipe connection in a vertical well, the liquid injection through the drill-string is stopped and the topside back-pressure choke valve opening is reduced so as to try to maintain a constant bottom-hole pressure (Pedersen et al., 2015; Nygaard et al., 2004). This means that liquid rate entering at the left boundary is reduced to a smaller amount accounting for the liquid that would typically be produced by the reservoir. Monitoring and controlling this operation effectively is of importance both for maintaining reservoir and well integrity, as well as for enabling characterization of the reservoir productivity and pore pressure while drilling (Suryanarayana et al., 2007a; Shayegi et al., 2012).

For this scenario, we include the lumped pressure dynamics of Section 4.3.3 where the flow out, q_c, is found from the multi-phase choke relation from Aarsnes et al. (2014b). On the left boundary, a constant gas injection rate is applied while the liquid rate and choke opening are varied according to Fig. 4.2.

The pressure trends in Fig. 4.2 and void profiles in Fig. 4.3 show the model's ability to qualitatively represent the essential dynamics for control and estimation applications in this scenario. We do, however, note the following errors and their causes:

- The steady state error in the downhole pressure $P(x{=}0)$ is due to the approximated momentum source term (4.44), in particular the failure of the approximation to account for the increased frictional pressure loss due to increase in gas velocity towards the rightmost part of the domain. This error can easily be amended by tuning the friction coefficient f.

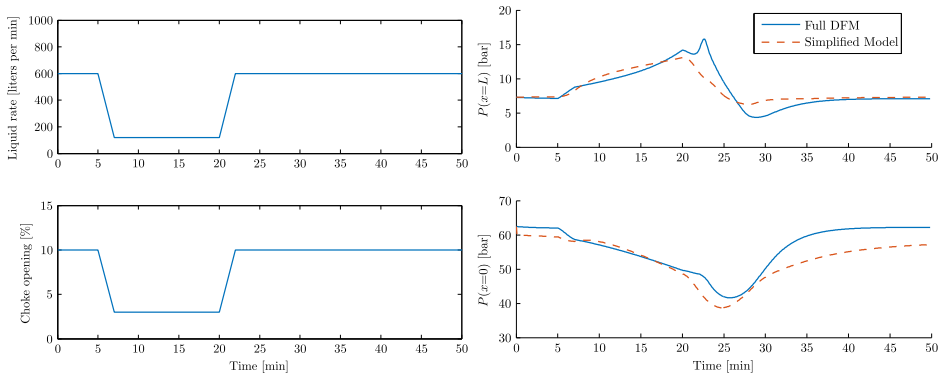

Figure 4.2.: Trends of the changing exogenous variables (**left**) and the topside and bottom-hole pressures (**right**) during the connection scenario.

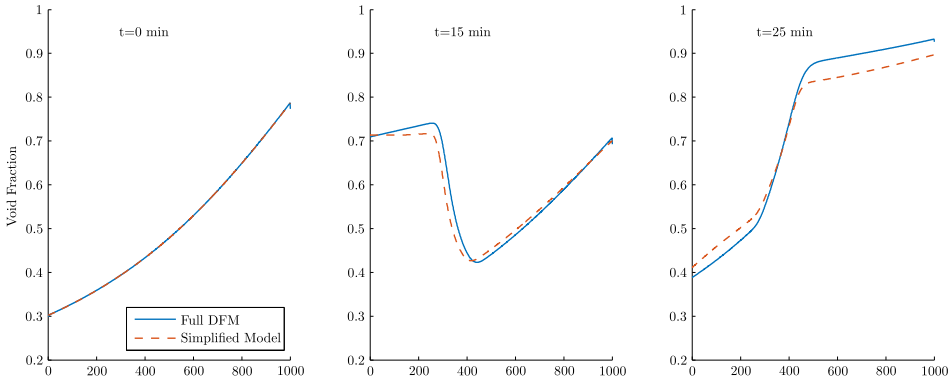

Figure 4.3.: Void fraction profiles before, during and after the connection.

- A significant transient error can be seen during the time periods 5–15 minutes, and 20–30 minutes. This error seems to be connected to the change in pressure at the right boundary which is not taken into account when the velocity profile is computed, see (4.54). This means that the simplified model over- and under-predicts the gas velocity, respectively in each of the two time periods, and this could cause the observed transient error.

These two errors are both due to the approximations done to enable the model to be cast in explicit form. For the time scales of importance in this scenario, the discarded pressure waves do not have significant impact on the accuracy of the results.

4.5. Summary and conclusions

In this paper we have presented a simplified two-phase flow model obtained by relaxing the distributed pressure dynamics, equivalent to using a quasi-steady momentum balance. The resulting model is a transport equation, with void fraction as the distributed state. The gas travels with an exponentially increasing (for negative pressure gradient), quasi-steady velocity driven by the gas expansion, which is modeled as a source term in the transport equation. The closure relations can be approximated as explicit functions and quadratures of the states and exogenous variables. This enables the implementation of simple, fast and robust two-phase simulators, which is amenable for control and estimation applications where simulation speed and robustness are of importance such as Model Predictive Control (Pedersen and Godhavn, 2013) and particle filters (Lorentzen et al., 2014).

To deal with cases where the right boundary condition is specified as a flow rate in place of a pressure, a relation is required to describe the pressure at the boundary. This is done by assuming a lumped pressure for the whole conduit, with dynamics modeled by an ODE coupled with the PDE. The resulting first order ODE model describing the lumped pressure dynamics can for some applications enable the use of established model-based algorithms in pressure control and estimation problems, where the full DFM is too complicated Aarsnes et al. (2016d).

Further work on this topic should deal with the following points not yet addressed:

- More elaborate phase behavior models
- Integrate the model with more accurate closure relations for the pressure drop (i.e. the momentum source term) and the slip law.
- Handle the phenomenon of phase separation in a shut-in scenario.

Chapter 5

Model-Based Estimation of Reservoir Inflow and Pore Pressure

This chapter is based on the work presented in Aarsnes et al. (2015); Ambrus et al. (2015, 2016).

Summary

The ability to perform accurate reservoir and pore pressure characterization during a kick incident is necessary, particularly when drilling in formations with narrow pressure margins. Current available techniques for pore pressure estimation and reservoir characterization either rely on empirical correlations requiring access to well logging data and other petrophysical information, or require downhole pressure sensing and advanced flow metering capabilities. This paper presents a model-based estimation technique which uses surface measurements commonly available in a Managed Pressure Drilling system, coupled with a novel transient two-phase model, capable of representing essential dynamics during a gas kick with reduced computational overhead, without sacrificing significant modeling accuracy . The model is validated in a kick scenario against experimental data and against a commercial multi-phase simulator, showing good agreement between key measured parameters and the model predictions, and thereby justifying the model applicability to field operations. Data from the commercial simulator case and also field data from an MPD operation are used to evaluate the proposed methodology for real-time reservoir characterization. The application yields promising results, where pore pressure and reservoir productivity are estimated within the uncertainty bounds, and the model-predicted flow out rate and surface back-pressure yield a reasonable match to their respective measurements.

5.1. Introduction

With the depletion of easily accessible hydrocarbon resources, the focus of the upstream oil and gas industry has shifted towards harsher environments such as

complex geo-pressured deepwater prospects (Karimi Vajargah et al., 2014). In wells drilled in such challenging environments, it is crucial to maintain the wellbore pressure at a value above both the reservoir pore pressure and the mud pressure required for wellbore stability. Furthermore, wellbore pressure should not exceed the fracture pressure at any time, which effectively limits the available pressure window for safe drilling. Of these pressure limits, the most critical is the pore pressure, as falling below this value in an uncased hole section (e.g. due to insufficient mud weight, poor hydraulics management, improper hole fill-up during tripping or an abnormally pressured zone) leads to influx of formation fluids (oil, water, gas, or a combination thereof) into the wellbore (Aarsnes et al., 2015). Influxes (also known as kicks) tend to be more hazardous when the formation fluids contain gas, which expands in the annulus causing large variations in annular pressure (Karimi Vajargah, 2013). An uncontrolled kick triggers a blow-out, which has potentially catastrophic consequences, impacting rig personnel safety, the surrounding environment, project economics, company and industry reputation (Karimi Vajargah et al., 2014). As a result, the proper planning and execution of well control operations is a major concern in any well being drilled, and the ability to model the gas influx dynamics in real-time, in addition to robustly estimating pore pressure, can significantly improve the success of a well control procedure (Aarsnes et al., 2015).

Managed Pressure Drilling (MPD) techniques enable real-time management of annular pressure and also facilitate dynamic pore pressure testing (Rostami et al., 2015). A particular variant of MPD which has become more prevalent in recent years is the constant bottom-hole pressure (CBHP) technique, which relies on a dedicated choke manifold for applying back-pressure on the annular side. Additionally, CBHP MPD systems include an accurate flow metering system, enabling early kick detection by constant monitoring of return flow in the closed-loop circulation system (Santos et al., 2003). The early kick detection, combined with immediate application of back-pressure by manipulating the size of the choke valve orifice, allows small and medium size kicks to be safely circulated out the of the well without the need for a conventional shut-in operation (Karimi Vajargah et al., 2014; Kinik et al., 2015; Aarsnes et al., 2016a).

In addition to state-of-the art actuation and sensing equipment, the CBHP MPD technique also requires a hydraulics model with multi-phase flow capabilities. Although advanced models have been developed to this end, their complexity makes them impractical for real-time applications such as model-based closed-loop control and estimation. As a result, most control systems in the industry still rely on single-phase dynamic models (e.g. Godhavn (2010); Kaasa et al. (2012); Reitsma and Couturier (2012)). Therefore, introducing a fit-for-purpose model which can capture the essential dynamics of gas expansion with limited computational expense and complexity is highly desirable (Aarsnes et al., 2016d; Ambrus et al., 2015). One potential application of such a model is the real-time estimation of pore pressure and reservoir productivity during a kick incident. This paper introduces a model-based estimation methodology employing a simplified two-phase flow model developed by the authors (Aarsnes et al., 2016b). Experimental test data is used to

validate the model, and subsequently the estimation algorithm is applied on a test case generated using a commercial multi-phase simulator and also field data from an MPD operation, both offering additional opportunities for model validation as well.

5.1.1. Background

The proper knowledge of pore pressure, together with fracture pressure and the pressure required for wellbore stability is a primary factor in the design of a well program prior to drilling the well (Rostami et al., 2015). Traditional methods for determining pore pressure in a drilling operation rely either on repeat formation tests and drill stem tests, or on empirical correlations to petrophysical logs, such as sonic, density and resistivity logs (Aadnøy et al., 2009). One of the most widely used correlation techniques is Eatons method, which is used to estimate pore pressure in shales based on normal compaction trends and data from resistivity and sonic logs, or normalized drilling parameters (d-exponent) Eaton (1975). Another notable technique for pore pressure estimation is Bowers method, which uses a correlation between sonic velocity and effective stress which accounts for the underlying causes of overpressure (Bowers, 1995).

The development of MPD techniques has enabled new approaches to real-time pore pressure estimation during kick incidents. Gravdal et al. (2013) used statistical modeling of the surface back-pressure build-up curve during shut-in to arrive at an estimate of pore pressure. A polynomial curve-fit was used to ascertain the wellbore pressure balanced the formation pressure, such that the measured bottom-hole pressure could be used as the new pore pressure estimate. Application of this algorithm requires a downhole pressure sensor, or an estimate thereof arrived at using a transient model such as the one suggested in this paper. Rostami et al. (2015) described a dynamic pore pressure test for statically underbalanced wells. The test consists of stepwise reduction in surface back-pressure until a micro-influx is detected. The downhole pressure is continuously monitored during the test using a Pressure While Drilling (PWD) tool, and the readings are used to calibrate previous pore pressure esitmates, obtained using Eatons d-exponent method or other similar techniques.

Real-time reservoir characterization has also been facilitated by underbalanced drilling (UBD), where the bottom-hole circulating pressure is intentionally kept below the pore pressure, effectively producing formation fluids while drilling (Vefring et al., 2002). In addition to minimizing reservoir impairment and maximizing production, UBD enables a better understanding of reservoir properties through comparison of real-time production rates to well logging data (Culen and Killip, 2005). Additional information can be inferred from pressure buildup data and gas and liquid flow metering on surface, leading to more accurate estimates of reservoir pressure and productivity index for different reservoir sections (Suryanarayana et al., 2007a; Shayegi et al., 2012).

In addition to the methodologies above, which are mostly empirical and/or

measurement-intensive, several researchers have attempted model-based estimation techniques, relying on physics-based models of the drilling hydraulics. Zhou et al. (2010) used an adaptive observer in conjunction with a single-phase hydraulic model and a linear reservoir model to estimate influx rate and pore pressure in an MPD system. Their estimation algorithm did not take gas expansion into account, which reduced performance when the gas was circulated out. An adaptive observer was also used by Hauge et al. (2012) for estimating the influx rate as well as the depth of the influx zone. A more sophisticated approach, using an infinite-dimensional boundary observer was applied to a transmission line model of the drilling hydraulics in order to estimate influx or lost circulation events occurring in an MPD setting (Hauge et al., 2013a).

In the context of UBD operations, Vefring et al. (2003) used an Ensemble Kalman Filter and the Levenberg-Marquardt method on the Drift-Flux Model coupled with a dynamic reservoir model to estimate reservoir pore pressure and permeability. Biswas et al. (2003) employed a genetic algorithm in conjunction with a transient two-phase reservoir simulator for the problem of estimating reservoir permeability as a function of depth. Aarsnes et al. (2014a) used the Drift-Flux Model in conjunction with an Extended Kalman Filter for on-line estimation the production index, while uncertain model parameters, such as friction factor, choke model coefficients and slip velocity, required off-line calibration.

5.2. The Reduced Drift Flux Model

The Drift-Flux Model (DFM) is one of the multi-phase models which is most frequently used in drilling applications. The DFM consists of separate mass balance equations and a combined momentum balance, together with several closure relations and a slip relation. Although widely employed in well control simulation software (Podio and Yang, 1986; Rommetveit and Vefring, 1991; Petersen et al., 2008), the DFM remains too unwieldy for real-time application in conjunction with model-based estimation and control techniques (Aarsnes et al., 2016d).

Finding efficient numerical solutions of the DFM is considered difficult due to strong non-linear coupling mechanisms and challenges associated with transition to single-phase regions (Evje and Wen, 2013). As such, a series of "reduced" DFMs, also called "No Pressure Wave" models, have been suggested (Taitel et al., 1989; Masella et al., 1998; Choi et al., 2013). These models represented attempts to simplify the classical DFM by imposing a quasi-equilibrium momentum balance, with the goal of simplifying the resulting model equations. The use of these models has been justified for applications where the relatively slow gas propagation dynamics are more important than the fast pressure dynamics. For applications such as MPD, where the transient evolution of the wellhead pressure as controlled by the back-pressure choke is of importance, a relation giving the dynamics of the pressure at the boundary is required (Ambrus et al., 2015). The proposed reduced DFM addresses this issue by adding a first-order ordinary differential equation represent-

ing the pressure dynamics, coupled with a transport equation for the propagation of the void fraction through the well.

In this paper we employ the model presented by Aarsnes et al. (2016b), augmented with the slip law of Shi et al. (2005) to improve performance when compared to full-scale wellbore operations. Main parts of the model are summarized in the following but the reader is referred to Aarsnes et al. (2016b) for details.

The model uses the void fraction $\alpha_{\mathrm{g}}(x,t)$ as the one distributed state, hence a function of the two independent variables x, t denoting position in the well and time. The lumped pressure dynamics is described by the wellhead back-pressure $P_c(t)$, and the dynamic equations are given as:

$$\frac{\partial \alpha_{\mathrm{g}}(x,t)}{\partial t} + v_{\mathrm{g}}(x,t)\frac{\partial \alpha_{\mathrm{g}}(x,t)}{\partial x} = E_{\mathrm{g}}(x,t), \qquad \text{Void wave advection,} \tag{5.1}$$

$$\frac{\partial P_c(t)}{\partial t} = \frac{\bar{\beta}(t)}{V}\big(q_\ell(t) + q_{\mathrm{g}}(t) - q_c(t) + T_{XE}(t)\big), \qquad \text{Lumped pressure.} \tag{5.2}$$

In the PDE (5.1) v_{g} is the gas velocity and E_{g} is a source term accounting for the local gas expansion, given as

$$E_{\mathrm{g}}(x,t) \equiv -\frac{\alpha_{\mathrm{g}}(x,t)(1 - C_0\alpha_{\mathrm{g}}(x,t))}{\gamma P(x,t)}\left(\frac{\partial P_c(t)}{\partial t} + v_{\mathrm{g}}(x,t)S(x,t)\right), \tag{5.3, 5.4}$$

where S is the momentum source term giving the pressure gradient, i.e.

$$P(x,t) = P_c(t) - \int_L^x \bar{S}(\xi,t)\mathrm{d}\xi, \tag{5.5}$$

$$\bar{S}(x,t) = -\bar{\rho}_M(x,t)\left(g\sin\theta(x) + \frac{2f(q_{\mathrm{g}}(t) + q_\ell(t)|q_{\mathrm{g}}(t) + q_\ell(t)|}{A^2 D}\right), \tag{5.6}$$

The gas velocity writes

$$v_{\mathrm{g}}(x,t) = e^{-I_v(x,t)}v_{\mathrm{g}0}(t) \tag{5.7}$$

$$I_v(x,t) = \int_0^x \frac{C_0\alpha_{\mathrm{g}}(\xi,t)}{P(\xi,t)\gamma}S(\xi,t)\mathrm{d}\xi, \tag{5.8}$$

$$v_{\mathrm{g}0}(t) \equiv \frac{C_0}{A}\big(q_{\mathrm{g}}(t) + q_\ell(t) + v_\infty\big), \tag{5.9}$$

where $q_{\mathrm{g}}(t), q_\ell(t)$ are the volumetric mass rates of gas and liquid entering the bottom of the well, and C_0, v_∞ are slip parameters. Finally, the boundary condition writes:

$$\alpha_{\mathrm{g}}(x{=}0,t) = \frac{q_{\mathrm{g}}(t)}{C_0(q_{\mathrm{g}}(t) + q_\ell(t)) + Av_\infty}. \tag{5.10}$$

For the lumped pressure dynamics (5.2), the effective bulk modulus $\bar{\beta}$ and total effective gas expansion T_{XE} are given as

(5.11)

$$\bar{\beta}(t) \equiv \frac{\beta_\ell}{1 + \frac{\beta_\ell}{L}\int_0^L \frac{C_0 \alpha_{\mathrm{g}}(x,t)}{\gamma P(x,t)} \mathrm{d}x}, \tag{5.12}$$

$$T_{XE}(t) = A\big(v_{\mathrm{g}}(L,t) - v_{\mathrm{g}0}(t)\big). \tag{5.13}$$

It should be noted that, due to the simplifying assumptions, the formulation does not handle scenarios where the well is completely shut-in (i.e. with both the blow-out preventers and choke closed), as it can prescribe only one boundary condition. In a shut-in case, an additional boundary condition is required to accommodate a zero net flow rate at the well head. This limitation can however be avoided if the slip velocity is low enough (or the well long enough) such that the gas bubble does not reach the well head before the circulation is resumed and the well control choke is opened. Furthermore, this is not an issue for well control operations in MPD, where up to a certain kick size, a complete shut-in is not required to safely bring the well back to overbalance.

5.2.1. Slip velocity Model

We use the slip velocity model of Shi et al. (2005), i.e.

$$v_\infty = \frac{1 - \alpha_{\mathrm{g}} C_0 K(\alpha_{\mathrm{g}}) v_c}{\alpha_{\mathrm{g}} C_0 \frac{\rho_{\mathrm{g}}}{\rho_\ell} + 1 - \alpha_{\mathrm{g}} C_0}, \tag{5.14}$$

where

$$v_c = \left(\frac{\sigma g(\rho_\ell - \rho_{\mathrm{g}})}{\rho_\ell^2}\right)^{\frac{1}{4}}, \tag{5.15}$$

$$K(\alpha_{\mathrm{g}}) = \begin{cases} \frac{1.53}{C_0}, & \alpha_{\mathrm{g}} \leq 0.2 \\ 3.182\Big(1 - e^{-\frac{\hat{D}}{9.3833}}\Big), & \alpha_{\mathrm{g}} > 0.4 \end{cases} \tag{5.16}$$

with

$$\hat{D} = \sqrt{\frac{g(\rho_\ell - \rho_{\mathrm{g}})}{\sigma}} D. \tag{5.17}$$

For values of α_{g} between 0.2 and 0.4, a linear interpolation between the $K(\alpha_{\mathrm{g}})$ values in Eq. (5.16) can be used.

5.3. Model Validation

The reduced DFM formulated in the previous is validated using commercial multi-phase simulator OLGA, and also using experimental data from a gas kick event simulated by injecting natural gas into a well used for test purposes.

Table 5.1.: Input data for OLGA simulator scenario.

Parameter	Value	Unit
Well depth	12,100	ft
Casing shoe depth	8,000	ft
Casing size	9.625	in
Hole size	8.5	in
Drill pipe outer diameter	3	in
Circulation rate	200	gpm
Mud weight	12	lb/gal
Fluid viscosity	30	cP
Bulk modulus	3105	psi
Annulus friction factor	7.210-3	-
Formation pore pressure	7750	psi
Choke valve coefficient	0.0694	ft^2
Choke gas expansion factor	0.3	-
Specific heat ratio	1.3	-
Surface temperature	60	F
Bottom-hole temperature	150	F
Slip law profile parameter	0	-

5.3.1. High fidelity simulator

The scenario generated using the commercial simulator is that of a 12,100 ft deep vertical land well drilled with a CBHP MPD system. For simplicity, it is assumed that drill pipe extends all the way to the bottom of the well, and that casing is set to a depth of 8,000 ft. 12-ppg water-based mud is circulated at a constant rate of 200 gpm. A dry gas reservoir with an average pore pressure of 7,750 psi is encountered at 12,090 ft. The well is initially underbalanced by approximately 300 psi, which results in a 10-bbl kick taken over a period of 10 minutes (time t=0 corresponds to the start of the kick). Choke opening is then decreased and the additional back-pressure brings the well to an overbalanced state. The amount of choke opening is subsequently adjusted by the software to maintain a constant bottom-hole pressure at 7,900 psi. A linear temperature profile is assumed throughout the simulation.

Table 5.1 summarizes the parameters used in this simulation scenario. The gas influx rate along with the choke opening profile generated by the simulator, presented in Figure 5.1, are entered as inputs to the reduced DFM.

As Figure 5.2 and Figure 5.3 indicate, there is a good agreement between the downhole and wellhead pressures, and also the flow out and pit gain computed by the proposed model and those obtained from the commercial simulator. Slight discrepancies towards the end of the simulation can be attributed to uncertainty in the choke flow model when gas reaches the choke. Examining the gas volume fraction profiles in Figure 5.4 also indicates a good agreement until the gas influx reaches the surface.

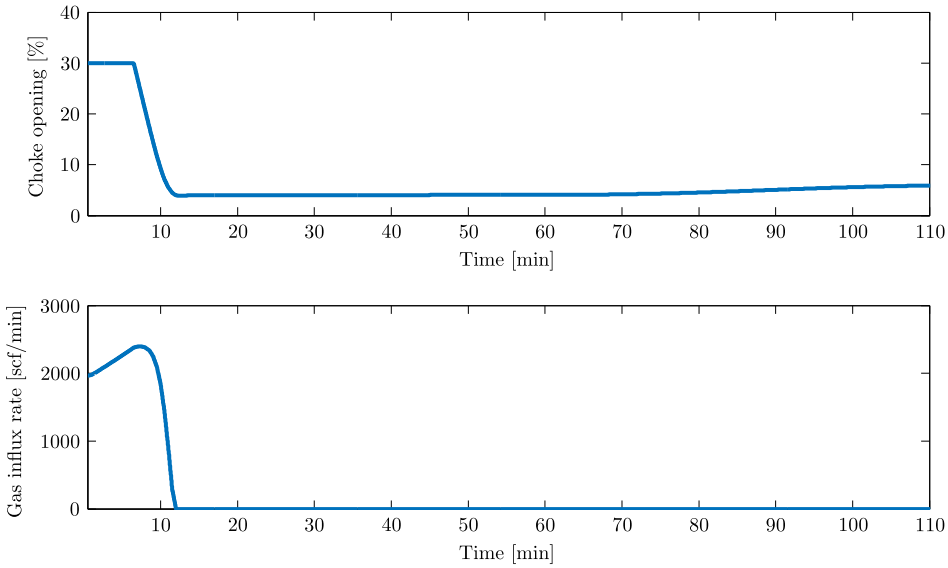

Figure 5.1.: Choke opening and gas influx rate used in the simulations.

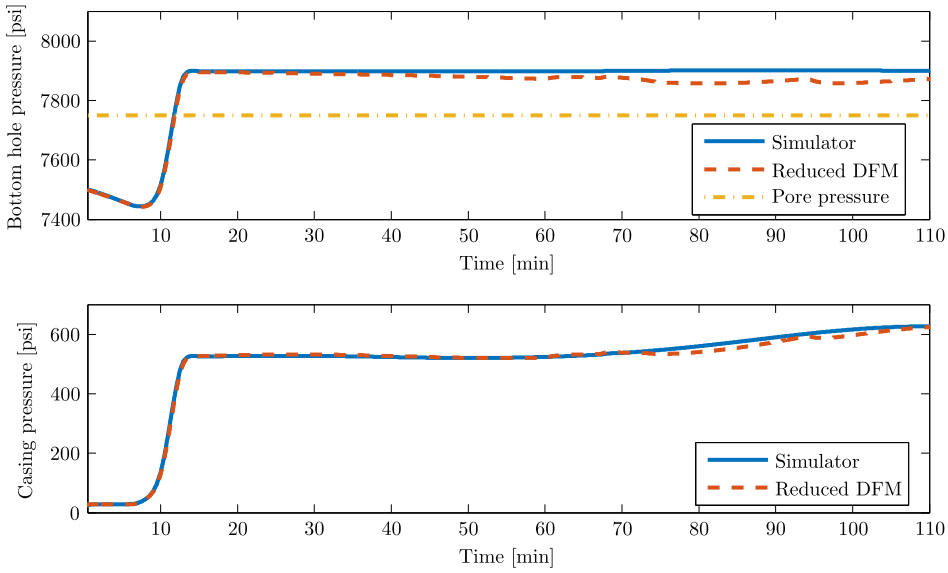

Figure 5.2.: Comparison of the commercial simulator with the reduced DFM, bottom-hole pressure (upper) and casing pressure (lower).

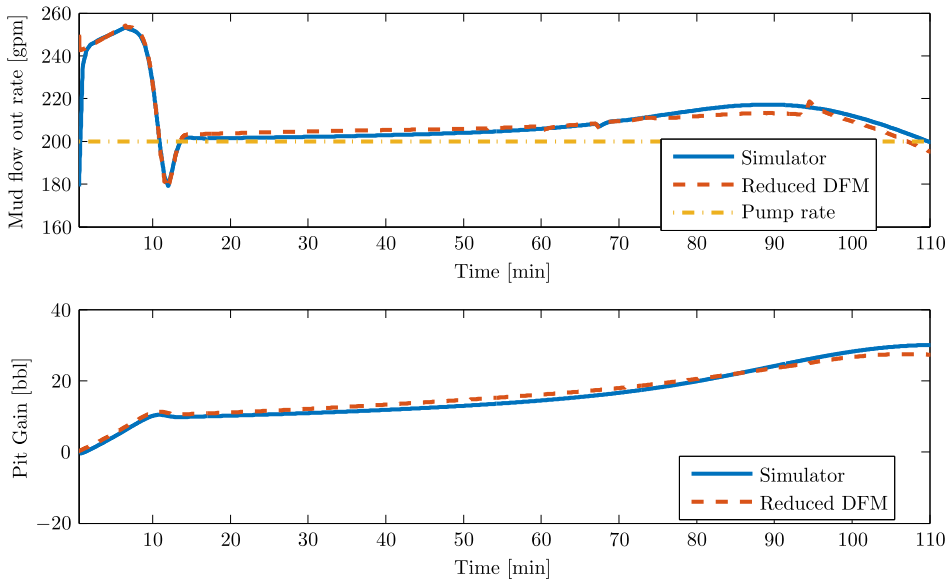

Figure 5.3.: Comparison of the commercial simulator with the reduced DFM, mud flow out (upper) and pit gain (lower).

5.4. Experimental data

The model described in the previous section was validated on an experimental data set obtained from a well control test conducted at Louisiana State University. The test setup, illustrated in Figure 5.6, was detailed by Chirinos et al. (2011). An 11-bbl gas kick was simulated by injecting natural gas inside the 1.25-in tubing while water-based mud was continuously pumped through the annulus formed by the 3.5-in drill pipe and the 1.25-in tubing, with returns taken through the annulus between the 9.625-in casing and the 3.5-in drill pipe. A manually operated choke manifold was used to provide back-pressure, with the goal of keeping a constant drill pipe pressure throughout the gas circulation. The mud circulation and gas injection rate recorded during the test were used as inputs to the model and are shown in Fig. 5.7. Well geometry, mud properties and other model inputs are detailed in Table 5.2.

The reduced DFM was implemented using an explicit, first-order upwind scheme with a time step of 1 second and 200 grid cells. The simulation results were compared to flow out and pit gain data (Fig. 5.8) as well as pressure data recorded from the experiment (Fig. 5.9), showing excellent match for pressure and reasonable agreement for the pit gain and flow out, as indicated by the percent errors in Table 5.3.

For flow out, it is noted that around the 100-minute mark in the simulation, the measured values became erratic, possibly due to the presence of gas in the

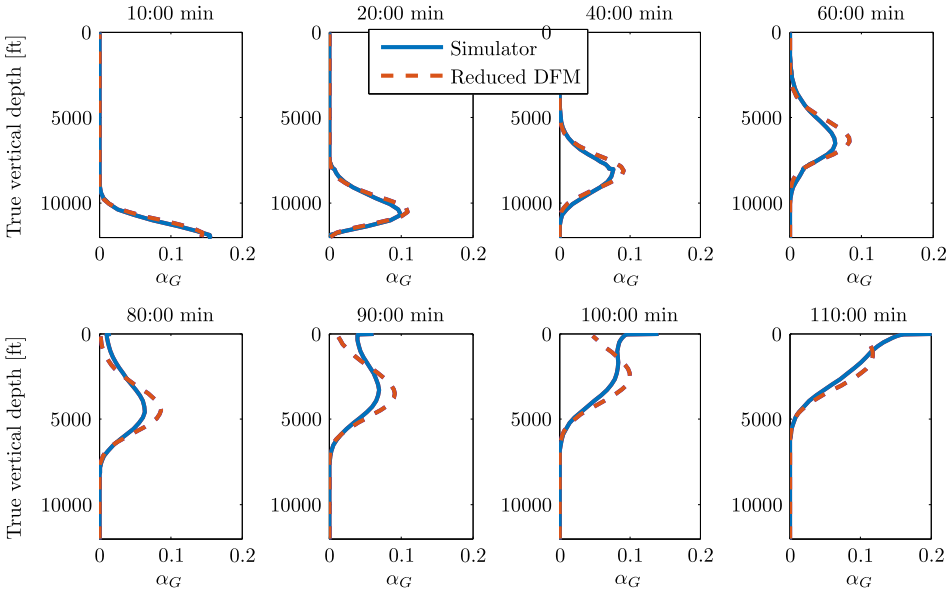

Figure 5.4.: Comparison of the commercial simulator with the reduced DFM, gas volume fraction along the depth during gas migration.

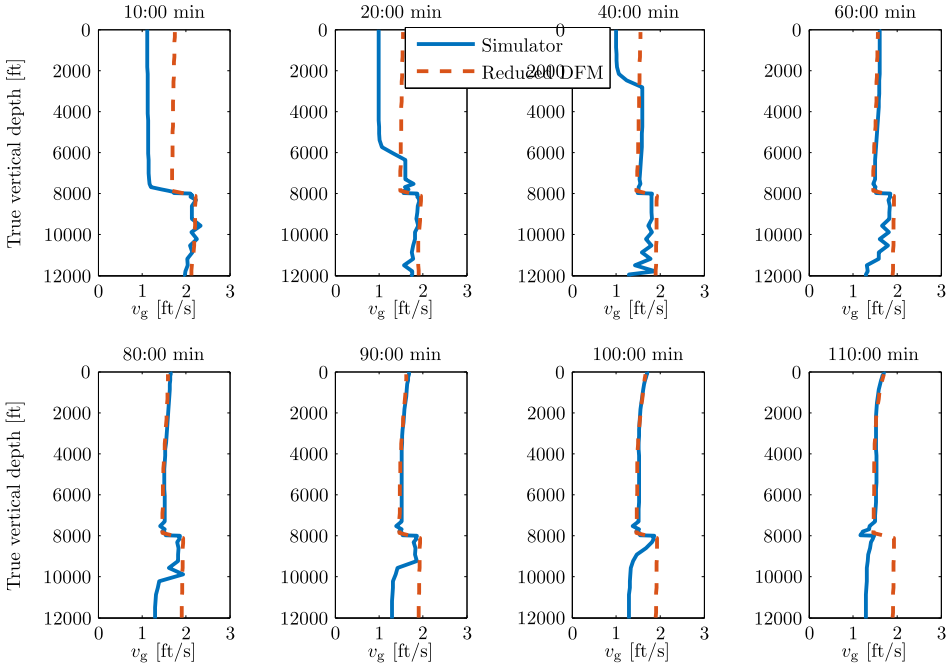

Figure 5.5.: Comparison of the gas velocities. Note that the discrepancy for when the $\alpha_g(x) = 0$ has no bearing on the actual simulation.

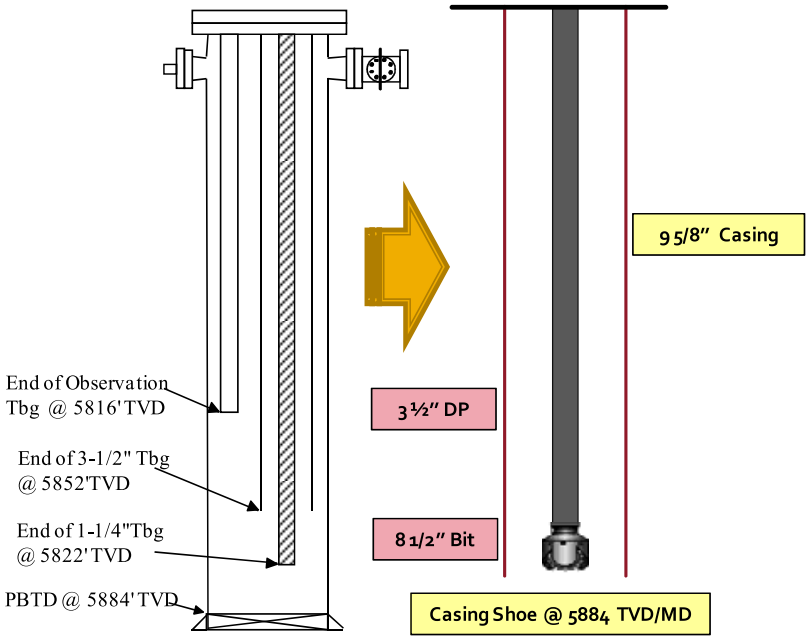

Figure 5.6.: Louisiana State University well schematic (Chirinos et al., 2011).

Table 5.2.: Input data for simulation on experimental data set.

Parameter	**Value**	**Unit**
Well depth	5,884	ft
Casing shoe depth	5,884	ft
Casing size	9.625	in
Drill pipe outer diameter	3.5	in
Gas injection tubing diameter	1.25	in
Circulation rate	90-150	gpm
Drilling fluid density	8.6	lb/gal
Plastic viscosity	8	cP
Yield point	2	lb/(100ft^2)
Bulk modulus	2.15105	psi
Annulus friction factor	7.410-3	-
Drill pipe friction factor	7.310-3	-
Choke valve coefficient	0.107	ft^2
Choke gas expansion factor	0.25	-
Specific heat ratio	1.3	-
Surface temperature	93	F
Bottom-hole temperature	140	F
Slip law profile parameter	0	-

Table 5.3.: Average percent error between experimental data and reduced DFM

Parameter	Average percent error
Bottom-hole pressure	0.5
Casing pressure	1.9
Flow out rate	28.9
Pit gain	10.4

flow meter. As far the pressure measurements are concerned, since there was no down-hole pressure sensor available in the experimental setup, the bottom-hole pressure was inferred from the drill pipe pressure (measured at the stand pipe) according to the following formula (Guo and Liu, 2011):

$$P_{bh} = P_d + \rho_\ell g h - \frac{2 f_d \rho_\ell q_\ell^2}{A_d D_d} L \tag{5.18}$$

where P_d is the recorded drill pipe pressure and f_d is the drill pipe friction factor.

5.5. Proposed Methodology for Pore Pressure and Reservoir Inflow Estimation

In this section, we present an approach for estimating the inflow rate and pore pressure of the flowing zone based on drilling parameters recorded during a kick. This requires a fit-for-purpose hydraulics model and a reservoir model, which correlates flow from the reservoir to the pressure drawdown, and also to a productivity index, a lumped parameter which is affected by the length of exposed zone, reservoir permeability, porosity, skin factor, reservoir fluid viscosity and compressibility (Vefring et al., 2003). For this application, we are more interested in the qualitative relationship between inflow rate, productivity and pore pressure, thus we use a qualitatively correct, linear inflow relationship (Shayegi et al., 2012):

$$q_{res} = J(P_{res} - P_{bh}), \tag{5.19}$$

with P_{res} the reservoir pressure and J the productivity index. In the above, it is assumed that $P_{res} > P_{bh}$ (i.e. well is underbalanced), otherwise, q_res is set to zero. Eq. (5.19) can be recast in a form more amenable for parameter estimation

$$q_{res} = \phi^T X, \tag{5.20}$$

where $X = \begin{bmatrix} JP_{res} \\ J \end{bmatrix}$ is the vector of unknown or uncertain parameters and $\phi = \begin{bmatrix} 1 \\ -P_{bh} \end{bmatrix}$ is the regressor. Since, for kick incident, q_{res} is not directly measured, we will instead use and estimate $\hat{q}_{res}$.

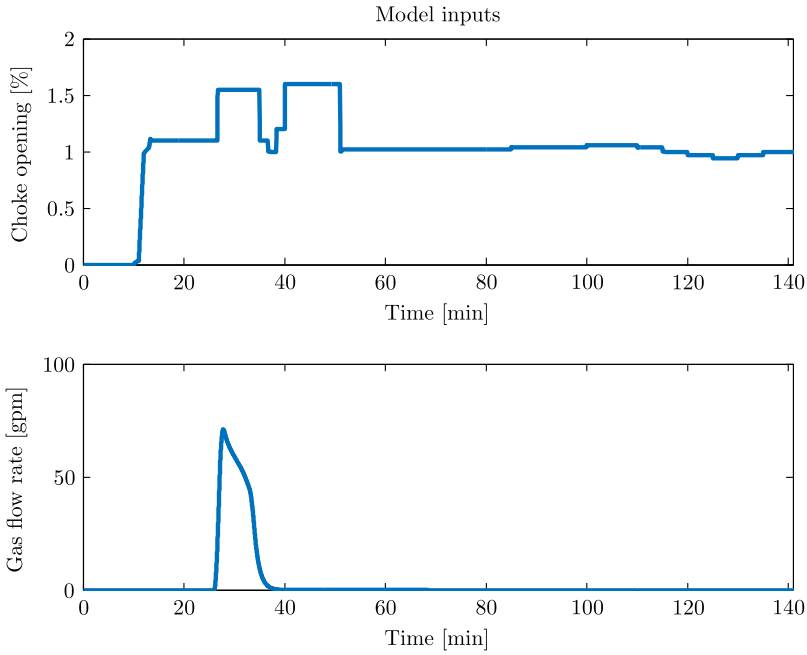

Figure 5.7.: Choke opening and gas injection rate for experimental test scenario.

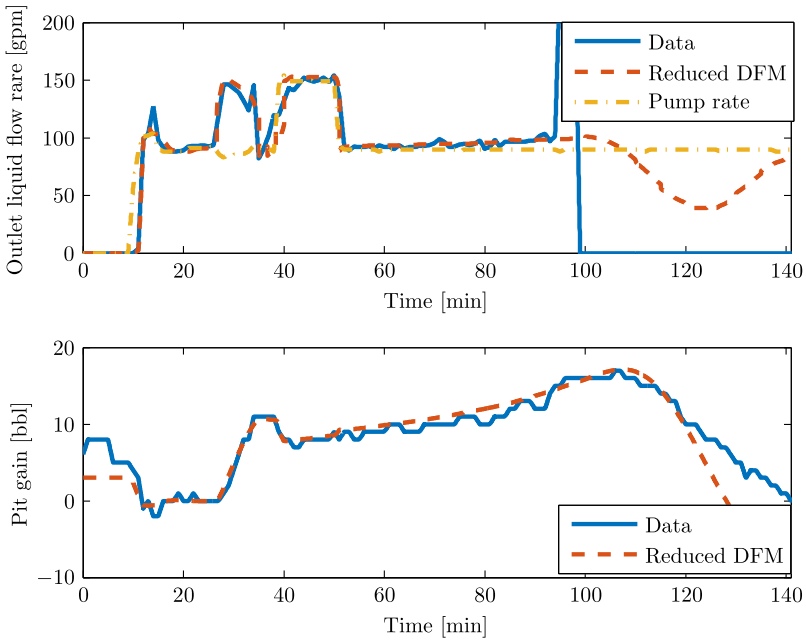

Figure 5.8.: Comparison of experimental data with the reduced DFM, mud flow out (upper) and pit gain (lower).

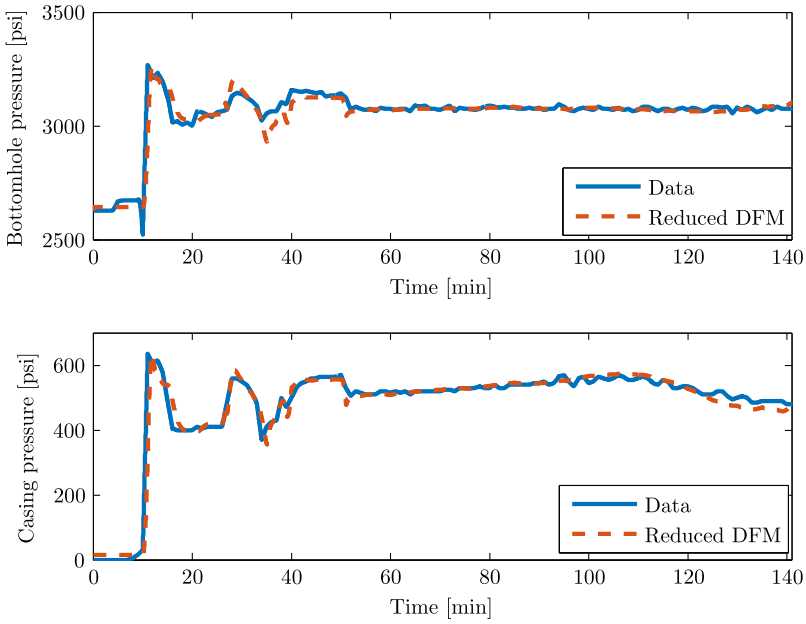

Figure 5.9.: Comparison of experimental data with the reduced DFM, bottom-hole pressure (upper) and casing pressure (lower).

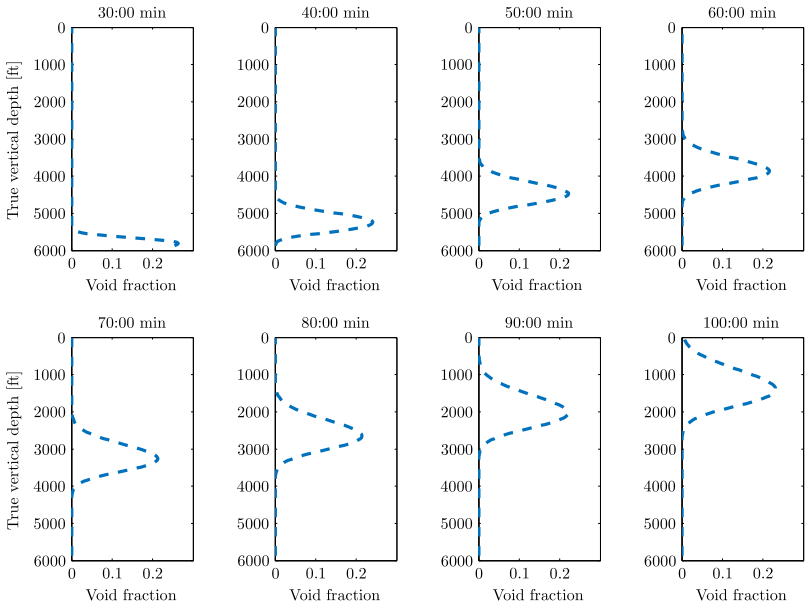

Figure 5.10.: Gas volume fraction along the depth, as predicted by reduced DFM.

As a baseline, we can compute $\hat{q}_{res}$ from the instantaneous mud flow out rate minus the mud injection rate, however, this is susceptible to measurement noise (particularly in flow out), and does not account for dynamics due to pressure changes and gas expansion as the kick is circulated. Therefore, we employ the first-order pressure dynamics from Eq. (5.2), where we use $\hat{q}_{res}$ in place of the gas source term q_{g} and we isolate all terms which explicitly depend on $\hat{q}_{res}$ (Note: in the following, all parameters which are estimated or derived from estimated quantities are denoted with a $\hat{}$ superscript):

$$\frac{\partial P_c}{\partial t} = \frac{\hat{\beta}}{V}\Big(q_\ell - q_c + \hat{q}_{res} + I_0 + 2(q_\ell + \hat{q}_{res})^2 I_1\Big), \tag{5.21}$$

with

$$I_0 = \int_0^L \frac{C_0 \hat{\alpha_{\mathrm{g}}}}{\gamma \hat{P}} \hat{v}_{\mathrm{g}} \hat{\rho}_M g \sin(\theta(x)) A \mathrm{d}x, \tag{5.22}$$

$$I_1 = \int_0^L \frac{C_0 \hat{\alpha_{\mathrm{g}}}}{\gamma \hat{P}} \hat{v}_{\mathrm{g}} \frac{f}{AD} \mathrm{d}x, \tag{5.23}$$

where I_0, I_1 account for gas expansion due to the hydrostatic and frictional pressure gradients, respectively. Note in the above that $\hat{v}_{\mathrm{g}}$ is computed from Eqs. (5.7)–(5.9) and the quantities $\hat{\beta}, \hat{P}, \hat{v}_{\mathrm{g}}, \hat{\alpha}_{\mathrm{g}}$ are also estimates of the true values as they all depend on $\hat{q}_{res}$. For MPD scenarios, where kick size is usually limited, we can assume $q_{res}^2 \ll q_\ell^2$, and thus neglect the quadratic q_{res} term in Eq. (5.21), which yields:

$$\frac{\partial P_c}{\partial t} = \frac{\hat{\beta}}{V}\Big(q_\ell - q_c + I_0 + 2q_\ell I_1 + \hat{q}_{\mathrm{g}}(1 + 4q_\ell I_1)\Big). \tag{5.24}$$

This equation can be low-pass filtered to remove noise in the measurements, and also to allow a mathematical formulation which enables linear regression techniques. Using Laplace transform notation for the low-pass filter $F(s) = 1/(\tau s + 1)$, we have

$$\frac{s}{\tau s + 1} P_c - \frac{1}{\tau s + 1}\frac{\hat{\beta}}{V}\Big(q_\ell + q_c + I_0 + 2q_\ell^2 I_1\Big) = \frac{1}{\tau s + 1}\left\{\frac{\hat{\beta}(1 + 4q_\ell I_1)}{V}\phi^t X\right\} \tag{5.25}$$

Denoting the left-hand side of (5.25) by y and the term $\frac{1}{\tau s+1}\left\{\frac{\hat{\beta}(1+4q_\ell I_1)}{V}\phi^t X\right\}$ by ψ allows us to finally write a linear equation of the form $y = \psi^T X$, which can be solved using an on-line regression technique, such as recursive least squares (RLS) Ljung (1999). Details of the RLS implementation are provided in Appendix 5.A. Using the notation above, an alternate approach to estimating influx rate is by computing the instantaneous estimate:

$$\hat{q}_{res}^{inst} = \frac{\mathbf{V}\mathbf{y}}{\hat{\beta}(1 + 4q_\ell I_1)}. \tag{5.26}$$

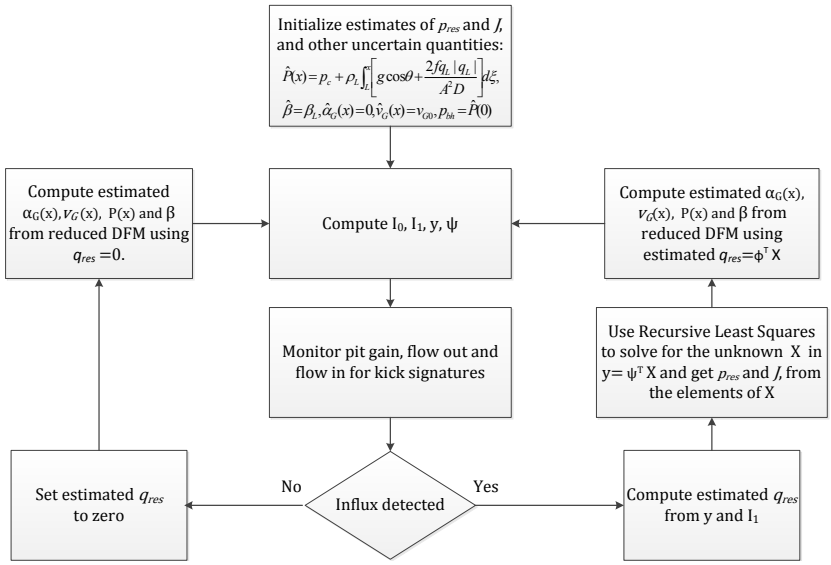

Figure 5.11.: Proposed estimation methodology.

The estimation methodology is summarized in Fig. 5.11. Since the reservoir model (5.19) is only valid while the well is underbalanced, the RLS algorithm can only be applied on a narrow time window starting from the detection of the kick up to the point when the well reaches an overbalanced state and inflow from the formation ceases. Thus, in order to ensure the estimated parameters do not diverge from the values computed while the well is underbalanced, the RLS method needs to be stopped as soon as the flow out and pit gain trends stabilize. As the gas percolates in the annular space, a slow increase in flow out and pit gain will be still observed, but the rate of change is much slower than when the kick enters the wellbore, and should not be misinterpreted as additional influx.

5.6. Validation of Estimation Methodology

5.6.1. Commercial Multi-Phase Simulator Case

The pore pressure and reservoir inflow estimation methodology was first tested on a MPD well control scenario generated using the commercial multi-phase simulator OLGA (Bendiksen et al., 1991). As a simulation case the same scenario from the validation section was used, see Table 5.1. At 12,090 ft the well intersected a dry gas reservoir with an average pore pressure of 7,750 psi, and a linear PI model was

Table 5.4.: Drilling parameters (Kinik et al., 2015).

Drill string	7,810ft 4" DP/w 253ft 4.5" BHA
Bit	5.25" PDC - 8x14" nozzles
Rig Pumps	2 triplex /w 12" Stroke x 5.5" Liner - 95% Efficiency
Auxiliary Pump	Triplex /w 6" Stroke x 4.5" Liner - 96% Efficiency
Intermediate Casing	34.2lb/ft 7"OD-6.36"ID at 6,535ft MD/TVD

used to simulate the reservoir influx. The initial underbalance of 300 psi resulted in a 10-bbl kick taken over a period of 10 minutes. The choke opening was then reduced with the resulting back-pressure bringing the well to an overbalanced state. The built-in controller in OLGA adjusted the choke opening to maintain a target bottom-hole pressure of 7,900 psi.

The flow out trend is shown in Fig. 5.12, together with the estimate of the gas influx rate, with both the RLS and instantaneous result. It should be noted that both show good agreement to the OLGA values during the kick, but the instantaneous estimate goes negative after the gas reaches the surface. Fig. 5.13 shows the estimates of pore pressure and PI, which converge in the proximity of the actual values (pore pressure estimate converged within 30 psi of the OLGA input, which is reasonable for practical purposes). This error can be further reduced if P_{bh} is directly measured from PWD equipment, instead of being computed from the reduced DFM. It is worth mentioning here that the RLS algorithm was started after an initial pit gain of 0.5 bbl, which is sufficiently early to capture the magnitude of the influx, however, if higher thresholds are used for starting the algorithm, some of the gas entering the well would not be accounted for by the model, leading also to larger estimation errors. These results are based on the RLS estimated q_{res}.

5.6.2. Field Data Case

The pore pressure and reservoir inflow estimation methodology was also implemented on data from a deviated well drilled in the western Canadian sedimentary basin. A methane kick was taken at a measured depth of 8,063 ft while drilling the build-up section with a 10.3 lbm/gal oil-based mud. The key drilling parameters are provided in Table 5.4, while the mud properties are detailed in Table 5.5. A CBHP MPD system was being used in the section, which enabled quick detection of the kick after a pit gain of 17 gal (Kinik et al., 2015), and back-pressure was subsequently applied from surface using an automatically controlled hydraulic choke. The driller picked up off bottom, stopping rotation and keeping circulation at 250 gpm while circulating the gas kick out of the well.

The top plot of Fig. 5.14 shows the mud flow out rate measured by a Coriolis flow meter, indicating the onset of the kick and the moment when overbalance in the well is restored as a result of the back-pressure applied from surface. The lower plot of Fig. 5.14 shows the estimated influx rate from the formation, using the RLS algorithm, as well as the instantaneous value. The RLS algorithm was initiated

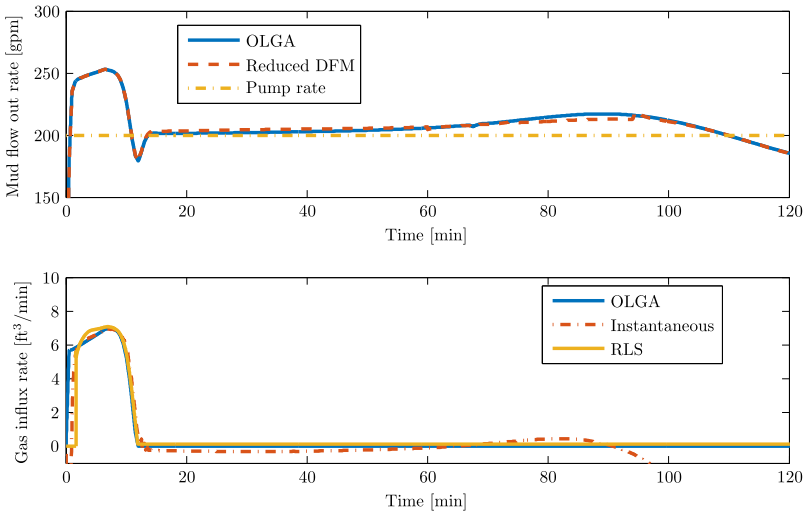

Figure 5.12.: Mud flow rate out from OLGA and predicted by the reduced DFM (upper); estimated gas influx rate (lower).

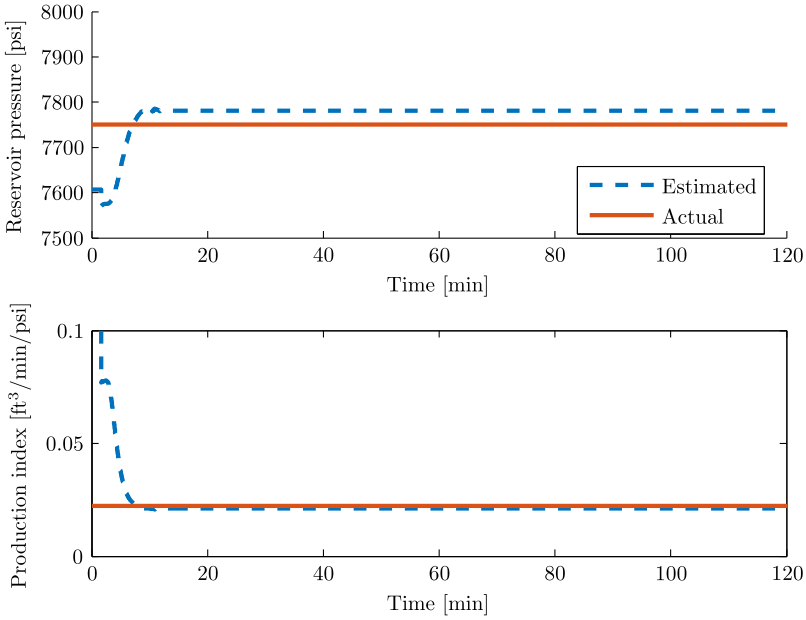

Figure 5.13.: Reservoir pore pressure (upper) and PI (lower) estimated by the RLS algorithm. Actual data are OLGA simulation inputs.

Table 5.5.: Drilling mud properties (Kinik et al., 2015).

Density	10.3ppg OBM Diesel Oil No2
Retort analysis	Water=16%, Oil=64%, (OWR = 81/19)
Fann35 Rheology	$\theta_{600}/\theta_{300}/\theta_3 = 337/21/4$ at 110°F
Thermal properties	Heat capacity = 0.42 Ntu/lb-ft, Thermal conductivity = 0.30 Btu/ft-°F-hr

after the differential flow rate (i.e. return flow minus flow in rate) exceeded 0.5 bbl over 30 seconds, and was stopped after the differential flow rate decreased to 0.1 bbl over 30 seconds. The instantaneous influx rate was computed throughout the simulation, yielding a reasonable pattern during the period of underbalance, but becoming erratic when the well is overbalanced and the kick is being circulated out. Thus, it is important to evaluate whether the algorithm detects actual influx or the effects of gas expanding as it travels upward in the annulus.

During the RLS estimation, measured flow out and back-pressure were fed back to the algorithm for determining $\hat{q}_{res}$ but after the influx ceased, the model was run in a feedforward mode (thus allowing comparison of predicted flow out and back-pressure to their measurements). The discrepancy in the flow out after 45 minutes could be attributed to gas breaking out of the drilling mud as the pressure falls below the bubble point pressure of the oil phase. It should be noted that he reduced DFM used in this simulation did not include mass transfer terms, and neglecting the gas dissolution in the oil-based mud may lead to erroneous prediction of the expansion, particularly once gas breaks out of the solution; however, the overall pit gain in an oil-based mud will normally be less than in water-based mud (Karimi Vajargah, 2013). While this modeling limitation was acknowledged, the data set was nevertheless pursued in order to evaluate the pore pressure and inflow estimation algorithm, which should not be affected by the phase behavior, as significant expansion and changes in mud compressibility would not happen during the period of active reservoir inflow.

The estimated values of pore pressure and PI are plotted in Fig 5.15. The estimated values were initiated with 4480 psi, and 1.461 ft^3/min/psi, respectively. Since the true value of pore pressure for this well was not available, a range of possible values was determined, based on offset well data (Contreras et al., 2013) and also based on the observed bottom-hole pressures before and after the kick event (used as hard limits which the pore pressure could not go beyond). This resulted in a 300 psi uncertainty margin. Similarly, a range of possible PI values were determined based on the estimated influx rates and the pressure draw-downs obtained using the minimum and maximum pore pressure values. As Fig. 5.15 indicates, the estimated values arrive within these limits once the kick is detected at 26.5 minutes in the simulation, and stay inside the region until the estimation algorithm is halted 3 minutes later, at which point the last valid estimates are saved. The algorithm ultimately determined a pore pressure of 4,916 psi and a PI

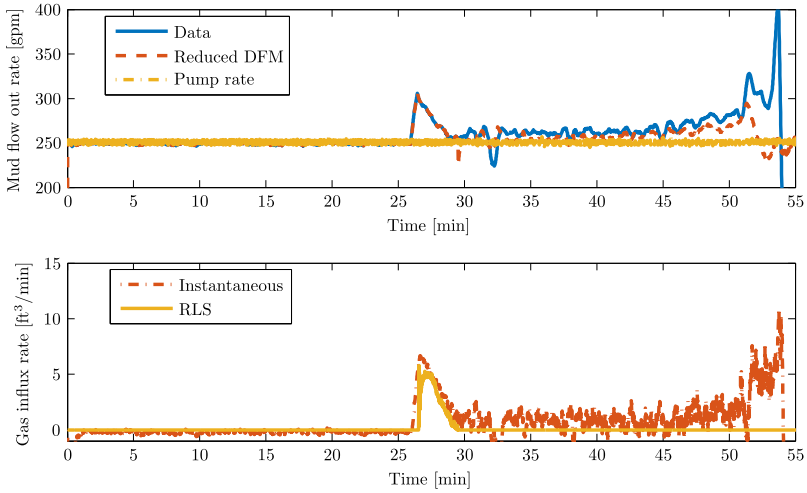

Figure 5.14.: Mud flow rate out measured and predicted by the reduced DFM (upper); estimated gas influx rate (lower).

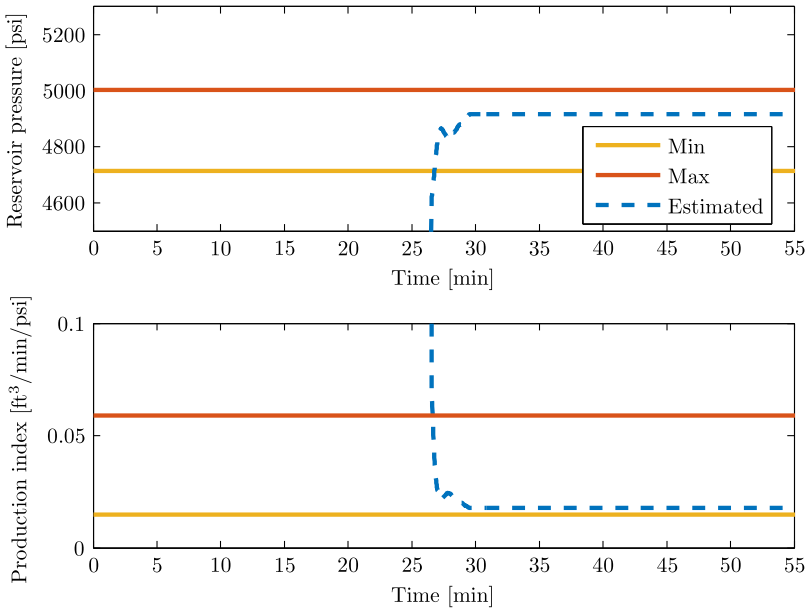

Figure 5.15.: Reservoir pore pressure (upper) and PI (lower) estimated by the RLS algorithm.

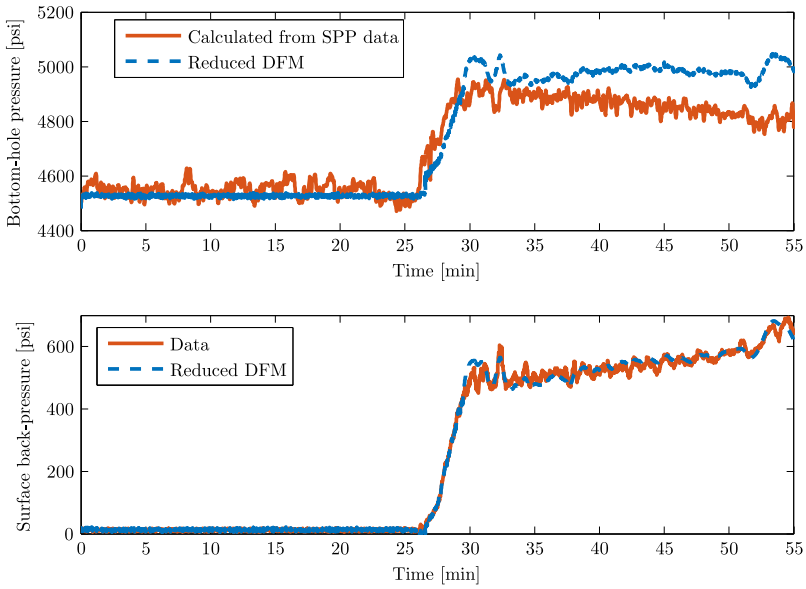

Figure 5.16.: Bottom-hole pressure from OLGA and predicted by the reduced DFM (upper); surface back-pressure from OLGA and predicted by reduced DFM (lower).

of 0.0178 ft3/min/psi.

Fig 5.16 shows bottom-hole pressure and surface back-pressure before and during the kick incident. The back-pressure predicted by the reduced DFM matches the actual data, with both indicating an increasing trend as the gas kick is circulated. Bottom-hole pressure was not directly measured in the well, but can be indirectly computed from the surface pressure data:

$$P_{bh} = P_d + P_{G,d} - P_{F,d} - P_{bot} \tag{5.27}$$

with P_d denoting the drill pipe or standpipe pressure (SPP), P_{bot} is the difference between on-bottom and off-bottom pump pressure, and $P_{G,d}, P_{F,d}$ are hydrostatic and frictional pressure drop in the various drillstring components (these include the pressure drop generated through the bit nozzles, mud motor etc.). The bottom-hole pressure computed using Eq. (5.27) agrees for the most part with the value from the reduced DFM, except for a portion towards the end of the simulation, possibly due to an under-estimation of the oil-based mud expansion. As shown in Fig. 5.15, the RLS estimated q_{res} is lower than the expected value based on instantaneous estimates, which implies that the reduced DFM may under-predict the influx, regardless of solubility considerations. This is a point of future work for this approach.

5.7. Conclusions

Proper determination of pore pressure and other parameters which affect the production of reservoir fluids is vital for successful well construction, particularly in geo-pressured environments where narrow margins between pore and fracture pressure present significant operational challenges to drilling and completion activities. While conventional methods for estimating pore pressure and / or reservoir productivity (or equivalently, the inflow rates obtained for a given pressure drawdown) resort to empirical correlations based on petrophysical logs, or require sophisticated multi-phase flow metering and downhole pressure measurements. This paper presents a novel approach which leverages a fast transient two-phase wellbore flow model, and a Recursive Least Squares regression technique. Preliminary validation on field data from an MPD kick incident highlights the potential of this model-based estimation method.

Further work on this topic, aside from validation on additional data sets and field scenarios, should extend the algorithms to accommodate more general reservoir inflow performance (Wiggins et al., 1996) and possible non-linear extensions to the least squares regression technique. To this end, techniques such as Extended Kalman filters, particle filters or neural network regression can be investigated. While this paper focused on MPD applications, the approach can be readily applied on UBD or conventional well control scenarios. Further improvements can also be made on the reduced DFM, particularly incorporating mass transfer and more elaborate phase behavior models. Ultimately, the estimation methodology together with the reduced DFM can be integrated within an automated well control decision-making framework (Karimi Vajargah et al., 2014).

Appendix

5.A. Recursive Least Squares Algorithm

We start from the linear model

$$y = \phi^T X \tag{5.28}$$

where y and ϕ represent measured parameters (y is a scalar, while ϕ is a vector) and X is the vector of unknown parameters. If we denote $\hat{X}(t)$ as the time-varying estimate of X, $P(t)$ the covariance matrix and $0 < \lambda \leq 1$ the forgetting factor, we have the RLS scheme (Ljung, 1999):

$$\mathbf{P}(t) = \frac{1}{\lambda}\Big[\mathbf{P}(t-1) - \epsilon(t)\phi^T(t)\mathbf{P}(t-1))\Big] \tag{5.29}$$

$$\hat{X}(t) = \hat{X}(t-1) + \epsilon(t)[y(t) - \phi^T(t)\hat{X}(t-1)]) \tag{5.30}$$

with

$$\epsilon(t) = P(t-1)\phi(t)\frac{1}{\lambda + \phi^T(t)P(t-1)\phi(t)}. \tag{5.31}$$

The RLS scheme, Eqs. (5.29)–(5.31), was initialized with the following values for the field data case:

$$\hat{X}(0) = \begin{bmatrix} 3.0885 \\ 10^{-7} \end{bmatrix}, \quad \mathbf{P}(0) = \begin{bmatrix} 0.0169 & 5.49 \times 10^{-10} \\ 5.49 \times 10^{-10} & 0 \end{bmatrix}, \quad \lambda = 1. \tag{5.32}$$

In field units, these values corresponding to an initial pore pressure of 4,480 psi and a PI of 1.461 ft3/min/psi.

Chapter 6

Robust Controller Design for Automated Kick Handling in Managed Pressure Drilling

Summary

The problem considered in this paper is that of controlling downhole pressure during oil and gas well drilling, with a particular focus on handling gas kicks leading to two-phase gas-liquid flow conditions. We identify a first-order approximation to the infinite-dimensional system which captures the dominating mode of the pressure dynamics in the frequency range of interest, while the high-frequency pressure dynamics are represented by a multiplicative uncertainty. This approximation is then modified to accommodate the changes to the dynamics introduced by the two-phase flow. The linearized plant has an open-loop time constant which varies between 2 and 600 seconds depending on operating point and gas distribution in the well. Robust controller design is then performed using Linear Matrix Inequalities (LMIs) via a polytopic norm-bounded description of both the high-frequency multiplicative, and the low-frequency parametric uncertainty. It is shown that, in order to achieve acceptable performance over such a large range of open loop time constants, a time-varying controller gain is required. The main contribution of the paper is to achieve this control objective systematically by formulating the control design problem as an LMI optimization problem. Then optimal solutions of the LMI problem can be obtained in polynomial time by using modern Interior Point Method (IPM) numerical solution algorithms.

6.1. Introduction

With the depletion of easily accessible hydrocarbon resources, the focus of the upstream oil and gas industry has shifted towards harsher environments such as complex geo-pressured deepwater prospects (Karimi Vajargah et al., 2014). When drilling wells in such environments, it is highly important to maintain the downhole drilling mud pressure at a value above the reservoir pore pressure and also the

pressure required for geomechanical wellbore stability, while keeping it below the formation fracture pressure(Karimi Vajargah et al., 2014).

This means, effectively, that the control goal is to keep the pressure at the bottom of the well within set constraints (Godhavn, 2010). The constant bottom-hole pressure Managed Pressure Drilling (MPD) technique addresses this problem by applying additional back-pressure via an automatically controlled choke valve at the well outlet (Godhavn, 2011). A key challenge associated with introducing automated choke control in drilling is dealing with influx of gas, referred to as a gas kick, which occurs when pressure in the open-hole section (i.e. the section of the well where casing and cement have not yet been set, exposing the well to formation fluids) is below the pressure in the surrounding reservoir. In such a scenario, the system response to actuation changes greatly due to the increased flow and compressibility introduced by the gas influx. At the same time, rapid and precise control becomes essential as the pressure in the well must be controlled to a higher set-point to stop the gas influx (Zhou et al., 2011). Failure to react appropriately to a kick incident can lead to a blow-out which has potentially catastrophic consequences, affecting not only rig personnel safety, but also the surrounding environment, project economics, and, ultimately, the company and industry reputation(Karimi Vajargah et al., 2014).

6.1.1. Control of Gas Kicks

Automatic choke control of gas kicks has previously been considered in the literature (Zhou et al., 2011; Carlsen et al., 2008, 2013; Hauge et al., 2012; Asgharzadeh Shishavan et al., 2015). These investigations typically consider single-phase flow and do not explicitly try to quantify and handle the significant effect the gas influx has on the system dynamics. Failure to do so may lead to degraded performance of the control algorithms and, in some cases, instability(Reitsma and Couturier, 2012).

This paper presents an approach to explicitly capture the effect of the gas influx and incorporate this in the controller design.

6.1.2. Key Challenges and Control Approach

The control problem poses the following key challenges for effective controller design:

- The distributed pressure dynamics are described by an infinite-dimensional model.
- The choke valve actuation is non-linear.
- Large variation in plant parameters in the presence of gas.

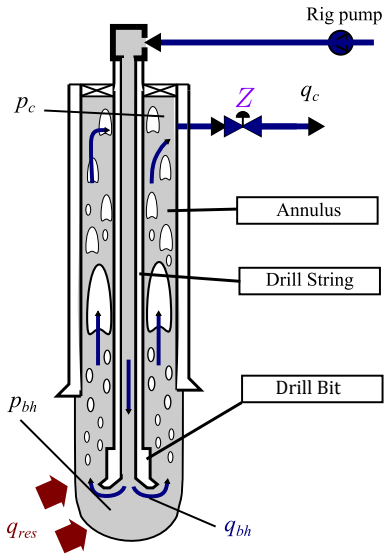

Figure 6.1.: Schematic of a vertical well with gas influx (from (Aarsnes et al., 2015)).

To address these challenges, the infinite-dimensional plant is approximated with a first-order model and the resulting high-frequency error is represented as a multiplicative uncertainty. The effect of the actuation non-linearity and changes in plant parameters due to gas influx is captured through explicit relations resulting in a linear time-varying first order plant with multiplicative uncertainty.

This plant is represented by a norm-bounded polytopic linear differential inclusion (LDI) which allows for robust controller design using LMIs (Boyd et al., 1994a). First, an approach is taken where a static feedback controller is designed, but due to the wide range of plant parameters encountered, the resulting performance of the controller is poor. To address this, a second approach is proposed where a robust, time-varying controller is designed using an estimate of the plant time constant and a bound on estimate uncertainty.

The controller is tested in simulations with an explicit numerical implementation of the Drift-Flux Model (DFM) representing the two-phase flow dynamics (Evje and Fjelde, 2002; Udegbunam et al., 2015).

6.1.3. Robust Control Using LMIs

Often when controller design is performed, there can be a disconnect between the control objective and the parameters that are adjusted to achieve it. For example, one could be trading off robustness versus performance by adjusting the relative weighting between control effort and error penalty in an LQR controller. Although this typically yields satisfactory results, in the present control problem, it is desirable to specify the control problem to be solved directly: i.e. maximize the

performance subject to the robustness constraint. For the present problem this can be achieved systematically by using LMIs, which motivates the approach taken in this paper.

LMIs present a rigorous framework to handle model uncertainties (Boyd et al., 1994b, 1997). They are used to bound the uncertainties in the model via convex constraints (Açıkmeşe and Corless, 2008), which result in convex optimization problems for control synthesis. The resulting optimization problems have linear inequality constraints on matrix solution variables, which are called LMIs and have been utilized to tackle many control problems (Packard et al., 1991; Gahinet and Apkarian, 1994; Açıkmeşe and Corless, 2002) as a systematic approach to ensure control design objectives within the uncertainties inherent in the system.

6.2. Model Description

Our goal in this section is to obtain a low-order approximation of the pressure dynamics in the wellbore annulus, and be able to quantify the resulting error in the frequency domain. This will enable us to design robust low-order controllers.

To this end, we will take the following steps:

1. Obtain an infinite-dimensional LTI representation of the single-phase dynamics in Section 6.2.1.

2. Approximate the infinite-dimensional LTI model with a first-order plant and quantify the resulting uncertainty, in Section 6.2.2.

3. Obtain a high-order LTI representation of the two-phase pressure dynamics, in Section 6.2.3.

4. Modify the first-order approximation from Step 2 to accommodate the effect of the two-phase dynamics and quantify the resulting uncertainty, in Section 6.2.4.

6.2.1. Single-Phase Infinite-Dimensional Model

As a starting point for understanding the implications of representing the distributed pressure dynamics with a low-order approximation, we consider a hydraulic transmission line model (Egeland and Gravdahl, 2002). The states of interest are the flow rate through the back-pressure choke $q_c(t)$, the flow rate into the bottom of the well $q_{bh}(t)$, and the pressure at the wellhead $p_c(t)$ and bottom $p_{bh}(t)$, see also Fig. 6.1.

We are concerned with the transient pressure behavior, which is captured by variables describing perturbations from an initial steady state. Assuming the system to initially be at rest at an equilibrium with states denoted by $\bar{q}_c = \bar{q}_{bh} \equiv \bar{q}$

and $\bar{p}_c, \bar{p}_{bh}$, we will use the perturbed variables:

$$\tilde{q}_c(t) = q_c(t) - \bar{q}, \qquad \tilde{q}_{bh}(t) = q_{bh}(t) - \bar{q}, \tag{6.1}$$

$$\tilde{p}_c(t) = p_c(t) - \bar{p}_c, \qquad \tilde{p}_{bh}(t) = p_{bh}(t) - \bar{p}_{bh}. \tag{6.2}$$

Perturbed downhole pressure, which we desire to control, and perturbed choke backpressure are related to the changes in flow through the choke by a wave equation describing distributed hydraulics in the well. For single-phase flow these dynamics can be expressed by the irrational transfer matrix derived in Appendix 6.A. Denoting the Laplace transformed variables with capital letters, and the Laplace variable with s, we can write:

$$\begin{bmatrix} P_{bh}(s) \\ P_c(s) \end{bmatrix} = \begin{bmatrix} G_1(s) \\ G_2(s) \end{bmatrix} Q_c(s). \tag{6.3}$$

This transfer matrix describes the pressure-flow dynamics in the well when the inflow at the bottom is constant.

6.2.2. First-Order Approximation

By discarding the distributed pressure dynamics in the well we can approximate the model with a single control volume representation (which is similar to the models used in (Pavlov et al., 2010; Kaasa et al., 2012)):

$$\dot{p}_c(t) = \frac{\beta}{V}\Big(q_{bh} - q_c(t)\Big), \tag{6.4}$$

where β is the drilling mud bulk modulus, and V is the annular volume. This model is obtained by discarding the fast pressure dynamics (Aarsnes et al., 2015), an implication of which is that we get the approximation:

$$\dot{p}_{bh}(t) \approx \dot{p}_c(t). \tag{6.5}$$

It is interesting to note that using the approximation $\tanh \Gamma(s) \approx \Gamma(s)$ (see Appendix 6.A) which is valid when $s \to 0 \implies \Gamma \to 0$, the distributed system transfer function (6.62) becomes identical to (6.4). This is the first-order series approximation to the irrational function $\sinh \Gamma$, and using higher-order approximations yield lumped models valid over a larger frequency range (Makinen et al., 2000). The match of this simple approximation at low frequencies can be seen in Fig. 6.2. The first-order approximation is valid up to the frequency range for which the distributed pressure dynamics start to become important.

6.2.3. Model Modifications for Two-Phase Flow

The gas propagation dynamics are significantly slower (on a time-scale of 10+ minutes) than the pressure dynamics. However, the gas *volume fraction profile* $\alpha_{\mathrm{g}}(x,t)$,

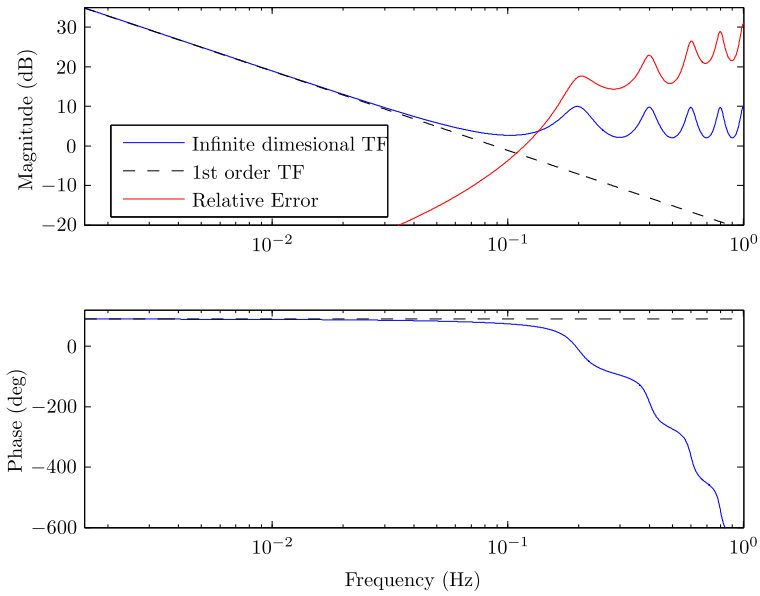

Figure 6.2.: Comparison of infinite-dimensional and first-order transfer function, $\tilde{p}_{bh}/\tilde{q}_c(s)$ (note that the magnitude is normalized).

strongly affects the magnitude and phase of the pressure dynamics. To reflect this, we will in this subsection develop a higher-order LTI model which approximates the pressure dynamics in a well for a given static gas profile: $\alpha_g(x,t) = \alpha_g(x)$. Then by considering different gas profiles, we can represent how the pressure dynamics changes over time as the kick progresses.

The response of this LTI model is then compared to that of the Drift-Flux Model, implemented with the explicit AUSM numerical scheme (see Appendix A), to validate the approach.

Next, we derive relations which allow us to approximate these two-phase dynamics with the first-order model from Section 6.2.2. We then compare the first-order model to the higher-order model to evaluate the match and the frequency range over which the first-order model is valid. The end result is a first-order model, representing a slow pressure mode, obtained by discarding both the slow gas propagation dynamics and the fast distributed pressure dynamics. This model is amenable for controller design as it gives a good representation of the dynamics around our desired cross-over frequency, and a quantification of the discarded high frequency dynamics such that robustness can be ensured.

Linear approximation of pressure dynamics

For controller design we seek LTI descriptions of the pressure dynamics that enable frequency domain analysis. The key is to attain a model useful for design

which gives a good representation of the dynamics in a frequency range around the crossover frequency. We consider the gas propagation effect on the bottom-hole circulating pressure (BHCP) through changing hydrostatic pressure as a slowly varying disturbance, and will handle this disturbance through integral action in the controller.

To capture the effect of the gas distribution on the pressure dynamics we use a modified version of the control volume model described in e.g. (Egeland and Gravdahl, 2002; Landet et al., 2012; Aarsnes et al., 2012) to obtain the desired LTI approximation. This approach has been shown to yield a good approximation at low frequencies while accuracy at higher frequencies can be retained by increasing the number of control volumes (Aarsnes et al., 2012).

To accommodate the effect of the gas distribution we modify the effective density, $\bar{\rho}$, and bulk modulus, $\bar{\beta}$, used in each control volume by accounting for the amount of gas in the volume. Using the definition of bulk modulus β in a volume V (White, 2003):

$$\beta = -V\frac{\mathrm{d}p}{\mathrm{d}V}, \tag{6.6}$$

where p is the pressure in the volume, we can find the effective bulk modulus, $\bar{\beta}$, of two different phases (i.e. gas and liquid) subject to the same pressure (treating each phase as a separate volume):

$$\bar{\beta} = -(V_1+V_2)\frac{\mathrm{d}p}{\mathrm{d}V_1+\mathrm{d}V_2} = \frac{(V_1+V_2)}{\frac{V_1}{\beta_1}+\frac{V_2}{\beta_2}}. \tag{6.7}$$

Consequently, denoting the gas volume fraction profile as $\alpha_{\mathrm{g}}(x,t)$, and noting that, for an ideal gas, the isothermal gas bulk modulus is equal to the pressure (White, 2003), we find the effective bulk modulus in a control volume where gas is present:

$$\bar{\beta}_j = \frac{\beta_\ell p(x_j)}{p(x_j)\big(1-\alpha_{\mathrm{g}}(x_j)\big)+\beta_\ell\alpha_{\mathrm{g}}(x_j)}, \tag{6.8}$$

where $p(x_j), \alpha_{\mathrm{g}}(x_j)$ denote that the pressure and void fraction quantities are averaged over control volume j, and β_ℓ denotes the bulk modulus of the liquid phase. The effective density in control volume j is given as

$$\bar{\rho}_j = \rho_\ell(1-\alpha_{\mathrm{g}}(x_j)) + \rho_{\mathrm{g}}\alpha_{\mathrm{g}}(x_j), \tag{6.9}$$

where ρ_ℓ and ρ_{g} are liquid and gas densities, respectively.

Using N control volumes, each of length $l = L/N$, and again only considering deviations from a steady state, we can write the lumped dynamics as:

$$\dot{p}_j = \frac{\bar{\beta}_j}{Al}(q_{j-1}-q_j), \qquad j = 1,\dots,N \tag{6.10}$$

$$\dot{q}_j = \frac{A}{l\bar{\rho}_j}(p_j-p_{j+1}) - kq_j, \qquad j = 1,\dots,N-1 \tag{6.11}$$

$$q_0 = 0, \qquad q_N = \tilde{q}_c, \tag{6.12}$$

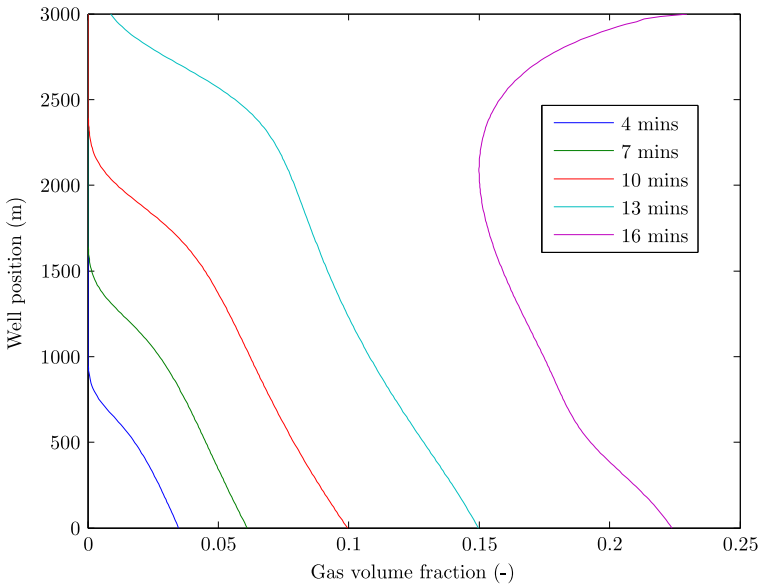

Figure 6.3.: Gas volume fraction profiles at different times after an uncontrolled kick incident.

and the resulting input–output descriptions can be denoted by the transfer functions

$$\begin{bmatrix} P_{bh}(s) \\ P_c(s) \end{bmatrix} = \begin{bmatrix} \tilde{G}_1(s) \\ \tilde{G}_2(s) \end{bmatrix} Q_c(s). \tag{6.13}$$

These high-order LTI models $\tilde{G}_1, \tilde{G}_2$ represent the pressure dynamics for a given gas distribution $\alpha_g(x,t)$ and pressure profile, $p(x,t)$, in the well. During a kick incident these models will change as the gas distribution propagates through the well. The impulse responses of the resulting high-order LTI models $\tilde{G}_1, \tilde{G}_2$ are compared to the impulse response simulated with the Drift-Flux Model (Udegbunam et al., 2015) in the next section.

6.2.4. Comparison with the Drift-Flux Model

Consider a Managed Pressure Drilling scenario where a well is drilled with a BHCP of 415 bar (a typical value for a 3000-meter deep vertical well (Aarsnes et al., 2015)) see Fig. 6.1, when encountering an over-pressured hydrocarbon reservoir at 421 bar of reservoir pressure causing gas influx into the well. If no response is taken, the well will tend to blow-out conditions over time as the lighter gas displaces the heavier drilling mud, causing yet more influx. The propagation of the gas profile in the well over time for this case can be seen in Fig. 6.3.

We are interested in how the pressure dynamics change during a kick from a control perspective, specifically how the BHCP reacts to changes in choke flow rate

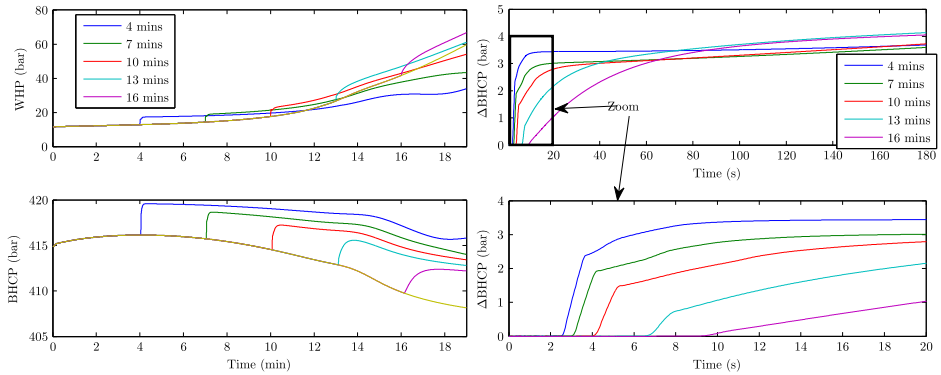

Figure 6.4.: Comparison of impulse responses of well head pressure (WHP) and bottom-hole pressure (BHCP) to an impulse in choke flow at different points in time after kick start (**left**) and the resulting perturbed response in the BHCP (**right**).

q_c. Fig. 6.4 shows the pressure responses simulated using the Drift-Flux Model when the system is subject to an impulse in choke flow at different times after the kick started, i.e. corresponding to the profiles in Fig 6.3.

Subtracting the nominal, undisturbed trajectories from the ones affected by the choke actuation we get Fig. 6.4 (**right**). This figure illustrates how the impulse response changes during a kick incident, from an early stage of a kick represented by the blue '4 min' curve (with the '4 min' α_g profile in Fig. 6.3), to an almost fully developed blow-out situation given by the purple '16 min' curve.

The impulse response of the high-order LTI system $\tilde{G}_1(s)$ is compared to that of simulations with the Drift-Flux Model (see Appendix A) at different points of gas distribution is shown in Fig. 6.5. The crossover frequency of the designed controller is expected to be in the range of 0.015–0.1 Hz, and we conclude that the LTI approximation is satisfactory for this range. For significantly lower frequencies the slow gas propagation dynamics, which are not captured by the LTI model, start to dominate (Aarsnes et al., 2016d).

Fig. 6.5, on the right, shows the Bode diagrams of the LTI models, illustrating the large variation in gain, as well as noteworthy change in the high-frequency pressure dynamics, caused by the gas. For a controller to be able to retain performance and robustness in handling such a kick, it is imperative to understand these changes in the system response.

Two-Phase First-Order Approximation

Returning to our first-order approximation (6.4), our two-phase equivalent writes:

$$\dot{p}_{bh}(t) \approx \frac{\bar{\beta}(t)}{V}\big(q_{bh} - q_c(t) + d\big), \tag{6.14}$$

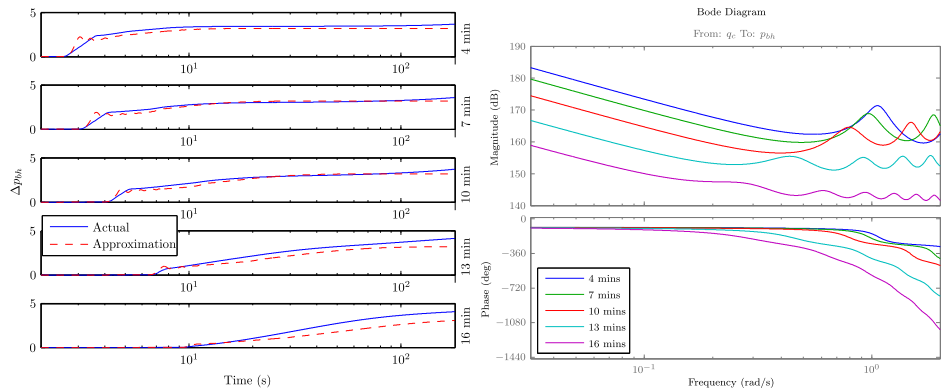

Figure 6.5.: Impulse responses of the lumped approximations $\tilde{G}_1(s)$ compared with the DFM simulation (**left**) and their Bode diagrams (**right**).

where d represents unmodeled two-phase dynamics which will be treated as a disturbance. For the two-phase dynamics we also have to modify the effective bulk modulus, $\bar{\beta}$, according to, see Eqs. (6.7)–(6.8);

$$\bar{\beta}(t) = \frac{L}{\int_0^L \left[\frac{\alpha_g(x,t)}{p(x,t)} + \frac{1-\alpha_g(x,t)}{\beta_\ell}\right] \mathrm{d}x}. \tag{6.15}$$

We further note that the change in the effective bulk modulus is responsible for the changes in system gain seen in Fig. 6.5.

Equation (6.14) is a first order time-varying linear approximate representation of the distributed non-linear dynamics described by the drift-flux model, see Appendix A. What motivates this approximation is that general control results of systems at the level of complexity of the drift-flux model do not exist, and while results exist for linearized versions of this system (Di Meglio and Aarsnes, 2015), these do not include robustness results and are exceedingly complicated. More tools are available for dealing with first order time-varying linear systems with high-frequency uncertainties.

In the next section we linearize the actuation nonlinearity and formalize representation of the high frequency uncertainty.

6.3. Proposed Controller Structure

We now turn to the task of developing a controller for the bottom-hole pressure p_{bh}.

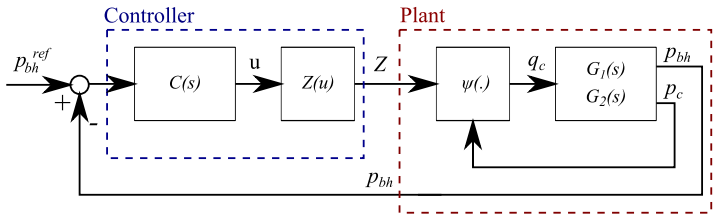

Figure 6.6.: Block diagram showing the controller with the proposed static mapping.

6.3.1. Choke Equation Non-Linearity

The flow rate out of the well is given by a choke equation relating it to choke pressure and choke opening (Godhavn, 2011):

$$q_c = \psi(z, p_c) \equiv \frac{C_v(z)}{\sqrt{\rho_\ell}} \sqrt{p_c - p_{c0}}, \tag{6.16}$$

where $C_v(z) > 0$ is the choke coefficient which, in the operating range of interest, is assumed to be an invertible function of the choke opening $z \in [0, 1]$ and p_{c0} is the pressure downstream of the choke.

With two-phase flow through the choke, the resulting equation becomes more involved. One possible such relation is considered in Appendix 6.B.

We introduce a static mapping between the controller output u and the choke opening z:

$$z(u) = C_v^{-1}\Big(q_{bh} \frac{\sqrt{\rho_\ell}}{\sqrt{u}}\Big), \tag{6.17}$$

where the mapping was chosen such that u corresponds to the steady state $\bar{p}_c - p_{c0}$ for $q_{bh} = q_c$ and liquid-only flow, for which (6.16) now writes

$$q_c = q_{bh} \frac{\sqrt{p_c - p_{c0}}}{\sqrt{u}}. \tag{6.18}$$

We note that this formulation does not require any feedback before the nominal controller design (see Fig. 6.6).

To conform to the Polytopic LDI formalism to be employed, the choke equation (6.18) is linearized and evaluated at a given operating point. For the general two-phase case, using the perturbation variables, we obtain a relation of the form (see Appendix 6.B for details):

$$\tilde{q}_c = K_p \tilde{p}_c - K_u \tilde{u}. \tag{6.19}$$

6.3.2. Linear Uncertain Plant

Combining (6.19) with (6.3) we get the linear perturbation dynamics represented by the plant transfer function

$$P_{bh} = P(s)U, \quad P(s) \equiv \frac{-G_1(s)K_u}{1 - G_2(s)K_p}.$$

Using the first-order approximation from (6.14) we obtain the nominal first-order plant $P_n(s)$ which, at equilibrium, can be written as

$$P_{bh} \approx P_n(s)U, \quad P_n(s) \equiv \frac{1}{\tau s + 1}, \tag{6.20}$$

$$\tau = V/(K_p\bar{\beta}), \quad K_p = \frac{1}{C_K}\frac{1}{\bar{u}}. \tag{6.21}$$

The time constant of the first-order plant will in practice be time-varying, i.e. $\tau = \tau(t)$, as it will change with the operating point and the amount of gas in the well through the 'effective bulk modulus' $\bar{\beta}$. Since this quantity is not directly measured it will be treated as uncertain and dealt with as such in the controller design.

The high-frequency dynamics that were discarded to obtain the first-order plant $P_n(s)$ also entail uncertainty that must be dealt with. The discarded dynamics are seen in the frequency domain as a series of resonances and anti-resonances caused by traveling and reflecting pressure waves in the well (see Fig. 6.2 and 6.5). Such resonances are difficult to model accurately as they change amplitude and location rapidly with changing choke opening (Aarsnes et al., 2014c). The Richardson annular effect, combined with possible Non-Newtonian rheology of the drilling mud, further complicates capturing the in-domain energy dissipation and consequently the amplitude of the resonances (Wahba, 2013; Stecki and Davis, 1986). This motivates discarding these dynamics as they would in any case have to be considered highly uncertain. We note that these effects reduce the amplitude of the resonances, meaning that ignoring them yield results that are conservative in terms of the significance of the resonances.

The discarded high-frequency dynamics are represented by a multiplicative uncertainty with the frequency weight $\tau_\Delta s$. That is, the full plant $P(s)$ is encompassed by the uncertain plant $P_\Delta(s)$ given as

$$P_\Delta(s) = \frac{1}{s\tau + 1}\Big(1 + \tau_\Delta s\Delta(s)\Big), \quad \|\Delta(s)\|_\infty \leq 1, \tag{6.22}$$

The constant τ_Δ is the period (in seconds) at which the high-frequency pressure dynamics become important. For the considered case, with a well depth of 3000 meters, $\tau_\Delta = 4$ seconds was chosen.

The corresponding fit of the nominal plant $P_n(s)$ when compared to $P(s)$ derived with the single-phase infinite-dimensional transfer functions $G_1(s), G_2(s)$ is seen on

the left in Fig 6.8. Similarly, we compare the nominal plant to the high-order LTI approximations of the 2-phase dynamics on the right in Fig 6.8. Here $\tau(t)$ changes with both the gas profile $\alpha_g(x,t)$ and the operating point $\bar{u}$. We see that the constant $\tau_\Delta = 4$ is sufficient to represent the error caused by the high frequency dynamics, while the relative error at lower frequencies is caused by uncertainty in $\tau(t)$.

6.4. Controller Design and Results

6.4.1. Case 1: Static Feedback Design

Recall the low-order uncertain plant formulation

$$P_{bh} = \frac{1}{s\tau + 1}\left(1 + \tau_\Delta s\Delta(s)\right)U \tag{6.23}$$

To represent the uncertainty, and obtain integral action in the control, the actuation $\tilde{u}$ is added as a state to allow representation of the time-derivative u_d of the actuation, and I_e for the integrated error (Ge et al., 2002). The system is then written in state space form as

$$\dot{\tilde{p}}_{bh} = -\frac{1}{\tau(t)}\left(\tilde{p}_{bh} + \tilde{u} + w + \tau_\Delta p\right) \tag{6.24}$$

$$\dot{\tilde{u}} = u_d \tag{6.25}$$

$$\dot{I}_e = \tilde{p}_{bh}, \tag{6.26}$$

where w is the disturbance, the open loop time constant $\tau(t)$ is time varying and the uncertainty due to the high-frequency pressure dynamics is represented through p given as

$$q = u_d \tag{6.27}$$

$$p = \Delta(t)q, \quad |\Delta(t)| \leq 1. \tag{6.28}$$

The resulting control problem is to find a state feedback gain, K, which robustly minimizes the $\mathbf{L}_2$ gain of the integrated error:

$$\sup_{\|w\|_2 \neq 0} \frac{\|I_e\|_2}{\|w\|_2}, \tag{6.29}$$

given the bound $\tau(t) \in [\underline{\tau}, \overline{\tau}]$. This problem formulation is summarized in Table 6.1.

To solve this problem we will represent the system as a *Linear Differential Inclusion* (LDI) (Boyd et al., 1994a). In state space form, we write:

$$\dot{x} = A(t)x + B_u u + B_w(t)w + B_p(t)p, \tag{6.34}$$

$$q = C_q x + D_{qu}u + D_{qp}p, \tag{6.35}$$

$$z = C_z x \tag{6.36}$$

$$p = \Delta(t)q, \quad |\Delta(t)| \leq 1, \tag{6.37}$$

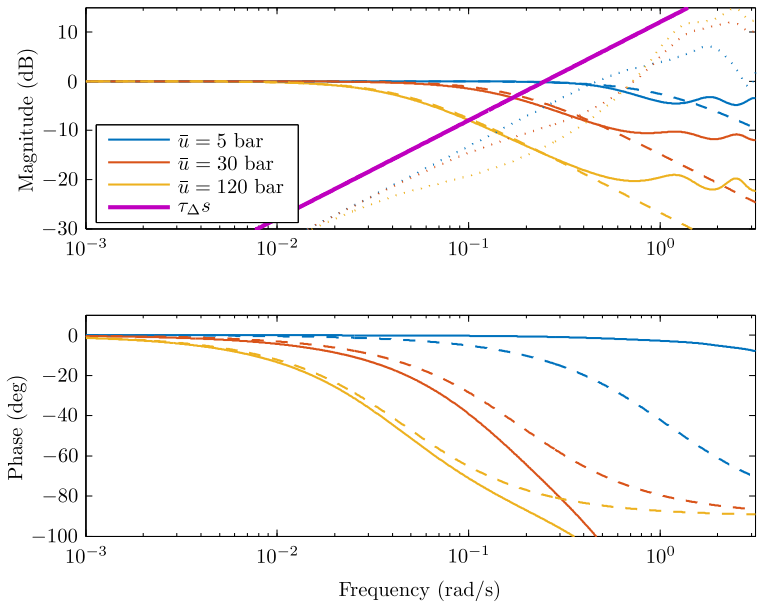

Figure 6.7.: Comparison of infinite-dimensional plants $P(s)$ (–) and first-order approximations $P_n(s)$ (- -), with the relative error $(\cdots)$ and error bound $\tau_\Delta s$ (with $\tau_\Delta = 4$ seconds) for different operating points $\bar{u}$, that is, with no gas in the well.

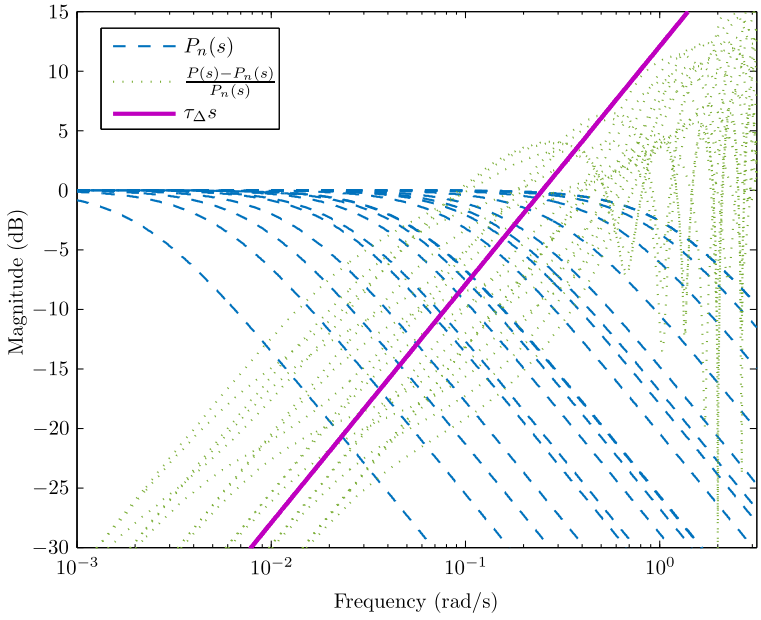

Figure 6.8.: The full complement of nominal plants and the resulting error, corresponding to the gas distributions in Fig. 6.3 (plus the three plants without any gas), is shown. The error bound $\tau_\Delta s$ covers the high frequency error while the error at lower frequencies is due to uncertainty in τ.

Table 6.1.: Control problem formulation

Control problem formulation

Find a controller $C(s)$ that robustly minimizes the $\mathbf{L}_2$ gain

$$\sup_{\|w\|_2 \neq 0} \frac{\|I_e\|_2}{\|w\|_2}, \tag{6.30}$$

subject to

$$\dot{\tilde{p}}_{bh} = \frac{1}{\tau(t)} \left(-\tilde{p}_{bh} + \tilde{u} + w + \tau_\Delta p \right), \tag{6.31}$$

$$\dot{I}_e = \tilde{p}_{bh}, \quad \tilde{u} = C(s)\tilde{p}_{bh}, \tag{6.32}$$

$$p = \Delta(t)\dot{\tilde{u}}, \quad \|\Delta(t)\| \leq 1, \quad \tau(t) \in [\underline{\tau}, \overline{\tau}]. \tag{6.33}$$

where $A(t)$ is the time varying system matrix, and the actuation, disturbance and norm-bound uncertainty enter through the input vectors $B_u, B_w(t), B_p(t)$ respectively. We use a quite general formulation for q in (6.35) as it will be needed for *Case 2*. With the bounds on $\tau(t) \in [\underline{\tau}, \overline{\tau}]$, and denoting $\tau_1 = \underline{\tau}, \tau_2 = \overline{\tau}$ the time varying plant (6.34)–(6.37) can be described as an LDI given by the set

$$\Omega = \mathbf{Co}\left\{ \begin{bmatrix} A_1 & B_u & B_{w,1} & B_{p,1} \\ C_q & D_{qp} & D_{qu} & 0 \\ C_z & 0 & 0 & 0 \end{bmatrix}, \begin{bmatrix} A_2 & B_u & B_{w,2} & B_{p,2} \\ C_q & D_{qp} & D_{qu} & 0 \\ C_z & 0 & 0 & 0 \end{bmatrix} \right\}. \tag{6.38}$$

with

$$A_i = \begin{bmatrix} \frac{-1}{\tau_i} & \frac{1}{\tau_i} & 0 \\ 0 & 0 & 0 \\ 1 & 0 & 0 \end{bmatrix}, B_{w,i} = \begin{bmatrix} \frac{1}{\tau_i} \\ 0 \\ 0 \end{bmatrix}, B_{p,i} = \begin{bmatrix} \frac{\tau_\Delta}{\tau_i} \\ 0 \\ 0 \end{bmatrix} \tag{6.39}$$

and

$$B_u = \begin{bmatrix} 0 \\ 1 \\ 0 \end{bmatrix}, C_q = \begin{bmatrix} 0 \\ 0 \\ 0 \end{bmatrix}^T, C_z = \begin{bmatrix} 0 \\ 0 \\ 1 \end{bmatrix}^T, \tag{6.40}$$

and finally $D_{qp} = 0, D_{qu} = 1$.

Formulation as an LMI

We synthesize a controller for this problem by solving the following eigenvalue problem (Boyd et al., 1994a) in the free variables Y, Q, γ, μ:

$$\text{minimize} \quad \gamma \tag{6.41}$$

$$\text{subject to:} \quad Q > 0, \mu > 0 \tag{6.42}$$

$$\begin{bmatrix} \begin{pmatrix} A_i Q + Q A_i^T \\ +B_u Y + Y^T B_u^T \\ +B_{w,i} B_{w,i}^T + \mu B_{p,i} B_{p,i}^T \end{pmatrix} & * & * \\ C_z Q & -\gamma^2 & * \\ \mu D_{qp} B_{p,i}^T + C_q Q + D_{qu} Y & 0 & -\mu \end{bmatrix} < 0, \tag{6.43}$$

$$i = 1, 2.$$

The solution of this problem yields the feedback gain: $\begin{bmatrix} k_1 & k_2 & k_3 \end{bmatrix}^T = YQ^{-1}$ of the state space formulation (6.24)–(6.26). Consequently, the controller can be written as the mapping $U = C(s)P_{bh}$ with

$$C(s) = \frac{k_1 s + k_3}{s(s - k_2)}. \tag{6.44}$$

We note that the minus in (6.59) is due to the formulation (6.41)–(6.43) assuming a positive feedback, meaning that $k_1, k_2, k_3 < 0$.

6.4.2. Case 2: Time-Varying Feedback Design

If we have some way of obtaining an estimate $\hat{\tau}$ of the value of $\tau(t)$, it is natural to conclude that better performance could be achieved by encoding this information into the controller actuation, effectively making the controller gain dependent on our estimate $\hat{\tau}$. This approach leads to a time-varying feedback law. By augmenting the plant with this time-varying feedback, it can be included in the LDI. Then we design a static feedback law for the augmented plant which ensures robust stability for the LDI and tries to optimize a performance index.

To facilitate such a controller we introduce an additional proportional feedback gain, $k_\tau(\hat{\tau})$, dependent on the estimated time constant $\hat{\tau}$. This additional feedback also enters into the the norm-bound uncertainty meaning that we have to modify the expression for q. Including this extra feedback gain, the state space description

becomes

$$\dot{\tilde{p}}_{bh} = -\frac{1+k_\tau(\hat{\tau})}{\tau(t)}\tilde{p}_{bh} + \frac{1}{\tau(t)}\left(\tilde{u} + w + \tau_\Delta p\right) \tag{6.45}$$

$$\dot{\tilde{u}} = u_d \tag{6.46}$$

$$\dot{I}_e = \tilde{p}_{bh}, \tag{6.47}$$

$$q = -\frac{1+k_\tau(\hat{\tau})}{\tau(t)}p_{bh} + \frac{1}{\tau(t)}\tilde{u} + u_d + \frac{k_\tau(\hat{\tau})}{\tau(t)}p \tag{6.48}$$

$$p = \Delta(t)q, \quad |\Delta(t)| \leq 1. \tag{6.49}$$

For $k_\tau(\hat{\tau})$ we would like a simple and explicit relation that can improve performance. In principle, there are a number of approaches to designing this mapping, but for our purposes the following function was found amenable:

$$k_\tau(\hat{\tau}) = (\sqrt{\rho\hat{\tau}+1} - 1), \tag{6.50}$$

where ρ is a tuning factor. (6.50) can be shown to be identical to an optimal Linear Quadratic Regulator with intregral action for the appropriately chosen tuning.

Having chosen a time-varying feedback gain, we proceed with the design. We have the same LDI as given by (6.38)–(6.40), except for the following changes:

$$A_i = \begin{bmatrix} -\frac{1+k_\tau(\hat{\tau}_i)}{\tau_i} & \frac{1}{\tau_i} & 0 \\ 0 & 0 & 0 \\ 1 & 0 & 0 \end{bmatrix}, \tag{6.51}$$

$$C_{q,i} = k_\tau(\hat{\tau}_i)\begin{bmatrix} -\frac{1+k_\tau(\hat{\tau}_i)}{\tau_i} & \frac{1}{\tau_i} & 0 \end{bmatrix}, \tag{6.52}$$

$$D_{qp} = k_\tau(\hat{\tau}_i)\frac{\tau_\Delta}{\tau}. \tag{6.53}$$

Here we need four edges to describe the polytope. Given a total range for τ: $\tau \in [\underline{\tau}, \overline{\tau}]$ and a bound on uncertainty given by r such that $\tau \in [\hat{\tau}r, \hat{\tau}/r]$, the parameters at the edges are

$$\tau_1 = \underline{\tau}, \qquad \hat{\tau}_1 = \underline{\tau}/r, \tag{6.54}$$

$$\tau_2 = \underline{\tau}/r^2, \qquad \hat{\tau}_2 = \underline{\tau}/r, \tag{6.55}$$

$$\tau_3 = \overline{\tau}r^2, \qquad \hat{\tau}_3 = \overline{\tau}r, \tag{6.56}$$

$$\tau_4 = \overline{\tau}, \qquad \hat{\tau}_4 = \overline{\tau}r. \tag{6.57}$$

Consequently, for $\rho = 0$ this formulation yields results identical to Case 1.

The controller $C(s)$ is now found the same way as before, and the full feedback is given as

$$U = (C(s) - k_\tau)P_{bh}. \tag{6.58}$$

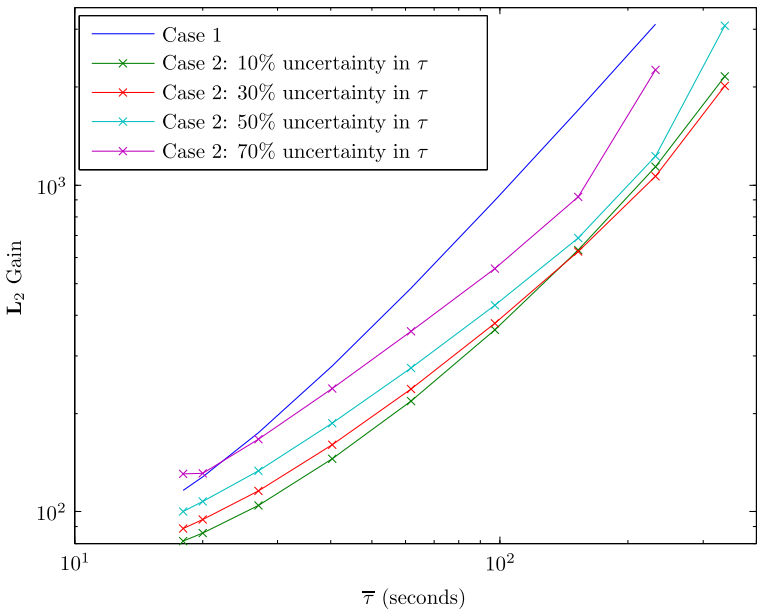

Figure 6.9.: Closed loop performance of controllers parametrized in robustness by the upper limit of τ: $\overline{\tau}$.

6.4.3. Design Results

A comparison of the performance achieved by the controllers, parametrized in the range of robustness, is shown in Fig. 6.9. Not surprisingly, the performance decreases rapidly with increasing upper bound on $\tau(t)$ denoted by $\overline{\tau}$ (the x-axis). The polytopic LDI formulation is known to be conservative in some cases due to the formulation requiring all conditions be met with a single Lyapunov function (implied by the matrix Q). This is likely to account for some of the decrease in performance.

Furthermore we note the success of the time-varying feedback controllers of Case 2 which are able to yield significant increases in performance even for large uncertainties in τ. The results shown are with $\rho = 0.08$ which was found to give the best results.

6.5. Simulations

To evaluate the performance of the controllers formulated in Section 6.4, we consider the dynamic handling of a gas kick in a Managed Pressure Drilling setting, similar to the one presented in Section 6.2.4, simulated with the DFM. During the kick removal process, the plant time constant, τ of (6.21), experiences very significant changes due to the required back-pressure, p_c, needed to attenuate the kick, and the

effect of the gas on the effective bulk modulus, $\bar{\beta}$ in (6.15). To test the performance and robustness of the controller, a particularly severe kick is simulated with a resulting range of τ between 2 and 600 seconds, see Fig. 6.10.

The pressure trends from the simulations with these controllers are shown in Figs. 6.11–6.13. The kick is initiated at 5 minutes, then attenuated at 7 minutes with a change of the downhole pressure setpoint p_{bh}^r, and then circulated out. The gas reaches the choke at around the 15 minutes mark, at which point the large expansion of the gas and its subsequent removal from the annulus through the choke cause large variations in hydrostatic pressure that must be compensated for.

6.5.1. Case 1

The pressure trends for the controller design with static feedback are shown in Fig. 6.11. Controllers designed with an upper bound $\overline{\tau}$ equal to $18, 61$ and 150 seconds, respectively, are shown. For the case of $\overline{\tau} = 18$ seconds the controller covers the time constants that can occur for single-phase flow, and in simulations without gas influx it showed excellent performance. For the kick scenario considered, however, the performance degrades when τ increases above this range due to the gas influx. In spite of the performance degradation, the controller does not seem to become unstable with the change in τ, which is not surprising as an increase in τ implies the system response is getting slower.

For the controllers designed for robustness to higher τ the performance is comparable. It seems clear that for the considered scenario, with such a large variation in τ, we are unable to increase performance significantly with a static, time invariant, controller. This motivates the approach of Case 2.

6.5.2. Case 2

The pressure trends for controller design with time-varying feedback are shown in Fig. 6.12. Controllers designed with an upper bound $\overline{\tau}$ equal to $18, 61$ and 150 seconds respectively, and a 30% uncertainty in τ, are shown. In all cases $\rho = 0.08$ was used for the time-varying feedback gain (6.50). For this initial investigation, the gas profile $\alpha_g(x, t)$ was assumed known and $\hat{\tau}(t)$ was calculated using (6.15) and (6.21).

The first thing to notice is that the conclusion from Section 6.4.3 holds in the simulations: using an estimate of the time constant τ in the feedback law allows for significantly improved performance. This is clearly seen by comparing Fig. 6.11 and Fig. 6.12.

Next we note that the controllers designed are quite conservative: the $\overline{\tau} = 18$ and $\overline{\tau} = 61$ controllers maintain good performance and do not show overly oscillatory behavior (a sign of vanishing phase margins), even when the actual $\tau(t)$ reaches values upwards of 600 seconds for a short time. Again, this is believed to be in large part due to the conservatism introduced by the LDI formulation wherein the same Lyapunov function is used throughout the range of $\tau \in [\underline{\tau}, \overline{\tau}]$. This can perhaps be

amended (with a resulting increase in performance) by dividing the interval $[\underline{\tau}, \overline{\tau}]$ into a set of overlapping sections, and using a separate Lyapunov function in each of them[1].

6.5.3. Wrong Estimate of τ

In our final simulation we consider the flip-side of assuming τ known: what happens when this assumption is wrong. Again we use a $\overline{\tau} = 18$ and a 30% uncertainty in τ. This time, however, the $\hat{\tau}$ is off by a factor of 4 compared to the τ calculated from the model state.

The $\hat{\tau} = 1/4\tau$ shows a degraded performance compared to $\hat{\tau} = \tau$ in being slower, with larger overshoots and poorer disturbance rejection. By linear analysis in a Nichols chart (not shown) the overshoots were found to be due to the degraded phase margins of this controller. However, under-predicting τ does not jeopardize stability because the poor phase margin is located at a low frequency where delays have little effect on the phase. Furthermore, under-predicting τ results in a large gain margin, which also accounts for the slower response.

The $\hat{\tau} = 4\tau$ controller becomes unstable when τ increases as the controller is overly aggressive. Specifically, the time-varying gain increases with $\hat{\tau}$, see (6.50), while the high-frequency uncertainty decreases with $\tau(t)$, see (6.24). Consequently, over-predicting τ may lead to instabilities.

6.6. Conclusion and Future Work

This paper proposed a controller structure and a first-order model approximation of two-phase flow in an oil and gas well which facilitates effective design of high-performance choke controllers for Managed Pressure Drilling. The accompanying analysis confirmed the proposition made in previous literature on this topic that the single-phase dynamics are dominated by a slow pressure mode, captured by the first-order approximation. It was shown that this fact also extends to the two-phase case.

Linearizing the choke actuation resulted in a first-order system with a time constant, τ, dependent on the operating point and the amount of gas in the well. For the severe kick scenario considered in this paper, a static feedback controller yielded poor performance due to the large variation in τ. Using a time-varying feedback and incorporating an uncertain assumption of τ, we were able to significantly improve performance while maintaining a satisfactory degree of robustness.

We did not elaborate on how the estimate of τ should be obtained, but possible approaches include techniques such as in (Aarsnes et al., 2015) or (Kaasa et al., 2011). Combining the estimation with the controller structure investigated in the

[1] Although the idea is simple, the required analysis to prove stability would presumably be quite involved as the system would have to stay within a section for sufficient time such that continued convergence can be shown even while the Lyapunov function changes.

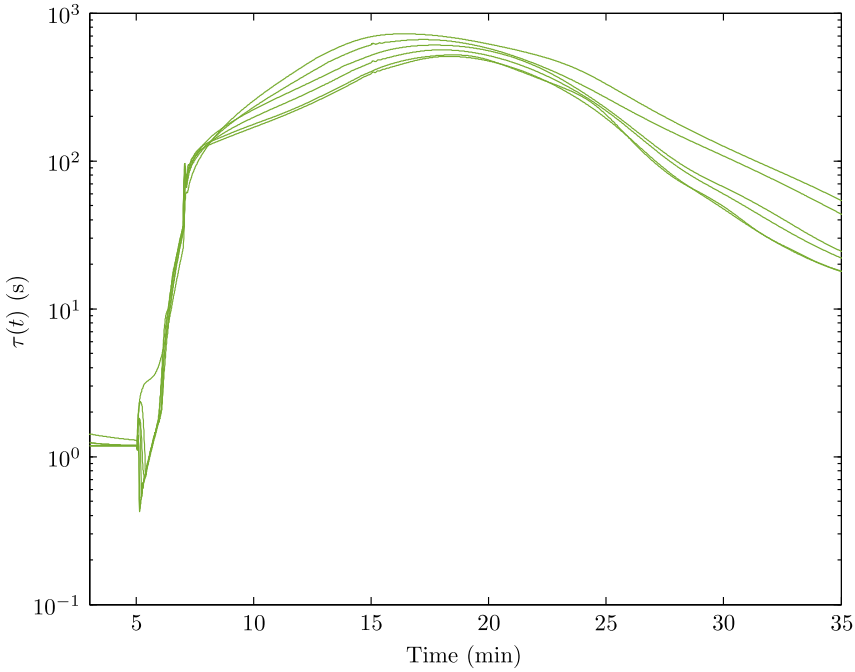

Figure 6.10.: Range of $\tau(t)$ trends.

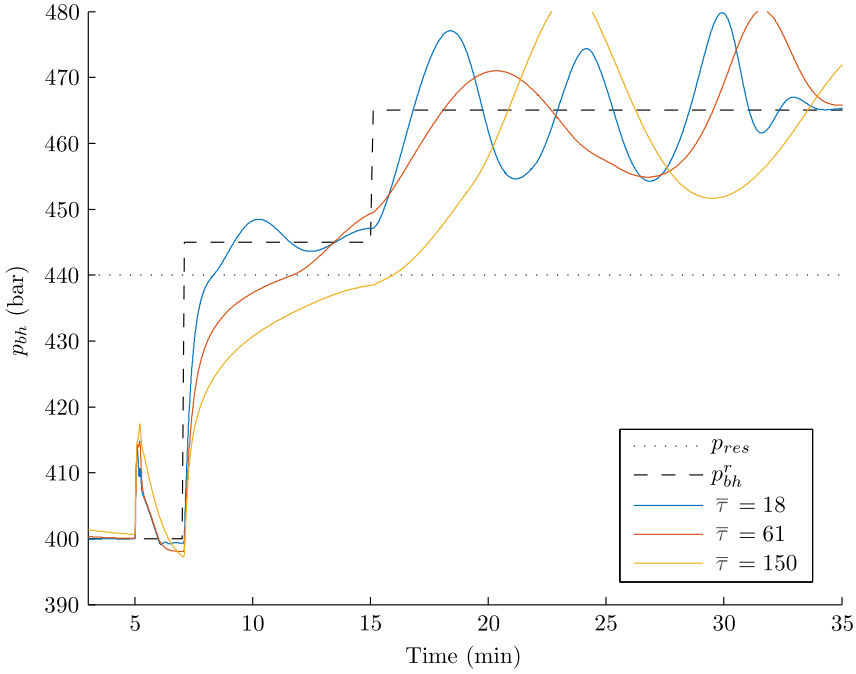

Figure 6.11.: **Case 1** controllers.

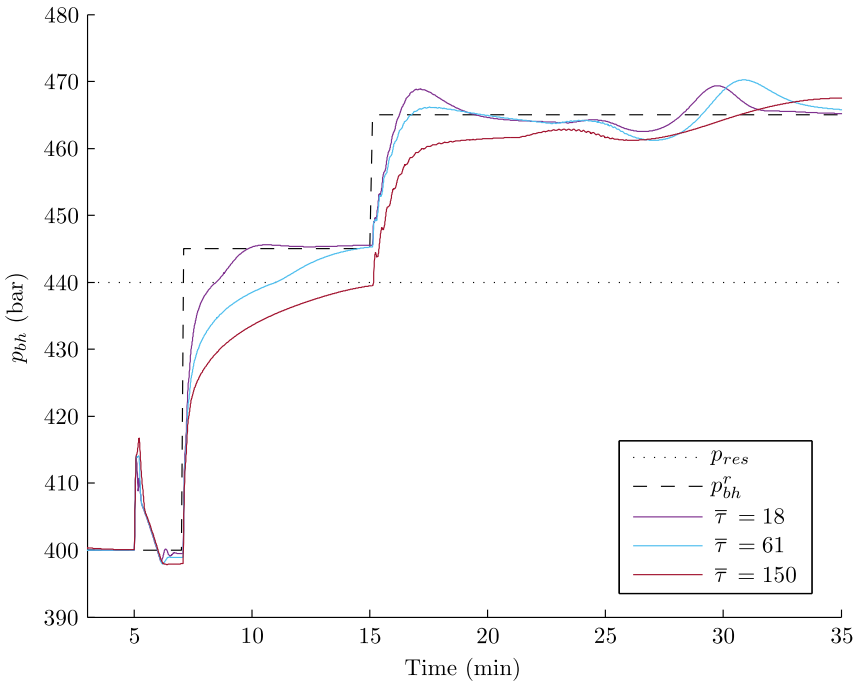

Figure 6.12.: **Case 2** controllers.

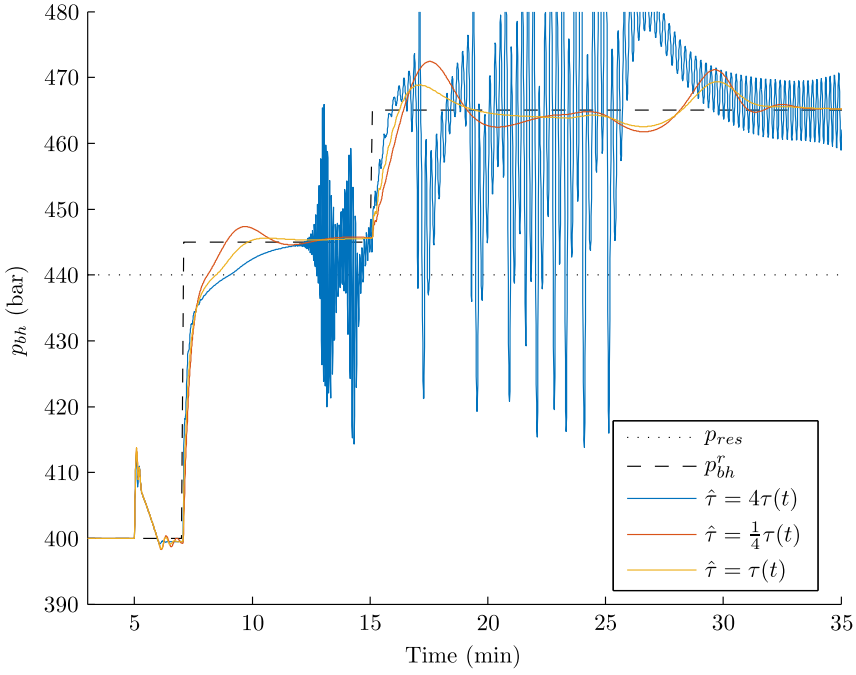

Figure 6.13.: **Case 2** controllers: the effect of under- or over-predicting $\tau(t)$.

current paper, i.e. designing adaptive controllers, is the goal of future work. In this context, the following conclusion is of importance:

- Assuming too low $\tau \rightarrow$ loss of performance.
- Assuming too high $\tau \rightarrow$ loss of robustness.

It was noted that the controllers designed seemed to be conservative when required to be robust for a large range of τ. It is believed that this is due to the LMI design approach requiring a single Lyapunov function to stabilize the whole set of polytopic uncertain plants. By splitting the envelope of τ into multiple overlapping sections when performing the controller design, thus allowing for the use of switched Lyapunov functions, it is believed that performance can be further improved.

Appendix

6.A. Hydraulic Transmission line modelling

Let $p(x,t), q(x,t)$ denote the profiles of pressure, respectively, volumetric flow rate in the well. We denote $t \in \mathbb{R}^+$ the time variable and $x \in [0, L]$ the position where $x = 0$ is the bottom of the well such that

$$\begin{aligned} p_{bh}(t) &= p(0,t), & p_c(t) &= p(L,t), \\ q_{bh}(t) &= q(0,t), & q_c(t) &= q(0,t). \end{aligned}$$

We are concerned with the transient behaviour of the well, and as such, we denote perturbations from some initial steady state profile $\bar{p}(x), \bar{q}$ (note that the steady state flow rate is constant while the steady-state pressure is dependent on position x)

$$\tilde{p}(x,t) = p(x,t) - \bar{p}(x), \qquad \tilde{q}(x,t) = q(x,t) - \bar{q}$$

In the following we drop the (x,t) arguments when this is obvious from the context.

Using the equation of continuity and the momentum balance coupled with the equation of state, respectively, we obtain

$$\frac{\partial \tilde{p}}{\partial t} + \frac{\beta}{A}\frac{\partial \tilde{q}}{\partial x} = 0 \tag{6.59}$$

$$\rho_0 \frac{\partial \tilde{q}}{\partial t} + A\frac{\partial \tilde{p}}{\partial x} = -k\tilde{q} \tag{6.60}$$

where β, ρ_0, A, k are the effective bulk modulus, nominal liquid density, cross-sectional flow area, and a viscous linear dissipation factor, respectively.

This model gives an excellent approximation of the single-phase flow dynamics in a well. The limiting factor of this model's performance is the simplicity of the linear, frequency-independent, friction factor. The above simplification should be valid given that:

- We are considering relatively small perturbations around the original steady state such that higher-order frictional effects are not significant.
- The resistive losses occurring at the boundaries are significantly higher than the viscous losses occurring along the line (Goodson and Leonard, 1972). This is typically satisfied in MPD operations as a partly open back-pressure choke is highly resistive. In cases where this assumption does not hold, frequency-dependent friction (Di Meglio and Aarsnes, 2015) or other more rigorous models could be used (Aarsnes et al., 2014c).

Using the model (6.59)-(6.60), the propagation operator Γ and characteristic line impedance Z_c are given as (Goodson and Leonard, 1972)

$$\Gamma(s) = \frac{sL}{c_0}\sqrt{1+\frac{k}{s}}, \quad Z_c(s) = \frac{\rho_0 c_0}{A}\sqrt{1+\frac{k}{s}}, \tag{6.61}$$

where $c_0 = \sqrt{\beta/\rho_0}$ is the sound velocity and s is the Laplace variable.

6.A.1. Irrational Transfer Function

The Laplace transformed, perturbed, pressure and flow dynamics (denoted by capital letters) can be written in standard form as (Goodson and Leonard, 1972)

$$\begin{bmatrix} P_{bh} \\ Q_{bh} \end{bmatrix}(s) = \begin{bmatrix} \cosh\Gamma & Z_c \sinh\Gamma \\ \frac{1}{Z_c}\sinh\Gamma & \cosh\Gamma \end{bmatrix} \begin{bmatrix} P_c \\ Q_c \end{bmatrix}(s),$$

where the propagation operator Γ, and characteristic line impedance Z_c are given in (6.61). For developing the desired transfer functions, the appropriate two-port configuration can be found in (Goodson and Leonard, 1972) (where we have Q_c defined as *flow out* of and Q_{bh} as *flow into* the well):

$$\begin{aligned} \begin{bmatrix} P_{bh} \\ P_c \end{bmatrix} &= Z_c \begin{bmatrix} \frac{\cosh\Gamma}{\sinh\Gamma} & -\frac{1}{\sinh\Gamma} \\ \frac{1}{\sinh\Gamma} & -\frac{\cosh\Gamma}{\sinh\Gamma} \end{bmatrix} \begin{bmatrix} Q_{bh} \\ Q_c \end{bmatrix}, \\ &\equiv \begin{bmatrix} -G_2(s) & G_1(s) \\ -G_1(s) & G_2(s) \end{bmatrix} \begin{bmatrix} Q_{bh} \\ Q_c \end{bmatrix}. \end{aligned} \tag{6.62}$$

6.B. Linearized Two-Phase Choke Equation

The topside flow out of the well is given by a two-phase choke equation relating the flow rate to choke pressure and choke opening. In the following we will consider the choke equation from (Aarsnes et al., 2014b):

$$\left[\frac{\rho_\ell v_\ell \alpha_\ell}{\sqrt{\rho_\ell}} + \frac{\rho_g v_g \alpha_g}{Y\sqrt{\rho_g}}\right]\Big|_{x=L} = \frac{C_v(z)}{A}\sqrt{p_c - p_{c0}}, \tag{6.63}$$

where $\rho_i, v_i, \alpha_i,\ i = G, L$ are the density, velocity and volume fraction of the gas and liquid, respectively, and $Y \in [0, 1]$ is a gas expansion factor for the gas flow. Herein, A, Y, ρ_ℓ, p_{c0} are assumed to be constant or slowly varying. We note that when the flow is liquid only (6.63) reduces to the classical single-phase choke equation (6.16).

Using the mapping (6.17) we are looking for a linearized approximation on the form

$$\tilde{q}_c = K_p \tilde{p}_c - K_u \tilde{u}, \tag{6.64}$$

Now denote $q_c = A v_M = A(\alpha_g v_g + \alpha_\ell v_\ell)\big|_{x=L}$ as the mixture flow through the choke. We have from (6.63), inserting (6.17), and assuming the slip law $v_g = C_0 v_M + v_\infty$, valid for $\alpha_g < 1/C_0$ (Zuber and Findlay, 1965):

$$q_c = \frac{1}{C_K}\left(\frac{\sqrt{p_c - p_{c0}}}{\sqrt{u}} + \frac{A}{2} v_\infty X_G\right), \tag{6.65}$$

$$C_K = 1 - \frac{1}{2} C_0 X_G, \quad X_G = \left[\alpha_g\left(1 - \frac{1}{Y}\frac{\sqrt{\rho_g}}{\sqrt{\rho_\ell}}\right)\right]\Big|_{x=L}. \tag{6.66}$$

$C_K \leq 1$ is to be understood as a two-phase modification factor equal to 1 for liquid-only flow.

Consequently, we have:

$$K_p = \frac{\bar{q}_{bh}}{C_K} \frac{1}{2\sqrt{p_c - p_{c0}}\sqrt{u}}, \tag{6.67}$$

$$K_u = \frac{\bar{q}_{bh}}{C_K} \frac{\sqrt{p_c - p_{c0}}}{2u\sqrt{u}}. \tag{6.68}$$

Combining (6.19) with (6.3) and using the first-order approximation from (6.14) we obtain the nominal first-order plant

$$P_{bh} \approx \frac{k_u}{\tau s + 1} U, \tag{6.69}$$

$$\tau = V/(K_p \bar{\beta}), \tag{6.70}$$

$$k_u = \frac{K_u}{K_p} = \frac{p_c - p_{c0}}{u}. \tag{6.71}$$

In the controller design we assume $k_u \approx 1$, which is valid at the equilibrium point. Furthermore, at the equilibrium we also have

$$\tau = \frac{V C_K 2\bar{u}}{\bar{\beta}\bar{q}_{bh}}. \tag{6.72}$$

Chapter 7

Concluding remarks

The drilling of petroleum wells often entail dynamics which are complex and/or non-intuitive, and monitored with limited measurement capabilities. As such researchers have, over the years, developed and validated mathematical models covering the full range of operations. This means that the drilling process is ripe for improvement through the application of the appropriate automated algorithms which could reduce risk, increase productivity and act as an enabling technology of the increasingly challenging prospects.

Such expectations have been slow to realize up until recently. But, the advent of back-pressure drilling, together with a larger industry pull for topside automation, have made available the necessary sensor and actuation equipment. Consequently automated pressure control using a backpressure choke for MPD is now readily offered, including such products as:

- **Expro PowerChokes®ABP Automatic Back Pressure Choke** (Expro, 2015).
- **Kelda Leidar®Control System** (Kelda Drilling Controls, 2015a).
- **Weatherford Microflux®Control System** (Weatherford, 2015).
- **MI Swaco @balance drilling** (MI Swaco, 2015).

It is natural to expect the standardization of automated pressure control that has happened in MPD to percolate to other back-pressure drilling approaches such as flow drilling and UBD. When this happens models of the two-phase flow encountered, that are amenable for control and monitoring algorithms, will be required. This thesis has attempted to provide a basis for designing and choosing such fit-for-purpose models. In particular, a heuristic has been proposed that suggests which type of dynamic dominates at different time scales (or equivalently, frequency ranges), summarized in Table 7.1.

Automatic pressure control of UBD has the potential of making a big impact, probably even more so than the automation that has occurred in MPD. The reason for this is that the dynamics encountered in UBD are more complicated and challenging to control, resulting in a larger potential for improvement from the conventional "bloke on the choke" to a state of the art control algorithm. Furthermore, the diverse operating conditions and challenges encountered in UBD means that

Table 7.1.: Time scale heuristic.

Time-scale	**Dominating dynamics**
$\sim$ 10 seconds	Distributed pressure dynamics
$\sim$ 1$-$10 minutes	Slow compression pressure mode
$\sim$ 10 minutes to hours	Void wave advection

automated pressure control has a potential as an enabling technology: e.g. avoiding large pressure transients in tight reservoirs.

Specific scenarios and procedures from UBD where these algorithms can make an impact were covered in the introduction. Of these, the following can be improved with automated feedback control of the back-pressure choke:

- Connection transients.
- Severe slugging.
- Extending the operating envelope to the unstable regime.

These transients are primarily driven by the void wave propagation dynamic (i.e. at the time scale of 10-minutes to hours). Consequently, by closing the feedback loop at a crossover frequency around 1–10 minutes, e.g. using the approach proposed in Chapter 6, these scenario can be effectively controlled and stabilized.

Appendix A

The Drift-Flux Model

This Appendix is based on the work presented in Aarsnes et al. (2014b) and Aarsnes et al. (2016a).

A.1. Governing Equations

The model consists in expressing the mass conservation law for the gas and liquid phases separately, and a combined momentum equation. The drilling mud, oil and water are lumped into one single liquid phase. In developing the model, we use the following mass variables

$$m = \alpha_\ell \rho_\ell, \qquad\qquad n = \alpha_{\mathrm{g}} \rho_{\mathrm{g}}$$

where for $k = \ell, \mathrm{g}$ denoting liquid or gas, ρ_k is the phase density, and α_k the volume fraction satisfying

$$\alpha_\ell + \alpha_{\mathrm{g}} = 1. \tag{A.1}$$

Further, v_k denotes the phase velocity, and p the pressure. All these variables are functions of time and space. We denote $t \geq 0$ the time variable, and $x \in [0, L]$ the space variable, corresponding to a curvilinear abscissa with x = 0 corresponding to the bottom of the well and x = L to the outlet choke position (see Fig. 6.1). The equations are as follows:

$$\frac{\partial}{\partial t} m + \frac{\partial}{\partial x}\big(m v_\ell\big) = 0, \tag{A.2}$$

$$\frac{\partial}{\partial t} n + \frac{\partial}{\partial x}\big(n v_{\mathrm{g}}\big) = 0, \tag{A.3}$$

$$\frac{\partial}{\partial t}\big(m v_\ell + n v_{\mathrm{g}}\big) + \frac{\partial}{\partial x}\big(P + m v_\ell^2 + n v_{\mathrm{g}}^2\big) = S. \tag{A.4}$$

In the momentum equation (A.4) we have the source term

$$S = -(m+n) g \sin\phi(x) - \frac{2 f (m+n) v_M |v_M|}{D}, \tag{A.5}$$

where the term $(m+n)g\sin\theta$ represents the gravitational source term, while $\frac{2f(m+n)v_M|v_M|}{D}$ accounts for frictional losses. The mixture velocity is given as

$$v_M = \alpha_{\mathrm{g}} v_{\mathrm{g}} + \alpha_\ell v_\ell. \tag{A.6}$$

Along with these distributed equations, algebraic relations are needed to close the system.

A.1.1. Closure Relations

Both the liquid and gas phase are assumed compressible. This is required for the model to handle the transition from two-phase to single-phase flow. The densities are thus given as functions of the pressure as follows

$$\rho_{\mathrm{g}} = \frac{P}{c_{\mathrm{g}}^2(T)}, \qquad \rho_\ell = \rho_{\ell,0} + \frac{P}{c_\ell^2}, \tag{A.7}$$

where c_k is the velocity of sound and $\rho_{\ell,0}$ is the reference density of the liquid phase given at vacuum. Notice that the velocity of sound in the gas phase c_G depends on the temperature as suggested by the ideal gas law. The temperature profile is assumed to be known and fed into the model.

Combining (A.7) with (A.1) we obtain the following relations for finding volume fractions from the mass variables:

$$\alpha_G = \frac{1}{2} - \frac{\frac{c_{\mathrm{g}}^2}{c_\ell^2} n + m + \sqrt{\Delta}}{2\rho_{\ell,0}},$$
$$\Delta = \left(\rho_{\ell,0} - \frac{c_\ell^2}{c_\ell^2} n - m\right)^2 + 4\frac{c_G^2}{c_L^2} n \rho_{\ell,0}$$

Then the pressure can be found by using a modified expression to ensure pressure is defined when the gas vanishes:

$$P = \begin{cases} \left(\frac{m}{1-\alpha_{\mathrm{g}}} - \rho_{\ell,0}\right) c_\ell^2, & \text{if } \alpha_{\mathrm{g}} \leq \alpha_{\mathrm{g}}^* \\ \frac{n}{\alpha_{\mathrm{g}}} c_{\mathrm{g}}^2, & \text{otherwise.} \end{cases} \tag{A.8}$$

Because the momentum equation (A.4) was written for the gas-liquid mixture, a so-called *slip law* is needed to empirically relate the velocities of gas and liquid. Traditionally, the Zuber-Findlay (Zuber and Findlay, 1965) slip law is used

$$v_{\mathrm{g}} = C_0 v_m + v_\infty$$

where C_0 and v_∞ are constant parameters. However, to handle the transition between single and two-phase flow, a more involved relation, with state-dependent parameters is needed (Evje, 2011; Shi et al., 2005). More precisely, we use the following slip law:

$$v_{\mathrm{g}} = (K - (K-1)\alpha_{\mathrm{g}}) v_M + \alpha_\ell S \tag{A.9}$$

where $K \geq 1$ and $S \geq 0$ are constant parameters.

A.1.2. Boundary Conditions

Boundary conditions on the left (downhole) boundary are given by the mass rates of gas and liquid injected from the drilling rig and flowing in from the reservoir. Denoting the cross sectional flow area by A, the boundary fluxes are given as:

$$mv_\ell|_{x=0} = \frac{1}{A}\Big(W_{L,res}(t) + W_{L,inj}(t)\Big), \tag{A.10}$$

$$nv_{\mathrm{g}}|_{x=0} = \frac{1}{A}\Big(W_{G,res}(t) + W_{G,inj}(t)\Big). \tag{A.11}$$

The injection mass rates of gas and liquid, $W_{G,inj}, W_{L,inj}$, are specified by the driller and can, within some constraints, be considered as manipulated variables. The inflow from the reservoir is dependent on the pressure on the left boundary, usually given by a Vogel-Type inflow performance relationship (IPR) (Wiggins et al., 1996), but within the range of drawdown (i.e. difference between reservoir and downhole pressure) considered here, an affine approximation should suffice, i.e.

$$W_{L,res} = k_L \max(P_{res} - P(0), 0)$$
$$W_{G,res} = k_G \max(P_{res} - P(0), 0)$$

Here P_{res} is the reservoir pore pressure and k_G, k_L are the production index (PI) of the gas and liquid, respectively.

The topside boundary condition is given by a choke equation relating topside pressure to mass flow rates

$$\Big[\frac{mv_\ell}{\sqrt{\rho_\ell}} + \frac{nv_{\mathrm{g}}}{Y\sqrt{\rho_{\mathrm{g}}}}\Big]\Big|_{x=L} = \frac{C_v(z)}{A}\sqrt{\max\left(P(x{=}L,t) - P_{c0}, 0\right)}, \tag{A.12}$$

where C_v is the choke opening given by the manipulated variable z, $Y \in [0,1]$ is a gas expansion factor for the gas flow and P_{c0} is the separator pressure, i.e. the pressure downstream of the choke. Changing the choke opening is the primary control actuation for the drilling system.

A.2. Numerical Implementations

Throughout the work, one out of the two numerical schemes were employed, depending on the requirements of the application.

1. The explicit AUSM scheme described in (Evje and Fjelde, 2002) for applications where resolution of the fast pressure waves was required.

2. A backward time, central space (BTCS) implicit scheme for long simulations where the slow gas propagation dynamics were of interest.

The implicit scheme is detailed below.

A.2.1. Implicit Scheme

Model (A.2)–(A.12) rewrites as the following nonlinear 3-state hyperbolic system of conservation laws (Masella et al., 1998)

$$\frac{\partial q_1}{\partial t} + \frac{\partial f_1(q_1, q_2, q_3)}{\partial s} = 0 \tag{A.13}$$

$$\frac{\partial q_2}{\partial t} + \frac{\partial f_2(q_1, q_2, q_3)}{\partial s} = 0 \tag{A.14}$$

$$\frac{\partial q_3}{\partial t} + \frac{\partial f_3(q_1, q_2, q_3)}{\partial s} = F_W(q_1, q_2, q_3) + F_G(q_1, q_2) \tag{A.15}$$

where $q = (q_1, q_2, q_3) = (n, m, nv_G + mv_L)$ is the set of conservative variables. Traditionally, explicit numerical schemes are favored for such systems, because they preserve shocks and limit numerical diffusion (Evje and Fjelde, 2002; Fjelde et al., 2003). However, to ensure their stability, the time and space steps Δt and Δs are required to satisfy, at all times, Courant-Friedrichs-Lewy (CFL) types of conditions, of the form

$$\left| \lambda_{\max}(\mathbf{u}) \frac{\Delta t}{\Delta s} \right| \leq 1 \tag{A.16}$$

where $\lambda_{\max}(\mathbf{u})$ is the largest (in absolute value) characteristic velocity of the problem, i.e. the largest eigenvalue of the matrix $\frac{\partial f}{\partial \mathbf{u}}(\mathbf{u})$. In the case of two-phase flow, the largest eigenvalue, which corresponds to the propagation of pressure waves in the gas, is of the order of 300 $\mathrm{m.s}^{-1}$. In the case of single-phase liquid flow, the order of magnitude jumps to around 1000 $\mathrm{m.s}^{-1}$. For, e.g., a 3000 meter-long well with 100 space steps, this imposes a time step of the order of $\Delta t < 0.1$s.

For this reason, we choose an unconditionally stable implicit scheme to numerically solve the equations, therefore not subject to CFL conditions. More precisely, consider a time-space grid $t \in \{0, \Delta t, ...\}$, $s \in \{0, \Delta s, ..., (P-1)\Delta s\}$. Denoting $\mathbf{q}(p\Delta s, n\Delta t) = \mathbf{q}^n(p)$, we consider the following approximate equations

$$\frac{q_{1,2}^n(p) - q_{1,2}^{n-1}(p)}{\Delta t} + \frac{f_{1,2}(\mathbf{q}^n(p+1)) - f_{1,2}(\mathbf{q}^n(p-1))}{2\Delta s} = 0 \tag{A.17}$$

$$\frac{q_3^n(p) - q_3^{n-1}(p)}{\Delta t} + \frac{f_3(\mathbf{q}^n(p+1)) - f_3(\mathbf{q}^n(p-1))}{2\Delta s} = F_W(\mathbf{q}^n(p)) + F_G(\mathbf{q}^n(p)) \tag{A.18}$$

These equations are valid for $p = 1, ..., P-2$, yielding $3 \times (P-2)$ implicit nonlinear equations to be solved at each time step. The boundary conditions (A.10)–(A.12) yield 3 more equations, that can be written in the following implicit form

$$h_{\mathrm{bottom},1}(\mathbf{q}^n(0)) = h_{\mathrm{bottom},2}(\mathbf{q}^n(0)) = h_{\mathrm{top}}(\mathbf{q}^n(P)) = 0 \tag{A.19}$$

The last 3 equations are given by using a de-centered second-order discretization of the spatial derivative at the boundaries

$$\frac{\partial f_{1,2}(\mathbf{q})}{\partial s}((P-1)\Delta s, n\Delta t) \approx \frac{3f_{1,2}(\mathbf{q}^n(P-1)) - 4f_{1,2}(\mathbf{q}^n(P-2)) + f_{1,2}(\mathbf{q}^n(P-3))}{2\Delta s} \tag{A.20}$$

$$\frac{\partial f_3(\mathbf{q})}{\partial s}(0, n\Delta t) \approx \frac{-3f_3(\mathbf{q}^n(0)) + 4f_3(\mathbf{q}^n(1)) - f_3(\mathbf{q}^n(2))}{2\Delta s} \tag{A.21}$$

This yields a set of $3P$ equations with $3P$ unknowns to be solved at each time step. To increase computational speed, the Jacobian of these equations is computed analytically, and a simple Newton algorithm is used to solve them. More precisely, the algorithm takes the following steps

1. At $t = 0$, pick a suitable initial condition, e.g. an equilibrium profile.
2. At $t = n\Delta t$, considering that $\mathbf{q}^{n-1}(p)$ is known for all $p = 0, ..., P-1$ from the previous iteration, do the following to compute $\mathbf{q}^n(p)$
   a) Use $\mathbf{q}^{n-1}(\cdot)$ as the initial guess of $\mathbf{q}^n(\cdot)$.
   b) Rewriting Equations (A.17)–(A.21) as $F(\mathbf{q}^n) = 0$, compute $F(\mathbf{q}^n)$.
   c) If the norm of F is low enough (given a pre-defined threshold value), the Newton algorithm has converged: go to step 3. The norm can be chosen, e.g., as a weighted 2-norm, i.e. $F^T W F$, where W is a suitably chosen weighing matrix.
   d) Compute the $3P \times 3P$ Jacobian matrix
   $$J = \frac{\partial F}{\partial \mathbf{q}^n} = \begin{pmatrix} \frac{\partial F}{\partial q_1^n(1)} & \cdots & \frac{\partial F}{\partial q_1^n(P-1)} & \frac{\partial F}{\partial q_2^n(1)} & \cdots & \frac{\partial F}{\partial q_3^n(1)} & \cdots \end{pmatrix} \tag{A.22}$$
   e) Update $\mathbf{q}^n$
   $$\mathbf{q}^n := \mathbf{q}^n - J^{-1}F(\mathbf{q}^n) \tag{A.23}$$
   f) Repeat steps (b)–(e) until the norm of F is low enough.
3. Increment n and go to step 1.

Remark: The choice of the norm in the stopping criterion for the Newton algorithm is critical to the algorithm performance and robustness. Particular attention should be given to scaling the equations to maximize the conditioning of matrix J.

Bibliography

Aadnøy, B. S., Cooper, I., Miska, S. Z., Mitchell, R., and Payne, M. (2009). *Advanced drilling and well technology*. Society of Petroleum Engineers.

Aamo, O. M. (2013). Disturbance rejection in 2 x 2 linear hyperbolic systems. *IEEE Trans. Automat. Contr.*, 58(5):1095–1106.

Aarsnes, U. J. F. and Aamo, O. M. (2016). Linear stability analysis of self-excited vibrations in drilling using an infinite dimensional model. *J. Sound Vib.*, 360:239–259.

Aarsnes, U. J. F., Aamo, O. M., and Pavlov, A. (2012). Quantifying Error Introduced by Finite Order Discretization of a Hydraulic Well Model. In *Aust. Control Conf.*, pages 54–59, Sydney, NSW.

Aarsnes, U. J. F., Acikmese, B., Ambrus, A., and Aamo, O. M. (2016a). Robust Controller Design for Automated Kick Handling in Managed Pressure Drilling. *J. Process Control*, In review.

Aarsnes, U. J. F., Ambrus, A., Di Meglio, F., Karimi Vajargah, A., van Oort, E., and Aamo, O. M. (2016b). A Simplified Two-Phase Flow Model Using a Quasi-Equilibrium Momentum Balance. *International Journal of Multiphase Flow*, 83(July):77–85.

Aarsnes, U. J. F., Ambrus, A., Karimi Vajargah, A., Aamo, O. M., and van Oort, E. (2015). A simplified gas-liquid flow model for kick mitigation and control during drilling operations. In *Proc. ASME 2015 Dyn. Syst. Control Conf.*, Columbus, Ohio, USA.

Aarsnes, U. J. F., Di Meglio, F., Aamo, O. M., and Kaasa, G.-O. (2014a). Fit-for-Purpose Modeling for Automation of Underbalanced Drilling Operations. In *SPE/IADC Manag. Press. Drill. Underbalanced Oper. Conf. Exhib.*, Madrid, Spain. Society of Petroleum Engineers.

Aarsnes, U. J. F., Di Meglio, F., Evje, S., and Aamo, O. M. (2014b). Control-Oriented Drift-Flux Modeling of Single and Two-Phase Flow for Drilling. In *ASME Dyn. Syst. Control Conf.*, page V003T37A003, San Antonio, Texas, USA. ASME.

Aarsnes, U. J. F., Di Meglio, F., Graham, R., and Aamo, O. M. (2016c). A Methodology for Classifying Operating Regimes in Underbalanced-Drilling Operations. *SPE Journal*, 21(02):243–433.

Aarsnes, U. J. F., Flåtten, T., and Aamo, O. M. (2016d). Models of gas-liquid two-phase flow in drilling for control and estimation applications. Submitted.

Aarsnes, U. J. F., Gleditsch, M. S., Aamo, O. M., and Pavlov, A. (2014c). Modeling and Avoidance of Heave-Induced Resonances in Offshore Drilling. *SPE Drill. Complet.*, 29(04):454–464.

Açıkmeşe, A. B. and Corless, M. (2002). Robust output tracking for uncertain/nonlinear systems subject to almost constant disturbances. *Automatica*, 38(11):1919–1926.

Açıkmeşe, B. and Corless, M. (2008). Stability analysis with quadratic lyapunov functions: Some necessary and sufficient multiplier conditions. *Systems & Control Letters*, 57(1):78–94.

Al-Saadi, A. J., Al-Bahlani, S., Al-Mahrooqi, S. M., Al-Riyamy, M. A., Carrera, M., Bowling, J., and Al-Balushi, A. (2006). Underbalanced Drilling Experience in PDO. In *Int. Oil Gas Conf. Exhib. China*. Society of Petroleum Engineers.

Ambrus, A., Aarsnes, U. J. F., Karimi Vajargah, A., Akbari, B., and van Oort, E. (2015). A Simplified Transient Multi-Phase Model for Automated Well Control Applications. In *Int. Pet. Conf.*, Doha, Qatar.

Ambrus, A., Aarsnes, U. J. F., Karimi Vajargah, A., Akbari, B., van Oort, E., and Aamo, O. M. (2016). Real-Time Estimation of Reservoir Influx Rate and Pore Pressure Using a Simplified Transient Two-Phase Flow Model for Managed Pressure Drilling Operations. *Journal of Natural Gas Science and Engineering*, To appear.

Anderson, B. D. and Moore, J. B. (1990). *Optimal Control Linear quadratic methods*. Courier Corporation.

Andréa-Novel, B., Coron, J.-M., and Bastin, G. (2009). On Lyapunov stability of linearised Saint-Venant equations for a sloping channel.

Anfinsen, H., Di Meglio, F., and Aamo, O. M. (2016a). Estimating the Left Boundary Condition of Coupled 1-D Linear Hyberbolic PDEs From Right Boundary Sensing. In *Submitt. to Eur. Control Conf.*, Aalborg, Sweeden.

Anfinsen, H., Diagne, M., Aamo, O. M., and Krstic, M. (2016b). An Adaptive Observer Design for n + 1 Coupled Linear Hyperbolic PDEs Based on Swapping. *Submitt. to IEEE Trans. Autom. Control. under Rev.*, pages 1–10.

Asgharzadeh Shishavan, R., Hubbell, C., Perez, H., Hedengren, J., and Pixton, D. (2015). Combined Rate of Penetration and Pressure Regulation for Drilling Optimization by Use of High-Speed Telemetry. *SPE Drill. Complet.*, (March).

Ashena, R. and Moghadasi, J. (2010). Mechanistic Modeling of Annular Two-Phase Flow While Underbalanced Drilling in Iran. In *SPE Int. Conf. Exhib.*

Åström, K. J. and Murray, R. M. (2010). *Feedback systems: an introduction for scientists and engineers*. Princeton university press, 2nd edition.

Bacon, W., Sugden, C., and Gabaldon, O. (2015). From Influx Management to Well Control; Revisiting the MPD Operations Matrix. In *SPE/IADC Drill. Conf. Exhib.* Society of Petroleum Engineers.

Baer, M. and Nunziato, J. (1986). A two-phase mixture theory for the deflagration-to-detonation transition (ddt) in reactive granular materials.

Bendiksen, K. H., Maines, D., Moe, R., and Nuland, S. (1991). The Dynamic Two-Fluid Model OLGA: Theory and Application. *SPE Prod. Eng.*, 6(02):171–180.

Bennion, D. B., Thomas, F. B., Bietz, R. F., and Bennion, D. W. (1996). Underbalanced Drilling, Praises and Perils. In *Permian Basin Oil Gas Recover. Conf.*, number December. Society of Petroleum Engineers.

Bhagwat, S. M. and Ghajar, A. J. (2014). A flow pattern independent drift flux model based void fraction correlation for a wide range of gas-liquid two phase flow. *Int. J. Multiph. Flow*, 59:186–205.

Biswas, D., Partners, B. E., Suryanarayana, P. V., and Frink, P. J. (2003). SPE 84176 An Improved Model to Predict Reservoir Characteristics During Underbalanced Drilling.

Bjorkevoll, K. S., Vollen, A. E., Barr Aas, I., and Hovland, S. (2010). Successful Use of Real Time Dynamic Flow Modelling to Control a Very Challenging Managed Pressure Drilling Operation in the North Sea. In *SPE/IADC Manag. Press. Drill. Underbalanced Oper. Conf. Exhib.* Society of Petroleum Engineers.

Bloemen, H., Belfroid, S., Sturm, W., and Verhelst, F. (2006). Soft sensing for gas-lift wells. *SPE J.*, 11(December):454–463.

Bourgoyne, A., Chenevert, M., Millheim, K., and Young, F. (1986). Applied Drilling Engineering.

Bourgoyne, Jr., A. (1997). Well Control Considerations for Underbalanced Drilling. In *Proc. SPE Annu. Tech. Conf. Exhib.*, San Antonia, Texas. Society of Petroleum Engineers.

Bowers, G. L. (1995). Pore Pressure Estimation From Velocity Data: Accounting for Overpressure Mechanisms Besides Undercompaction. *SPE Drill. Complet.*, 10(02):89–95.

Boyd, S., El Ghaoui, L., Feron, E., and Balakrishnan, V. (1994a). *Linear Matrix Inequalities in System and Control Theory*. Society for Industrial and Applied Mathematics, Philadelphia.

Boyd, S., El-Ghaoui, L., Feron, E., Balakrishnan, V., and Yaz, E. (1997). Linear matrix inequalities in system and control theory. *Proceedings of the IEEE*, 85(4):698–699.

Boyd, S. P., El Ghaoui, L., Feron, E., and Balakrishnan, V. (1994b). *Linear matrix inequalities in system and control theory*, volume 15. SIAM.

Bruce Stewart, H. and Wendroff, B. (1984). Two-phase flow: Models and methods. *J. Comput. Phys.*, 56(3):363–409.

Carlsen, L. A., Nygaard, G., Gravdal, J. E., Nikolaou, M., and Schubert, J. (2008). Performing the Dynamic Shut-In Procedure Because of a Kick Incident When Using Automatic Coordinated Control of Pump Rates and Choke-Valve Opening. In *SPE/IADC Manag. Press. Drill. Underbalanced Oper. Conf. Exhib.* Society of Petroleum Engineers.

Carlsen, L. A., Nygaard, G., and Nikolaou, M. (2013). Evaluation of control methods for drilling operations with unexpected gas influx. *J. Process Control*, 23(3):306–316.

Cayeux, E., Daireaux, B., Dvergsnes, E. W., Florence, F., and Varco, N. O. (2013). SPE / IADC 163440 Toward Drilling Automation : On the Necessity of Using Sensors That Relate to Physical Models. In *SPE/IADC Drill. Conf. Exhib.*, Amsterdam, The Netherlands.

Chen, G.-Q., Levermore, C. D., and Liu, T.-P. (1994). Hyperbolic conservation laws with stiff relaxation terms and entropy. *Commun. Pure Appl. Math.*, 47(6):787–830.

Chirinos, J. E., Smith, J. R., and Bourgoyne, D. A. (2011). A Simplified Method to Estimate Peak Casing Pressure During MPD Well Control. In *SPE Annu. Tech. Conf. Exhib.*, number 2010. Society of Petroleum Engineers.

Choi, J., Pereyra, E., Sarica, C., Lee, H., Jang, I. S., and Kang, J. (2013). Development of a fast transient simulator for gasliquid two-phase flow in pipes. *J. Pet. Sci. Eng.*, 102:27–35.

Choi, J., Pereyra, E., Sarica, C., Park, C., and Kang, J. M. (2012). An efficient drift-flux closure relationship to estimate liquid holdups of gas-liquid two-phase flow in pipes. *Energies*, 5(12):5284–5306.

Contreras, O., Hareland, G., and Aguilera, R. (2013). Pore Pressure Modelling and Stress-Faulting-Regime Determination of the Montney Shale in the Western Canada Sedimentary Basin. *J. Can. Pet. Technol.*, 52(05):349–359.

Crowe, C. T., Schwarzkopf, J. D., Sommerfeld, M., and Tsuji, Y. (2011). *Multiphase flows with droplets and particles*. CRC press.

Culen, M. and Killip, D. (2005). Forensic Reservoir Characterisation Enabled with Underbalanced Drilling. *SPE Eur. Form. Damage Conf.*

Danielson, T. J., Bansal, K. M., Djoric, B., Duret, E.-D., Johansen, S. T., and Hellan, O. (2011). Testing and Qualification of a New Multiphase Flow Simulator. In *Offshore Technol. Conf.*, pages 1–16. Offshore Technology Conference.

de Kruif, B., Leskens, M., Linden, R., and Alberts, G. (2008). Soft-Sensing for Multilateral Wells With Downhole Pressure and Temperature Measurements. *Proc. Abu Dhabi Int. Pet. Exhib. Conf.*

Di Meglio, F. (2011). *Dynamics and control of slugging in oil production*. Phd thesis, ParisTech.

Di Meglio, F. and Aarsnes, U. J. F. (2015). A distributed parameter systems view of control problems in drilling. In *2nd IFAC Work. Autom. Control Offshore Oil Gas Prod.*, Florianopolis, Brazil.

Di Meglio, F., Bresch-Pietri, D., and Aarsnes, U. J. F. (2014). An Adaptive Observer for Hyperbolic Systems with Application to UnderBalanced Drilling. In Edward, B., editor, *IFAC World Congr. 2014, South Africa*, pages 11391–11397, Cape Town, South Africa.

Di Meglio, F., Kaasa, G.-O., and Petit, N. (2009). A first principle model for multiphase slugging flow in vertical risers. In *Proc. 48h IEEE Conf. Decis. Control held jointly with 2009 28th Chinese Control Conf.*, pages 8244–8251. IEEE.

Di Meglio, F., Kaasa, G.-o., Petit, N., and Alstad, V. (2010). Model-based control of slugging flow: An experimental case study. In *Proc. 2010 Am. Control Conf.*, pages 2995–3002. IEEE.

Di Meglio, F., Vazquez, R., and Krstic, M. (2013). Stabilization of a System of n+1 Coupled First-Order Hyperbolic Linear PDEs With a Single Boundary Input. *IEEE Trans. Automat. Contr.*, 58(12):3097–3111.

Doan, Q., Oguztoreli, M., Masuda, Y., Yonezawa, T., Kobayashi, A., Naganawa, S., and Kamp, A. (2003). Modeling of Transient Cuttings Transport in Underbalanced Drilling (UBD). *SPE J.*, 8(02):160–170.

Eaton, B. A. (1975). The Equation for Geopressure Prediction from Well Logs. In *Fall Meet. Soc. Pet. Eng. AIME*. Society of Petroleum Engineers.

Egeland, O. and Gravdahl, J. (2002). *Modeling and simulation for automatic control*. Marine Cybernetics.

Eikrem, G. O., Aamo, O. M., and Foss, B. (2006). Stabilization of Gas-Distribution Instability in Single-Point Dual Gas Lift Wells.

Eikrem, G. O., Aamo, O. M., and Foss, B. (2008). On Instability in Gas Lift Wells and Schemes for Stabilization by Automatic Control.

Esmaeil, J. and Skogestad, S. (2011). Simplified Dynamical Models for Control of Severe Slugging in Multiphase Risers. In Sergio, B., editor, *Proc. 18th IFAC World Congr. 2011*, pages 1634–1639, Milano, Italy.

Evje, S. (2011). Weak solutions for a gas-liquid model relevant for describing gas-kick in oil wells. *SIAM J. Math. Anal.*, 43(4):1887–1922.

Evje, S. and Fjelde, K. K. (2002). Hybrid Flux-Splitting Schemes for a Two-Phase Flow Model. *J. Comput. Phys.*, 175(2):674–701.

Evje, S. and Flåtten, T. (2006). CFL-Violating Numerical Schemes for a Two-Fluid Model. *J. Sci. Comput.*, 29(1):83–114.

Evje, S. and Wen, H. (2013). Weak solutions of a gas-liquid drift-flux model with general slip law for wellbore operations. *Discret. Contin. Dyn. Syst.*, 33(10):4497–4530.

Evje, S. and Wen, H. (2015). Global Solutions of a Viscous Gas-Liquid Model with Unequal Fluid Velocities in a Closed Conduit. *SIAM J. Math. Anal.*, 47(1):381–406.

Expro (2015). Automatic Back Pressure Choke: Designed for Superior Performance. http://www.expropowerchokes.com/Innovation/, accessed 09-12-2015.

Eykhoff, P. (1994). Every good regulator of a system must be a model of that system. *Model. Identif. Control A Nor. Res. Bull.*, 15(3):135–139.

Fjelde, K. K. and Karlsen, K. H. (2002). High-resolution hybrid primitiveconservative upwind schemes for the drift flux model. *Comput. Fluids*, 31(3):335–367.

Fjelde, K. K., Rommetveit, R., Merlo, A., and Lage, A. C. (2003). Improvements in Dynamic Modeling of Underbalanced Drilling. In *IADC/SPE Underbalanced Technol. Conf. Exhib.*, number 3, Houston, Texas. Society of Petroleum Engineers.

Flåtten, T. and Lund, H. (2011). Relaxation two-phase flow models and the subcharacteristic condition. *Math. Model. Methods Appl. Sci.*, 21(12):2379–2407.

Gabaldon, O., Culen, M., Brand, P., and Partners, B. E. (2014). OTC-25256-MS Enhancing Well Control Through Managed Pressure Drilling. (May):5–8.

Gahinet, P. and Apkarian, P. (1994). A linear matrix inequality approach to h_∞ control. *International journal of robust and nonlinear control*, 4(4):421–448.

Gauthier, P. J., Hussain, H., Bowling, J., Edwards, J. E., and Herold, B. (2007). Determination of Water Producing Zones While Under-balanced Drilling Horizontal Wells - Integration of Sigma Log and Real-Time Production Data. In *SPE Middle East Oil Gas Show Conf.* Society of Petroleum Engineers.

Gavrilyuk, S. and Fabre, J. (1996). Lagrangian coordinates for a drift-flux model of a gas-liquid mixture. *Int. J. Multiph. flow*, pages 453–460.

Ge, M., Chiu, M.-S., and Wang, Q.-G. (2002). Robust PID controller design via LMI approach. *J. Process Control*, 12(1):3–13.

Godhavn, J.-M. (2010). Control Requirements for Automatic Managed Pressure Drilling System. *SPE Drill. Complet.*, 25(3):336–345.

Godhavn, J.-M. (2011). Drilling Seeking Automatic Control Solutions. In Sergio, B., editor, *18th IFAC World Congr. Milano*, pages 10842–10850, Milano, Italy.

Goodson, R. E. and Leonard, R. G. (1972). A Survey of Modeling Techniques for Fluid Line Transients. *J. Basic Eng.*, 94(2):474.

Graham, R. A. and Culen, M. S. (2004). Methodology For Manipulation Of Wellhead Pressure Control For The Purpose Of Recovering Gas To Process In Underbalanced Drilling Applications. In *Proc. SPE/IADC Underbalanced Technol. Conf. Exhib.*, Houston, Texas. Society of Petroleum Engineers.

Gravdal, J. E., Nikolaou, M., Breyholtz, Y., and Carlsen, L. A. (2013). Improved Kick Management During MPD by Real-Time Pore-Pressure Estimation. In *SPE Annu. Tech. Conf. Exhib.*, number March, pages 4–7. Society of Petroleum Engineers.

Gryzlov, A. N. (2011). *Model-based estimation of multi-phase flows in horizontal wells*. PhD thesis, Technische Universiteit Delft.

Guillard, H. and Viozat, C. (1999). On the behaviour of upwind schemes in the low Mach number limit. *Comput. Fluids*, 28(1):63–86.

Guo, B. (2002). Balance between Formation Damage and Wellbore Damage: What Is the Controlling Factor in UBD Operations? In *Int. Symp. Exhib. Form. Damage Control*. Society of Petroleum Engineers.

Guo, B. and Ghalambor, A. (2002). An Innovation in Designing Underbalanced Drilling Flow Rates: A Gas-Liquid Rate Window (GLRW) Approach. In *Proc. IADC/SPE Asia Pacific Drill. Technol.* Society of Petroleum Engineers.

Guo, B. and Ghalambor, A. (2006). A Guideline to Optimizing Pressure Differential in Underbalanced Drilling for Reducing Formation Damage. In *Proc. Int. Symp. Exhib. Form. Damage Control*. Society of Petroleum Engineers.

Guo, B. and Liu, G. (2011). *Applied Drilling Circulation Systems: Hydraulics, Calculations and Models*. Gulf Professional Publishing.

Hasan, A. (2014). Disturbance attenuation of n + 1 coupled hyperbolic PDEs. In *53rd IEEE Conf. Decis. Control*, number 978, pages 2058–2064. IEEE.

Hasan, A., Kabir, C., and Srinivasan, S. (1994). Countercurrent bubble and slug flows in a vertical system. *Chem. Eng. Sci.*, 49(16):2567–2574.

Hasan, A. R. and Kabir, C. S. (1983). Pressure Buildup Analysis: A Simplified Approach (includes associated papers 11862 and 11867 and 11925 and 11926 and 13676). *J. Pet. Technol.*, 35(01):178–188.

Hauge, E. (2013). *Automatic Kick Detection and Handling in Managed Pressure Drilling Systems*. PhD thesis, NTNU.

Hauge, E., Aamo, O. M., and Godhavn, J.-M. (2012). Model-based estimation and control of in/out-flux during drilling. In *2012 Am. Control Conf.*, pages 4909–4914. IEEE.

Hauge, E., Aamo, O. M., and Godhavn, J.-m. (2013a). Application of an Infinite-Dimensional Observer for Drilling Systems Incorporating Kick and Loss Detection. In *Eur. Control Conf.*, pages 1065–1070, Zürich, Switzerland.

Hauge, E., Godhavn, J., Molde, D., Cohen, J., Stave, R., and Toftevaag, K. (2015). Analysis of Field Trial Well Control Results with a Dual Gradient Drilling System. In *Offshore Technol. Conf.* Offshore Technology Conference.

Hauge, E., Stamnes, Ø. N., Aamo, O. M., and Godhavn, J.-M. (2013b). A Dynamic Model of Percolating Gas in a Wellbore. *SPE Drill. Complet.*, 27(02):204–215.

Hérard, J.-M. (2007). A three-phase flow model. *Math. Comput. Model.*, 45(5-6):732–755.

Holmås, K. and Løvli, A. (2011). FlowManager(TM) Dynamic: A Multiphase Flow Simulator for Online Surveillance, Optimization and Prediction of Subsea Oil and Gas Production. In *15th Int. Conf. Multiph. Prod. Technol.*, pages 241–254, Cannes, France.

Hu, B. (2004). *Characterizing gas-lift instabilities*. PhD thesis, NTNU.

Hu, L., Di Meglio, F., Vazquez, R., and Krstic, M. (2015). Control of Homodirectional and General Heterodirectional Linear Coupled Hyperbolic PDEs. *arXiv Prepr.*, pages 1–33.

Ishii, M. (1977). One-dimensional drift-flux model and constitutive equations for relative motion between phases in various two-phase flow regimes. Technical report, Argonne National Laboratory (ANL), Argonne, IL (United States).

Jansen, F., Shoham, O., and Taitel, Y. (1996). The elimination of severe sluggingexperiments and modeling. *Int. J. Multiph. Flow*, 22(6):1055–1072.

Kaasa, G.-O., Stamnes, Ø. N., Imsland, L., and Aamo, O. M. (2011). Intelligent Estimation of Downhole Pressure Using a Simple Hydraulic Model. In *Proc. IADC/SPE Manag. Press. Drill. Underbalanced Oper. Conf. Exhib.*, number April, Denver, Colerado. Society of Petroleum Engineers.

Kaasa, G.-O., Stamnes, Ø. N., Imsland, L. S., and Aamo, O. M. (2012). Simplified hydraulics model used for intelligent estimation of downhole pressure for a managed-pressure-drilling control system. *SPE Drill. Complet.*, 27(March):127—-138.

Karimi Vajargah, A. (2013). *Pressure Signature of Gas Influx*. PhD thesis, U. of Tulsa.

Karimi Vajargah, A., Hoxha, B. B., and van Oort, E. (2014). Automated Well Control Decision-Making during Managed Pressure Drilling Operations. In *SPE Deep. Drill. Complet. Conf.* Society of Petroleum Engineers.

Kelda Drilling Controls (2015a). Leidar®Pressure Controller. http://www.kelda.no/products/leidar/, accessed 2015-12-09.

Kelda Drilling Controls (2015b). Straume(TM) Hydraulic Simulator. http://www.kelda.no/products/straume/, accessed 2015-10-08.

Khalil, H. K. (2002). *Nonlinear systems*. Prentice hall Upper Saddle River, 3 rd edition.

Kinik, K., Gumus, F., and Osayande, N. (2015). Automated Dynamic Well Control With Managed-Pressure Drilling: A Case Study and Simulation Analysis. *SPE Drill. Complet.*, 30(02):110–118.

Krstic, M., Protz, J., Paduano, J., and Kokotovic, P. (1995). Backstepping designs for jet engine stall and surge control. *Proc. 1995 34th IEEE Conf. Decis. Control*, 3(December):3049–3055.

Lage, A., Fjelde, K., and Time, R. (2000). Underbalanced Drilling Dynamics: Two-Phase Flow Modeling and Experiments. In *IADC/SPE Asia Pacific Drill. Technol.*, volume 8, pages 61–70, Kuala Lumpur, Malaysia. Society of Petroleum Engineers.

Lage, A. and Time, R. (2000). Mechanistic Model for Upward Two-Phase Flow in Annuli. *Proc. SPE Annu. Tech. Conf. Exhib.*, (1):1–11.

Lage, A. and Time, R. (2002). An Experimental and Theoretical Investigation of Upward Two-Phase Flow in Annuli. *SPE J.*, 7(3):16–18.

Landet, I. S., Mahdianfar, H., Aarsnes, U. J. F., Pavlov, A., and Aamo, O. M. (2012). Modeling for MPD Operations With Experimental Validation. In *IADC/SPE Drill. Conf. Exhib.*, San Diego, California.

Landet, I. S., Pavlov, A., and Aamo, O. M. (2013). Modeling and Control of Heave-Induced Pressure Fluctuations in Managed Pressure Drilling. *IEEE Trans. Control Syst. Technol.*, 21(4):1340–1351.

Linga, G. (2015). A Hierarchy of Non-Equilibrium Two-Fluid Models. *SIAM J. Appl. Math.*, (Submitted).

Ljung, L. (1999). *System identification : theory for the user*. Prentice Hall, Upper Saddle River, 2nd edition.

Lorentzen, R., Fjelde, K., Jonny, F., Lage, A., Geir, N., and Vefring, E. (2001). Underbalanced and Low-head Drilling Operations: Real Time Interpretation of Measured Data and Operational Support. *Proc. SPE Annu. Tech. Conf. Exhib.*

Lorentzen, R. J. and Fjelde, K. K. (2005). Use of slopelimiter techniques in traditional numerical methods for multi-phase flow in pipelines and wells. *Int. J. Numer. Methods Fluids*, 48(7):723–745.

Lorentzen, R. J., Nævdal, G., and Lage, A. C. V. M. (2003). Tuning of parameters in a two-phase flow model using an ensemble Kalman filter. *Int. J. Multiph. Flow*, 29(8):1283–1309.

Lorentzen, R. J., Saevareid, O., and Naevdal, G. (2010). Rate Allocation: Combining Transient Well Flow Modelling and Data Assimilation. In *SPE Annu. Tech. Conf. Exhib.*, pages 1–9. Society of Petroleum Engineers.

Lorentzen, R. J., Stordal, A., Nævdal, G., Karlsen, H. A., and Skaug, H. J. (2014). Estimation of Production Rates With Transient Well-Flow Modeling and the Auxiliary Particle Filter. *SPE J.*, 19(01):172–180.

Lorentzen, R. J., Stordal, A. S., Luo, X., and Nævdal, G. (2015). Estimation of Production Rates by Use of Transient Well-Flow Modeling and the Auxiliary Particle Filter: Full-Scale Applications. *SPE Prod. Oper.*, 19(01):172–180.

Lukawski, M. Z., Anderson, B. J., Augustine, C., Capuano, L. E., Beckers, K. F., Livesay, B., and Tester, J. W. (2014). Cost analysis of oil, gas, and geothermal well drilling. *J. Pet. Sci. Eng.*, 118:1–14.

Lund, H. (2012). A Hierarchy of Relaxation Models for Two-Phase Flow. *SIAM J. Appl. Math.*, 72(6):1713–1741.

Luo, X., Lorentzen, R. J., Stordal, A. S., and Nævdal, G. (2014). Toward an enhanced Bayesian estimation framework for multiphase flow soft-sensing. *Inverse Probl.*

Makinen, J., Piche, R., and Ellman, A. (2000). Fluid Transmission Line Modeling Using a Variational Method. *J. Dyn. Syst. Meas. Control*, 122(1):153.

Malloy, K. P., Stone, R., Medley, G. H., Hannegan, D. M., Coker, O. D., Reitsma, D., Santos, H. M., Kinder, J. I., Eck-Olsen, J., McCaskill, J. W., May, J. R., Smith, K. L., and Sonnemann, P. (2009). Managed-Pressure Drilling: What It Is and What It Is Not. In *IADC/SPE Manag. Press. Drill. Underbalanced Oper. Conf. Exhib.*, number Figure 2. Society of Petroleum Engineers.

Masella, J., Tran, Q., Ferre, D., and Pauchon, C. (1998). Transient simulation of two-phase flows in pipes. *Int. J. Multiph. Flow*, 24(5):739–755.

Maxwell, J. C. (1867). On Governors. *Proc. R. Soc. London*, 16:270–283.

MI Swaco (2015). @balance Control Services. http://www.slb.com/services/miswaco/services /mpd_ubd/at_balance/control_services.aspx, accessed 2015-12-09.

Minami, K. and Shoham, O. (1994). Transient two-phase flow behavior in pipelines-experiment and modeling. *Int. J. Multiph. Flow*, 20(4):739–752.

Mykytiw, C., Davidson, I., and Frink, P. (2003). Design and Operational Considerations to Maintain Underbalanced Conditions with Concentric Casing Injection. In *IADC/SPE Underbalanced Technol. Conf. Exhib.* Society of Petroleum Engineers.

Mykytiw, C., Suryanarayana, P., and Brand, P. (2004). Practical Use of a Multiphase Flow Simulator for Underbalanced Drilling Applications Design - The Tricks of the Trade. In *SPE/IADC Underbalanced Technol. Conf. Exhib.* Society of Petroleum Engineers.

Nævdal, G., Mannseth, T., and Vefring, E. H. (2002). Near-Well Reservoir Monitoring Through Ensemble Kalman Filter. In *SPE/DOE Improv. Oil Recover. Symp.*, number 1, pages 1–9. Society of Petroleum Engineers.

Nguyen, C., Somerville, J., and Smart, B. (2009). Predicting the Production Capacity During Underbalanced-Drilling Operations in Vietnam. *Proc. IADC/SPE Manag. Press. Drill. Underbalanced Oper. Conf. Exhib.*

Nikoofard, A., Aarsnes, U. J. F., Johansen, T. A., and Kaasa, G.-O. (2015). Estimation of States and Parameters of a Drift-Flux Model with Unscented Kalman Filter. In *2nd IFAC Work. Autom. Control Offshore Oil Gas Prod.*, Florianopolis, Brazil.

Nikoofard, A., Johansen, T. A., and Kaasa, G.-O. (2014a). Design and comparison of adaptive estimators for Under-balanced Drilling. In *2014 Am. Control Conf.*, pages 5681–5687. IEEE.

Nikoofard, A., Johansen, T. A., and Kaasa, G.-O. (2014b). Nonlinear Moving Horizon Observer for Estimation of States and Parameters in Under-Balanced Drilling Operations. In *Vol. 3 Ind. Appl. Model. Oil Gas, Control Validation, Estim. Control Automot. Syst. Multi-Agent Networked Syst. Control Syst. Des. Phys. Human-Robot Interact. Rehabil. Robot. Sensin*, page V003T37A002. ASME.

Nikoofard, A., Johansen, T. A., Mahdianfar, H., and Pavlov, A. (2013). Constrained MPC design for heave disturbance attenuation in offshore drilling systems. In *2013 MTS/IEEE Ocean. - Bergen*, pages 1–7. IEEE.

Nygaard, G. and Nævdal, G. (2005). Modelling two-phase flow for control design in oil well drilling. In *Proc. 2005 IEEE Conf. Control Appl. 2005. CCA 2005.*, pages 675–680, Toronto, Ont. IEEE.

Nygaard, G., Vefring, E., Fjelde, K.-k., and Nævdal, G. (2007a). Bottomhole pressure control during drilling operations in gas-dominant wells. *SPE J.*, (December 2006):11–12.

Nygaard, G. H., Imsland, L. S., and Johannessen, E. A. (2007b). Using NMPC based on a low-order model for controlling pressure during oil well drilling. In Bjarne, F., editor, *8th Int. IFAC Symp. Dyn. Control Process Syst.*, volume 3, pages 159–164.

Nygaard, G. H., Vefring, E. H., Mylvaganam, S., and Fjelde, K. K. (2004). Underbalanced Drilling: Improving Pipe Connection Procedures Using Automatic Control. In *SPE Annu. Tech. Conf. Exhib.* Society of Petroleum Engineers.

Packard, A., Zhou, K., Pandey, P., and Becker, G. (1991). A collection of robust control problems leading to lmis. In *Decision and Control, 1991., Proceedings of the 30th IEEE Conference on*, pages 1245–1250. IEEE.

Patankar, S. and Spalding, D. (1972). A calculation procedure for heat, mass and momentum transfer in three-dimensional parabolic flows. *Int. J. Heat Mass Transf.*, 15(10):1787–1806.

Pauchon, C. and Dhulesia, H. (1994). TACITE: A Transient Tool for Multiphase Pipeline and Well Simulation. In *SPE Annu. Tech. Conf. Exhib.*, number 58, pages 62–77. Society of Petroleum Engineers.

Pavlov, A., Kaasa, G.-O., and Imsland, L. S. (2010). Experimental Disturbance Rejection on a Full-Scale Drilling Rig. In Lorenzo, M., editor, *IFAC Symp. Nonlinear Control Syst.*, pages 1338–1343.

Pedersen, T. and Godhavn, J.-M. (2013). Model Predictive Control of Flow and Pressure in Underbalanced Drilling. In *10th IFAC Int. Symp. Dyn. Control Process Syst.*, pages 307–312.

Pedersen, T., Godhavn, J.-M., and Schubert, J. (2015). Supervisory control for underbalanced drilling operations. *IFAC-PapersOnLine*, 48(6):120–127.

Perez-Tellez, C. (2003). *Improved bottomhole pressure control for underbalanced drilling operations*. PhD thesis, Louisiana State University.

Perez-Tellez, C., Smith, J., and Edwards, J. (2003). A New Comprehensive, Mechanistic Model for Underbalanced Drilling Improves Wellbore Pressure Prediction. *SPE Drill. Complet.*, 18(3):199–208.

Petersen, J., Rommetveit, R., Bjørkevoll, K. S., and Froyen, J. (2008). A General Dynamic Model for Single and Multi-phase Flow Operations during Drilling, Completion, Well Control and Intervention. In *Proc. IADC/SPE Asia Pacific Drill. Technol. Conf. Exhib.*, pages 1–12, Jakarta, Indonesia. Society of Petroleum Engineers.

Pickles, R., Brand, P., and Savage, P. (2004). Utilization of Underbalanced Drilling Techniques to Exploit a Low-Pressure Reservoir in Indonesia. In *SPE/IADC Underbalanced Technol. Conf. Exhib.* Society of Petroleum Engineers.

Podio, A. and Yang, A.-P. (1986). Well Control Simulator for IBM Personal Computer. In *SPE/IADC Drill. Conf.*, number June, pages 159–173. Society of Petroleum Engineers.

Reitsma, D. G. and Couturier, Y. (2012). New Choke Controller for Managed Pressure Drilling. *2012 IFAC Work. Autom. Control Offshore Oil Gas Prod. Nor. Univ. Sci. Technol. 31 May - 1 June 2012, Trondheim, Norw.*, pages 223–230.

Roe, P. (1981). Approximate Riemann solvers, parameter vectors, and difference schemes. *J. Comput. Phys.*, 43(2):357–372.

Rommetveit, R., Bjorkevoll, K. S., Gravdal, J. E., Goncalves, C. J., Lage, A. C. V., Campos, J. E., Aragao, A. F., Arcelloni, A., and Ohara, S. (2005). Ultra-Deepwater Hydraulics and Well Control Tests with Extensive Instrumentation: Field Tests and Data Analysis. *SPE Drill. Complet.*, 20(04):251–257.

Rommetveit, R., Fjelde, K., Frøyen, J., Bjørkevoll, K., Boyce, G., and Eck-Olsen, J. (2004). Use of Dynamic Modeling in Preparations for the Gullfaks C-5A Well. In *Proc. SPE/IADC Underbalanced Technol. Conf. Exhib.* Society of Petroleum Engineers.

Rommetveit, R. and Lage, A. C. V. M. (2001). Designing Underbalanced and Lightweight Drilling Operations; Recent Technology Developments and Field Applications. In *Proc. SPE Lat. Am. Caribb. Pet. Eng. Conf.*, Buenos Aires, Argentina. Society of Petroleum Engineers.

Rommetveit, R. and Vefring, E. (1991). Comparison of Results From an Advanced Gas Kick Simulator With Surface and Downhole Data From Full Scale Gas Kick Experiments in an Inclined Well. In *SPE Annu. Tech. Conf. Exhib.* Society of Petroleum Engineers.

Rostami, S. A., Kinik, K., Gumus, F., and Kirchhoff, M. (2015). Dynamic Calibration of the Empirical Pore Pressure Estimation Methods Using MPD Data. In *Offshore Technol. Conf.*, number 2004. Offshore Technology Conference.

Santos, H., Leuchtenberg, C., and Shayegi, S. (2003). Micro-Flux Control: The Next Generation in Drilling Process. In *SPE Lat. Am. Caribb. Pet. Eng. Conf.* Society of Petroleum Engineers.

Santos, H. M., Catak, E., Kinder, J. I., Nogueira, E. F., Lage, A. C. V., and Sonnemann, P. (2007). First Field Applications of Microflux Control Show Very Positive Surprises. In *IADC/SPE Manag. Press. Drill. Underbalanced Oper.* Society of Petroleum Engineers.

Saponja, J. (1998). Challenges with Jointed Pipe Underbalanced Operations. *SPE Drill. Complet.*, 13(02):121–128.

Saponja, J., Adeleye, A., and Hucik, B. (2006). Managed-Pressure Drilling (MPD) Field Trials Demonstrate Technology Value. In *IADC/SPE Drill. Conf.* Society of Petroleum Engineers.

Shayegi, S., Kabir, C. S., If, F., Christensen, S., Ken, K., Casasus-Bribian, J., Hasan, A. K., and Moos, D. (2012). Reservoir Characterization Begins at First Contact With the Drill Bit. *SPE Drill. Complet.*, 27(01):11–21.

Shi, H., Holmes, J., Durlofsky, L., Aziz, K., Diaz, L., Alkaya, B., and Oddie, G. (2005). Drift-Flux Modeling of Two-Phase Flow in Wellbores. *SPE J.*, 10(1):24–33.

Sinegre, L. (2006). *Dynamic study of unstable phenomena stepping in gas-lift activated systems.* PhD thesis, MINES ParisTech.

Sinegre, L., Petit, N., and Ménégatti, P. (2005). Distributed delay model for density wave dynamics in gas lifted wells. In *IEEE CONFERENCE ON DECISION AND CONTROL*, pages 7390–7397. IEEE.

Sinegre, L., Petit, N., and Menegatti, P. (2006). Predicting instabilities in gas-lifted wells simulation. In *2006 Am. Control Conf.*, page 8 pp. IEEE.

Smith, J. R. and Patel, B. M. (2013). A Proposed Method for Planning the Best Initial Response to Kicks Taken During Managed-Pressure-Drilling Operations. *SPE Drill. Complet.*, 27(02):194–203.

Solem, S., Aursand, P., and Flåtten, T. (2015). The dispersive wave dynamics of a two-phase flow relaxation model. *ESAIM Math. Model. Numer. Anal.*, 49(2):601–619.

Stamnes, Ø. N., Aamo, O. M., and Kaasa, G.-O. (2011a). Adaptive Redesign of Nonlinear Observers. *IEEE Trans. Automat. Contr.*, 56(5):1152–1157.

Stamnes, Ø. N., Aamo, O. M., and Kaasa, G.-O. (2011b). Redesign of adaptive observers for improved parameter identification in nonlinear systems. *Automatica*, 47(2):403–410.

Stecki, J. and Davis, D. (1986). Fluid transmission linesdistributed parameter models part 1: A review of the state of the art. *Proc. Inst. Mech. Eng. Part A J. Power Energy*, 200(4):215–228.

Storkaas, E., Skogestad, S., and Godhavn, J.-M. (2003). A low-dimensional dynamic model of severe slugging for control design and analysis. In *11th Int. Conf. Multiph. flow*, pages 117–133, San Remo, Italy.

Suryanarayana, P., Smith, B. E., Hasan, A. K., Leslie, C., Buchanan, R. W., and Pruitt, R. D. (2006). Basis of Design for Coiled-Tubing Underbalanced Through-Tubing Drilling in the Sajaa Field. *SPE Drill. Complet.*, 21(02):125–132.

Suryanarayana, P., Vaidya, R. N., and Wind, J. (2007a). Use of a New Rate-Integral Productivity Index in Interpretation of Underbalanced Drilling Data for Reservoir Characterization. In *Prod. Oper. Symp.* Society of Petroleum Engineers.

Suryanarayana, P., Wu, Z., Ramalho, J., and Himes, R. E. (2007b). Dynamic Modeling of Invasion Damage and Impact on Production in Horizontal Wells. *SPE Reserv. Eval. Eng.*, 10(04):348–358.

Taitel, Y. (1986). Stability of severe slugging. *Int. J. Multiph. Flow*, 12(2):203–217.

Taitel, Y. and Barnea, D. (1983). Counter current gas-liquid vertical flow, model for flow pattern and pressure drop. *Int. J. Multiph. Flow*, 9(6):637–647.

Taitel, Y. and Barnea, D. (1997). Simplified transient simulation of two phase flow using quasi-equilibrium momentum balances. *Int. J. Multiph. Flow*, 23(3):493–501.

Taitel, Y., Shoham, O., and Brill, J. (1989). Simplified transient solution and simulation of two-phase flow in pipelines. *Chem. Eng. Sci.*, 44(6):1353–1359.

Teixeira, B. O., Castro, W. S., Teixeira, A. F., and Aguirre, L. a. (2014). Data-driven soft sensor of downhole pressure for a gas-lift oil well. *Control Eng. Pract.*, 22:34–43.

Thorogood, J., Aldred, W. D., Florence, F., and Iversen, F. (2010). Drilling Automation: Technologies, Terminology, and Parallels With Other Industries. *SPE Drill. Complet.*, 25(04):419–425.

Torre, A., Schmidt, Z., Blais, R., Doty, D., and Brill, J. (1987). Casing Heading in Flowing Oil Wells. *SPE Prod. Eng.*, 2(04):297–304.

Udegbunam, J. E., Fjelde, K. K., Arild, ø., Ford, E., and Lohne, H. P. (2013). Uncertainty-Based Approach for Predicting the Operating Window in UBO Well Design. *SPE Drill. Complet.*, 28(04):326–337.

Udegbunam, J. E., Fjelde, K. K., Evje, S., and Nygaard, G. (2014). A Simple Transient Flow Model for MPD and UBD Applications. In *SPE/IADC Manag. Press. Drill. Underbalanced Oper. Conf. Exhib.*, number April, pages 8–9. Society of Petroleum Engineers.

Udegbunam, J. E., Fjelde, K. K., Evje, S., and Nygaard, G. (2015). On the Advection-Upstream-Splitting-Method Hybrid Scheme: A Simple Transient-Flow Model for Managed-Pressure-Drilling and Underbalanced-Drilling Applications. *SPE Drill. Complet.*, 30(02):098–109.

Vefring, E., Gerhard, N., Fjelde, K., Lorentzen, R., Geir, N., and Antonino, M. (2002). Reservoir Characterization during Underbalanced Drilling: Methodology, Accuracy, and Necessary Data. In *Proc. SPE Annu. Tech. Conf. Exhib.*, San Antonia, Texas. Society of Petroleum Engineers.

Vefring, E., Gerhard, N., Lorentzen, R., Geir, N., and Fjelde, K. (2003). Reservoir Characterization During UBD: Methodology and Active Tests. In *Proc. IADC/SPE Underbalanced Technol. Conf. Exhib.*, number 1, pages 1–9, Houston, Texas. Society of Petroleum Engineers.

Wahba, E. (2013). Non-Newtonian fluid hammer in elastic circular pipes: Shear-thinning and shear-thickening effects. *J. Nonnewton. Fluid Mech.*, 198:24–30.

Wallis, G. B. (1969). *One-dimensional two-phase flow*. McGraw-Hill, New-York.

Weatherford (2015). Microflux Control System. http://www.weatherford.com/products-services/drilling-formation-evaluation/ secure-drilling-services/managed-pressure-drilling/microflux-control-system, accessed 2015-12-09.

White, F. (2003). *Fluid Mechanics*. McGraw-Hill international editions. McGraw-Hill.

Wiggins, M., Russell, J., and Jennings, J. (1996). Analytical Development Of Vogel-Type Inflow Performance Relationships. *SPE J.*, 1(4):355–362.

Willersrud, A. (2015). *Model-Based Diagnosis of Drillin Incident*. PhD thesis, Norwegian University of Science and Technology.

Willersrud, A., Blanke, M., and Imsland, L. (2015a). Incident detection and isolation in drilling using analytical redundancy relations. *Control Eng. Pract.*, 41:1–12.

Willersrud, A., Blanke, M., Imsland, L., and Pavlov, A. (2014). Fault diagnosis of downhole drilling incidents using adaptive observers and statistical change detection. *J. Process Control*, 30:90–103.

Willersrud, A., Blanke, M., Imsland, L., and Pavlov, A. (2015b). Drillstring Washout Diagnosis Using Friction Estimation and Statistical Change Detection. *IEEE Trans. Control Syst. Technol.*, 23(5):1886–1900.

Willersrud, A., Imsland, L., Pavlov, A., and Kaasa, G.-o. (2013). A Framework for Fault Diagnosis in Managed Pressure Drilling Applied to Flow-Loop Data. In *10th IFAC Int. Symp. Dyn. Control Process Syst.*, Mumbai, India.

Wu, Z. and Suryanarayana, P. (2011). Reservoir Characterization through Automatic History Matching of Underbalanced Drilling (UBD) Data in a Horizontal Well. In *SPE Eur. Annu. Conf. Exhib.*, volume 1, pages 23–26. Society of Petroleum Engineers.

Xu, Z. G. and Golan, M. (1989). Criteria for operation stability of gas-lift wells. *SPE Prod. Oper. Journals*.

Zhou, J., Nygaard, G., Godhavn, J., Breyholtz, O., and Vefring, E. H. (2010). Adaptive observer for kick detection and switched control for bottomhole pressure regulation and kick attenuation during managed pressure drilling. In *Am. Control Conf. (ACC), 2010*, pages 3765–3770.

Zhou, J., Stamnes, Ø. N., Aamo, O. M., and Kaasa, G.-O. (2011). Switched Control for Pressure Regulation and Kick Attenuation in a Managed Pressure Drilling System. *IEEE Trans. Control Syst. Technol.*, 19(2):337–350.

Zuber, N. and Findlay, J. A. (1965). Average Volumetric Concentration in Two-Phase Flow Systems. *J. Heat Transfer*, 87(4):453.